Université de Montréal

# Uncovering the role of misfolded SOD1 in the pathogenesis of Amyotrophic Lateral Sclerosis

par
Sarah Pickles

Département de Biochimie et médicine moléculaire, Université de Montréal
Faculté de médicine

Thèse présentée à la Faculté médicine
en vue de l'obtention du grade de doctorat
en Biochimie

Avril 2015

Université de Montréal

Cette thèse intitulée:

# Uncovering the role of misfolded SOD1 in the pathogenesis of Amyotrophic Lateral Sclerosis

Présentée par
Sarah Pickles

a été évaluée par un jury composé des personnes suivantes:

Dr. Luis Rokeach, Président rapporteur

Dr. Christine Vande Velde, Directeur de recherché

Dr. Christopher Rose, Membre du jury

Dr. Daryl Bosco, Examinateur externe

Dr. Jean-Claude Labbé, Représentant du doyen

# Résumé

La sclérose latérale amyothrophique (SLA) est une maladie neurodégénérative charactérisée par la perte des neurones moteurs menant à la paralysie et à la mort. Environ 20% des cas familiaux de la SLA sont causés par des mutations de la superoxyde dismutase 1 (SOD1), conduisant vers un mauvais repliement de la protéine SOD1, ce qui a comme conséquence un gain de fonction toxique. Plusieurs anticorps spécifiques pour la forme mal repliée de la protéine ont été générés et utilisés comme agent thérapeutique dans des modèles précliniques. Comment le mauvais repliement de SOD1 provoque la perte sélective des neurones moteurs demeure non résolu. La morphologie, le bilan énergétique et le transport mitochondrial sont tous documentés dans les modèles de la SLA basés sur SOD1, la détérioration des mitochondries joue un rôle clé dans la dégénération des neurones moteurs. De plus, la protéine SOD1 mal repliée s'associe sélectivement sur la surface des mitochondries de la moelle épinière chez les modèles de rongeurs de la SLA. Notre hypothèse est que l'accumulation de la protéine SOD1 mal repliée sur les mitochondries pourrait nuire aux fonctions mitochondriales. À cette fin, nous avons développé un nouvel essai par cytométrie de flux afin d'isoler les mitochondries immunomarquées avec des anticorps spécifiques à la forme malrepliée de SOD1 tout en évaluant des aspects de la fonction mitochondriale. Cette méthode permettra de comparer les mitochondries portant la protéine SOD1 mal repliée à celles qui ne la portent pas. Nous avons utilisé un anticorps à conformation spécifique de SOD1, B8H10, pour démontrer que la protéine mal repliée SOD1 s'associe avec les mitochondries de la moelle épinière des rat $SOD1^{G93A}$ d'une manière dépendante du temps. Les mitochondries avec la protéine mal repliée SOD1 B8H10 associée à leur surface ($B8H10^{+}$) ont un volume et une

production excessive de superoxyde significativement plus grand, mais possèdent un potentiel transmembranaire comparable aux mitochondries B8H10$^{-}$. En outre, la présence de la protéine mal repliée SOD1 reconnue par B8H10 coïncide avec des niveaux plus élevés de la forme pro-apoptotique de Bcl-2. L'immunofluorescence de sections de moelle épinière du niveau lombaire avec l'anticorps spécifique à la conformation B8H10 et AMF7-63, un autre anticorps conformationnel spécifique de SOD1, démontre des motifs de localisations distincts. B8H10 a été trouvé principalement dans les neurones moteurs et dans plusieurs points lacrymaux dans tout le neuropile. Inversement, AMF7-63 a marqué les neurones moteurs ainsi qu'un réseau fibrillaire distinctif concentré dans la corne antérieure. Au niveau subcellulaire, SOD1 possèdant la conformation reconnu par AMF7-63 est aussi localisée sur la surface des mitochondries de la moelle épinière d'une manière dépendante du temps. Les mitochondries AMF7-63$^{+}$ ont une augmentation du volume comparé aux mitochondries B8H10$^{+}$ et à la sous-population non marquée. Cependant, elles produisent une quantité similaire de superoxyde. Ensemble, ces données suggèrent qu'il y a plusieurs types de protéines SOD1 mal repliées qui convergent vers les mitochondries et causent des dommages. De plus, différentes conformations de SOD1 apportent une toxicité variable vers les mitochondries. Les protéines SOD1 mal repliées réagissant à B8H10 et AMF7-63 sont présentes en agrégats dans les fractions mitochondriales, nous ne pouvons donc pas prendre en compte leurs différents effets sur le volume mitochondrial. Les anticorps conformationnels sont des outils précieux pour identifier et caractériser le continuum du mauvais repliement de SOD1 en ce qui concerne les caractéristiques biochimiques et la toxicité. Les informations présentes dans cette thèse seront utilisées pour déterminer le potentiel thérapeutique de ces anticorps.

**Mots-clés** : SLA, SOD1, SOD1 mal repliée, mitochondrie, cytométrie de flux.

# Abstract

Amyotrophic Lateral Sclerosis (ALS) is a neurodegenerative disorder characterized by the loss of motor neurons resulting in paralysis and death. Approximately 20% of familial ALS cases are caused by mutations in superoxide dismutase (*SOD1)*, which leads to misfolding of the SOD1 protein, resulting in a toxic gain of function. Several antibodies have been generated that are specific for the misfolded form of the protein, and have been used as therapeutics in pre-clinical models. How misfolded SOD1 provokes a selective loss of motor neurons remains unresolved. Mitochondrial morphology, bioenergetics and transport are all documented is SOD1-mediated ALS models, thus mitochondrial impairment plays a key role in motor neuron degeneration. Moreover, misfolded SOD1 selectively associates with the surface of spinal cord mitochondria in ALS rodent models. We hypothesize that the accumulation of misfolded SOD1 on mitochondria could impair mitochondrial function. To this end, we developed a novel flow cytometric assay to immunolabel isolated mitochondria with misfolded SOD1 antibodies while also evaluating aspects of mitochondrial function. This method will allow for a comparison of mitochondria bearing misfolded SOD1 to those without. We utilized the B8H10 conformation specific SOD1 antibody to demonstrate that misfolded SOD1 associates with $SOD1^{G93A}$ rat spinal cord mitochondria in a in a time dependent manner. Mitochondria with B8H10-reactive misfolded SOD1 associated with their surface ($B8H10^{+}$) have a significantly larger volume and produce excessive amounts of superoxide, but have a similar transmembrane potential compared to $B8H10^{-}$ mitochondria. In addition, the presence of B8H10-reactive misfolded SOD1 coincides with higher levels of the pro-apoptotic form of Bcl-2. Staining of lumbar spinal cord sections with both B8H10 and another conformation specific SOD1 antibody, AMF7-63, yielded distinct localization patterns. B8H10 was found predominantly in motor neurons and

numerous puncta throughout the neuropil. Conversely, AMF7-63 marked motor neurons as well as a distinctive fibrillar network that was concentrated in the anterior horn. At the subcellular level, AMF7-63-reactive misfolded SOD1 also localized to the mitochondrial surface of spinal cord mitochondria in a time-dependent manner. AMF7-63$^{+}$ mitochondria have an increased volume compared to B8H10$^{+}$ mitochondria and the unlabelled subpopulation. However, they produce similar amounts of superoxide. Together, these data suggest that there are multiple species of misfolded SOD1 that converge at the mitochondria to cause damage. Moreover, different SOD1 conformations may ellicit varying toxicities towards mitochondria. Both B8H10 and AMF7-63-reactive misfolded SOD1 are present in aggregates in mitochondrial fractions and can therefore not account for any different effects produced in terms of mitochondrial volume. Conformational antibodies are invaluable tools to identify and characterize the continuum of misfolded SOD1 species with regards to biochemical characteristics and toxicity. The information presented in this thesis will be used in determining the future therapeutic potential of these antibodies.

**Keywords** : ALS, SOD1, misfolded SOD1, mitochondria, flow cytometry

# Table of contents

# List of tables

# List of figures

## I. Introduction



## II. Chapter 2 : Immunodetection of outer membrane proteins by flow cytometry of isolated mitochondria



## III. Chapter 3: Mitochondrial damage revealed by immunoselection for ALS-linked misfolded SOD1.

# List of acronyms and abbreviations

3'UTR: Three prime untranslated region

AA: Antimycin A

AAV: Adeno-associated virus

ALS Bi: Amyotrophic Lateral Sclerosis with behavioral impairment

ALS/Ci: Amyotrophic Lateral Sclerosis with cognitive Impairment

ALS: Amyotrophic Lateral Sclerosis

APOA2: ApolipoproteinA-II

ASP: Antisense oligonucleotides

ATFS-1: Activating transcription factor associated with stress-1

ATP: Adenosine triphosphate

ATX2: Ataxin-2

Bcl-2: B cell lymphoma 2

BiP: Binding immunoglobulin protein

*C. elegans*: *Caenorhabditis elegans*

C9ORF72: Chromosome 9 open reading frame 72

CCCP: Carbonyl cyanide *m*-chlorophenyl hydrazone

CCS: Copper chaperone for superoxide dismutase

CFTR: Cystic fibrosis transmembrane conductance regulator

CHCHD10: Coiled-coil helix coiled-coil helix domain 10

CHOP: C/EBP homologous protein

CNS: Central nervous system

CREST or SS18L1: Synovial sarcoma translocation gene on chromosome 18-like component of neuron-specific nBAF chromatin remodeling complex

CyPH: Cyclophilin D

DCA: Dichloroacetate

DENN: Differentially expressed in normal neoplastic cells

Derlin-1: Degradation in endoplasmic reticulum protein

DNA: Deoxyribonucleic acid DNA

DRG: Dorsal root ganglia

Drp1: Dynamin-related protein 1

DSE2: Disease specific epitope

EDTA: Ethylenediaminetetraacetic acid

eIF2A: Eukaryotic translation initiation factor 2A

ER: Endoplasmic reticulum

ERAD: Endoplasmic-reticulum-associated protein degradation

Erv1: Essential for respiration and vegetative growth

ERα: Estrogen receptor alpha

ETC: Electron transport chain

FALS: Familial Amyotrophic Lateral Sclerosis

Fis1: Fission 1

FSC: Forward side scatter

FTD: Frontotemporal Dementia

FUS/TLS: Fused in Sarcoma/Translocated in Sarcoma

$G_4C_2$: GGGGCC

GEFs: Guanine Exchange Factors

GRP-78: 78 kDa glucose-related protein

Grx2: Dithiol glutaredoxin

hESC: Human embryonic stem cells

HIV-1: Human immunodeficiency virus 1

hnRNP: Heterogeneous nuclear ribonucleoproteins

IL-4: Interleukin 4

IMM: Inner mitochondrial membrane

IMS: Intermembrane space

iPSC: Induced pluripotent stem cell

JNK: c-Jun N-terminal kinases

KARS: Lysyl-tRNA synthetase

kDa: Kilo Dalton

LC3: Microtubule-associated protein 1A/1B-light chain 3

LC3-II: LC3-phosphatidylethanolamine conjugate (LC3-II)

MAMs: Mitochondria-associated membranes

MAP: Mitogen activated protein

MFI: Mean fluorescence intensity

Mfn1/2: Mitofusin 1/2

Mia40: Mitochondrial intermembrane space assembly 40

MIF: Macrophage migration inhibitory factor

MS758: Misfolded SOD1 clone 758

MSC: Mesenchymal stem cells

MTG: MitoTracker Green

mtDNA: mitochondrial DNA

MTS: Mitochondrial targeting sequence

NADPH: Nicotinamide adenine dinucleotide phosphate

NEFL: Neurofilament

NES: Nuclear export sequence

NF-κB: Nuclear factor-kappa B

NLS: Nuclear localization sequence

NMJ: Neuromuscular junction

NRF1: Nuclear respiratory factor-1

NSC: Neural stem cells

OBMPFD: Inclusion body myopathy with early-onset Paget disease and Frontotemporal dementia

OMM: Outer mitochondrial membrane

OMMAD: Outer mitochondrial membrane associated degradation

Opa1: Optic atrophy 1

PGC1-α: NAD-dependent protein deacetylase, or peroxisome proliferator-activated receptor gamma, coactivator 1 alpha

P: Post-natal day

SQSTM1: p62/Sequestosome 1

PERK: protein kinase RNA-like endoplasmic reticulum kinase

POAG: Primary open angle glaucoma

PTP1P15: Protein tyrosine phosphatase-interacting protein-51

QGSY: Gln-Gly-Ser-Tyr

RAN translation: Repeat associated non-ATG translation

RGG: Arg-Gly-Gly

RIP-1: Receptor interacting-1 protein

RNA: Ribonucleic acid

ROS: Reactive oxygen species

RRM: RNA recognition motifs

SALS: Sporadic Amyotrophic Lateral Sclerosis

SCA2: Spinocerebellar ataxia type 2

scFv: Secretable single-chain fragment variable

SDS: Sodium dodecyl sulfate

SEDI: SOD1 exposed dimer interface

shRNA: short hairpin RNA

SIRT3: Sirtuin 3

SNPH: Synaptaphilin

SOD1: Superoxide dismutase

T cells: T lymphocytes

TALEN: Transcription activator-like effector nucleases

TDP-43: Transactive response DNA binding protein 43

TMRM: Tetramethylrhodamine methyl ester

$UPR^{mt}$: Mitochondrial unfolded protein response

USOD: Unfolded SOD1

VAPB: Vesicle–associated membrane protein-associated protein B

VDAC1: Voltage dependent anion channel 1

VEGF: Vascular endothelial growth factor

*To my family*

# Acknowledgements

It is said that it takes a village to raise a child. In my experience it takes a whole research community to graduate a PhD candidate.

On that note, I would like to thank the whole CRCHUM, old and new. I am blown away by the creativity, expertise and generosity of everyone at this research center, especially the Neuroscience Axis. In particular, I would like the thank Nathalie Arbour, for all her support and advice.

To my current and former lab mates, Laurie Destroismaisons, Sarah Peyrard, Yousra Khalfalah, Sabrina Semmler, Guillaume Caron and Jade-Emmanuelle Deshaies, Karli McDonald, Anais Aulas and Stephanie Stabile, it has been has been a pleasure and honor working with you day in and day out. We have shared successes, setbacks, expertise, advice, cocktails, jokes and occasionally some science. I wish you all nothing but success for the future and have the utmost confidence you will all do great things. To the Mito-Team, Sabrina and honorary member Laurie, thank you for all your hard work, I know I could not have done it without you both, keep up the good fight. To Christine, I most wholeheartedly want to thank you for this opportunity and your continued support. You have not just been my supervisor, but also my mentor, career adviser and cheerleader. I sincerely enjoyed my time in your lab and hope to be half the scientist you are.

To my surrogate lab, the Parker Lab, current and past members, you are the best neighbours. We have shared a tiny office and now a lab space and I have enjoyed all the time spent with you all and wish you the best.

To my family, Mom, Dad and Grandma, thank you for always being there, thank you for your support, and thank all your for all your love. All those poster projects finally paid off! I love all so much and am so grateful for having you in my life. To my husband, Matthew, thank you for your love, patience, counsel, and calmness. I love you and am excited to begin this next chapter in our lives.

# 1. Introduction

## 1.1. Amyotrophic lateral sclerosis

Amyotrophic Lateral Sclerosis (ALS) was first described by Jean-Martin Charcot as a progressive paralysis of voluntary muscles ultimately leading to death [1]. Charcot classified these symptoms under the name of ALS with amyotrophic meaning atrophy of muscles, and lateral sclerosis referring to the hardening of tissue in the lateral part of the spinal cord. In North America, ALS is also called Lou Gehrig's disease, in honour of the New York Yankees player who died of this disease in 1941. In France, the disease is known as Charcot's disease, named after its founder, whereas in the United Kingdom and Australia it is commonly referred to simply as Motor Neuron Disease.

## 1.2. Epidemiology

ALS is a late onset neurodegenerative disorder. The mean age of onset is 61.8 ± 3.8 years [2]. The range of disease onset is quite broad, with symptoms beginning from twenty to ninety years old [3]. Juvenile and early adult onset are occasionally reported and associated with specific genetic lesions [4, 5]. ALS is relatively rare with an incidence of 1.8/100, 000 in North America [2]. The incidence in men is slightly higher than woman [6]. The prevalence of ALS disease is 3.4 per 100, 000 in North America [2]. These figures underscore the lifetime risk of ALS, which is 1 in 350 for men and 1 in 400 for women [7]. ALS is a relentless progressive disease resulting in the majority of patients expiring within three to four years of disease onset and only about 10% surviving ten years after onset [8].

Although clinically identical, ALS patients can be segregated into two groups, sporadic (SALS) and familial ALS (FALS) [9]. SALS is used to describe individuals that have no family history of ALS, which is contrasted with FALS which is used to refer to individuals who have a first or second degree relative with ALS [10]. Approximately 5 to 10% of ALS cases are classified as familial [11], leaving the vast majority due to sporadic and not fully defined etiologies.

While the cause(s) of SALS is largely undefined, it is postulated that symptoms can result from genetic susceptibility in combination with environmental factors and time [12]. Increased age and tobacco use are associated with increased incidence of ALS [12]. Other proposed risk factors are athleticism [13], pesticide exposure [14], and trauma [15], however, the validity of these risk factors remains to be confirmed. The complexity and cost of determining environmental risk factors of SALS make it a daunting task, and thus limit the available strategies to model SALS in a research setting.

Classically, ALS is considered a disease with a purely motor phenotype, however this view is gradually changing. It is now appreciated that many patients exhibit cognitive defects, and in fact, ALS overlaps significantly with Frontotemporal Dementia (FTD). Following Alzheimer's, FTD is the second most common form of dementia, and manifests as executive and language dysfunction with changes in behaviour and personality [16]. The prevalence of FTD is between 10 and 30 cases per 100,000 in people aged 45 to 60 years [17]. Approximately 50 % of ALS patients have a loss of function in neurological tests examining frontal lobe function. These patients are referred to as ALS with cognitive or behavioral impairment (ALS Ci/ALS Bi). Fifteen percent of ALS patients have a significant enough decline in frontal lobe function to be

officially diagnosed with FTD, and are classified as ALS-FTD [18]. ALS also clusters with certain neurodegenerative and neuropsychiatric diseases, for instance diagnosis of schizophrenia is higher in families with ALS, as well as rates of suicide [19]. Genetic susceptibility to neurological and neurophysiological factors may be at play for increasing risk in families with known ALS cases, however these factors are yet to be identified.

### 1.3. Clinical presentation

ALS is characterized by the degeneration of upper motor neurons in the cerebral cortex, and lower motor neurons in the brain stem and spinal cord [20]. Symptoms of lower motor neuron degeneration include muscle cramping and fasciculations (involuntary muscle contractions), muscle atrophy and corresponding weakness [20]. Symptoms caused by the loss of upper motor neurons include motor symptoms, such as uncoordinated and slow movement, spastic tone, as well as non-motor symptoms such as executive dysfunction [20]. Loss of upper motor neurons can also produce some Parkinson-like symptoms, including muscle rigidity and tremor [20].

In the majority of patients (65-75%), onset of disease begins in the limbs (spinal onset), usually unilateral [21]. About one-third of patients have a bulbar onset, where they experience speech and swallowing dysfunction first, characterized by flaccid or spastic dysarthria, dysphagia, hoarseness, tongue wasting, weakness and fasciculations [21]. Limb onset is associated with prolonged survival, as well as younger age at presentation of symptoms [20]. Conversely, bulbar onset, older age at presentation and early respiratory muscle involvement are linked to reduced survival time [21] Uniquely, sensory neurons, ocular motor neurons, and neurons in the Onuf's nucleus are preserved [22, 23] or only affected at late stages of disease [24]. Symptomatic members of the same family, with the same mutation can have variable times

of onset, symptom presentation, and rate of disease progression, highlighting that ALS is clinically heterogeneous [25].

### 1.4. ALS Genetics (Table 1)

#### 1.4.1. Superoxide Dismutase 1

In 1993, *SOD1* (superoxide dismutase 1), found on chromosome 21q22.22 was identified as the first gene to cause FALS [26]. This finding was surprising given that SOD1 had been known as an abundant detoxifying enzyme for years [27]. There are over 170 reported mutations in SOD1 that cause ALS ([28], ALSoD: http://alsod.iop.kcl.ac.uk/) **(Fig. 1)**. This is remarkable given that the entire gene encodes five exons and produces a protein of only 153 amino acids, even more surprising is that there are over 75 different amino acid mutations [29]. A major area of study in ALS research is determining what properties the SOD1 mutations have in common, and which of these are important for pathogenesis. Minor amino acid substitutions, such as G93A, (glycine to alanine) lead to disease, suggesting that almost any alteration in protein structure will result in ALS. The validity of some of the identified *SOD1* mutations as causative of ALS remains contentious [30]. ALS causative mutations in *SOD1*, are found in all five exons of SOD1, with no clear hotspots [31]. However, six mutations are reported at residue G93: A, C, D, R, S or V. Each mutation produces a variable phenotype with G93V being most aggressive, G93A with intermediate aggressiveness (2 to 3 years from diagnosis to death), G93S, C and D being least severe, and G93R having a variable phenotype [32]. The majority of SOD1 mutations (80%) are missense with only a few insertions and deletions [33]. In almost all ALS kindreds, mutations in *SOD1* are dominantly inherited with the exception of the D90A mutation, which is recessively inherited [34]. Mutations in *SOD1* constitute approximately 12

**Table 1:**
**Genes implicated in ALS**

| Gene | Protein Function | Inheritance | Diagnosis | Percentage (%) of cases | | References |
|---|---|---|---|---|---|---|
| | | | | FALS | SALS | |
| *SOD1* | Superoxide metabolism | AD, AR | ALS, PMA | 12 | 3 | Rosen et al., 1993 |
| *TARDP* | RNA metabolism | AD | ALS, ALS-FTD | 4 | 1 | Kabashi et al., 2008; Sreedharan et al.,2008 |
| *FUS* | RNA metabolism | AD, AR | ALS, ALS-FTD | 4 | 1 | Kwiatkowski et al., 2009; Vance et al., 2009 |
| *C9ORF72* | DENN protein, unknown function | AD | ALS, ALS-FTD, FTD | 40 | 7 | DeJesus-Hernandez et al., 2011; Renton et al., 2011 |
| *SQSTM1* | Ubiquitination, autophagy | AD | ALS, ALS-FTD | 1 | <1 | Fecto et al., 2011 |
| *VCP* | Proteasome | AD | ALS, ALS-FTD, FTD, IBMPFD | 1 | 1 | Johnson et al., 2010 |
| *OPTN* | Autophagy | AD, AR | ALS, POAG | <1 | <1 | Maruyama et al., 2010 |
| *PFN1* | Cytoskeletal dynamics | AD | ALS | <1 | <1 | Wu et al., 2012 |
| *UBQLNS* | Ubiquitination, autophagy | X-linked | ALS, ALS-FTD | <1 | <1 | Deng et al., 2011 |
| *VAPB* | Vesicular trafficking | AD | ALS, SMA | <1 | <1 | Nishimura et al., 2004 |
| *hnRNPA2B1/A1* | RNA metabolism | AD | ALS, IBMPFD, FTD | <1 | <1 | Kim et al., 2013 |

**Table 1: Genes implicated in ALS.** Adapted from Renton *et al*., 2014 [35] and Leblond *et al*., 2014 [10]. Values represent the percentage of ALS cases explained by each gene. AD, autosomal dominant; AR, autosomal recessive; XD, X-linked dominant; PMA, progressive muscular atrophy; IBMPFD, inclusion body myopathy with Paget's disease and frontotemporal dementia; POAG, primary open-angle glaucoma; SMA, spinal muscular atrophy; DENN, differentially expressed in normal and neoplasia.

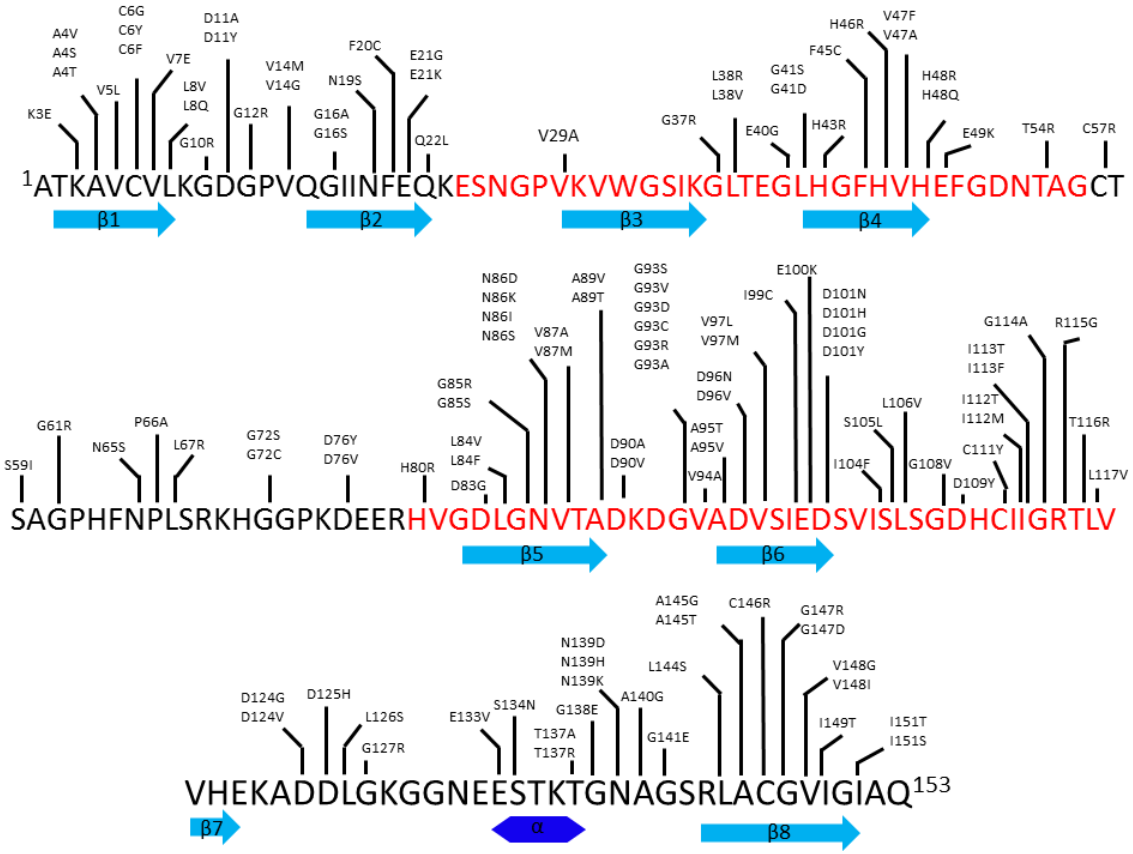


**Figure 1: ALS-causing SOD1 mutations**. Adapted from Fujisawa *et al*., 2012 [36]. Schematic depicting SOD1 mutations. Primary sequence for wild-type SOD1 is depicted. Color change denotes exons, exon 1, 3 and 5 (black) and 2 and 4 (red). Secondary structure displayed below, β strands (light blue arrows) and α helix (dark blue hexagon).

to 20% of FALS, and 1-2% of SALS cases [37]. Due to a founder effect, about 50% of North American ALS patients carry the A4V mutation [38]. The second most prevalent mutation in North America is I113T. In contrast, the H46R mutation is more prevalent in Japan, with about 40% of SOD1-FALS patients carrying this particular mutation [38]. The population of Scandinavia has a high prevalence of the recessively inherited D90A mutation [12].

Genotype-phenotype predictions in ALS are difficult to make as the clinical presentation is quite heterogeneous. Exceptions include the A4V mutation, which is characterized by a short survival period, typically one year after diagnosis [39]. The H46R, D90A, G27R and D110Y mutations usually display slow disease progression with patients surviving 10 to 15 years after diagnosis [38-41]. Patients with SOD1 mutations usually have a younger age of onset, predominance of lower motor neuron involvement (limb-onset), and a lack of cognitive or behavioural difficulties [25].

### 1.4.2. Trans active response DNA binding protein 43

Identification of ubiquitinated transactive response DNA binding protein 43 (TDP-43) in cytoplasmic inclusions within spinal cords of ALS and FTD patients [42] led shortly thereafter to the discovery of mutations in *TARDBP* as causative for ALS [43-45] and FTD [46]. Prior to its association with ALS, TDP-43 was identified as a transcriptional repressor of human immunodeficiency virus 1 (HIV-1) [47]. Forty-seven *TARDBP* mutations have been described [46]. ALS causing *TARDBP* mutations are inherited dominantly, and are mainly clustered in the prion like domain. They make up approximately 4% of FALS cases and 1% of SALS cases. Typically, FALS cases with TDP-43 mutations present with earlier age of onset, with symptoms usually starting in the upper extremities and a long disease course [20].

TDP-43 is a highly conserved, ubiquitously expressed protein of 414 amino acids [48]. TDP-43 has a predominantly nuclear localization, although it can shuttle between the nucleus and cytoplasm [49]. Structurally, TDP-43 contains two ribonucleic acid (RNA) recognition motifs (RRM), that can bind RNA and deoxyribonucleic acid (DNA), a C-terminal glycine-rich prion-like domain [50], an N-terminal nuclear localization sequence (NLS), and a nuclear export sequence (NES) located in RRM2 [51]. Recently, TDP-43's previously ignored N-terminus has garnered attention and is now considered important for TDP-43 aggregation [52-55].

TDP-43 is part of a family of proteins referred to as heterogeneous nuclear ribonucleoproteins (hnRNPs) that are involved in multiple stages of RNA processing. TDP-43 also binds DNA and is involved in transcription. TDP-43 functions in RNA splicing, regulating the splicing of cystic fibrosis transmembrane conductance regulator (*CFTR*) [56] and apolipoproteinA-II (*APOA2*) [57]. In addition, TDP-43 is involved in the generation of microRNA, RNA transport, translation and the formation of stress granules [49]. TDP-43 binds approximately 6000 mRNA transcripts in the brain and decreasing the level of TDP-43 expression affects the splicing and abundance of hundreds of RNAs [58]. Therefore the precise physiological role of TDP-43 in the central nervous system (CNS) is quite complex.

It is still unknown whether mutations in *TARDBP* result in disease by either a loss or a toxic gain of function, or even a combination of a nuclear loss of function and a cytoplasmic gain of function. In either case, TDP-43 levels are tightly regulated [59-61] via auto regulation by self-splicing and/decreased translation [58, 62].

### 1.4.3. Fused in Sarcoma/Translocated in Sarcoma

In 2009, mutations in the *FUS* gene, located on chromosome 16p11.2, were linked to ALS [63, 64]. The protein Fused in Sarcoma/Translocated in Sarcoma (FUS) was first investigated as an oncogene in liposarcoma [65]. The discovery of a second mRNA binding protein connected to ALS garnered much excitement, and confirmed the importance of mRNA processing in neurodegeneration.

FUS is a 526 amino acid protein. Structurally, it is composed of an N-terminal transcriptional activation domain, an RRM, three Arg-Gly-Gly (RGG1-3) repeat domains, a zinc-finger motif, a NES, and a C-terminal non-classical NLS [66, 67]. FUS also contains two predicted prion domains, in the N-terminal Gln-Gly-Ser-Tyr (QGSY) region and in the C-terminal RGG2 domain [50]. Under physiological conditions FUS is localized to the nucleus, although like TDP-43, it has the ability to shuttle between the nucleus and cytoplasm [68]. FUS functions in many cellular processes including DNA repair, transcriptional regulation, microRNA processing, splicing and stress response [67]. FUS, like TDP-43, also binds thousands of mRNA targets in the brain, and deletion of FUS leads to alterations in the splicing and abundance of hundreds of mRNAs [69]. Interestingly, the majority of binding targets of TDP-43 and FUS are distinct [69].

Of the approximately fifty reported dominantly inherited *FUS* mutations [25], the majority are missense, however deletions, insertions and mutations in the three prime untranslated region (3'UTR) are also documented [67]. Most FUS mutations are found in the zinc-finger motif, RGG2 and RGG3, and the NLS [67]. The others are in the QGSY-rich domain and RGG1 [67]. Mutations in FUS account for about 4% and 1% of FALS and SALS cases, respectively [25]. In addition to ALS, FUS mutations cause or increase the risk for essential

tremor and FTD [70-72]. Clinically, FUS mutations associate with a younger age of onset (less than 40 years old [25]), a bulbar presentation and shorter disease course. The P525L mutation has an extremely early onset, often in childhood, with an aggressive progression [73, 74]. Similar to TDP-43, whether *FUS* mutations cause ALS by a way of loss of function or gain of a toxic function remains an area of intense investigation.

### 1.4.4. Chromosome 9 open reading frame 72

In 2011, two groups independently identified a hexanucleotide (GGGGCC or $G_4C_2$) repeat expansion in the non-coding region of the chromosome 9 open reading frame 72 (*C9ORF72)* gene on chromosome 9p21 [35, 75]. This finding sparked considerable excitement in the field, as the *C9ORF72* expansion was responsible for over one third (~40%) of FALS cases, and about 7% of SALS cases [37], thereby constituting the most frequent cause of genetically inherited ALS. In addition, the *C9ORF72* expansion is the first intronic expansion linked to ALS [37]. The *C9ORF72* expansion is also associated with approximately 25% of familial FTD cases and 6% of sporadic FTD [76], again strengthening the premise that ALS and FTD constitute a disease spectrum.

Epidemiologically, the *C9ORF72* expansion is most prevalent in European populations and correlates with early onset, typically bulbar, cognitive and behavioural changes, as well as increased incidence of neuropsychiatric illness [11, 20]. Similar to other nucleotide repeat expansion disorders like Huntington's disease, ataxias, and myotonic dystrophy, the number of repeats is critical to pathogenesis [77]. Healthy people have between 2 to 30 hexanucleotide repeats in *C9ORF72*, whereas ALS patients have between 700 to 2400 repeats [20]. The number of repeats has been characterized in a number of tissues, and is larger in neuronal tissues than

in the blood [78, 79]. A firm correlation of expansion length with disease phenotype has not yet been established [80].

The function of chromosome 9 open reading frame 72 (C9ORF72) remains elusive. Unlike the other major FALS linked proteins, SOD1, TDP-43 or FUS, C9ORF72 was unknown before its association to ALS. Bioinformatic studies reveal homology to differentially expressed in normal neoplastic cells (DENN) domain proteins, which primarily function as Rab-Guanine Exchange Factors (GEFs) [81]. These proteins play a prominent role in membrane trafficking, including endocytosis and autophagocytosis [82]. C9ORF72 interacts with several Rabs (Rab1, Rab5, Rab9 and Rab11) as well as parts of the autophagic machinery, including ubiquilin-2 and microtubule-associated protein 1A/1B-light chain 3 (LC3)-positive vesicles [83], supporting its putative role in membrane trafficking.

Despite not knowing the precise physiological role of the C90RF72 gene product, there are three proposed mechanisms of pathogenicity. Collectively, decreased levels of the *C9ORF72* transcript in ALS patient lymphoblasts [75] and the finding that *Danio rerio* and *Caenorhabditis elegans* loss of function models show axonal degeneration of motor neurons and locomotor defects [84, 85], point towards haploinsufficency as a cause of disease. Conversely, gain-of-function models based on toxicity of RNA or dipeptide proteins generated by repeat associated non-ATG (RAN) translation are also suggested. In repeat diseases, translation can occur at various sites of the repeat, as opposed to the ATG initiation site, although the mechanisms are currently unclear, RNA structure likely plays a role in RAN-translation [86]. RNA foci are found in the brains and in induced pluripotent stem cell (iPSC)-differentiated neurons derived from patients with *C9ORF72* expansions [87, 88]. RNA foci may trap certain RNA-binding proteins, causing a loss in their respective functions [89]. RNA foci and other cellular defects

are reversed when iPSC-differentiated neurons are treated with antisense oligonucleotides (ASO) against the $G_4C_2$ expansion [87]. RAN generated di-peptides containing (antisense: Pro-Arg, Pro-Ala, Gly-Pro, and sense: Gly-Ala, Gly-Arg, Gly-Pro) cytoplasmic aggregates have also been detected in C9ORF72 patient brains [88, 90]. Recently, a study examined all three pathogenic hypotheses simultaneously. The Pro-Arg dipeptide, in particular, is extremely toxic to primary mouse cortical and motor neurons. Expression of the C9ORF72 expansion is also toxic to primary neurons, while knock-down of the C9ORF72 transcript had no effect on cell survival [91]. Interestingly, RNA and dipeptide related toxicity are linked, as the toxicity of Pro-Arg aggregates and the C9ORF72 expansion are synergistic [91]. The idea that these two mechanisms of toxicity may converge is in agreement with the finding that both RNA foci and dipeptide aggregates are present in post-mortem tissue of ALS patients [90].

### 1.4.5. Rare Variants

Reviews of ALS genetics are rapidly out-dated due to the high speed in which novel genes are discovered. Newly discovered genes include, *OPTN* [92], *VCP* [93], *UBQLN2* [94], *DAO* [95], *hnRNPA2B1/A1* [96], *CHCHD10* [96], *MATR3* [97] and *TBK1* [98], to name a few. These genes and their protein products will be instrumental in revealing novel pathways involved in ALS, although they are rare causes of ALS [37]. Several of these genes are causative for other diseases including FTD, primary open angle glaucoma (POAG), and inclusion body myopathy with early-onset Paget disease and frontotemporal dementia (IBMPFD).

### 1.4.6. *De novo* mutations

*De novo* mutations are the subject of intense research as of late and are linked to many neurological conditions, including autism [99]. *De novo* mutations are not inherited from parent to child, rather they occur through genetic copying error or during cell division [100]. *De novo* mutations of previously known ALS genes *SOD1* [101] , and *FUS* [102-106] are found SALS cases. Exome sequencing of ALS trios (affected patients, and non-affected parents) identifies a mutation in SS18L1 (Synovial sarcoma translocation gene on chromosome 18-like component of neuron-specific nBAF chromatin remodeling complex) or *CREST*, a gene encoding a calcium-regulated transcriptional activator [107]. While this constitutes an interesting finding that implicates chromatin remodelling as a novel pathway in ALS, the pathogenicity of all *de novo* mutations requires further validation [3].

### 1.4.7. Genetic risk factors

Twenty-three percent of SALS cases are proposed to be the result of a genetic defects [108]. Identified genetic modifiers include *PGRN*, *KIFAP3*, *EPHA4* and *UNC13A*, although they require further validation [3]. A yeast screen of potential modifiers of TDP-43 toxicity finds poly-(A)-binding protein (Pab1p)-binding protein (*PBP1)* as a potent enhancer of toxicity [109]. The human orthologue is Ataxin-2. Mutations in *ATX2* lead to a CAG expansion that causes Spinocerebellar ataxia type 2 (SCA2). ALS patients have a greater number *ATX2* CAG repeats than healthy controls, but less than SCA2 patients [109], thereby implicating intermediate *ATX2* repeat length as a potential genetic modifier of ALS.

### 1.5. Pathology

A pathological hallmark of ALS is the presence of intracellular protein inclusions in the soma and axons of neurons. Inclusions found in ALS patients can be placed into three categories, skein-like, bunina bodies, and hyaline, based on morphology and the identity of proteins found within the inclusion [110]. Skein-like and hyaline inclusions usually contain ubiquitin, while bunina bodies are ubiquitin negative [111]. Skein-like inclusions and bunina bodies are found in all ALS cases. SOD1, TDP-43 and FUS localize to skein-like inclusions while hyaline inclusions, containing SOD1, are mostly limited to SOD1-mediated FALS [112].

The protein inclusions found in the brain and spinal cords of ALS patients contains ubiquitinated proteins and the majority (~97%) of these inclusions are composed of TDP-43. Neurons from ALS patients have an accumulation of TDP-43 in the cytoplasm and a loss of nuclear TDP-43 [49]. TDP-43 present within inclusions is hyperphosphorylated, ubiquitinated and cleaved to generate C-terminal fragments [49] and recently found to be acetylated. TDP-43 inclusions are found in neurons and occasionally in glial cells in the brain (hippocampus and neocortex) as well as in spinal cord motor neurons [48]. That TDP-43 inclusions are found in the majority of ALS patients, even without TDP-43 mutations, suggest its involvement in almost all ALS cases. FUS immunoreactive cytoplasmic inclusions are present in less than 1% of ALS cases, and segregate with patients carrying mutations in *FUS* [63, 64]. TDP-43 inclusions are not found in these individuals, which may indicate that FUS acts downstream of TDP-43 [37] or by independent mechanisms. FUS inclusions are prominently cytoplasmic, although nuclear inclusions are also sometimes observed [113], and are present in neurons and less frequently in the glia [64]. Patients with the C9ORF72 expansion also have TDP-43 and sequestosome 1

(SQSTM1) or p62 inclusions. These inclusions are increasingly found in the frontal region, and in hippocampal neurons [114]. With the identification of new genes linked to ALS, their associated protein are increasingly studied for their presence in patient inclusions. Optineurin and ubiquilin-2 have been found within inclusions in some sporadic ALS cases [115]. The prevalence of these inclusions as well as their overlap with TDP-43 positive inclusions, or other protein inclusions remains to be fully characterized.

SOD1 inclusions are present in patients that carry a genetic defect in SOD1, which represents roughly 2% of all inclusions found in ALS patients [49]. SOD1 is found in both skein-like and hyaline inclusions [116, 117]. TDP-43 containing inclusions are not usually found in patients with SOD1-mediated ALS [118], implying SOD1-mediated FALS may be distinct. SOD1 positive inclusions are reported in some sporadic ALS patients [116, 117], however the validity of this finding is currently under debate [119]. The incorporation of SOD1 into inclusions implies that it is aggregated and likely misfolded. In the following sections mutant SOD1 folding/misfolding and aggregation will be discussed in depth. Furthermore, the literature confirming the prescence of misfolded SOD1 in ALS patient inclusions will examined.

## 1.6. The role of SOD1 in ALS pathogenesis

### 1.6.1. Function

SOD1 is a ubiquitously expressed, well conserved metalloenzyme that binds copper and zinc [120]. Its principle function is to convert superoxide into hydrogen peroxide [27].

$$2O_2^- + 2H^+ \rightarrow H_2O_2 + O_2$$

SOD1 is mainly cytosolic [121], although a small portion localizes to the intermembrane space (IMS) in mitochondria [122], where as in the cytosol, its main function is to convert the free

radical superoxide into hydrogen peroxide [27]. In addition to the cytosol and IMS, SOD1 is also reported to localize to the nucleus [123], peroxisomes [124], endoplasmic reticulum (ER) and Golgi apparatus [125]. SOD1 is an abundant protein, especially in the CNS where it constitutes 1-2% of total soluble protein [126]. SOD1 belongs to a family of three proteins (SOD1-3) with the same function. SOD2, is found in the mitochondrial matrix, and unlike SOD1, binds manganese instead of copper and zinc [127]. SOD3 is found in the extracellular matrix and like SOD1, also requires copper and zinc for its enzymatic activity [127].

SOD1 mutations were initially suspected as being causative for ALS due to a loss of function resulting in the accumulation of reactive oxygen species (ROS), however, the observation that many SOD1 mutants retain their dismutase activity at levels comparable to wild-type SOD1 refuted this claim [128]. Furthermore, SOD1 null mice do not develop symptoms resembling ALS [129]. In contrast, transgenic animals over-expressing mutant human SOD1 die early from a progressive paralytic disease [130], providing strong evidence that SOD1 mutations cause a toxic gain of function in ALS. Although SOD1 null mice do not develop ALS, and live to a reasonably old age, they are hypersensitive to axotomy [129] and cerebral ischemia [131] indicating that they have abnormal phenotypes associated with both motor neurons and neurons in general. A partial loss of SOD1 function may be involved in SOD1-linked ALS [29].

Recently, some non-canonical functions for SOD1 have come to light. Mutant SOD1 binds the 3'UTR of vascular endothelial growth factor (VEGF), a neurotrophic factor for motor neurons, causing destabilization of the transcript and loss of VEGF expression [132]. Similarly, mutant SOD1 regulates low molecular weight neurofilament (*NEFL*) mRNA through its 3' UTR resulting in a loss of protein expression in neuronal cells [133]. Correction of the SOD1 mutation

in iPSC-derived motor neurons using transcription activator-like effector nucleases (TALEN)-mediated homologous recombination rescued the loss of NFL expression [134]. SOD1 is also reported to act as a transcription factor. In response to high levels of ROS, SOD1 translocates to the nucleus to increases the expression of genes related to oxidative stress resistance and cellular repair [135]. High levels of respiration causing production of oxygen and glucose, lead to SOD1-mediated stabilization of a group of proteins that downstream result in the repression of respiration [136]. These non-traditional functions of SOD1 clearly indicate there is much more to be discovered about the signalling functions of this molecule, as it regulates gene expression at multiple levels. Furthermore, how SOD1 is transcriptionally regulated remains to be fully explored, but uncovering the factors that modulate its expression could be vital for therapeutics aimed at changing SOD1 expression.

### 1.6.2. Structure, folding and post-translational modifications

Several post-translational modifications are required to form the mature SOD1 protein. Following translation, SOD1 is loaded with zinc by an unidentified mechanism, then copper by the copper chaperone for superoxide dismutase (CCS), which also facilitates the formation of an intramolecular disulfide bond between Cys57 and Cys146, and finally SOD1 forms a homodimer [137]. SOD1 can acquire copper by a CCS-independent pathway, involving reduced glutathione [138]. CCS may also regulate SOD1 activity in response to oxidative stress [139]. Zinc binding structurally organizes the immature polypeptide, while copper binding is responsible for SOD1 activity [140, 141].

Structurally, the SOD1 homodimer is arranged as an eight-stranded Greek key beta barrel, with an immunoglobulin-like fold [142]. SOD1 has two loops: the zinc-loop (residues

49-83) located between β-strands 4 and 5 and the electrostatic loop (residues 121-142) which is formed between β-strands 7 and 8. Both loops contribute to the active site, where the superoxide anion interacts with copper to be reduced [142].

SOD1 is an unusually stable protein capable of resisting denaturation at high heat (SOD1 has a melting temperature of approximately 92°C), whereas most proteins unfold between 40-60°C [143]. This stability is reflected in the ability of the mature SOD1 protein to withstand high concentrations of denaturants, 6M guanidine chloride and 10M urea, detergents, 4% sodium dodecyl sulfate (SDS), and treatment with 1 mg/mL proteinase K [144-147]. The stability of SOD1 is attributed to its metal occupancy, disulfide bond formation, and dimerization, which are all interdependent [110, 148]. Absence of metals will promote dissolution of the disulfide bond [149]. SOD1 without metals or an intact disulfide bond cannot form dimers [148, 150 {Arnesano, 2004 #703, 151], whereas presence of the metals and disulfide bond will promote dimerization [152].

The high stability of wild-type SOD1 is rather surprising given that almost any mutation leads to disease. Indeed, an intense area of investigation is to determine similarities and differences in the biochemical properties amongst the various mutant proteins, although it remains possible that there is no one common property [141]. Several mutants have a decreased thermostability, approximately 5-10°C lower than wild-type SOD1, comparable to apo SOD1 [153]. However, a number of mutants also have stabilities that are similar to wild-type SOD1 [154]. Furthermore, most mutants have wild-type-like activities [155, 156] and with the exception of the metal binding mutants, there are very few structural differences compared to wild-type SOD1 [157-160]. These findings suggests that the majority of mutant SOD1 is well folded. Examination of SOD1 folding in a cell-free rabbit reticulocyte lysate assay reveals

SOD1 mutants are unable to fold as efficiently as wild-type SOD1, although many mutants were able to eventually reach a well-folded state, as determined by resistance to proteinase k digestion [141]. This delay in folding kinetics leads to the accumulation of a pool of immature/intermediate SOD1 forms, which have decreased stability and may negatively affect a diverse array of cellular functions [141].

SOD1 lacking its complement of metals has a drastically reduced stability, as evidenced by a decreased melting temperature 50 to 59°C [161]. SOD1 with its proper complement of metals is referred to as holo, whereas SOD1 in the demetalated state is referred to as apo. Probing the metalation and activity status of recombinant mutant SOD1 proteins demonstrates that several mutants do not contain their full complement of metals and some lack dismutase activity, suggesting that copper is missing from the active site [156]. Soluble wild-type and mutant (G37R, H46R/H48Q and G93A) SOD1 from the brains and spinal cords of transgenic mice contain the proper complement of metals, except for H46R/H48Q, which lacks copper binding and has reduced zinc binding [162]. However, insoluble SOD1 had a low occupancy of metals [162]. Due to the high affinity of SOD1 for copper and zinc, the authors propose loss of metals was not probable *in vivo* and the origin of demetalated insoluble SOD1 originates from immature peptides which have yet to incorporate metals [162]. In support of this proposal, in-cell NMR experiments document that a portion of mutant SOD1 protein exists in an unstructured state incapable of zinc binding. Furthermore, toxic oligomers likely originate from this precursor [163]. Zinc can also aberrantly bind immature forms of SOD1 (apo SOD1 dimers, monomers and reduced monomers) at both the zinc and copper sites thereby leading to a pool of misfolded SOD1 [164]. Expression of CCS decreases the pool of unstructured SOD1 species suggesting

that in addition to its function in copper loading, it may also act as a chaperone [163] thereby decreasing levels of immature SOD1 [163].

Reduction of the disulfide bond in apo SOD1 substantially decreases the melting temperature from 52 °C [154] to 43°C [153], indicating the disulfide bond provides additional stability for SOD1 structure. Mutant SOD1 is more prone to reduction than wild-type SOD1 [149] and reduced SOD1 is destabilized compared to holo SOD1 [165].

As an alternative to the theory that SOD1 mutations retard protein folding kinetics leading to increased levels of unstable immature precursors, ALS mutations may predispose the protein to misfold in response to stress that the wild-type protein would normally withstand. One such stress is oxidation. SOD1 is exposed to ROS as part of its normal function and oxidative stress has been linked to ALS [166]. Increased levels of oxidative stress are documented in tissues from ALS patients [167, 168] as well as SOD1 mouse models [169]. Oxidation of SOD1 mutants causes destabilization of the protein mediated by oxidation of metal binding histidine residues [170]. Furthermore, oxidation leads to release of bound metals and exposure of hydrophobic residues, which is further enhanced when SOD1 is mutated [171]. Oxidation of either wild-type or mutant SOD1 leads to monomerization, followed by protein destabilization [172]. Treatment of SOD1 with denaturants causes unfolding with metal depleted monomers as an intermediate, thus confirming the plausibility of this precursor as an intermediate in SOD1 unfolding [173, 174].

#### 1.6.2.1 SOD1 aggregation

Immature forms of SOD1 caused by the loss of one or more post-translational modifications, or genetic mutation, destabilizes the protein structure and likely underlies the

formation of aggregates [110]. Indeed, mutant SOD1 forms inclusions within spinal cord motor neurons in both FALS patients with SOD1 mutations and SOD1 rodent animal models [175-179]. One such subset of aggregates have a fibrillar appearance and are composed of β-sheets [180]. Interestingly, fibrils have the ability to self-regulate, once a fibril is formed it has the ability to nucleate or seed fibrils from properly folded protein [181, 182].

Fibrils are found in numerous neurodegenerative diseases including Parkinson's, Huntington's and Alzheimer's disease [182]. The presence of fibrils in SOD1-mutated FALS remains debated, as reports of fibrils in spinal cords are conflicting [119, 183]. In ALS rodent models, SOD1 inclusions stain positive for Thioflavin T, a molecule that upon binding to β-sheets exhibits enhanced fluorescence [184]. Based on Thioflavin T fluorescence, mutant and apo SOD1 readily form fibrils *in vitro* [152, 185]. Moreover, structural studies demonstrate ALS-linked mutations and apo SOD1 form fibrils [158, 186, 187]. *In silico* analysis of the SOD1 sequence reveals four regions predicted to fibrillize [188]. Two C-terminal segments of SOD1, residues 101-107 and 147-153, accelerate fibril formation of apo wild-type and mutant SOD1 *in vitro* [188]. It has been proposed that metal deficient and disulfide reduced SOD1 would only be required for the nucleation of fibril formation, followed by incorporation of more stable forms of SOD1, due to the self-seeding property of fibrils [110]. Thus, implying an initially small pool of unstructured SOD1 could spontaneously increase over time. Treatment of apo reduced wild-type SOD1 aggregates with proteases and subsequent analysis by mass spectrometry reveals three protease resistant peptides making up the core of the SOD1 aggregates. SOD1 mutants use some of these same regions, but have distinct cores. Distinct aggregate structures would affect the solubility and possibly toxic potentcy [189].

Whether or not SOD1 aggregates are toxic and by what mechanisms remains undefined. SOD1 monomers [190], oligomers [191] and aggregates [192] have all been proposed to mediate toxicity. Similarly, soluble SOD1 versus insoluble SOD1 is suggested to underlie SOD1-linked toxicity [193]. Regardless of what the toxic species is *in vivo*, there is consensus that misfolding of SOD1 protein is the initiating event.

#### 1.6.2.2. Additional post-translational modifications

In addition to the post-translation modification required for the proper folding of SOD1, several other modifications have been described that can modify SOD1 aggregation propensity or SOD1 protein levels. The maturation of SOD1 consists of removal of the initiating methionine and acetylation of the N-terminal residue [194]. A recent study suggest that acetylsalicylic acid acetylates several lysine residues in mutant apo SOD1 which prevents its association into amyloid like fibrils [195]. Whether SOD1 is acetylated within cell culture, animal models, or in ALS patients remained unknown. In response to increased oxidative stress, wild-type and mutant SOD1 are glutathionylated at Cys111, which causes destabilization of the SOD1 dimer [196, 197]. Phosphorylation at Thr2 and Thr58 or Ser59 in SOD1 is reported in human erythrocytes [197]. SUMO (small ubiquitin-like modifier) proteins are a family of protein that are post-translationally and reversibly attached to proteins to modify their transport, regulation, stability, and response to stress [198]. SOD1 is sumoylated at Lys9 and Lys75 by both SUMO1 and SUMO2/3 [199, 200]. Sumoylation increases SOD1 stability and the formation of aggregates [199, 200]. Taken together, these findings provide evidence that SOD1 is post-translationally regulated in multiple ways, however the relevance of many of these modifications in ALS pathogenesis remains uninvestigated.

Insoluble SOD1 from the spinal cords of symptomatic $SOD1^{G93A}$ mice was found to be mono and oligoubiquitinated [201]. Ubiquitination was observed in the spinal cord but not hippocampus, and is confined to Lys48, suggesting proteasome-mediated degradation of SOD1 [201]. Several E3 ubiquitin ligases are reported to ubiquitinate SOD1 for degradation, including E6-AP [202], Dorfin [203], neuronal homologous to E6AP carboxyl terminus (HECT)-type ubiquitin-protein isopeptide ligase (NEDL1) [204], and the ER-associated E3 ubiquitin ligase Gp78 [205]. Several of these E3 ubiquitin ligases, such as E6-AP and Dorfin, are found within mutant-SOD1 inclusions [202, 203].

### 1.6.3. SOD1 animal models

The first transgenic mouse model of ALS ($SOD1^{G93A}$) was developed by expressing SOD1 mini-genes, containing human genomic fragments driven by the endogenous SOD1 promoter and regulatory regions. This mouse develops a progressive and fatal paralysis that closely resembles ALS [130]. Many other transgenic models over-expressing human SOD1 missense mutations have been developed, as well as three C-terminal truncation mutations and several experimental mutations [130, 177, 179, 184, 206-215] (**Table 2**). The $SOD1^{G93A}$ mouse is the most extensively studied, and for the time being is the gold-standard for testing therapeutic agents [25]. The $SOD1^{G37R}$ and $SOD1^{G85R}$ models are the second most frequently used mouse models. In addition two rat models exist, expressing the G93A [216] and H46R [217] mutation in human *SOD1* (**Table 3**).

**Table 2**
**Transgenic SOD1 mouse models**

| Mutation | Disease onset (months) | Reference |
|---|---|---|
| A4V a | 8 | Deng et al., 2006 |
| G37R | 4 to 6 | Wong et al., 1995 |
| G37R b * | 11 to 13 | Boillee et al., 2006 |
| H46R | 5 | Chang-Hong et al., 2005 |
| H46R/H48Q | 4 to 6 | Wang et al., 2002 |
| H46R/H48Q/H63G/H120G | 8 to 12 | Wang et al., 2003 |
| L84V | 5 to 6 | Tobisawa et al., 2003 |
| G85R | 8 to 14 | Brujin et al., 1997 |
| G86R c | 3 to 4 | Ripps et al., 1996 |
| D90A | 12 | Jonsonn et al., 2006 |
| G93A | 3 to 4 | Gurney et al., 1994 |
| L126X | 7 to 9 | Wang et al., 2005 |
| L126X | 11 | Deng et al., 2006 |
| L126delTT | 15 | Watanabe et al., 2005 |
| G127X d | 8 | Jonsson et al., 2004 |
| Wild-type * | non symptomatic | Tu et al., 1998 |

**Table 2: Transgenic SOD1 mouse models.** Adapted from Turner and Talbot 2008 [206]. . Double transgenic for $SOD1^{WT}$ (a). SOD1 gene floxed (b). Mouse gene (c). Homozygous for mutation (d). Animals used in this thesis (*).

**Table 3**
**Transgenic SOD1 rat models**

| Mutation | Disease onset (months) | Reference |
|---|---|---|
| G93A * | 3.5 to 4 | Howland et al., 2002 |
| H46R | 4 to 5 | Nagai et al., 2001 |
| Wild-type * | non-symptomatic | Chan et al., 1998 |

**Table 3: Transgenic SOD1 rats models.** Adapted from Turner and Talbot 2008 [206].

Animals used in this thesis (*).

Characterization of SOD1$^{G93A}$ mice reveals disease onset at 3 months (higher levels of transgene expression lead to earlier disease onset) with weakness, and weight loss due to muscle atrophy that progresses to paralysis and then death at about 4 months [130] (**Fig. 2**). Denervation of neuromuscular junctions begins around 47 days, with axon loss at 80 days and motor neuron loss at 100 days [218, 219]. Other prominent pathological features include fragmentation of the Golgi apparatus [219], mitochondrial morphological alterations [220, 221], SOD1 positive aggregates [176], gliosis of astrocytes and microglia [222]. Although the SOD1$^{G93A}$ rats have not been characterized as extensively as the mouse modeld, they share many common features including an age dependent muscle atrophy progressing to paralysis (~3.5-4 months), motor neuron loss and gliosis [216, 223, 224] (**Figure 3**). Characterization of disease progression in the SOD1$^{G93A}$ rat model is challenging as there exist colony differences [224, 225]. Therefore careful reporting of disease onset, surivial and major pathological hallmarks are required for each colony.

Small SOD1 animal models exist, however they receive far less attention than rodent models. Expression of mutant SOD1 in *Danio Rerio* causes dose dependent axonopathy, motor neuron loss, muscle atrophy, and these fish have less endurance and decreased survival, compared to wild-type controls [226, 227]. Expression of mutant or wild-type SOD1 in *Drosophila* motor neurons decreases the flies' ability to climb, causes defects in neural electrophysiology, accumulation of SOD1 in neurons, and induces stress in surrounding glial cells, but does not lead to motor neuron loss or death [228]. The lack of specificity of phenotype between mutant and wild-type could indicate toxicity of wild-type SOD1. *C. elegans* models of ALS expressing mutant SOD1 selectively in neurons or muscle demonstrate modest locomotion defects and aggregation of SOD1, but normal survival [229, 230].

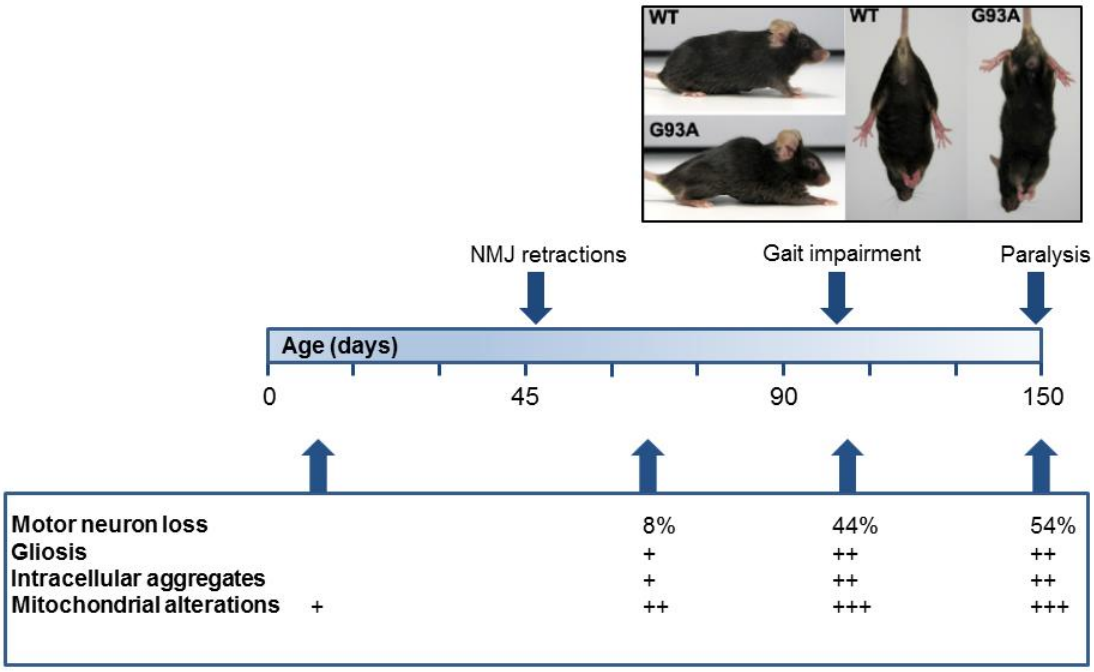


**Figure 2: Timeline of selected histopathological and clinical changes relevant to disease in SOD1$^{G93A}$ mice.** Adapted from Bendotti and Carri 2004 [231], Fischer *et al*., 2004 [218] and Turner and Talbot *et al*., 2008 [206]. Mitochondrial morphology and structure are altered prior to motor neuron loss and other hallmarks of disease.

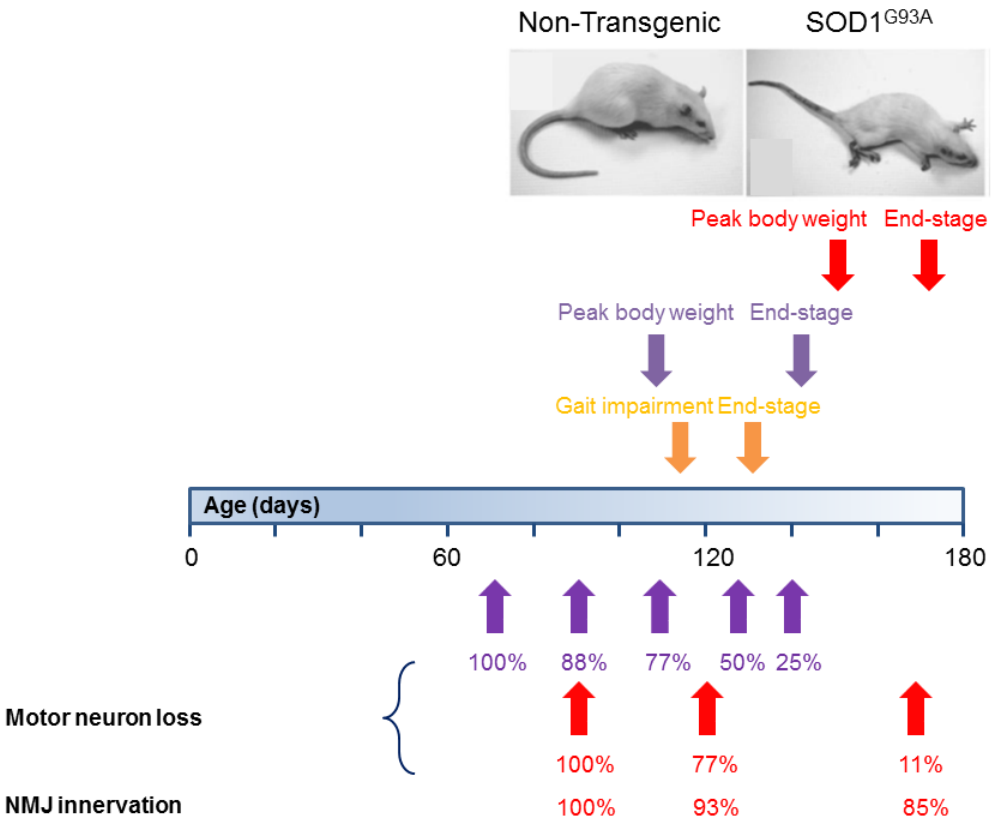


**Figure 3: Timeline of selected histopathological and clinical changes relevant to disease in SOD1$^{G93A}$ rats**. Data pooled from Howland *et al*., 2002, [216] (orange), Matsumoto *et al*., 2006 [223] (purple) and Thompsen *et al*., 2014 [224] (red). Peak body weight: the point at which rats begin to loose weight due to muscle atrophy; Gait-impairment: the point at which animals being to limp; End-stage: the point at which the rat cannot right itself; NMJ: Neuromuscular junction.

### 1.6.4. Misfolded SOD1

Mutant SOD1 adopts a similar structure to wild-type SOD1 [157-160], however a portion of mutant SOD1 adopt a non-native "misfolded" conformation, as demonstrated by loss of Proteinase K resistance [232, 233{Vande Velde, 2008 #2, 234]. It is increasingly appreciated that SOD1-mediated disease pathogenesis is a result of misfolded SOD1. In an effort to specifically study misfolded SOD1, several groups have developed conformation specific antibodies that selectively target certain conformations of SOD1 (reviewed in [33, 235]). These antibodies were generated by immunizing animals with either apo $SOD1^{G93A}$ protein(A5C3, B8H10, C4F6 and D3H5) or SOD1 peptides consisting of residues that are normally buried within the folded protein, Disease specific epitope (DSE2 3H1 and DSE1a 10C12), SOD1 exposed dimer interface (SEDI), unfolded SOD1 (USOD), mutant SOD1 specific antibody clone (MS758), AJ10 and a series of polyclonal peptide antibodies produced by Forsberg and colleagues (**Fig. 3**). Collectively, these antibodies recognize epitopes only available when SOD1 adopts a non-native conformation. These tools have allowed the field to probe the spatial and temporal localization of misfolded SOD1 as well as examine mechanisms to modulate its abundance. While initially designed as therapeutics, their potential is just now emerging. Hopefully these reagents will allow the field to answer why motor neurons selectively degenerate in SOD1-mediated FALS and in SALS as a whole, and by what mechanisms.

#### 1.6.4.1. Misfolded SOD1 in SOD1-mediated FALS

Misfolded SOD1 antibodies SEDI, USOD, C4F6, AJ10, DSE2 and DSE1a label inclusions, mostly hyaline and skein-like, in SOD1-mediated FALS patient spinal cords, but not controls [119, 236-239] . The polyclonal peptide antibodies made by Forsberg and colleagues detect misfolded SOD1-immunoreactive inclusions in some FALS patients, and surprisingly in two patients with another motor neuron disease, spinal bulbar muscular atrophy (SBMA) [240]. Despite some reactivity of the SOD1 peptide antibodies in controls, the misfolded SOD1 conformational antibodies are specific for SOD1 caused FALS and confirm that non-native misfolded SOD1accumulates in spinal cord of patients.

The SEDI antibody preferential labels neurons within the ventral horn, as well as motor neuron axons, and axonal processes in the spinal cords of several ALS mouse models, but not the dorsal spinal cord [241]. In agreement, the C4F6 antibody preferentially labels the ventral spinal cord of $SOD1^{G93A}$ mice [236]. In contrast, the AJ10 antibody labels motor neurons in the ventral spinal cord and sensory neurons of the dorsal root ganglia in $SOD1^{G93A}$ mice [241]. This group also found extensive degeneration of dorsal sensory neurons, which has not been widely reported in this model [242], and previously reported no AJ10 labelling in the dorsal spinal cord, thereby casting some confusion on whether misfolded SOD1 is truly found in sensory neurons [239]. Misfolded SOD1 as detected by the D3H5 and AJ10 antibodies is found in neurons of the cortex [224, 239, 243].

**Table 4**

**Misfolded SOD1 specific antibodies**

| Antibody | Epitope | Mitochondrial Localization | Reactive for FALS tissue | | Reactive for SALS tissue | Therapeutic | References |
|---|---|---|---|---|---|---|---|
| | | | SOD1 | non-SOD1 | | | |
| A5C3 | Exon 4 | + | nd | nd | nd | - | Gros-Louis et al., 2010; Vande Velde et al., 2011; Sexena et al., 2014 |
| B8H10 | Exon 3 | + | nd | nd | nd | nd | Gros-Louis et al., 2010; Ezzi et al., 2010; Parone et al., 2013; Patel et al., 2014; Patel et al., 2015; Isrealson et al., 2015 |
| C4F6 | Exon 4 | - | + | nd | + | nd | Urushitani et al., 2006; Bosco et al., 2010; Prudencio et al., 2011; Brotherton et al., 2012; Ayers et al., 2014; Brown et al., 2014; Rotunno et al., 2014; Xu et al., 2015; Redler et al., 2014 |
| D3H5 | Exon 2 | nd | nd | nd | nd | + | Gros-Louis et al., 2010; Patel et al., 2014; Saxena et al., 2014 |
| DSE2 3H1 & DSE1a 10C12 | residues 125-142 | + | + | + | + | nd | Vande Velde et al., 2008; Isrealson et al., 2010; Grad et al., 2011; Pokrishevsky et al., 2012; Grad et al., 2014; |
| SEDI | residues 143-151 | + | + | nd | - | + | Rakhit et al., 2007; Liu et al., 2009, 2012; Kerman et al., 2010; Prudencio et al., 2011; Mulligan et al., 2012 |
| USOD | residues 42-48 | nd | + | nd | - | nd | Kerman et al., 2010; Mulligan et al., 2012 |
| MS758 | residues 6-16 | nd | nd | nd | nd | nd | Fujisawa et al, 2012 |
| peptides | residues 4-20, 57-72, 131-153 | nd | + | nd | + | nd | Forsberg et al., 2010 |
| AJ10 | residues 29-57 | + | + | nd | - | nd | Sabado et al., 2013; Sabado et al., 2014 |

**Table 4: Misfolded SOD1 specific antibodies.** Adapted from Pickles *et al*., 2012 and Rotunno and Bosco, 2014 [33]. Not determined (nd); positive results (+); negative result (-).

The SEDI antibody labels both neurons and occasionally astrocytes in SOD1 mouse models [241], whereas the D3H5 predominately labels motor neurons, with occasional labelling in astrocytes and microglia at advanced age [243]. Glial cells were not significantly labelled with the misfolded SOD1 specific antibody AJ10 either [239]. A systematic evaluation of misfolded SOD1 accumulation in glial cells has not been done for any misfolded SOD1 specific antibodies. Therefore, the question of whether misfolded SOD1 expression in glia contributes to non-cell autonomous toxicity remains open.

#### 1.6.4.2. Misfolded SOD1-linked toxicity

The C4F6 antibody recognizes both a sequence specific epitope (G93A mutation) when denatured and a conformational epitope of mutant SOD1 and wild-type SOD1 oxidized at Cys 111, in native conditions [244]. Application of recombinant mutant SOD1, but not wild-type SOD1, significantly inhibit anterograde axonal transport in isolated squid axoplasm [244]. Hydrogen peroxide oxidized wild-type SOD1 recapitulated the defects seen by mutant SOD1, indicating that mutant and misfolded wild-type SOD1 share the ability to inhibit vesicle transport [244]. This same assay was employed in another study revealing that SOD1 mutants inhibit anterograde transport of vesicles through the p38 (mitogen activated protein) MAP kinase pathway [244, 245]. Two groups have reported the epitope to which the C4F6 antibody binds. Through mutagenesis and structural alignment, the Borchelt group found that the C4F6 epitope minimally contains residues 90-93, which are located in the beta-turn of the loop between beta sheets 5 and 6 [246]. The Bosco group, through chemical cross-linking, mass spectrometry and mutagenesis, identify residues 92-96 as critical for binding by the C4F6 antibody [247]. Exposure of this epitope is modulated by the zinc binding and electrostatic

loops, as removal of the loops greatly increases C4F6 binding [247]. Exposure of the C4F6 epitope correlates with SOD1 toxicity to microglia [247]. Thus, C4F6-reactive misfolded SOD1 is linked to both defective axonal transport and non-cell autonomous toxicity.

The SEDI and B8H10 antibodies identify misfolded SOD1 in microsomal fractions from SOD1 mouse models [248, 249], thereby potentially linking misfolded SOD1 to the endoplasmic reticulum. A5C3-reactive misfolded SOD1 and ER marker binding immunoglobulin protein (BiP) also known as 78 kDa glucose-related protein (GRP-78) co-localize in motor neurons from $SOD1^{G93A}$ mice, placing misfolded SOD1 at the ER [250].

Interestingly, misfolded SOD1 levels (as detected by A5C3 and/or D3H5) increase with age paralleling levels of the endoplasmic reticulum (ER) stress response protein, BiP in $SOD1^{G93A}$ mouse motor neurons. Treatment with ER-stress inducing drugs thapsigargin and tunicamycin both increase levels of misfolded SOD1 [250]. In contrast treatment with salubrinal, which inhibits eukaryotic translation initiation factor 2A (eIF2A) phosphatases and attenuates ER-stress, decreases the levels of misfolded SOD1 and delays disease progression and the appearance of other disease markers [251]. Strengthening the connection between misfolded SOD1 and the ER, 124 of 132 SOD1 mutants bind to the ER protein Derlin-1 (degradation in endoplasmic reticulum protein), via residues 6-16. Immunization of rats with a peptide containing the Derlin-1 interacting domain produced the misfolded SOD1-specific antibody clone 78 (MS785). MS785 recognizes almost all SOD1-Derlin-1 interacting mutants. Derlin mediates an ER stress response to regulate cellular processes when zinc levels are low [252].

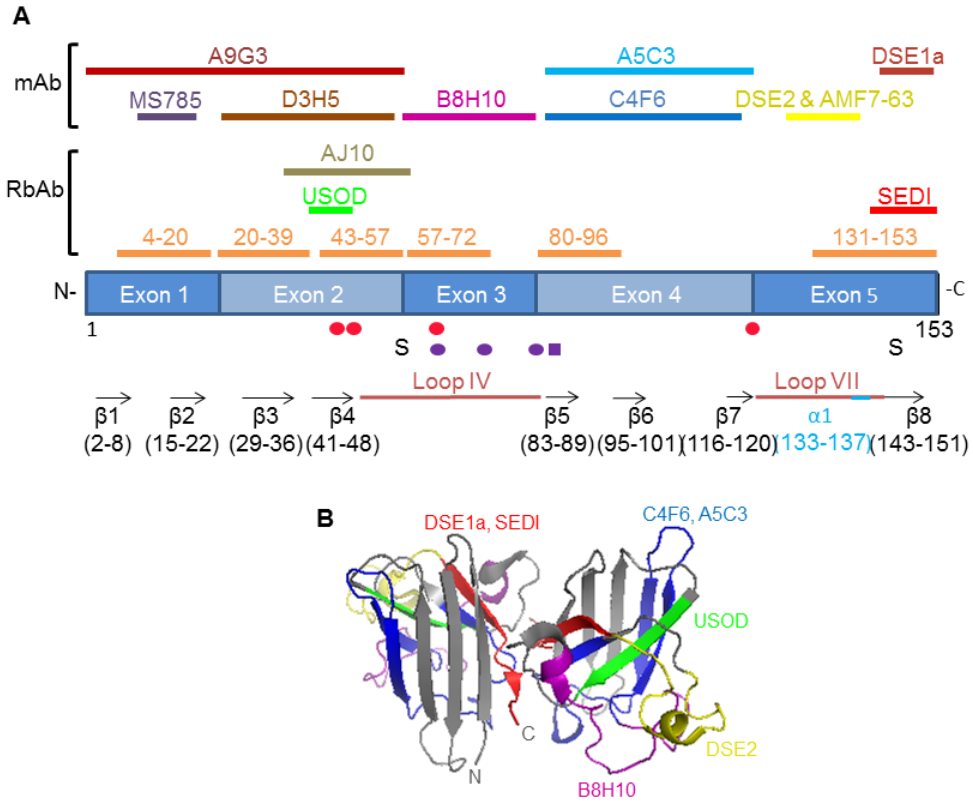


**Figure 4: Misfolded SOD1 specific antibodies.** Adapted from Pickles *et al*., 2012 [235]. A) Epitopes recognized by misfolded SOD1 antibodies mapped onto the SOD1 structure. Structural features are as indicated: β-strand (black), loops (pink), α helix (blue), disulfide bonds between Cys57 and Cys146 (S), copper-binding residues His46, His48, His63 His120 (red circles) and zinc-binding residues His63, His71, His80 and Asp83 (His, purple circles and Asp, purple square). B) Three dimensional reconstruction of SOD1 homodimer (PBD: 2C9V) showing the location of DSE1a/ SEDI (red), A5C3/C4F6 (blue), USOD (green), B8H10 (purple).

Collectively these studies strongly suggest misfolded SOD1 is at the heart of toxicity in SOD1 linked FALS, as it has been linked to several major proposed models of toxicity, including axonal transport defects, ER stress and non-cell autonomous toxicity.

#### 1.6.4.3. Motor neuron vulnerability

A major questions in ALS research is why SOD1 toxicity specifically causes motor neuron degeneration, or put another way, why are motor neurons particularly vulnerable? Motor neuron death follows a temporal sequence, with fast twitch fatigable (FF) motor neurons degenerating first, followed by fast twitch fatigable resistance (FR) motor neurons, and then the smaller slow (S) motor units in $SOD1^{G93A}$ mouse models [253]. This pattern is likely consistent in humans, as the twitch force of FF motor neurons decreases the earliest in SALS patients [254]. Why FF are preferentially lost in ALS remains elusive, although it is likely they have intrinsic properties rendering them more vulnerable than other neuronal populations.

In the $SOD1^{G93A}$ mouse model, FF motor neurons selectively exhibit ER-stress [251]. Misfolded SOD1 (as detected by A5C3 and/or D3H5) accumulates in FF motor neurons and parallels levels of the ER stress marker BiP, as determined by retrograde labeling via the gastrocnemius muscle in $SOD1^{G93A}$ mice [250]. ER stress-causing agents selectively exacerbate misfolded SOD1 accumulation in motor neurons, although ER stress proteins are elevated in all cell types [250]. Indicating a motor neuron specific vulnerability whereby misfolded SOD1 accumulates upon ER stress activation.

Macrophage migration inhibitory factor (MIF) was identified as the cytosolic chaperone of SOD1 that is abundant in liver, but not spinal cord [249]. Although motor neurons express

high levels of MIF transcript, protein levels are low. Increasing MIF expression in neuronal cells led to a diminution of misfolded SOD1 in a dose-dependent manner and augmenting MIF levels in murine motor neurons by viral infection led to increased cell survival [249].

Together these two studies indicate motor neurons are intrinsically less equipped to handle misfolded SOD1. Motor neurons as opposed to other neuronal populations are prone to misfolded SOD1 accumulation in stressed conditions. Moreover, motor neurons lack chaperones, MIF and likely others that could regulate misfolded SOD1 levels.

#### 1.6.4.4. Modulating levels of misfolded SOD1

Misfolded SOD1 antibodies are frequently used to monitor levels of the toxic protein species, as corollaries of survival or improved performance. Immunization of $SOD1^{G37R}$ mice with recombinant apo $SOD1^{G93A}$ results in a 30 day increase in survival, with a corresponding decrease in C4F6-reactive misfolded SOD1 [255]. B8H10-reacive misfolded SOD1 levels are reduced in $SOD1^{G93A}$ mice treated with Withaferin A, an inhibitor of nuclear factor-kappa B (NF-κB), compared to vehicle control [256]. Withaferin A treated animals live longer, had decreased signs of neuroinflammation and higher counts of motor neurons [256]. Decreasing levels of SOD1 in corticospinal motor neurons in the brain by injection of AAV9 encoding short hairpin RNA (shRNA) targeted against SOD1 decreases D3H5-reactive misfolded SOD1, and increases survival by 20 days compared to $SOD1^{G93A}$ rats injected with AAV9 encoding GFP [224]. Neuronal activity is shown to modulate misfolded SOD1 levels, as enhancing motor neuron excitability pharmacogenetically in $SOD1^{G93A}$ mice decreased misfolded SOD1 levels whereas inhibition of activity augmented misfolded SOD1 accumulation in motor neurons [250]. iPSC-derived motor neurons from an ALS patient with a SOD1 mutation are intrinsically

hyperexcitable compared to motor neurons that were genetically corrected [257]. The models used, an *in vivo* mouse model over-expressing mutant SOD1 versus an *in vitro* human model with only one copy of mutant SOD1, were very different and could possibly account for the inconsistencies. Conversely, motor neurons could increase activity in order to compensate for mutant SOD1 toxicity. Although not a treatment *per se*, gene editing to correct a SOD1 mutation in ALS patient iPSC-derived motor neurons causes a loss of A5C3 antibody-reactivity [134].

### 1.6.5. Non-cell autonomous toxicity of SOD1

For many years motor neurons were the primary focus of ALS research as they are the cell type that selectively degenerates. Increasingly, many non-neuronal cell types are now considered intimately linked with motor neuron death and disease.

Generation of transgenic mice expressing mutant SOD1 under the control of cell-type specific promoters for motor neurons [258-260] and astrocytes [261] were generally unsuccessful at provoking motor neuron death. Furthermore, the development of chimeric mice that expressed mutant SOD1 in motor neurons, but not in non-neuronal cells, resulted in increased survival of the animals, indicating the importance of glial cells in modulating disease course [262].

Selectively reducing expression of mutant SOD1 in a cell specific fashion led to a novel understanding of the contribution of each cell type to disease onset and progression and the hypothesis that SOD1 may exert non-cell autonomous toxicity [263, 264]. Collectively these experiments reveal that SOD1 expression in motor neurons [265] and oligodendrocytes [266] mediates disease onset and expression of mutant SOD1 in astrocytes and microglia affect disease progression [265, 267]. Surprisingly, this approach has also revealed that decreased

expression of dismutase active $SOD1^{G37R}$ in Schwann cells accelerates disease, likely due to decreased dismutase activity [268]. Removal of SOD1 in endothelial cells which form part of the blood-CNS barrier of the brain and spinal cord or muscle, had no effect on disease [269, 270]. T lymphocytes are also implicated in ALS pathogenesis. Although the CNS is thought of as an immune privileged area, T cells are detected post-mortem in the spinal cords of SALS patients [271], as well as in the spinal cords of SOD1 mouse models [272]. Several studies document that a compromised immune system decreases the lifespan of $SOD1^{G93A}$ mice [273, 274], whereas addition of healthy T effector or T regulatory cells prolongs survival [275]. The increased survival afforded to ALS animal models likely involves the ability of T regulatory cells to modulate microglia [276]. Perisynaptic Schwann cells, glial cells located at the neuromuscular junction, exhibit improper coding activity in response to endogenous activity in $SOD1^{G37R}$ mice [277], thus adding another cell-type as a culprit of toxicity in ALS.

In an effort to determine how microglia and astrocytes expressing mutant SOD1 cause motor neuron degeneration, a number of *in vitro* studies have employed primary co-cultures of motor neurons and glial cells from various sources. Mutant SOD1 expressing microglia from ALS animal models are toxic to wild-type motor neurons due to release of cytokines and free radicals [278, 279] whereas modulation of microglia by secretion of the cytokine interleukin 4 (IL-4) by T cells is protective [280, 281]. Astrocytes from SOD1 mouse models are toxic to wild-type motor neurons derived from both animal models [282] and human embryonic stem cells (hESC) [283, 284]. Astrocytes isolated post-mortem from FALS (with SOD1 mutations) and SALS patients increase the death of mouse motor neurons compared to astrocytes from a healthy individual [285]. A fully humanized co-culture study demonstrates that astrocytes

derived from SALS patients are toxic to hESC-derived motor neurons, and further identifies that receptor interacting-1 protein (RIP1) mediates motor neuron death via necroptosis [286].

Despite a large body of evidence indicating that glial cells are important in ALS, the mechanisms remained undefined. Whether glial cells influence disease in other forms of FALS is only now emerging.

### 1.6.6. SOD1 and sporadic ALS

While SOD1 inclusions are a typical hallmark of FALS cases with underlying SOD1 mutations, SOD1 positive inclusions are found in some SALS cases [116, 117]. Additional studies are required to reinforce this finding. Despite SOD1 being highly stable, lack of the metal co-factors and the reduction of the disulfide bond leads to the formation of fibrils and aggregates [152, 287]. Metal-depleted wild-type SOD1 can be immunoprecipitated by the misfolded SOD1 specific antibodies D3H5, MS785 (lack of zinc) [36, 243] and $SOD1^{G93A}$ mice immunized with recombinant apo $SOD1^{WT}$ live longer than mice treated with vehicle alone [288]. Taken together, modified wild-type SOD1 can mimic structural features of misfolded SOD1. Treatment of N2a cells expressing $SOD1^{WT}$ with hydrogen peroxide causes SOD1 ubiquitination, same as is observed for mutant SOD1 [289]. Oxidized $SOD1^{WT}$ protein applied to cultured motor neurons induces toxicity equivalent to that of mutant SOD1 [289]. In SALS patient lymphoblasts, oxidized SOD1 is detected in a subset of patients with bulbar onset [290]. Like mutant SOD1, oxidized SOD1 interacts with Bcl-2 causing a toxic conformational shift that alters mitochondrial morphology [290]. Oxidation of Cys111, a residue known to be important for SOD1 stabilization and toxicity [291, 292], underlies the ability of the misfolded SOD1 specific antibody C4F6 to recognize $SOD1^{WT}$ [244]. Suppressing SOD1 expression in

astrocytes, derived from post-mortem tissue of both FALS and SALS patients, leads to a dose-dependent decrease in toxicity when co-cultured with murine motor neurons [285]. These findings add to the accumulating evidence that wild-type SOD1 is central to ALS. However, another study found that decreasing SOD1 levels in astrocytes from SALS patients had no effect on motor neurons derived from human embryonic stem cells [286].

C4F6-reactive misfolded SOD1 was detected in 4 of 9 sporadic ALS spinal cords by immunohistochemistry, and no misfolded SOD1 immunolabeling was found in controls (17 cases) [244]. Misfolded SOD1 isolated from SALS tissue and perfused into a squid axoplasm assay inhibited axonal transport, and the transport defect was reversed with the addition of C4F6 antibody [244]. Taken together these experiments demonstrate that misfolded SOD1 is present in SALS patients. Yet two additional studies were unable to detect C4F6-reactive misfolded SOD1 in SALS cases (a combined 50 cases), even when multiple epitope retrieval techniques were tested [236, 246]. It is not apparent why conflicting results were obtained. One could speculate that variability in collection/processing of tissue could be at play, or loss of antibody affinity or specificity between the first study and subsequent studies. Regardless of the cause of the discrepancy, a consensus on this issue has yet to emerge. SALS patient iPSC-derived motor neurons may be an ideal system in which to unequivocally determine if misfolded SOD1 is found in SALS. They would provide a framework where many patient cell lines prepared under equivalent conditions could be evaluated. Misfolded SOD1 has already been detected in iPSC-derived motor neurons from FALS patients demonstrating the feasibility of this approach [134].

DSE2 and DSE1a antibodies detect misfolded SOD1 in SALS patients in two separate studies (a combined total of 48 cases), but not in neurological or non-neurological controls [238, 293]. Interestingly, misfolded SOD1 was found in non-SOD1 mediated FALS. Analysis of

SALS patients with TDP-43 pathology also had limited amounts of misfolded SOD1 reactivity. Misfolded SOD1 was also detected in a FALS patient with the $FUS^{R521C}$ mutation with an absence of TDP-43 inclusions. In cell culture models simultaneously overexpressing $SOD1^{WT}$ with FUS or TDP-43 resulted in the detection of misfolded SOD1 [238]. This finding remains to be independently confirmed, but is particularly intriguing given that it provides a link between RNA binding proteins and SOD1, which are not thought to act in the same pathway. The SOD1 peptide antibodies positively label misfolded SOD1 in several SALS cases, as well as disease controls, leading to doubt regarding the specificity of the antibody [240]. Misfolded SOD1 was not found in SALS cases using the USOD, SEDI or AJ10 antibodies [119, 239]

Considerable excitement and controversy surrounds the finding of misfolded wild-type SOD1 in SALS patient material. If so what is the magnitude of SOD1 contribution to SALS? These answers will greatly impact the broader utility of therapeutics aimed at modulating total levels of SOD1 or just misfolded SOD1.

### 1.6.7. Propagation of mutant SOD1

The spread of ALS throughout the neuroaxis is reminiscent of prion disease, which involves the self-propagation of a pathogenic protein [294]. Increasing evidence supports that SOD1 and TDP-43 behave as prion-like proteins in that they can each cause misfolding of their native counterparts [294]. *In vitro* evidence suggests this is possible, as both wild-type and mutant SOD1 are capable of seeding fibrils and aggregates [110]. Spinal cord homogenates from wild-type and mutant SOD1 animal models, but non-transgenic littermates cause recombinant wild-type and mutant SOD1 to form fibrils [295]. This is specific to SOD1 as spinal cord homogenates from a Huntington's disease mouse model or a human patient with FTD do not

seed SOD1 fibrils [295]. As compelling as these data are, they do not directly identify SOD1 as prion-like molecule since these experiments used complex homogenates, containing nucleic acids, cytokines and other factors, any of which could have elicited SOD1 fibrillation. Transfection of mutant $SOD1^{G85R}$ and $SOD1^{G127X}$ into neuronal cells lines causes endogenous wild-type SOD1 to misfold as demonstrated by detection with misfolded SOD1 antibodies DSE2 and DSE1a. This finding identified mutant SOD1 as the necessary factor for misfolding [232]. Moreover, incubation of recombinant $SOD1^{G127X}$ and $SOD1^{WT}$ in a cell-free system caused $SOD1^{WT}$ to become misfolded, suggesting that mutant SOD1 is sufficient to induce misfolding [232]. Injection of spinal cord homogenates from paralyzed $SOD1^{G93A}$ animals into the spinal cords of post-natal day (P) P0 $SOD1^{G85R\text{-}YFP}$ (which do not develop paralysis due to sub threshold levels of mutant SOD1) mice resulted in paralysis in 6 of 10 injected mice and correlated with the presence of SOD1 inclusions in the spinal cord [296]. Interestingly, injection of homogenates from $SOD1^{WT}$ mice caused paralysis in 1 of 3 animals, again reasserting that misfolded wild-type SOD1 can be pathogenic [296]. Introduction of homogenates from paralyzed recipient $SOD1^{G85R\text{-}YFP}$ mice into naïve $SOD1^{G85R\text{-}YFP}$ mice led to an early-onset paralysis in all animals tested [296]. This is the first *in vivo* evidence that mutant/misfolded is transmissible, although with the caveat that spinal cord homogenates, containing multiple factors besides mutant/misfolded SOD1, were utilized.

Another feature of prion-like proteins is the ability to spread from cell to cell. The mechanism of propagation from cell to cell depends on the extracellular release of mutant SOD1 aggregates or exosomes containing misfolded SOD1 which are able to enter nearby cells by micropinocytosis [293, 297]. Mutant SOD1 can be secreted extracellularly through its interaction with chromogranins [298]. Increasing levels of Chromogranin A in neurons

## 2.1. Author Contributions

SP preformed all experiments. SP analyzed the data in consultation with NA and CVV. SP and CVV wrote the manuscript.

## 2.2. Abstract

Methods to detect and monitor mitochondrial outer membrane protein components in animal tissues are vital to study mitochondrial physiology and pathophysiology. This protocol describes a technique where mitochondria isolated from rodent tissue are immunolabeled and analyzed by flow cytometry. Mitochondria are isolated from rodent spinal cords and subjected to a rapid enrichment step so as to remove myelin, a major contaminant of mitochondrial fractions prepared from nervous tissue. Isolated mitochondria are then labeled with an antibody of choice and a fluorescently conjugated secondary antibody. Analysis by flow cytometry verifies the relative purity of mitochondrial preparations by staining with a mitochondrial specific dye, followed by detection and quantification of immunolabeled protein. This technique is rapid, quantifiable and high-throughput, allowing for the analysis of hundreds of thousands of mitochondria per sample. It is applicable to assess novel proteins at the mitochondrial surface under normal physiological conditions as well as those proteins which may become mislocalized to this organelle during pathology. Importantly, this method can be coupled to fluorescent indicator dyes to report on certain activities of mitochondrial subpopulations and is feasible for mitochondria from the central nervous system (brain and spinal cord) as well as liver.

accelerated death in SOD1$^{G37R}$ mice and increased levels of B8H10-reactive misfolded SOD1 [299].

Together, these studies indicate that mutant SOD1 causes native SOD1 protein to misfold, thus behaving like a prion. Moreover, this property of SOD1 can explain how misfolded SOD1 propagates from cell to cell and eventually region to region. Future studies will elucidate the precise mechanisms of transmission. Immunization with misfolded SOD1 specific antibodies, in addition to lowering the burden of misfolded SOD1, have the potential to limit cell to cell spread and therefore slow/halt disease progression.

### 1.6.8. SOD1-mediated toxicity

In the 22 years since the identification of *SOD1* mutations as causative for ALS, several targets and pathways have been implicated in SOD1 toxicity. The most prominent include glutamate excitoxicity, induction of ER stress, inhibition of the proteasome, mitochondrial dysfunction, secretion of SOD1 and microglial activation, induction of extracellular superoxide by nicotinamide adenine dinucleotide phosphate (NADPH) oxidase, altered axonal transport, disruption of the blood-brain-barrier, and dysfunction of autophagy [264] (**Figure 5**).

#### 1.6.8.1. Mitochondria as a target for SOD1 toxicity

Mitochondria are principally known to produce ATP through oxidative phosphorylation. However, they also participate in a number of other cellular functions, including signalling, apoptosis and calcium handling. A mitochondrion is composed of distinct compartments, the outer mitochondrial membrane (OMM), the intermembrane space (IMS), the inner

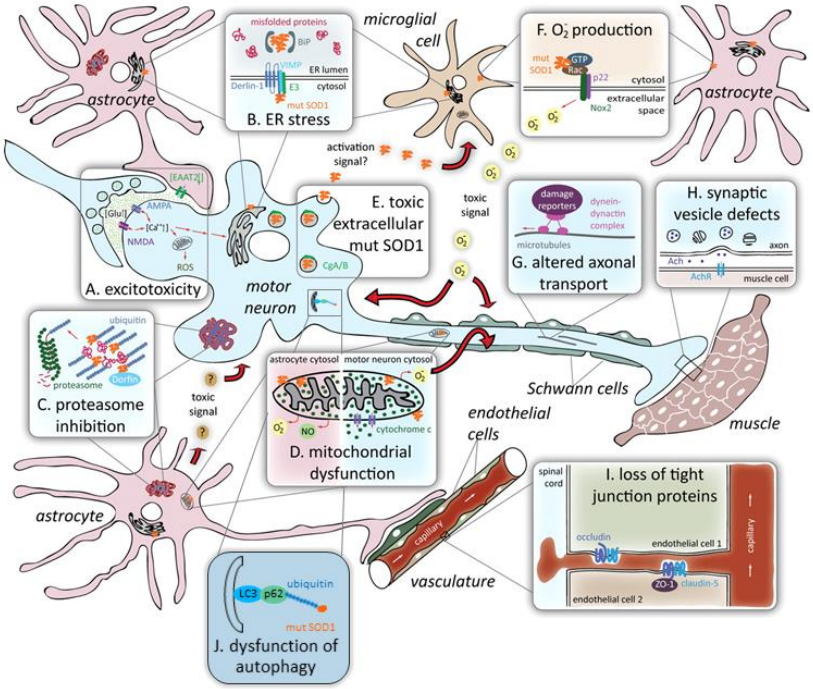


**Figure 5: Proposed mechanisms of toxicity in SOD1-mediated ALS.** Adapted from Ilieva *et al.,* 2009 [264]. A) Excitotoxicity. B) ER stress. C) Inhibition of the proteasome. D) Mitochondrial dysfunction. E) Extracellular release of mutant SOD1. F) Superoxide production. G) Altered axonal transport. H) Synaptical vesicle defects. I) Disruption of blood-spinal barrier. J) Dysfunction of autophagy.

mitochondrial membrane (IMM), the cristae space, formed by the folding of the inner membrane and the matrix. Mitochondria have their own genetic material encoding thirteen polypeptides, which are part of the oxidative phosphorylation machinery. Given the polarity and high activity of motor neurons, they are thought to be especially vulnerable to mitochondrial dysfunction [300] and to SOD1 mediated toxicity (**Figure 6**).

#### 1.6.8.1.1. Mitochondrial morphology

The observation that mitochondrial morphology is altered in SALS patients led to the hypothesis that mitochondria are linked with disease. Ultrastructural analysis of post-mortem spinal cords of SALS patients show aggregated, swollen mitochondria with cristae disorganization in the anterior horn [301, 302]. In addition, granular fibril structures associate with mitochondria [303]. Mitochondrial abnormalities are also evident in the motor cortex [304] and surprisingly in dorsal root ganglion cells [305]. Motor neurons derived from iPSCs of FALS patients with SOD1 mutations confirm post-mortem findings, that mitochondria have a disorganized structure, appear swollen, and clustered together in neurites [306]. Correction of the SOD1 mutation using zinc-finger nucleases rescued the mitochondrial phenotype.

Similar morphological defects were mirrored in the spinal cords of ALS mouse models, mostly $SOD1^{G93A}$, but also $SOD1^{G37R}$, $SOD1^{G85R}$ and $SOD1^{L126X}$ [208, 220, 221, 307-313]. A longitudinal study of mitochondrial ultrastructure reveals swollen, vacuolated mitochondria, and the frequent appearance of mega mitochondria, in spinal cords of $SOD1^{G93A}$ mice [221]. Quantification reveals fewer, but larger mitochondria. Mitochondrial morphological abnormalities are also observed at the neuromuscular junction (NMJ) [221]. Mitochondrial structure in both the spinal cord and pre-synaptic terminal of the NMJ is altered as early as P7

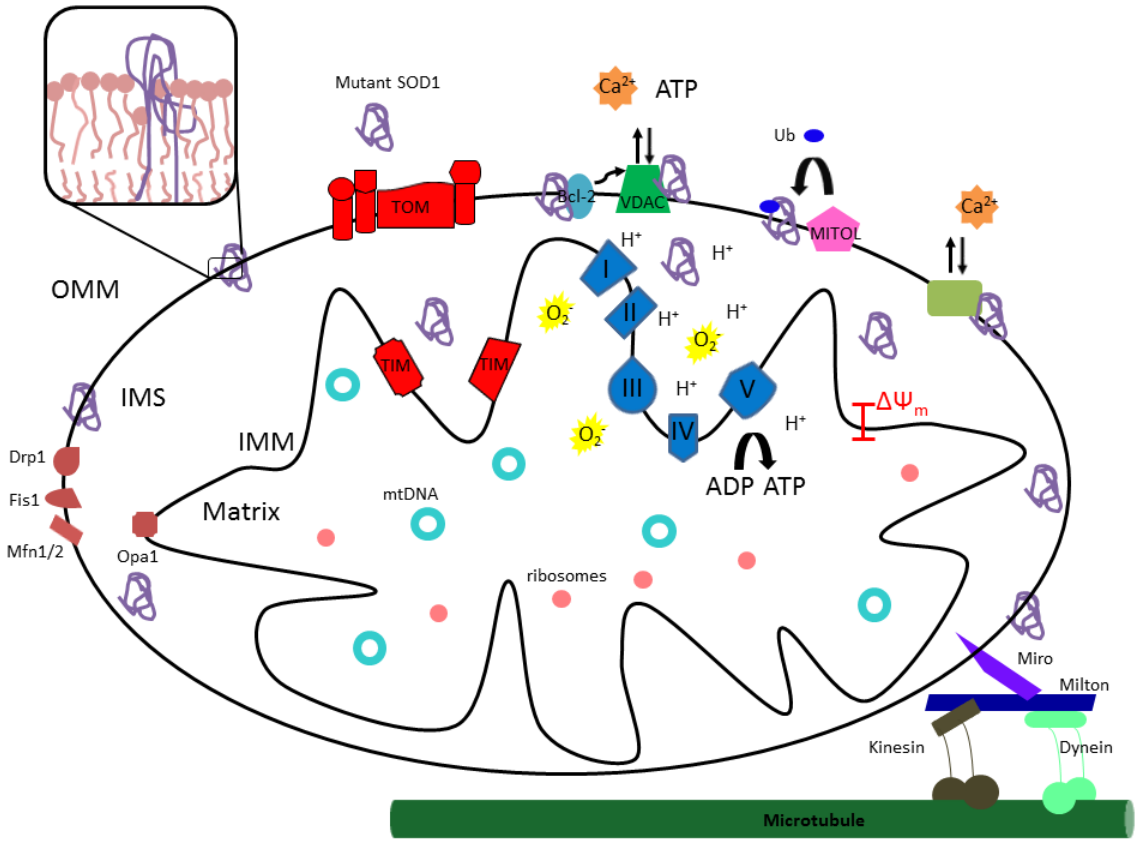


**Figure 6: Mutant SOD1 and mitochondria in ALS**. Mutant SOD1 associated with the OMM in tissues affected by ALS and is also imported into the IMS. Outlined are the mechanisms by which mutant SOD1 is propped to damage mitochondria, including altering levels of mitochondrial fission and fusion proteins, altering permeability of the outer membrane, blocking the protein import machinery of the mitochondria, translocase of outer membrane (TOM) and translocase of inner membrane (TIM) complezes, interaction with mitochondrial proteins, Bcl-2, VDAC and MITOL, altering bioenergetics (including the productions of ATP, transmembrane potential and generation of superoxide), decreasing calcium buffer and halting transport of mitochondria to axons. Together, these mechanisms are propsed to disturb cellular function leading to motor neuron death that is characteristic of ALS.

[221]. Using a mouse model with motor-neuron restricted expression of mitochondrial-targeted EGFP, crossed to $SOD1^{G37R}$ and $SOD1^{G85R}$ mice reveals increased spherical mitochondria compared to controls in motor neuron somata [310]. In the motor neuron axons of $SOD1^{G85R}$ mice, mitochondria are elongated pre-symptomatically, and mitochondrial elongation is exacerbated with symptom progression [310]. Together these studies clearly demonstrate that mitochondrial morphology is significantly disturbed in both human disease and animal models.

Mitochondria are dynamic organelles that fuse and divide forming a network or existing as individual entities [314]. Mitochondrial morphology is controlled by a balance of proteins mediating fission, dynamin-related protein 1 (Drp1) and fission 1 (Fis1) and proteins resulting in fusion, mitofusin 1 and 2 (Mfn1, Mfn2) and optic atrophy 1 (Opa1) [314]. Levels of these proteins are tightly regulated, as mitochondrial morphology is linked to organelle function [315]. Therefore, one way to affect morphology would be to dysregulate the balance of fission and fusion proteins. Alterations in mitochondrial morphology could arise by other means, including ionic homeostasis, although this has yet to be investigated in the context of ALS.

Transient transfection of mutant SOD1 in NSC-34 cells results in swollen mitochondria [316]. In agreement with this, mitochondrial fragmentation, determined as a decrease in length was observed in both the soma and dendrites of NSC-34 cells stably expressing mutant SOD1 [317]. NSC-34 and SH-SY5Y cells expressing mutant SOD1 show increased mitochondrial fragmentation, swelling, cristae disorganization, decreased levels of fusion protein Opa1 and increased levels of fission protein Drp1 [318]. An imbalance towards increased fission is corroborated in the $SOD1^{G93A}$ mouse models, as levels of Opa1 and Mfn2 decrease with age in the anterior spinal cord, whereas fission proteins remain constant [319]. Actual mitochondrial fusion rates are lower in $SOD1^{G93A}$ motor neuron cultures compared to controls [320].

Moreover, mitochondrial length is decreased in the distal axons for $SOD1^{G93A}$ motor neurons [320] and sciatic nerves [321]. These disturbances were cell type specific, as cortical neurons from $SOD1^{G93A}$ animals had properties similar to controls [320].

Collectively, these results suggest that mutant SOD1 causes mitochondrial fragmentation, likely via decreased mitochondrial fusion mediated by an imbalance of fusion and fission proteins, as well as mitochondrial swelling and cristae disorganization. How mutant SOD1 alters mitochondrial fusion, or the imbalance of fission and fusion remains unknown, despite being an important avenue of research.

#### 1.6.8.1.2. Mitochondrial transport

Early on, defects in axonal transport were linked to ALS [322, 323], and the observations that mitochondrial distribution was also altered in ALS mouse models led credence to the proposition that defects in mitochondrial transport may be a relevant disease mechanism [310, 313, 324]. Motor neurons from $SOD1^{G93A}$ mice show decreased anterograde transport, causing depletion of mitochondria in axons [325]. Furthermore, the decrease in transport is associated with mitochondrial damage, namely depolarization and mitochondrial rounding [325]. Altered mitochondrial movement, both in the anterograde and retrograde directions is found in NSC-34 cells expressing mutant SOD1, thereby affecting the density of mitochondria in neurites [317]. In a follow-up study, the same authors, now using motor neurons expressing mutant SOD1 show retrograde axonal transport was selectively affected, and attributed this to reduced velocity and frequency of movements. This was selective for the transport of mitochondria as the movement of membrane bound organelles was not affected by mutant SOD1, and cell type-specific as cortical neurons exhibited normal mitochondrial transport [320]. Both anterograde and

retrograde transport of mitochondria is decreased in motor neurons from $SOD1^{G93A}$ rats [326]. Expression of mutant SOD1 with a dominant negative form of $Drp1^{K38A}$ inhibits fission leading to partial rescue of mitochondrial fragmentation and a full rescue of transport defects [326]. These data intriguingly link morphology and transport. *In vivo* imaging of sciatic nerves reveals mitochondrial retrograde transport defects appear first, followed by defects in anterograde transport [321], while another group claims that mitochondrial movement in both directions is affected [327]. Motor neurons-derived from iPS cells from an ALS patient with an SOD1 mutation had fewer motile mitochondria and this phenotype is rescued by gene editing to correct the mutant SOD1 allele [306]. Unfortunately, the direction of mitochondrial movement was not assessed in this study.

Synaptaphilin (SNPH) is a docking receptor for mitochondria. Decreased docking as a consequence of genetic deletion of SNPH leads to increased mitochondrial mobility. Crossing of $SOD1^{G93A}$ mice with SNPH-null mice increases axonal mitochondrial mobility in dorsal root ganglia (DRG) neurons, but does not prolong survival, preserve motor neuron counts or attenuate neuroinflammation [328]. Imaging of nerve explants from $SOD1^{G93A}$ mice confirms transport defects, but this was not specific to mutant SOD1 as slowed transport was also observed in $SOD1^{WT}$ mice [329]. Conversely, mitochondrial transport in $SOD1^{G85R}$ mice is comparable to wild-type (non-transgenic) mice [329]. These results imply motor neuron death is not necessarily a consequence of axonal transport defects, given that transport defects are detected in wild-type animals with intact motor neurons, and no transport defects were found in $SOD1^{G85R}$ mice, where there is substantial age-dependent motor neuron loss. Moreover, it provides evidence that different mouse models, expressing different SOD1 mutations (with

different activities) can yield varying results. Collectively, these findings imply decreased mitochondrial motility/transport is insufficient to cause motor neuron death.

#### 1.6.8.1.3. Mitochondrial calcium handling

Calcium acts as an intracellular signalling molecule to regulate multiple cellular functions. Calcium signalling is modulated by transient increases in cytosolic calcium concentration, which are normally kept low by releasing calcium extracellularly or sequestering it in the ER and mitochondria [330]. Therefore, mitochondria's ability to buffer cytosolic calcium is vital to proper calcium signalling and cell survival and has emerged as a relevant disease mechanism in ALS.

Mitochondrial calcium buffering defects are reported in a number of different ALS models, including neuronal cell culture lines [331], isolated brain and spinal cord mitochondria derived from SOD1 mice [332], and within brain slices extracted from $SOD1^{G93A}$ mouse models [333, 334]. The inability to buffer cytosolic calcium is suggested to be a result of a reduction of the mitochondrial calcium uniporter to uptake calcium into the mitochondria [334]. Muscle fiber mitochondria from $SOD1^{G93A}$ mice also have increased amounts of calcium [335]. Calcium defects are selective for spinal cord and brain mitochondria, as calcium buffering in liver mitochondria is unaffected [332]. Similarly, calcium defects are only observed in vulnerable hypoglossal neurons, but not oculomotor neurons which are resistant to degeneration in ALS [333]. Increased mitochondrial calcium levels precede accumulation of calcium in the ER and cytosol in motor neurons of dissociated mouse dorsal root ganglia cultures, implying that alterations in calcium buffering could originate from dysfunctional mitochondria [336].

Cyclophilin D (CyPD) is a component of the mitochondrial permeability transition pore, which allows calcium to enter mitochondria [337]. Numerous studies have crossed CyPD null mice to SOD1 mice to determine if enhanced mitochondrial buffering capacity can attenuate disease. Early studies did support this hypothesis as $SOD1^{G93A}CyPD^{-/-}$ female mice had an increased lifespan [338]. A second study reports female $SOD1^{G93A}$ mice had an increased survival compared to male mice, however crossing into a CyPD null background resulted in a decreased survival for female mice, now comparable to their male counterparts [339]. The survival rate in female $SOD1^{G93A}CyPD^{-/-}$ mice was mechanistically linked to 17b-oestradiol, which decreased calcium retention in brain mitochondria only when CyPD was present [339]. Yet another study examined deletion of CyPD in three different ALS mouse models ($SOD1^{G93A}$, $SOD1^{G37R}$, and $SOD1^{G85R}$) and reported no effect on survival, despite increased calcium buffering in isolated spinal cord mitochondria [340]. These studies offer conflicting results, which may be attributed to the different genetic backgrounds of the $CyPD^{-/-}$ lines used (C57/BL/6 versus C57BL/6J) [339, 340]. However, it does question the relevancy of calcium buffering with respect to mitochondrial dysfunction in ALS.

#### 1.6.8.1.4. Mitochondrial Bioenergetic defects

Five multi subunit complexes (Complex I-V) located in the IMM make up the electron transport chain (ETC). Electrons from the citric acid cycle flow through each complex eventually producing oxygen and energy in the form of ATP. During this process protons are pumped out of the matrix into the IMS creating a separation of charge and generating a transmembrane potential across the IMM. This membrane potential drives ATP synthesis through the terminal complex of the ETC [341].

Decreases in complex I activity and reduced ATP/ADP ratios are documented in lymphoblasts from SALS patients [342]. Oxygen consumption and electron transport activity are globally reduced [343] in the $SOD1^{G93A}$ mouse, or specifically reduced in complexes I and IV [344] or in only complex IV [345], in the spinal cord and/or brain. Conversely, no change in ATP levels in isolated brain and/or spinal cord mitochondria from pre-symptomatic $SOD1^{G93A}$ mice [332], or rats [346]. In cultured neuronal cells, defects in electron transport chain activity are reported with associated diminution of ATP levels [347], and specifically complex I and IV defects are found [316]. Overall across many ALS models there is decreased mitochondrial activity.

As mitochondrial transmembrane potential and energy production are linked many groups use membrane potential as a read-out for mitochondrial function. Mitochondrial transmembrane depolarization is linked with mutant SOD1 expression in primary neurons [320, 325, 336], motor neuron terminals [348] and cultured neuronal cell lines [349]. Interestingly, mitochondrial transmembrane potential in the proximal segment of motor neurons of $SOD1^{G93A}$ mice are hyperpolarized compared to $SOD1^{WT}$ mice, while more distal mitochondria are depolarized, thereby revealing compartment specific differences in mitochondrial bioenergetics [320]. Differences in mitochondrial morphology are also documented in cell body versus axon [310]. Further comparison of somatic and synaptic mitochondrial dysfunction is warranted and could reveal compartmental specific mitochondrial alterations. No difference in transmembrane potential is observed in isolated spinal cord mitochondria from $SOD1^{G93A}$ and $SOD1^{WT}$ rats [346]. Conversely, mitochondrial hyperpolarization is reported in NSC-34 cells transiently expressing mutant SOD1, compared to cells transfected with wild-type SOD1 [350]. Lymphoblasts from SALS patients are hyperpolarized compared to healthy controls [351].

Discrepancies in how mutant SOD1 affects mitochondrial transmembrane potential may be attributed to the varying model systems used, *in vivo* versus *in vitro*, as well as the specific experimental conditions.

Mitochondria produce superoxide from complex I and complex III as a by-product of oxidative phosphorylation [352 224]. Inefficiencies in the electron transport chain typically lead to increased superoxide production. In neuronal cells lines expressing mutant SOD1, mitochondrial superoxide is elevated [349, 353]. Isolated mitochondria from the spinal cord and brain of $SOD1^{G93A}$ rats produce higher levels of reactive oxygen species compared to mitochondria isolated from their non-transgenic littermates [354]. Mitochondrial derived superoxide could lead to increased oxidative stress in ALS. In fact, levels of oxidative stress markers, such as protein carbonyls, lipid peroxidation and DNA damage are elevated in SOD1 mouse models [169, 355-357] and in neuronal tissue from ALS patients [168].

While the bulk of what is known about mitochondrial impairments in ALS, has focused on whole tissue or neurons, relatively little effort has been made to identify non-neuronal mitochondrial dysfunction. In fact, mitochondrial dysfunction in astrocytes may also participate in disease. Astrocyte mitochondria from $SOD1^{G93A}$ rats have decreased electron transport activity, decreased transmembrane potential, and increased superoxide production compared to controls [358]. Co-culture of motor neurons with astrocytes pre-treated with mitochondrial toxins (rotenone, antimycin A, sodium azide, flurocitrate) results in diminished motor neuron survival, demonstrating astrocytes with defective mitochondria cannot adequately support motor neurons [358]. Astrocytes from $SOD1^{G93A}$ rats are less able to sustain motor neurons than astrocytes from non-transgenic animals, however treatment with mitochondrially targeted antioxidants (ubiquinone and carboxy-proxyl nitroxide) resulted in significantly increased

motor neuron survival to levels comparable to controls [358]. Lastly, motor neurons (expressing either mutant or wild-type SOD1) co-cultured with $SOD1^{G93A}$ astrocytes have decreased mitochondrial transmembrane potential and elevated mitochondrial calcium levels [359]. Collectively these studies indicate that mitochondrial dysfunction in astrocytes causes toxicity to motor neurons. Moreover, defective astrocytic mitochondria can induce mitochondrial abnormalities in motor neurons *in vitro*.

#### 1.6.8.1.5. Altered mitochondrial protein import

Given the mitochondria's unique structure, the vast majority of its protein components must be transported across one or two membranes. Thus, this organelle has evolved a mechanism to import all nuclear encoded proteins through a series of proteins in the outer and inner membrane [360]. Proteomic analysis of spinal cord mitochondria reveals a substantial increase in proteins involved in mitochondrial import, including translocase of the outer membrane 40 (TOM40), TOM20, and TOM22 [346]. Import of two different mitochondrial substrates is slowed in spinal cord mitochondria isolated from $SOD1^{G93A}$ rats. Addition of recombinant mutant SOD1, but not α-synuclein, a protein implicated in Parkinson's disease, to mitochondria isolated from healthy animals significantly inhibited mitochondrial import [346].

#### 1.6.8.1.6. SOD1 at the mitochondria

Clearly, the presence of mutant SOD1 negatively impacts multiple aspects of mitochondrial function, but how does this mainly cytosolic protein deleteriously affect mitochondria? Mutant SOD1 may damage mitochondria directly, as a small portion of SOD1 localizes to the mitochondrial IMS under normal physiological conditions [122]. In agreement

with this, numerous studies demonstrate SOD1 is localized to mitochondria in the $SOD1^{G93A}$ mouse [309, 343, 361, 362]. Biochemical studies find SOD1 in the IMS [363, 364] and demonstrate that IMS-targeted SOD1 in the absence of cytosolic SOD1 is protective against oxidative damage in yeast [364]. That SOD1 is found in the IMS is particularly interesting given the lack of a mitochondrial targeting sequence (MTS) [365]. However, there is precedence for proteins localizing to mitochondria in the absence of a MTS. For SOD1, this is likely due its interaction with CCS, as several studies show localization of SOD1 in the IMS is CCS-dependent [364, 366]. CCS is a substrate of the mitochondrial intermembrane space assembly (Mia40)-essential for respiration and vegetative growth (Erv1) import pathway. In this pathway, proteins with disulfide bonds diffuse freely across the outer membrane through the translocase of the outer membrane (TOM) proteins. CCS then interacts with oxidized Mia40, forming disulfide bonds with CCS, and eventually leading to a fully folded oxidized CCS. Mia40 is reoxidized by Erv1. Mia40 and Erv1 constitute a disulfide relay system, which fold proteins in the IMS, resulting in their retention (or trapping) in the IMS [367]. Erv1 is re-oxidized by transferring electrons from oxygen or cytochrome c, thus coupling the Mia40-Erv1 system to oxidative phosphorylation [368]. SOD1 must be in its reduced apo state to enter mitochondria [366] and all of four cysteine residues are required for import [369]. In N2a cells, wild-type SOD1 localization to the IMS is dependent on CSS, Mia40 and Erv1 activity or redox state, which is regulated by oxygen levels and respiratory chain activity. Conversely, this regulation is absent for SOD1 mutants [369]. Mutant SOD1 has a tendency to accumulate to high levels in/on mitochondria compared to $SOD1^{WT}$ in NSC-34 cells [347]. Therefore, more mutant SOD1 is associated with mitochondria, and is no longer regulated by normal physiological parameters. As a proof of principle, IMS-targeted mutant SOD1 in NSC-34 cells causes significant

mitochondria defects, mitochondrial fragmentation, decreased cell viability, transport defects, and sensitivity to stress [317, 370]. A mouse model expressing IMS-targeted mutant SOD1 in an SOD1-null background shows impaired mitochondria respiratory chain activity and calcium handling defects, motor neuron loss, decreased motor function, and weakness, however NMJs remained innervated [371]. Thus, mutant SOD1 present only in the IMS causes mitochondrial damage, but is insufficient to cause the full presentation of ALS.

SOD1 is reported to be in mitoplasts, mitochondria stripped of outer membrane, and localizing to the mitochondrial matrix [372]. However, this finding has yet to be replicated and there is no mechanism known for SOD1 import into the matrix. Lastly, accumulation of mutant SOD1 on the mitochondrial surface is also reported [234, 373, 374]. The conformational specific antibodies, SEDI [248], DSE2 [233, 234, 249], A5C3 [310], and AJ10 [239]) detect misfolded SOD1 at the mitochondria, revealing this organelle as an and intersecting point for misfolded SOD1. DSE2-reactive misfolded SOD1 selectively associates with the cytoplasmic face of the outer mitochondrial membrane in $SOD1^{G93A}$ rat spinal cords [234], and motor neuron mitochondria, from $SOD1^{G85R}$ and $SOD1^{G37R}$ are labelled by the misfolded SOD1 specific antibody A5C3 [310]. Furthermore, the SOD1 chaperone MIF precludes misfolded SOD1 association to liver mitochondria [249].

Given that SOD1 molecule destined for import into the mitochondria must traverse the OMM in the apo reduced state, it is possible that mitochondria are a collection point for unfolded/misfolded SOD1.

#### 1.6.8.1.7. Mitochondrial aggregates

SOD1 aggregation at the mitochondria is described in both cell culture and animal models and in various mitochondrial compartments (OMM, IMS, and matrix) [207, 318, 370, 372-374]. How these aggregates perturb mitochondrial function remains speculative at best. In recent years, numerous studies, outlined below, suggest that mutant SOD1 disrupts lipid membranes, and intriguingly many studies focus on mitochondrial membranes. When mutant SOD1 is added to a reconstituted lipid membrane, it forms a tetrameric functional pore, in which ions can pass [375]. This same phenomenon is also observed for the amyloid beta peptide in Alzheimer's Disease [376]. Wild-type and mutant SOD1 readily form fibrils and expose hydrophobic regions, when incubated in reducing conditions and high temperatures. Addition of SOD1 fibrils (both wild-type and mutant) to rat liver mitochondria cause a loss of membrane integrity [377, 378]. Using atomistic molecular dynamics simulations, both the electrostatic and zinc binding loops of apo SOD1 are predicted to bind phospholipid bilayers and suggest SOD1 insertion could further seed aggregation [379]. Nuclear Magnetic Resonance (NMR) studies reveal that mutant, zinc-depleted wild type and reduced wild-type SOD1 anchor in lipid bilayers by forming energetically favorable alpha-helixes [380]. These data support earlier work demonstrating that misfolded SOD1 behaves like an integral membrane protein in spinal cord mitochondria from $SOD1^{G93A}$ rats [234]. α-synuclein can also adopt a helical configuration in lipids [381]. Taken together, mutant SOD1 has the capacity to destabilize lipid membranes with the potential of causing numerous deleterious consequences.

#### 1.6.8.1.8. Mitochondrial interacting partners

Identifying protein interactors at the mitochondria may be key to unravelling how mutant/misfolded SOD1 contributes to disease. To that end, several interactors of mutant/misfolded SOD1 at the mitochondria are reported. Mutant SOD1 and to a lesser extent wild-type SOD1, interact with B cell lymphoma 2 (Bcl-2) at the mitochondria in N2a cells, $SOD1^{G93A}$ mice and human FALS patient material [374]. This interaction induces a conformational change in Bcl-2, exposing the normally buried pro-apoptotic BH3 domain [382]. Exposure of the BH3 domain causes the SOD1/Bcl-2 complex to interact with VDAC1, leading to decreased permeability of the mitochondrial membrane to ADP, and downstream to mitochondrial hyperpolarization and decreased cellular viability [350]. Using SOD1 blocking peptides it was determined that the SOD1/Bcl-2 complex is mediated by the amino acid stretch encoded by exon 2 of SOD1. Addition of the exon 2 peptide in NSC-34 cells expressing $SOD1^{G93A}$ reduces Bcl-2 binding and rescues mitochondrial dysfunction. Similarly, addition of the exon 2 peptide increases ADP permeability in isolated spinal cord mitochondria from $SOD1^{G93A}$ mice [350]. Therefore, the ability of the exon 2 peptide to block the interaction of SOD1 with Bcl-2 suggests mutant SOD1 must be in a non-native misfolded conformation that exposes all or some residues located in exon 2 to interact with Bcl-2. Interestingly, the epitopes of D3H5 and USOD are localized to exon 2 of SOD1 [33, 235]. One could speculate that Bcl-2 would co-immunoprecipitate with both of these antibodies. Moreover, it would be tempting to speculate that D3H5 or USOD could be used interchangeably with the exon 2 peptide to rescue mitochondrial dysfunction induced by mutant SOD1.

DSE2-reactive misfolded SOD1 interacts with the voltage dependent anion channel 1 (VDAC1), an outer mitochondrial membrane protein important for the movement of substrates

across the membrane [233]. *In vitro* functional studies demonstrate that recombinant mutant SOD1, but not wild-type SOD1, decreases VDAC1 conductance in a reconstituted lipid bilayer. Furthermore, ADP levels are reduced in the spinal cords of ALS animal models [233]. However, crossing $SOD1^{G37R}$ mice with VDAC1 null mice results in accelerated disease and shortened survival [233]. Other misfolded SOD1 binding partners at the mitochondrial surface are expected, as DSE2-reactive misfolded SOD1 associates with spinal mitochondria in ALS animal models even in the absence of VDAC1 [346].

In COS-7 cells, MITOL/MARCH5, a mitochondrial outer membrane-resident ubiquitin ligase, ubiquitinates mutant SOD1, but not wild-type SOD1 [383]. Over-expression of MITOL in N2a cells causes the proteasome-dependent degradation of mutant SOD1 and slightly decreases ROS production, whereas knock down of MITOL enhances ROS production, and decreases both ATP levels and cell viability [383]. The *in vivo* significance of this interaction and in the context of disease has yet to be determined [383].

An interaction between mutant SOD1 and lysyl-tRNA synthetase (KARS) was initially found using a yeast-two hybrid screen [384]. In COS-7 cells and SOD1 mouse models, mutant SOD1 interacts with the mitochondrial targeted form of this protein, mitoKARS [385]. Mutant SOD1 and mitoKARS form aggregates on the mitochondrial surface prior to mitoKARS import, effectively causing decreased mitochondrial translation [385]. In addition, expression of both mutant SOD1 and mitoKARS alters mitochondrial morphology and decreases cell viability [385].

Collectively, these studies strongly implicate aberrant protein interactions with mutant/misfolded SOD1 at the mitochondrial surface in the disruption of various pathways, including membrane permeability, protein degradation and protein synthesis.

#### 1.6.8.1.9. Mitochondrial targeted interventions

Several cell culture studies successfully show that mitochondrial targeted interventions can reverse mutant SOD1-mediated mitochondrial damage. In neuronal cell lines, over-expression of mutant SOD1 and dithiol glutaredoxin (Grx2), a protein localized in the mitochondrial matrix, increases SOD1 solubility, rescues mitochondrial morphology, restores the balance of fission and fusion proteins, preserves mitochondrial function and increases cell survival [318]. The mechanisms by which this matrix protein affects SOD1, which is mostly localized to the IMS or OMM, remains unidentified. Treatment of $SOD1^{G93A}$ rat motor neurons with sirtuin 3 (SIRT3), an NAD-dependent protein deacetylase, or peroxisome proliferator-activated receptor gamma, coactivator 1 alpha (PGC1-α) rescues fragmentation and reduces mitochondrial transport defects attributed to mutant SOD1 [326]. *In vivo* experiments have been less clear in demonstrating that improving mitochondrial function has any benefit with regards to disease onset and/or progression. Several anti-oxidant compounds reduce astrocyte toxicity to motor neurons including mitochondrial targeted catalase [359]. However introduction of catalase to $SOD1^{G93A}$ mice did not result in any benefit in terms of survival [386]. $SOD1^{G93A}$ mice administered dichloroacetate (DCA), a drug that stimulates pyruvate dehydrogenase complex activity, had increased NMJ innervation, higher motor neuron counts and led to an extension of survival by two weeks compared to untreated mice [387]. In complementary *in vitro* experiments, DCA improves mitochondrial respiration in astrocytes [387]. Increasing levels of PGC-1α in muscle of $SOD1^{G93A}$ mice led to increased mitochondrial biogenesis and activity and animals had improved strength and endurance, but there was no effect on survival, supporting the view that mutant SOD1 expression muscle does not contribute to disease.

Nevertheless, increasing PGC-1α in the spinal cord of SOD1 animal models may be viable experimental approach [388]. As mentioned previously, modulating calcium buffering capacity through CyPD gene deletion produces mixed results, with the latest study showing no effect on survival. Ablation of CyPD improves mitochondrial morphology, ATP synthesis, partially rescues motor neuron loss and decreases levels of misfolded SOD1. However, it did not rescue muscle denervation or axonal degeneration [340]. Thus suggesting that even low levels of misfolded SOD1 are sufficient to modulate disease.

## 1.7. Therapeutics

At present, riluzole is the only approved drug for the treatment of ALS, and its efficacy is limited, resulting in a 3-6 month extension of life [389]. That only one compound is available after 50 years of trials and testing of over 150 drugs/therapies [390], is disappointing to say the least. Many features of ALS make it challenging to find treatments. It is a rare heterogeneous disease, with a short survival time and no known biomarkers [25]. Furthermore delivering a compound or other active agents into the spinal cord requires invasive delivery methods [391].

Several trials in various phases are currently testing compounds that target a variety of disease related mechanisms; mitochondrial dysfunction, neuroinflammation, and autophagic flux [392]. In addition, cell replacement therapy using mesenchymal stem cells (MSC) isolated from bone marrow or blood, and neural stem cells (NSC), isolated from fetal tissue, have been investigated for their ability to support degenerating cells in the spinal cord by releasing trophic support or immune modulatory factors. Both MSC and NSC are effective at prolonging survival in SOD1 animal models [393, 394]. Human trials have demonstrated the feasibility and safety of these treatments. However, the efficacy remains unknown and larger scale studies are

required [395-397]. MSC administered intravenously were later found in the spinal cord, suggesting that invasive delivery methods can be circumvented [395]. iPS cells are a recent technology where a patient's own fibroblasts can be expanded and differentiated *ex vivo* to replace motor neurons in the brain or spinal cord [398]. This approach is challenging given that motor neurons must project axons long distance and reform functional connections with muscle [390]. Despite this, these cells are useful as models of disease and for high throughput screening of drug compounds [391].

Another active area of therapeutics is antisense oligonucleotides (ASO), single-stranded oligonucleotides that duplex with mRNA, thus rendering the ASO-bound mRNA to be degraded by the endonuclease RNAse H [399]. ASO therapy is currently under consideration for FALS patients with C9ORF72 expansion, as numerous studies reveal decreased expression of C9ORF72 has favourable outcomes [87, 400]. Application of this approach to C9ORF72 patients should be done cautiously as it is still under debate whether the disease mechanism is loss of function or gain of function and knowledge on cellular functions of C9ORF72 is still limited.

### 1.7.1. Reducing levels of SOD1

ASO may also prove effective for SOD1-mediated FALS. As a proof of principle several groups demonstrate that decreasing SOD1 protein through various RNA interference approaches has beneficial effects on survival in SOD1 animal models [401-403]. Furthermore, clinical trials indicate that intrathecal delivery of ASO is tolerated and relatively safe [404]. Further trials are required to definitively conclude if treatment with ASO against SOD1 decreases SOD1 expression in the spinal cord, to what level and whether this will prove

beneficial to patients. Another point of consideration is whether a systemic decrease in SOD1 could have negative consequences for ALS patients, especially because it is likely that we have yet to uncover the entirety of pathways where SOD1 is implicated. At present, this treatment would target FALS patients with SOD1 mutations, however mounting evidence suggests that SOD1 is involved in SALS and could therefore be applied to more patients.

Many other therapeutic interventions are under consideration, including reduction of misfolded SOD1 using delivery of misfolded SOD1 specific antibodies by conventional delivery methods or virus-meditated delivery.

### 1.7.2. Reducing levels of misfolded SOD1

Some of the SOD1 conformational antibodies have been efficacious in pre-clinical animal models. Passive immunization of $SOD1^{G93A}$ mice with misfolded SOD1 antibodies A5C3 and D3H5, led to divergent outcomes with regards to survival. Immunizing with the A5C3 antibody produces no effect on survival, whereas the D3H5 antibody extended survival 6-9 days, depending on the duration of immunization and when the treatment was started [243]. Increased survival as well as increased innervation at the NMJ and attenuation of gliosis in the spinal cord correlated with decreased levels of B8H10-reactive misfolded SOD1 following immunization [243]. Incorporation of the variable chains of the misfolded SOD1 antibody D3H5 into an adeno-associated virus (AAV) vector encoding secretable single-chain fragment variable (scFv) antibody and administered to $SOD1^{G93A}$ mice via intrathecal injection results in increased survival, up to 40 days [405]. Importantly, survival correlated with virus titer in animal spinal cords [405]. Animals receiving the viral vector encoding scFv D3H5 had decreased gliosis,

increased maintenance of motor neurons and decreased levels of B8H10-reactive misfolded SOD1 [405].

$SOD1^{G37R}$ and $SOD1^{G93A}$ mice actively immunized with the SEDI-peptide (residues 143-151) show an increased survival of 40 and 12 days, respectively [190]. Mice treated with the SEDI-peptide have decreased gliosis, a higher preservation of motor neurons, decreased levels of misfolded SOD1 and a nearly complete loss of oligomeric SOD1 complexes within the spinal cord [190].

Decreasing levels of SOD1 in corticospinal motor neurons in the brain by injection of AAV9 encoding short hairpin RNA (shRNA) targeted against SOD1 decreases D3H5-reactive misfolded SOD1, and increases survival by 20 days compared to $SOD1^{G93A}$ rats injected with AAV9 encoding GFP [224].

Collectively these results indicate that misfolded SOD1 is a viable therapeutic target. Moreover, decreased misfolded SOD1 level associates with prolonged lifespan and attenuation of disease markers.

### 1.8. Overview and rationale for thesis

ALS-linked mutations in *SOD1*, lead to the misfolding of the SOD1 protein. In an effort to specifically identify non-native conformations of SOD1, several groups have generated misfolded SOD1 antibodies that recognize epitopes exposed only when SOD1 adopts a non-native conformation (reviewed in [33, 235]). In addition to the detection of misfolded SOD1, these antibodies have proven efficacious at reducing misfolded SOD1 levels in pre-clinical models and are therefore a viable therapeutic option for SOD1-mediated ALS [190, 243].

Mitochondrial morphological abnormalities are one of the earliest features of disease in $SOD1^{G93A}$ mice and multiple aspects of mitochondrial physiology are disrupted in both mutant SOD1 cell culture and animal models (reviewed in [406]). Misfolded SOD1 localizes to the cytoplasmic face of spinal cord mitochondria, and more specifically to motor neuron mitochondria, in ALS rodent models [234, 310]. We hypothesize that the presence of misfolded SOD1 at the surface of spinal cord mitochondria negatively impacts mitochondrial function and thus contributes to the disease process.

Herein, we describe a novel flow cytometric assay whereby mitochondria isolated from rats or mice are immunolabeled with an antibody of interest and simultaneously probed for aspects of mitochondrial function, including size/volume, transmembrane potential and superoxide production. Uniquely, this method allows us to independently assess the function of mitochondrial subpopulations (**Chapter 2: Immunodetection of outer membrane proteins by flow cytometry of isolated mitochondria**).

The application of this method to rodent models of ALS ($SOD1^{G93A}$ rats and $SOD1^{G37R}$ mice) using the misfolded SOD1 antibody B8H10, reveals two spinal cord mitochondrial subpopulations, one with misfolded SOD1 deposited at the surface versus another without. This permitted a comparative analysis of mitochondrial volume, transmembrane potential and superoxide production (**Chapter 3: Mitochondrial damage revealed by immunoselection for ALS-linked misfolded SOD1**).

Data from our group and others suggest that there exists multiple misfolded SOD1 species with varying biochemical properties [407, 408]. We hypothesize that there exists a continuum of misfolded SOD1 species with varied localizations, properties and potencies. Moreover, misfolded SOD1 antibodies have the potential to tease out such differences, and

ideally identify toxic misfolded species versus more benign conformations. Using a combination of approaches, including our novel flow cytometric assay, we compare the differences between AMF7-63 and B8H10-reactive misfolded SOD1 (**Chapter 4: ALS-linked misfolded SOD1 species have divergent impacts on mitochondria**).

# Chapter 2

## Immunodetection of outer membrane proteins by flow cytometry of isolated mitochondria

Pickles, S., Arbour, N., Vande Velde, C. Immunodetection of outer membrane proteins by flow cytometry of isolated mitochondria. J Vis Exp., 2014 September 18; (91): e51887.

If different forms of misfolded SOD1 can have unique protein interactors, perhaps their biochemical properties are also distinct. Prudencio *et al*., found that SEDI-reactive misfolded SOD1 forms inclusions, while C4F6-reactive misfolded SOD1 has a diffuse localization, and is likely more soluble, leading the authors to conclude that misfolded SOD1 adopts multiple misfolded conformations [408]. B8H10, DSE2 and AMF7-63-reactive misfolded SOD1 form aggregates in both spinal cord homogenates and isolated mitochondria from symptomatic $SOD1^{G93A}$ rats, although fibrils are predominantly detected with the DSE2 and AMF7-62 antibodies (**Chp. 4**). Using a panel of SOD1 peptide binding antibodies two different strains of misfolded aggregates were detected in SOD1 mouse spinal cords [407]. One strain correlated with earlier disease onset and decreased survival, therefore demonstrating different potencies of these two strains [407]. Conversely, C4F6-reactive misfolded SOD1 is not found in aggregates (**Chp. 4**), consistent with low C4F6-reactivity to SOD1 in oligomeric complexes from HEK293 lysates [457] and its localization in soluble fractions both *in vitro* and *in vivo* [236, 408]. The relative solubilities of AMF7-63 and B8H10-reactive misfolded SOD1 conformers has yet to be evaluated, and remains a potential explanation for the increased toxicity of AMF7-63-reactive misfolded SOD1.

The effectiveness of the misfolded SOD1 antibody D3H5 as a therapeutic versus the failure of the A5C3 antibody [243], adds to the evidence that misfolded SOD1 assumes a continuum of misfolded states. One could speculate that immunization with the A5C3 antibody did not reduce the levels of B8H10-reactive misfolded SOD1 as effectively as the D3H5 antibody. It remains unknown whether immunization with either antibody decreased B8H10-reactive misfolded levels at the mitochondria and/or mitigated mitochondrial damage. A5C3 weakly associates with spinal cord mitochondria (**Chp. 4**). It is tempting to speculate that its weak localization at

## 2.3. Introduction

Mitochondria are highly dynamic organelles that undergo multiple rounds of fission and fusion, are transported to sites of high energy demand and respond rapidly to physiological stimuli [409]. Since it is increasingly recognized that mitochondria within different tissues, even different cellular compartments, have distinct functional profiles, new methods are needed to identify these distinct mitochondrial subsets.

Microscopy provides a means whereby individual mitochondria can be visualized and the presence of a protein at or in mitochondria can be determined by immunofluorescence[234]. However, quantitative analysis by this method is labor intensive and is more suitable for experiments using immortalized or primary cell lines. The study of individual mitochondria derived from tissue is significantly more difficult and most methods do not allow for easy identification of mitochondrial subsets concurrently with the evaluation of mitochondrial function [410].

In order to address this hurdle, a novel method to immunolabel mitochondria isolated from rodent tissues and subsequently analyzed by flow cytometry has been developed. This allows for the rapid detection and quantification of proteins localized to the mitochondrial outer membrane, which compared to analysis by microscopy, is much less labor intensive and permits the analysis of thousands of mitochondria in a single sample. This assay can be applied to monitor the fate and relative amount of mitochondrial outer membrane proteins that are thought to be constitutively present at the mitochondria, the recruitment of proteins to the mitochondrial surface, or the detection of proteins mislocalized to the mitochondria in pathological conditions. Moreover, the incorporation of conventional fluorescent indicator dyes permits the simultaneous evaluation of certain aspects of mitochondrial function in distinct mitochondrial subpopulations.

## 2.4. Protocol

Animals used in this study were treated in strict accordance to a protocol (N08001CVsr) approved by the Centre de Recherche du Centre Hospitalier de l'Université de Montréal (CRCHUM) Institutional Committee for the Protection of Animals which follows national standards as outlined by the Canadian Council on Animal Care (CCAC).

Prepare all reagents required to perform this protocol (**Table 1**). All other details regarding equipment, supplies and suppliers can be found in **Table 2**.

### I. Collection of rat spinal cord

**I.i**. Deeply anaesthetize the rat (Sprague Dawley) with 4% isoflorane. Verify anaesthetization by a lack of reflex upon pinching of the forepaw. Euthanize the rat by decapitation via guillotine. This method of euthanasia is preferred over others which might distort the spinal cord.

**I.ii.** Cut the skin of the back to expose the spine. Cut the spinal column with bone scissors just above the pelvic bone. Visualize the opening of the vertebral column.

**I.iii.** Insert a 10 mL syringe, with a 200 μL pipette tip (attached via melting slightly over flame), filled with Phosphate Buffered Saline (PBS), into the vertebral column.

**I.iv**. Flush out the spinal cord by applying a medium amount of pressure to the plunger.

| Buffer | Composition | Step used | Comments |
|---|---|---|---|
| Homogenization Buffer (HB) | 210 mM Mannitol<br>70 mM Sucrose<br>10 mM Tris pH 7.5<br>1 mM EDTA | II.i-II.viii | Protease inhibitors can be added |
| HB+ KCL | HB, as above with the addition of 50 mM KCl | II.iii | Protease inhibitors can be added |
| M-Buffer | 220 mM Sucrose<br>68 mM Mannitol<br>10 mM KCl<br>5 mM KH2PO4<br>2 mM MgCl2<br>500 µM EGTA<br>5 mM Succinate<br>5 µM Rotenone<br>10 mM HEPES pH 7.2<br>0.1 % fatty-acid free Bovine Serum Albumin | III.iii-III.ix | Protease inhibitors can be added. This buffer is supplmented with succinate a complex II substrate and rotenone and inhibitor of complex I to prevent reverse electron transport. |

**Table 1: Buffer Compositions.**

| Name of Material/ Equipment | Company | Catalog Number | Comments/Description |
|---|---|---|---|
| Rats | Charles River | Strain code 400 | Adult (9 weeks to 18 weeks) male or female rats can be used for the isolation protocol. Weight of rats is dependent on gender and age (males between 300 to 500 g and females between 200 to 350 g) are typically used. |
| Dounce homogenizer | Kontes Glass Co. | 885450-0022 | Duall 22 |
| Microcentrifuge | Thermo Scientific | | Sorvall Legend Micro 17 R |
| Ultracentrifuge tubes | Beckman Coultier | 344057 | Transparent, thin walled |
| Sorvall Ultracentrifuge | Thermo Scientific | | Sorvall WX UltraSeries |
| AH-650 rotor and buckets | Thermo Scientific | | |
| Opti-prep | Axis-Shield | 1114542 | Iodixanol, density gradient medium |
| Fatty acid free Bovine Serum Albumin | Sigma | A8806 | Must be fatty acid free for mitochondria |
| Sodium succinate dibasic hexahydrate | Sigma | S9637 | |
| Rabbit anti-Mitofusin2 antibody | Sigma | M6319 | |
| Rabbit IgG | Jackson Immuno Research | 011-000-003 | |
| Anti-Rabbit IgG PE | eBioscience | 12-4739-81 | |
| Micro titer tube | Bio-Rad | 223-9391 | For sample acquisition by flow cytometry |
| MitoTrackerGreen (MTG) | Invitrogen | M7514 | 100 nM: Ex490 nm/Em516 nm |
| TMRM | Invitrogen | T668 | 100 nM: Ex548 nm/Em574 nm |
| CCCP | Sigma | C2759 | |
| MitoSOX Red | Invitrogen | M36008 | 5 μM: Ex540 nm/Em600 nm |
| Antimycin A | Sigma | A8874 | |
| LSR II flow cytometer | BD | | |
| BS FACSDiva Software | BD | | |
| FlowJo | TreeStar Inc. | | Software used for analysis |
| BCA protein assay kit | Pierce/Thermo Scientific | 23225 | Bradford assay is not recomended as it is not compatible with high concentrations of SDS |

**Table 2: Materials.**

**I.v.** If any blood is present on the spinal cord, rinse with PBS before proceeding to the next step.

**Note:** This method has also been validated for brain and liver. If including these tissues, collect half the brain from the euthanized rat and a piece of liver equal in weight to the spinal cord. All other steps remain identical.

## II. Isolation of spinal cord mitochondria (adapted from Vande Velde *et al.[411]*

**II.i.** Collect the whole intact spinal cord and place in 5ml glass homogenizer with 5 volumes (~3.25 ml) Homogenization Buffer (HB). For optimal recovery of isolated mitochondria, perform all steps on ice or in cold room. Homogenize tissue by hand until no large pieces of tissue remain, approximately eight strokes. Place homogenate in two (2 mL) or three (1.7 mL) microcentrifuge tubes. Centrifuge 1300 x g for 10 mins at 4 ˚C in a benchtop microcentrifuge.

**II.ii.** Recover supernatant and place in a 5mL ultracentrifuge tube. Add 750 µL (~0.5 volumes) HB to the pellet-containing microcentrifuge tube and gently resuspend the pellet. Repeat centrifugation and resuspension steps two more times. Pool all supernatants (S1a and S1b) into the same 5 mL ultracentrifuge tube above. This step serves to remove small debris.

**II.iii.** Centrifuge pooled S1 using an ultracentrifuge equipped with a swinging bucket rotor and centrifuge at 17, 000 x g for 15 mins at 4 ˚C.

**II.iv.** Keep supernatant (S2) for further processing if the cytosolic fraction is of interest (for example for Western blot analysis). Resuspend the pellet (P2), the crude mitochondrial fraction,

in 4 mL HB+50 mM KCl. Centrifuge 17, 000 x g for 15 mins at 4 ˚C in a swinging bucket rotor. Discard the supernatant and gently resuspend the pellet (P3) in 800 µL HB.

**Note:** Mitochondria are washed with HB+50mM KCl to remove any non-specific mitochondrially-associated contaminants.

**II.v**. In a new 5 mL ultracentrifuge tube, add 200 µL Iodixanol (density gradient medium).

**II.vi**. To this tube add, 800 µL of resuspended pellet (P3), thereby creating a final concentration of 12% Iodixanol. Mix the contents of the tube gently via pipetting with a P1000. Centrifuge in an ultracentrifuge equipped with a swinging bucket rotor at 17, 000 x g for 15 mins at 4 ˚C.

**Note:** Liver does not contain myelin and therefore this step is not necessary if only the liver is being processed. However, if liver is being processed concurrently with CNS mitochondria, it is recommended to treat all tissues equally.

**II.vii.** Aspirate the layer of myelin at the top of the tube and carefully remove and discard the supernatant. Pellet may be loose. Resuspend the pellet in 4 mL HB. Centrifuge again at 17, 000 x g for 10 mins at 4 ˚C. Discard the supernatant and resuspend the pellet in 4 mL HB. Repeat the centrifugation and remove the supernatant.

**II.viii**. Resuspend the final pellet (P7) in 100-200 µL HB and transfer to a 1.7 ml microcentrifuge tube. This sample contains isolated mitochondria.

**II.ix**. Proceed to protein quantification. Dilute samples and the standard curve in 2% sodium dodecyl sulfate (SDS) to ensure adequate solubilization of mitochondria during protein quantification.

## III. Immunolabeling of isolated mitochondria for flow cytometry

**III.i**. For each staining mix to be tested, pipette 25 µg of isolated mitochondria into a 1.7 mL microcentrifuge tube. Include an unstained sample in each experiment; and for each antibody, be sure to include a sample for the appropriate isotype control.

**III.ii**. Centrifuge at 17, 000 x g for 2 mins at 4 ˚C in a bench-top microcentrifuge.

**III.iii**. Remove supernatant and resuspend isolated mitochondria in 50 µL Mitochondria Buffer (M Buffer) supplemented with 10% fatty-acid free BSA for 15 mins at 4 ˚C (blocking step).

**Note:** During labeling, perform incubations in a refrigerator at 4 ˚C.

**III.iv.** Add primary antibody (rabbit anti-Mfn2, 20 µg per mL) to tube and incubate for 30 mins at 4 ˚C.

**Note:** Determine optimal concentration of each antibody empirically by titration. Due to variability in concentration and/or purity, different lots of the same antibody from the same

manufacturer may lead to different results; therefore titration is needed for each new lot of antibody.

**III.v.** Wash out unbound primary antibody: Centrifuge at 17, 000 x g for 2 mins at 4 ˚C. Remove the supernatant and gently resuspend the pellet in 200 µL M Buffer. Centrifuge at 17, 000 x g for 2 mins at 4 ˚C. Remove supernatant and resuspend the pellet in 50 µL M Buffer.

**III.vi.** Add secondary antibody (Donkey anti-rabbit IgG Phycoerythrin (PE), 0.5 µg per ml) to tube and incubate samples for 30 mins at 4 ˚C, protected from light.

**III.vii.** Wash out unbound secondary antibody: Centrifuge at 17, 000 x g for 2 mins at 4 ˚C. Remove the supernatant and resuspend the pellet in 200 µL M Buffer. Centrifuge at 17, 000 x g for 2 mins at 4 ˚C. Remove supernatant and resuspend the pellet in 500 µL M Buffer.

**III.viii.** To ensure events are in fact mitochondria, stain isolated mitochondria with a mitochondria specific fluorescent dye for 15 mins at room temperature, protected from light. If staining of other functional parameters (mitochondrial transmembrane potential or superoxide production) is desired, proceed to step IV. If not, proceed to step V for acquisition.

**Note:** It is important to verify that the emission spectra of the secondary antibody is compatible with that of the functional dyes. For example, if verifying mitochondrial purity with a commercial dye with spectral properties similar to FITC and transmembrane potential with Tetramethylrhodamine methyl ester (TMRM), a viable secondary antibody would be

allophycocyanin (APC: Ex650 nm/Em660 nm). Add compensations controls, i.e. a sample immunolabeled or stained with a single fluorophore, when applicable.

**III.ix.** Transfer to a tube suitable for loading flow cytometer. (To facilitate the small sample size, a microtiter tube is placed inside 3 ml flow cytometer tube.) Keep samples on ice and proceed immediately to flow cytometer for acquisition.

## IV. Assaying mitochondrial transmembrane potential and mitochondrial superoxide production by flow cytometry

**IV.i.** Verify that isolated mitochondria have an intact transmembrane potential by staining with 100 nM TMRM (Ex548 nm/Em574 nm)[412], at step 3.8, for 15 mins at room temperature, protected from light. For comparison of transmembrane potential between samples and populations, use of lower/non-quenching concentrations of TMRM (1 to 30 nM), may be more appropriate [413].

**IV.ii.** As a control for TMRM staining, stain isolated mitochondria with 100 nM TMRM in the presence of 100 μM carbonyl cyanide m-chloro phenyl hydrazine (CCCP), a mitochondrial uncoupler that will depolarize mitochondria. The concentration of CCCP required to depolarize the mitochondria may be less if lower concentrations of dye are used.

**IV.iii.** Verify that isolated mitochondria produce mitochondrial superoxide by staining with an appropriate mitochondrial superoxide indicator [414], also at step 3.8, for 15 mins at room

temperature, protected from light.

**IV.iv.** As a control for mitochondrial superoxide production, stain isolated mitochondria with dye in the presence of 10 μM Antimycin A, an inhibitor of complex III of the respiratory chain that will augment mitochondrial superoxide production.

## IV. Acquisition and analysis of immunolabeled isolated mitochondria by flow cytometry

**IV.i.** Instrument set up: Switch voltages from linear to log mode to facilitate analysis of isolated mitochondria and set voltages (FSC: 450; SSC: 250). Ensure that events are collected in FSC-A (area) mode as well as FSC-W (width) and FSC-H (height), to be able to exclude doublets (ie. two events, passing through the detector at the same time) in analysis post-data collection. Set the number of events to be collected to 100, 000. Acquire compensation controls, if applicable.

**IV.ii.** Data acquisition: Before data acquisition, avoid vortexing samples. Instead mix by gently tapping tube. Initially collect events at a low pressure, during gating. Gate on total population. Adjust voltages of histograms accordingly, usually the peak of the unstained sample will correspond to the second decade ($10^2$). Once gates are established, and samples are being processed, the pressure can be switched to high.

**IV.iii.** Analysis: Visualize doublets by plotting FSC-W versus FSC. Identify singlets and doublets. Gate on singlets. Select the mitochondrial population by gating on events that are stained positively with a mitochondrial-selective dye.

**IV.iv.** Determine background labeling from isotype control. Using the isotype control sample, determine the percentage of the mitochondrial population labeling positive for Mfn2 antibody.

### 2.5. Representative results

Mitochondria derived from rat spinal cords can be immunolabeled with an antibody targeted to Mitofusin2 (Mfn2), a protein implicated in the fusion of the outer membrane of mitochondria[415]. Following isolation and labeling with a Mfn2 specific antibody and a fluorescently conjugated secondary antibody, mitochondria are processed by flow cytometry (**Fig. 1**). Following data acquisition, samples are analyzed using flow cytometry analysis software, by first visualizing all collected events on a dot plot (**Fig. 2A**). Doublets and singlets are differentiated when the events are plotted in FSC, width (W) versus area (A) (**Fig. 2B**). Once singlets are selected, gate the mitochondrial population via FSC/SSC (**Fig. 2C**), and verify the number of events staining positive for mitochondria-specific dye by co-plotting a histogram of the unstained sample with a sample stained with the mitochondria-specific dye. To determine the mitochondrial events, place a gate at the intersection of the two peaks (**Fig. 2D**). For spinal cord preparations, typically >90 % of the events are positive for the mitochondria-specific dye. For other tissues such as liver, ~98 % of the events will label with the dye (data not shown). After selecting only events that label positively for the mitochondria-specific dye, determine background labeling with the isotype control by selecting a gate ($Mfn2^{+}$) that includes 1 % or

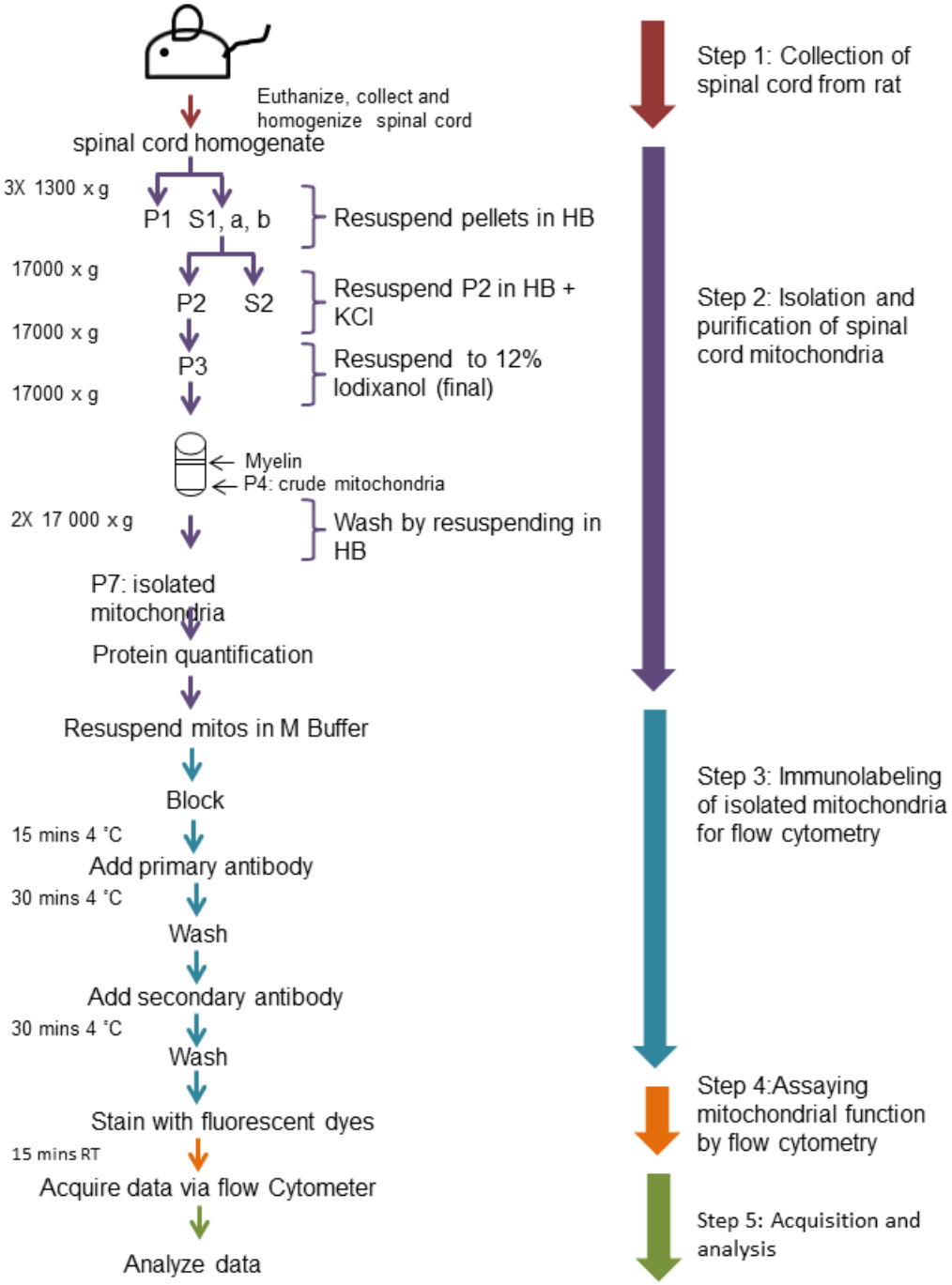
Euthanize, collect and homogenize spinal cord
spinal cord homogenate
3X 1300 x g
P1 S1, a, b
Resuspend pellets in HB
17000 x g
P2 S2
Resuspend P2 in HB + KCl
17000 x g
P3
Resuspend to 12% Iodixanol (final)
17000 x g
Myelin
P4: crude mitochondria
2X 17 000 x g
Wash by resuspending in HB
P7: isolated mitochondria
Protein quantification
Resuspend mitos in M Buffer
Block
15 mins 4 °C
Add primary antibody
30 mins 4 °C
Wash
Add secondary antibody
30 mins 4 °C
Wash
Stain with fluorescent dyes
15 mins RT
Acquire data via flow Cytometer
Analyze data
Step 1: Collection of spinal cord from rat
Step 2: Isolation and purification of spinal cord mitochondria
Step 3: Immunolabeling of isolated mitochondria for flow cytometry
Step 4:Assaying mitochondrial function by flow cytometry
Step 5: Acquisition and analysis

**Figure 1: Schematic of isolation, immunolabeling and analysis of mitochondria. Step 1:** Collect tissue and homogenize. **Step 2:** The isolation procedure contains eight centrifugation steps. Myelin, a major containment of central nervous system tissue is removed by diluting mitochondria in Iodixanol (density gradient medium) and centrifuging, resulting in the myelin floating to the top of the tube, while the mitochondria are pelleted. **Step 3**: Following isolation and quantification, mitochondria are blocked, labeled with primary antibody and washed. A secondary antibody conjugated to a fluorophore is then added. Unbound antibody is washed out. **Step 4**: At this point fluorescent dyes that report on mitochondrial purity, or mitochondrial function can be added. **Step 5**: Mitochondria are now ready to be analyzed by flow cytometry.

less isotype labeling (**Fig. 2E, *left***). Apply this gate uniformly to all samples labeled with antibody Mfn2 to determine the percentage of mitochondria with Mfn2 present on the outer mitochondrial membrane (**Fig. 2E, *right***). In this experiment, 30% of mitochondria derived from spinal cord label positive for Mfn2. It is important to note here, that although Mfn2 is considered to be a ubiquitously expressed mitochondrial outer membrane protein, it has not been previously quantified. Moreover, an immunocytochemical analysis of Mfn2 in cultured cells shows a non-homogenous labeling of individual mitochondria[416]. Of note, the antibody in this study was generated using a synthetic peptide to the N-terminus (amino acids 38-55). There is a predicted splice variant of Mfn2 lacking the first 302 amino acids, although this variant has yet to be confirmed experimentally (UniProt database). Thus, this assay is unable to detect alternatively spliced Mfn2 lacking the N-terminal sequence, given the antibody used.

Mitochondrial transmembrane potential ($\Delta\Psi_m$) and superoxide production can be assessed in this assay. Across the inner mitochondrial membrane, there is a separation of charge which drives ATP production via oxidative phosphorylation. TMRM is a cationic dye that accumulates within the mitochondria in a membrane potential dependent manner[412], and therefore can be used as a reporter of mitochondrial transmembrane potential. The majority of mitochondria (95%) are TMRM positive after staining, compared to the unstained control (**Fig. 3A**). However, when the uncoupler CCCP is added there is a significant decrease in the number of mitochondria able to retain TMRM (**Fig. 3A**). CCCP allows the free passage of ions across the inner mitochondrial membrane, essentially destroying the separation of charge and depolarizing the membrane.

Mitochondria release superoxide as a normal byproduct of oxidative phosphorylation from complex I and III of the electron transport chain. Mitochondrial superoxide can be

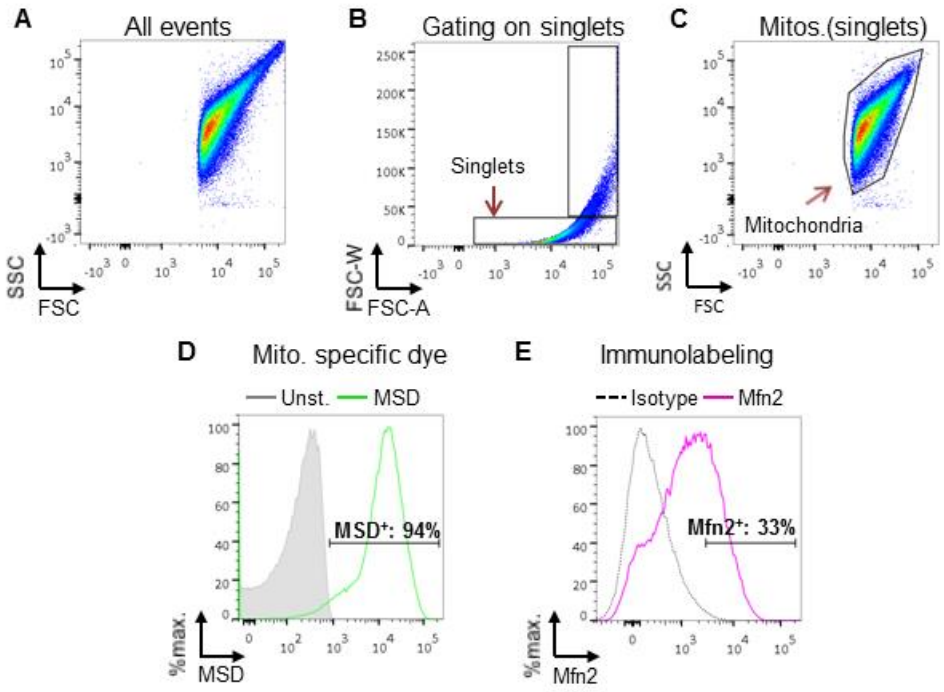


**Figure 2: Strategy for the analysis of isolated mitochondria by flow cytometry.** The Forward Scatter (FSC) and Side Scatter (SSC) voltages must be adjusted for small events, using both parameters in logarithmic mode. FSC width (FSC-W) data must be collected to exclude doublets. Note, on most flow cytometers, the default setting for FSC and SSC is linear mode. **A)** Visualize all collected events on a dot plot. **B)** Doublets, two mitochondria passing by the laser at the same time, can be distinguished from singlets by plotting FSC versus FSC-W (linear mode). Events are excluded if the FSC-W value is more than twice the mean FSC-W value of the majority of events, ie. those that are part of the dense cloud. Events under this threshold are gated as singlets. **C)** Again, visualize the events in a dot plot, and gate on the remaining events. **D)** Plot a histogram of the unstained sample (solid, grey, filled) and sample stained with a mitochondrial specific dye (MSD: solid, green). Gate the events staining positive for the MSD ($MSD^+$). **E)** Histogram of the isotype control, rabbit IgG (dashed, black) and Mfn2 labeled

sample (solid, pink). Set the gate so as to yield ≤ 1% $Mfn2^+$ on the isotype control peak and apply this same gate to experimental sample to determine the percentage of events labeling positive for Mfn2 ($Mfn2^+$).

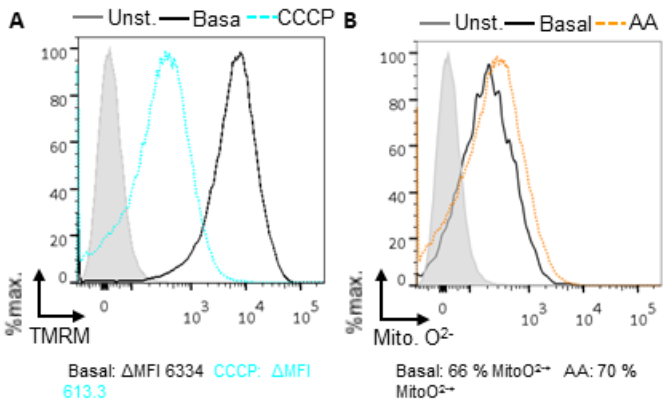


**Figure 3: Assaying mitochondrial transmembrane potential ($\Delta\Psi_m$) and superoxide production in isolated mitochondria by flow cytometry. A)** Under basal conditions all active mitochondria will label with TMRM (solid, black), compared to unstained control (solid, grey, filled) because the dye accumulates in mitochondria with a transmembrane potential. Addition of the protonophore CCCP (dashed, blue) dissipates the transmembrane potential causing the mitochondria to depolarize and retain less dye compared to basal conditions. Data is reported as the delta mean fluorescent intensity (ΔMFI), which is the mean fluorescent intensity of the unstained control subtracted from the mean fluorescent intensity of the sample. **B)** Under basal conditions, mitochondria produce superoxide as a by-product of oxidative phosphorylation. This mitochondrial source of superoxide can be assayed with a mitochondrial superoxide indicator, ($MitoO^{2-}$: solid, black) compared to unstained control (solid, grey, filled). Addition of the complex III inhibitor, Antimycin A (dashed, orange) results in increased superoxide production, compared with basal levels. Data is reported as percent of cells staining positive for the $MitoO^{2-}$ indicator.

measured via a membrane permeable dye that is targeted to mitochondria and becomes fluorescent following a reaction with superoxide [414]. Functional mitochondria produce a basal amount of superoxide compared to unstained samples (**Fig. 3B**). Addition of the complex III inhibitor Antimycin A yields an increase in superoxide, as seen by a rightward shift in florescence and a higher number of mitochondria (typically ~10% ) that are fluorescent with this mitochondrial superoxide indicator dye (**Fig. 3B**).

### 2.6. Discussion

It is increasingly evident that mitochondria are key players in both normal physiology and disease. While immunoblotting can determine which proteins are found within mitochondria or at the mitochondrial surface in a certain condition, this method reports on the average of the entire population. This method cannot yield information about relative abundances of mitochondrial subpopulations or subsets. While it has been previously assumed that all mitochondria are created equally, the field is increasingly recognizing that mitochondria within a cell have extensive variability in terms of morphology and/or function [417].

Fluorescent microscopy approaches do take into account the heterogeneity of mitochondria. However, quantification of this type of data is labor intensive. Furthermore, this approach is better suited to studies using cultured cells, as labeling of mitochondria *in vivo*/*in situ* is difficult due to the excessive number of mitochondria present, making differentiation of individual organelles inherently difficult. In most immunocytochemistry protocols, it is also not possible to simultaneously label outer mitochondrial membrane proteins and assess mitochondrial function due to the cellular permeabilization step required for antibody labeling. The current method works with isolated mitochondria, and thus does not require a

permeabilization step. In addition, the visualization of individual mitochondria is only possible via electron microscopy which is not amenable to the analysis of mitochondrial function. That being said, we recognize that isolation of mitochondria from tissue leads to disruption of the mitochondrial network and this could affect some elements of mitochondrial function. However, comparisons of functional aspects of isolated mitochondria from tissues that are processed similarly remains valid.

This method of immunolabeling of tissue-derived isolated mitochondria and subsequent analysis by flow cytometry allows for a rapid and quantifiable method to detect and monitor the presence of a protein located on the outer membrane. Detection of a highly abundant mitochondrial protein (like Mfn2) is possible with this technique. Similarly, this method can detect low abundance proteins that are only deposited on the mitochondrial membrane in disease, like misfolded SOD1 in the context of Amyotrophic Lateral Sclerosis (ALS)[418]. In addition, this method could be useful to monitor those proteins which transiently associate with the mitochondrial surface as part of their normal function. Examples include Dynamin-Related protein-1 (Drp1), a cytosolic protein that is recruited to the mitochondria to promote mitochondrial fission [419] and tumor necrosis factor receptor-associated factor 6 (TRAF6), which translocates to mitochondria to augment mitochondrial reactive oxygen species as a part of an innate immune response [420].

At present this technique is amenable only to proteins located at the mitochondrial surface, as standard permeabilization protocols for intracellular labeling require a detergent which disrupts the structural integrity of mitochondria. While a number of possible reagents have been tried (unpublished), further optimization of the immunolabeling protocol is still needed to make this protocol amenable to detecting intra-mitochondrial components.

This technique has broad applications and can be used to detect the presence or recruitment of one or more proteins to the mitochondria under different experimental paradigms. Furthermore, mitochondria can be co-labeled with two different antibodies, as well as with fluorescent indicators [418]. Other fluorescent probes could also be incorporated to characterize additional aspects of mitochondrial function. For example, commercially available dyes to monitor mitochondrial pH [421], calcium uptake with Calcium green-5N [422], and ATP levels [423] are possible.

## 2.7. Acknowledgments

We thank Laurie Destroismaisons and Sarah Peyrard for outstanding technical support and Dr. Alexandre Prat for access to the flow cytometer. We would also like to acknowledge Dr. Timothy Miller for his contribution regarding the removal of myelin from the preparations. This work was supported by the Canadian Institutes of Health Research (CIHR) Neuromuscular Research Partnership, Canadian Foundation for Innovation, ALS Society of Canada, the Frick Foundation for ALS Research, CHUM Foundation and Fonds de la Recherche en Santé du Québec (C.V.V.). Both C.V.V. and N.A. are Research Scholars of the Fonds de la Recherche en Santé du Québec and CIHR New Investigators. S.P. is supported by the Tim Noël Studentship from the ALS Society of Canada.

# Chapter 3

# Mitochondrial damage revealed by immunoselection for ALS-linked mutant SOD1

Pickles, S., Destroismaisons, L., Peyrard, SL., Cadot, S., Rouleau, GA., Brown, RH Jr., Julien, JP., Arbour, N., Vande Velde, C. Mitochondrial damage revealed by immunoselection for ALS-linked misfolded SOD1. Hum Mol Genet, 2013 October 1; 22 (19): 3947-59.

### 3.1. Author Contributions

Contribution: SP preformed majority of experiments. LD assisted in flow cytometry experiments on rats and mice, and in immunohistochemistry experiment. SLP collected some tissue from rats for immunohistochemistry. SC preformed initial pilot experiments on patient cells, which were redone by SP. RHB and GR contributed patient cells lines. SP analyzed data in consultation with NA and CVV. SP and CVV wrote the manuscript.

### 3.2. Abstract

Mutant superoxide dismutase 1 (SOD1) selectively associates with spinal cord mitochondria in rodent models of SOD1-mediated amyotrophic lateral sclerosis. A portion of mutant SOD1 exists in a non-native/misfolded conformation that is selectively recognized by conformational antibodies. Misfolded SOD1 is common to all mutant SOD1 models, is uniquely found in areas affected by the disease, and is considered to mediate toxicity. We report that misfolded SOD1 recognized by the antibody B8H10 is present in greater abundance in mitochondrial fractions of $SOD1^{G93A}$ rat spinal cords compared to oxidized SOD1, as recognized by the C4F6 antibody. Using a novel flow cytometric assay, we detect an age-dependent deposition of B8H10-reactive SOD1 on spinal cord mitochondria from both $SOD1^{G93A}$ rats and $SOD1^{G37R}$ mice. Mitochondrial damage, including increased mitochondrial volume, excess superoxide production and increased exposure of the toxic BH3 domain of Bcl-2 tracks positively with the presence of misfolded SOD1. Lastly, B8H10 reactive misfolded SOD1 is present in the lysates and mitochondrial fractions of lymphoblasts derived from ALS patients carrying SOD1 mutations, but not in controls. Together these results highlight misfolded SOD1 as common to two ALS rodent animal models and familial ALS patient

lymphoblasts with four different SOD1 mutations. Studies in the animal models point to a role for misfolded SOD1 in mitochondrial dysfunction in ALS pathogenesis.

### 3.3. Introduction

Amyotrophic Lateral Sclerosis (ALS) is a late onset neurodegenerative disease characterized by the loss of motor neurons [263]. Twenty percent of familial cases are due to mutations in superoxide dismutase 1 (*SOD1*) leading to the gain of an unknown toxicity. Mitochondria have long been considered a target of SOD1 toxicity due to reports of abnormal mitochondrial morphology in both patients [424] and animal models [307, 312, 361]. Several aspects of mitochondrial function are reported as disturbed in ALS models including decreased electron transport activity [343, 425], deregulated calcium handling [332, 336], impaired protein import [346], increased exposure of the Bcl-2 BH3 domain [382] and diminished conductance of the voltage-dependent anion channel (VDAC1) [233]. Whether such mitochondrial abnormalities actively contribute to the initiation or progression of ALS pathology, or rather are affected secondarily, remains unresolved.

SOD1 associates with mitochondria in an age-dependent and tissue-selective manner in multiple SOD1 rodent models and in ALS patient material harbouring SOD1 mutations [234, 373, 374]. A portion of SOD1 does localize to the intermembrane space (IMS) [363], but forced localization of SOD1 to the IMS is inadequate to provoke sufficient mitochondrial damage so as to yield motor neuron loss or paralysis [371]. While a proportion of mutant SOD1 protein is tightly bound to the cytoplasmic face of the outer membrane of spinal cord mitochondria [234], whether such surface-bound mutant SOD1 contributes to disease pathogenesis remains an open question. To date, studies demonstrating mitochondrial dysfunction, whether *in vivo* or *in vitro*,

report on the total mitochondrial population. However, only a portion of mitochondria have mutant SOD1 deposited on their outer membrane, leading to uncertainty as to which mitochondrial damage is linked to the association of mutant/misfolded.

A subset of SOD1 within spinal cord samples from ALS patients and SOD1 rodent models exists in an altered/non-normal conformation as demonstrated by a series of conformation restricted antibodies [119, 232, 234, 240, 243, 244, 248]. Increasing evidence suggests that these alternative forms, collectively referred to as misfolded SOD1, underlie the inherent toxic nature of SOD1 mutations [236, 244] as it is enriched in the motor neurons of both ALS rodent models and patient samples [240, 243, 244]. We previously demonstrated that mitochondrial-associated SOD1 is misfolded [234] and localized within motor neurons *in vivo* [310]. It remains undefined what type of mitochondrial damage is associated with this pool of mitochondrial-associated misfolded SOD1.

Using an antibody specifically detecting a misfolded form of SOD1, the clone B8H10, we provide evidence that B8H10-reactive misfolded SOD1 robustly associates with a subset of mitochondria isolated from SOD1 rodent models but not from wild-type controls. Moreover, this antibody identifies a subset of damaged spinal cord mitochondria in both $SOD1^{G93A}$ rats and *Lox*$SOD1^{G37R}$ mice. Mitochondrial defects appear prior to disease onset, clinical disease symptoms, gliosis and motor neuron loss. We also demonstrate for the first time that spinal cord mitochondria with surface-bound misfolded SOD1 have increased labelling for the toxic BH3 domain of Bcl-2, elevated production of mitochondrial superoxide, and deregulated volume homeostasis. Lastly, we demonstrate B8H10-reactive misfolded SOD1 is present in lymphoblasts derived from ALS patients with SOD1 mutations and not in controls.

## 3.4.Results

### 3.4.1. Differential detection of misfolded SOD1 on mitochondria by conformation-restricted antibodies

Recent progress in the field is marked by the development of a number of antibodies targeted to non-native conformations of SOD1, termed collectively as "misfolded SOD1". One such antibody, the mouse monoclonal C4F6 antibody, has been shown to preferentially recognize $H_2O_2$-oxidized SOD1 [244] while the reactivity of other misfolded SOD1 specific monoclonal antibodies, such as A5C3, B8H10 and D3H5, to particular SOD1 subtypes remains undefined. B8H10 has been used to effectively monitor misfolded SOD1 in a $SOD1^{G93A}$ mouse model following passive immunization with the D3H5 antibody, targeted to a different epitope of misfolded SOD1 [243]. Importantly, decreased levels of B8H10-reactive misfolded SOD1 correlated positively with increased survival, increased motor neuron counts and attenuated gliosis in these D3H5-treated animals [243]. Thus, we sought to determine if B8H10 and C4F6 were equally able to detect misfolded SOD1 in subcellular fractions enriched for spinal cord mitochondria isolated from symptomatic $SOD1^{G93A}$ rats. Interestingly, immunoprecipitation with B8H10, but not C4F6, robustly detected misfolded SOD1 in mitochondrial and cytosolic fractions from these animals (**Fig. 1A**). Since C4F6 has not been previously published in an immunoprecipitation assay, we considered that the antibody may not be well suited for this application and thus performed non-denaturing gel analysis for an independent evaluation of the mitochondrial association of misfolded SOD1 with these reagents. Specifically, we loaded a titration of purified mitochondria from the same animal on non-denaturing gels and blotted with B8H10 and C4F6. In this assay, densitometry determined that B8H10 immunoreactivity was detected 1.7 times more readily in mitochondrial fractions compared to C4F6 (**Fig. 1B**).

Mitochondrial and cytosolic fractions were verified by immunoblotting with VDAC and Hsp70, respectively (**Fig. 1D**). To ensure that the C4F6 antibody was indeed able to recognize $SOD1^{G93A}$ protein and oxidized wild-type protein as published, we treated recombinant mutant and wild-type SOD1 protein with $H_2O_2$, as previously described [244]. As a control, we also treated the recombinant proteins with Ethylenediaminetetraacetic acid (EDTA), another agent which has been previously published to provoke SOD1 misfolding, presumably via chelation of the zinc co-factor that is necessary for the structural integrity of SOD1 [243]. Note, this method also likely chelates the copper which is required for dismutase activity, but is not considered essential for SOD1 toxicity [209]. In agreement with previously published data, the C4F6 antibody robustly detects recombinant $SOD1^{G93A}$ protein and $H_2O_2$ treated wild type protein, albeit with much lower affinity to the latter. (Note the increased exposure time of immunoblots for recombinant $SOD1^{WT}$ compared to recombinant $SOD1^{G93A}$ protein). C4F6 had only minor reactivity for untreated and EDTA-treated wild-type protein, confirming the published specificity of this antibody for $SOD1^{G93A}$ mutant protein and oxidized wild-type protein (**Fig. 1C**). Collectively, these data suggest that these two antibodies recognize distinct SOD1 conformers with B8H10, but not C4F6, recognizing a conformer that demonstrates enhanced association with mitochondria.

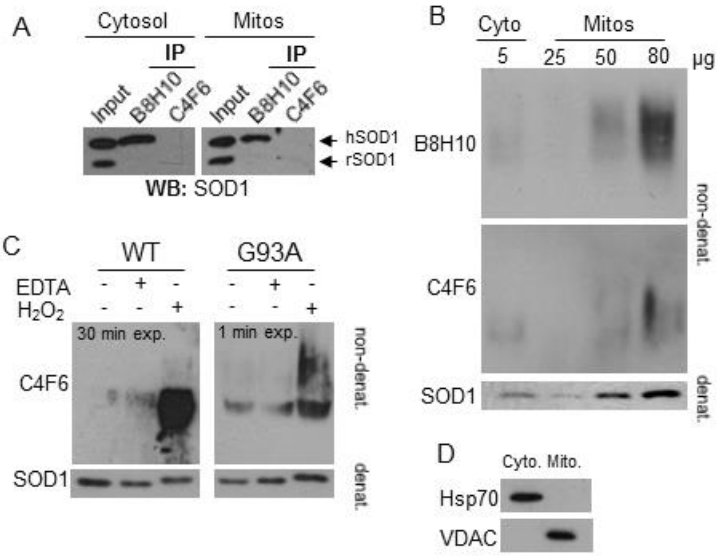


**Figure 1: Preferential detection of B8H10 reactive misfolded SOD1 associated with mitochondria**. The capacity of B8H10 and C4F6 antibodies to detect misfolded SOD1 was compared using mitochondrial and cytosolic protein fractions isolated from spinal cord of symptomatic $SOD1^{G93A}$ rat or recombinant SOD1 using different conditions. A) Immunoprecipitation of cytosolic or mitochondrial fractions from a symptomatic $SOD1^{G93A}$ rat with B8H10 or C4F6 misfolded SOD1 specific antibodies and blotted for SOD1. Input is 2 µg of each fraction. Upper and lower bands corresponds to human (hSOD1) and rat SOD1 (rSOD1), respectively. Experiment shown is representative of three independent trials. B) Non-denaturing gel of cytosolic fraction (5 µg) or increasing amounts of the mitochondrial fraction (25, 50 and 80 µg) blotted with misfolded specific antibodies B8H10 and C4F6. *Bottom*: Denaturing gel showing total amount of SOD1 present. Experiment shown is representative of three independent trials. C) Non-denaturing gel of recombinant SOD1 proteins (6 µg) treated with EDTA or $H_2O_2$, to demonstrate specificity of C4F6 antibody for $SOD1^{G93A}$ protein and oxidized

$SOD1^{WT}$ protein. Note the specificity of the C4F6 antibody for $SOD1^{G93A}$ protein (1 minute exposure) compared to labelling of $SOD1^{WT}$ protein (30 minute exposure). *Bottom*: Denaturing gel showing total SOD1 present. D) Immunoblotting of cellular fractions for VDAC and Hsp70 confirmed identity of mitochondrial and cytosolic fractions, respectively.

### 3.4.2. Immunodetection of mitochondrial-bound misfolded SOD1 by flow cytometry

Misfolded SOD1 associates with the mitochondrial surface of spinal cord mitochondria [233, 234]. We hypothesized that the presence of misfolded SOD1 may negatively affect key aspects of mitochondrial function. Given the prominence of a B8H10-reactive misfolded SOD1 species associated with $SOD1^{G93A}$ rat spinal cord mitochondria, we exploited this property to develop a quantitative flow cytometric assay whereby the function of mitochondria bearing misfolded SOD1 could be directly and selectively assessed using fluorescent immunodetection with B8H10 coupled with indicator dyes. In this assay, isolated mitochondria derived from the spinal cords of $SOD1^{G93A}$ rats, are first selected/gated according to light scattering properties (**Fig. 2A**). Secondly, mitochondrial identity is confirmed via positive labelling with the mitochondria-specific, membrane potential independent fluorescent probe MitoTracker Green (MTG; **Fig. 2B**). These criteria demonstrate that 92.3 ± 1.5% (n=13) of collected events represent mitochondria. Of this mitochondrial population, selected based on MTG labelling, the B8H10 antibody selectively identifies a subset of spinal cord mitochondria with surface-bound misfolded SOD1 ($B8H10^{+}$) in samples from symptomatic $SOD1^{G93A}$ rats but not age-matched transgenic $SOD1^{WT}$ rats which express comparable total levels of human $SOD1^{WT}$ protein, or non-transgenic littermates (**Fig. 2C**). Analysis of multiple similarly-aged animals indicates that 14.5 ± 0.6% of $SOD1^{G93A}$ spinal cord mitochondria label positively for B8H10, while only 0.6 ± 0.1% and 0.5 ± 0.1% are detected in $SOD1^{WT}$ and non-transgenic rats, respectively (**Fig. 2D**). Importantly, preparations of liver mitochondria from the same $SOD1^{G93A}$ animals exhibited negligible levels of misfolded SOD1 labelling (0.5 ± 0.2%; $p<0.0001$, n=3 animals per genotype). Misfolded SOD1 was also minimal in liver mitochondria from $SOD1^{WT}$ (0.6 ± 0.2%)

and non-transgenic rats (0.4 ± 0.1%) (**Fig. 2D**). Collectively, these data establish a novel cytofluorometric assay to detect misfolded SOD1 and are in agreement with previous work documenting the association of misfolded SOD1 to be preferentially enriched on spinal cord mitochondria [233, 234].

### 3.4.3. The deposition of misfolded SOD1 onto spinal cord mitochondria is age-dependent and occurs just prior to disease onset

Previous work using immunoprecipitation and immunofluorescence demonstrated qualitatively that misfolded SOD1 is associated with mitochondria in late-staged/symptomatic ALS animals [233, 234, 310]. In order to refine these observations, we used B8H10 detection via flow cytometry to quantitatively assess the amount and kinetics of misfolded SOD1 deposition on the surface of spinal cord mitochondria in the $SOD1^{G93A}$ rat model. We analyzed spinal cord and liver preparations from 36 animals spanning pre-symptomatic to symptomatic stages (8-18 weeks) (**Fig. 2E**). In our cohort, misfolded SOD1 was appreciably detected on the surface of spinal cord mitochondria starting at 14 weeks, with a progressive age-dependent increase in the percentage of spinal cord mitochondria labelling for B8H10 over time (**Fig. 2E**). Misfolded SOD1 was not significantly detected on the surface of liver mitochondria from the same animals (**Fig. 2E**). Using a least square regression model, age was determined to have a significant effect on the association of misfolded SOD1 to spinal cord mitochondria ($p<0.0001$), but not liver mitochondria ($p<0.6227$).

By monitoring our colony with biweekly measurement of body weight and observation of clinical/phenotypic disease behaviour, we determined that the deposition of misfolded SOD1 onto mitochondria occurs just prior to disease onset, as defined by peak body weight (**Fig. 2F**).

This definition is objective and reliable, having been applied in other ALS animal models [426]. At the time of disease onset, animals display a normal gait, normal hindlimb spread reflex, and have full motility. In our $SOD1^{G93A}$ rat colony, onset was observed at 15.3 weeks (107 ± 1.5 days, n=43) while the symptomatic stage, as determined by observation of gait defects, including limping or hopping, occurs at 18.0 weeks (126 ± 1.8 days, n=42) (**Fig. 2G**). These data demonstrate that misfolded SOD1 is associated with the surface of spinal cord mitochondria just prior to disease development in the $SOD1^{G93A}$ rat model. The timing of misfolded SOD1 association to mitochondria may suggest its involvement in disease onset.

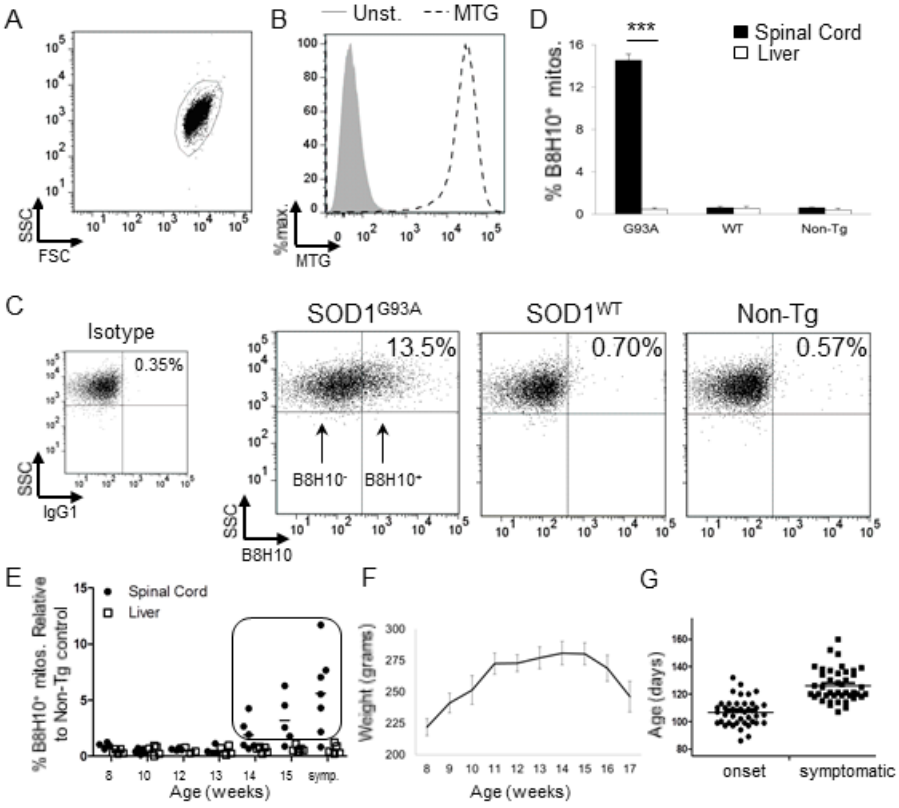


**Figure 2: Detection of mitochondrial-bound misfolded SOD1 by flow cytometry.** Mitochondria were isolated from spinal cord and liver of SOD1$^{G93A}$, SOD1$^{WT}$ and non-transgenic rats and characterized by flow cytometry. A) Isolated mitochondria are first gated by size (forward side scatter, FSC) and granularity (side scatter, SSC). B) Mitochondria are then selected by staining with MitoTracker Green (MTG, black, dashed) a mitochondrial specific dye, compared to unstained control (grey, filled). C) Mitochondria that label positive for B8H10 (B8H10$^{+}$), compared to background labelling with isotype control (IgG1), are selected and mitochondrial function of the two-subpopulations (B8H10$^{+}$ vs. B8H10$^{-}$) can then be compared. D) Quantification of B8H10$^{+}$ mitochondria derived from spinal cord (black) or liver (white) of symptomatic SOD1$^{G93A}$ rats (18.0 ± 1.1 weeks) and age-matched SOD1$^{WT}$ (17.6 ± 0.8 weeks) and non-transgenic rats (16.9 ± 0.9 weeks). Data is represented as percentage of B8H10$^{+}$

mitochondria (mean ± SEM), n=3 animals per genotype and tissue, *** $p < 0.0001$. E) By flow cytometry the amount of mitochondria labelled with the B8H10 antibody increases over time in spinal cord (black circle), but not liver (white square) samples derived from $SOD1^{G93A}$ rats. Animals with greater than 1% of mitochondria labelling positive for B8H10 (boxed) were included in the functional analysis. n=4-7 animals per time point. F) Weight curve of $SOD1^{G93A}$ females rats were weighed and evaluated bi-weekly (n=4-10 per time point). G) Disease onset and symptomatic phase for all $SOD1^{G93A}$ rats used in this study. In our colony, onset of disease, as defined by reaching peak body weight, corresponds to 15.2 weeks (107 ± 1.5 days, n=43) and the appearance of symptoms, namely gait defects, occurred at 18.0 weeks (126 ± 1.8 days, n=42). Based on these observations the association of misfolded SOD1 with mitochondria begins prior to disease onset.

### 3.4.4. B8H10$^{+}$ mitochondria have disrupted mitochondrial volume homeostasis

Animals displaying B8H10$^{+}$ labelling of ≥1% of the total collected events, corresponding to a minimum of 1000 individual mitochondria, were included in subsequent functional analyses (**Fig. 2E**, *boxed points*). Specifically, subpopulations of mitochondria either coated with misfolded SOD1 (B8H10$^{+}$) or not (B8H10$^{-}$) were independently gated and compared for mitochondrial volume/size. Using flow cytometry, the intensity of light scattered at small angles from an incident laser beam, referred to as forward light scatter (FSC), is proportional to particle volume and thus can be used to estimate particle size [427, 428]. By this measurement, B8H10$^{+}$ mitochondria demonstrate an increased volume/size compared to B8H10$^{-}$ mitochondria within the same preparation (**Fig. 3A**). Quantification of the geometric means of FSC revealed that the B8H10$^{+}$ mitochondrial subpopulation was 1.5 to 2.0x larger than B8H10$^{-}$ mitochondria. This observation was present at 14 weeks, the earliest time point where mitochondria labelled positive for B8H10-reactive misfolded SOD1 and persisted throughout the course of the disease (**Fig. 3B**; $p<0.0001$). These data were confirmed with the mitochondrial-specific and potential-independent dye MitoTracker Green where increased mean fluorescent intensity (ΔMFI) reflects increased mitochondrial uptake of the dye which positively correlates with volume [429] (**Fig. 3C**). Starting at 14 weeks, B8H10$^{+}$ mitochondria displayed ~3.0x higher ΔMFI, a measure of the average fluorescent intensity of each mitochondrion, compared to B8H10$^{-}$ mitochondria (**Fig. 3D**; $p<0.0001$). Overall, these results show that mitochondria bearing misfolded SOD1 have a greater mitochondrial volume compared to their counterparts not carrying such protein.

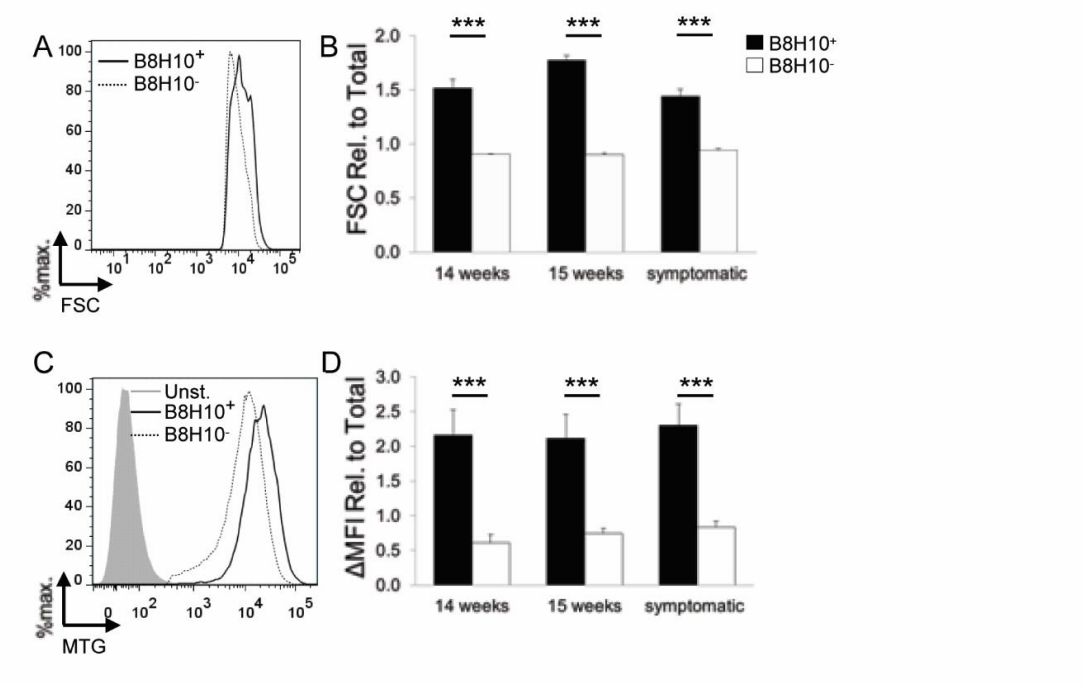


**Figure 3: Mitochondria with misfolded SOD1 associated have a greater mitochondrial volume.** Mitochondria isolated from spinal cords of $SOD1^{G93A}$ rats at different time points were characterized by flow cytometry. A) Representative histogram of FSC of $B8H10^{+}$ mitochondria (solid line) versus $B8H10^{-}$ mitochondria (dotted line) of a symptomatic $SOD1^{G93A}$ rat B) Quantitation of geometric mean of FSC of $B8H10^{+}$ mitochondria (black) and $B8H10^{-}$ mitochondria (white) relative to total population (mean ± SEM) at 14 and 15 weeks of age and symptomatic $SOD1^{G93A}$ rats. C) Representative histogram of $B8H10^{+}$ (solid line) and $B8H10^{-}$ (dotted line), mitochondria stained with MTG, compared to unstained control (grey, filled). D) Delta mean fluorescent intensity (ΔMFI) of MTG staining of mitochondrial sub-populations relative to total population (mean ± SEM). *** $p < 0.0001$

### 3.4.5. B8H10$^+$ mitochondria produce excessive superoxide in the absence of depolarization

Our method of surface labelling isolated mitochondria does not include membrane permeabilization and thus preserves mitochondrial integrity. Thus, this methodology permits the use of membrane-permeable fluorescent indicators dyes to assess key features of mitochondrial function. Superoxide is a natural by-product of normal mitochondrial respiration arising from complexes I and III of the mitochondrial electron transport chain (ETC), being released asymmetrically to both sides of the inner membrane [352]. The superoxide released to the matrix-side is essentially trapped due to the inherent impermeability of the inner membrane to superoxide and is efficiently detected by the fast-reacting membrane-permeable fluorescent indicator dye MitoSOX Red. MitoSOX Red becomes fluorescent following reaction with superoxide [352, 430, 431] as demonstrated by increased fluorescence following treatment with the complex III inhibitor Antimycin A (**Fig. 4A**). To determine if mitochondrial superoxide levels are perturbed by the association of misfolded SOD1, we performed simultaneous B8H10 labelling and MitoSOX Red staining. A greater percentage of B8H10$^+$ mitochondria labelled with MitoSOX Red compared to B8H10$^-$ mitochondria (**Fig. 4B**). Beginning at the earliest time point at which B8H10$^+$ mitochondria were detected (14 weeks) and continuing to the symptomatic phase, an average of 1.9 times more B8H10$^+$ mitochondria demonstrated elevated superoxide production, even when data were normalized for the increased size of B8H10$^+$ mitochondria (**Fig. 4C**; $p<0.05$ and $p<0.01$). These data indicate that mitochondria coated with misfolded SOD1 produce excessive amounts of superoxide. Within the B8H10$^+$ population, a positive correlation was noted between enlarged mitochondria (high FSC) and elevated superoxide levels (**Fig. 4D**).

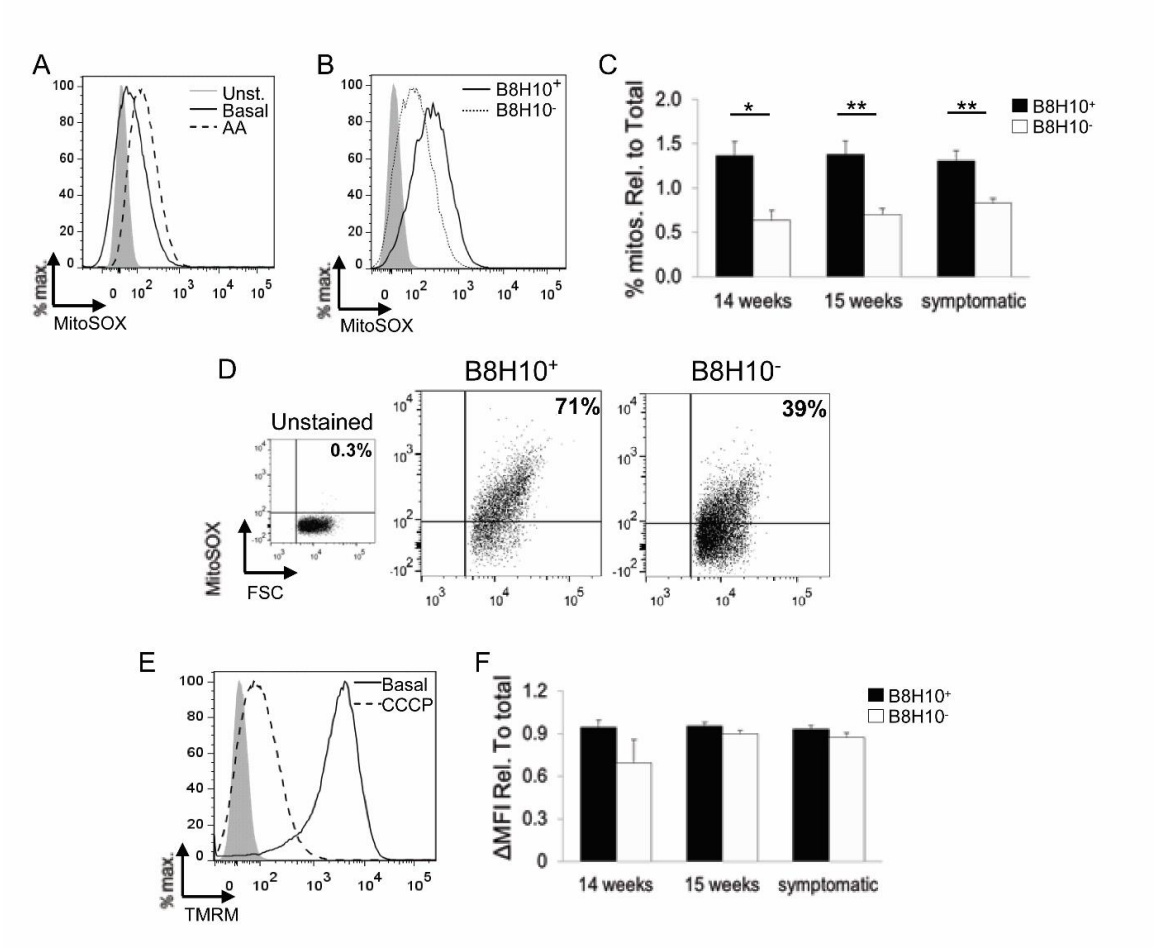


**Figure 4: Mitochondria with misfolded SOD1 associated exhibit an increased production of mitochondrial superoxide but retain a normal transmembrane potential.** Mitochondria isolated from spinal cord of $SOD1^{G93A}$ at different time points were characterized by flow cytometry for superoxide production and mitochondrial transmembrane potential. A) Mitochondrial superoxide can be assayed with MitoSOX Red. Addition of the complex III inhibitor Antimycin A (AA) causes an increase in superoxide production (dashed line), compared to basal levels (solid line), and unstained control (grey, filled). B) Representative histogram of mitochondrial superoxide production of $B8H10^{+}$ (solid line) and $B8H10^{-}$ (dashed line) mitochondria from the spinal cord of a symptomatic $SOD1^{G93A}$ rat. C) Quantification of

percentage of MitoSOX$^{+}$ mitochondria in the B8H10$^{+}$ (black) and B8H10$^{-}$ (white) populations, relative to MTG staining and the total mitochondrial population. D) Representative dot plots demonstrating that the B8H10$^{+}$ population has a higher percentage of larger mitochondria (as determined by FSC) that produce excessive mitochondrial superoxide (as measured by MitoSOX Red). E) Histogram demonstrating that mitochondrial transmembrane potential can be assayed with TMRM. Under basal conditions almost all mitochondria stain positive for TMRM (solid line), but transmembrane potential is dissipated with the addition of the protonophore CCCP (dashed lined). F) Quantification of ΔMFI of TMRM staining of B8H10$^{+}$ and B8H10$^{-}$ mitochondria relative to MTG staining and the total mitochondrial population. * $p < 0.05$; ** $p < 0.01$.

Mitochondrial transmembrane potential ($\Delta\Psi_m$) refers to the separation of charge across the inner mitochondrial membrane and is essential to drive ATP production via oxidative phosphorylation. Isolated spinal cord mitochondria were simultaneously labelled for misfolded SOD1 with B8H10 antibody and stained with tetramethylrhodamine (TMRM). TMRM is a cationic dye that rapidly and reversibly equilibrates across the mitochondrial membrane in a voltage-dependent manner according to the Nernst equation [432]. This can be demonstrated by treatment with the potent protonophore, Carbonyl cyanide *m*-chlorophenyl hydrazone (CCCP) which results in a significant dissipation of $\Delta\Psi_m$ (**Fig. 4E**). While disturbances in ROS production are often linked to mitochondrial depolarization [433], we observed $\Delta\Psi_m$ to be comparable between B8H10 sub-populations when data are normalized for size (**Fig. 4F**). These observations indicate that mitochondria carrying misfolded SOD1 have normal membrane potential. Conversely, superoxide production is increased suggesting that targeted mitochondrial damage tracks with the mitochondrial association of misfolded SOD1.

### 3.4.6. Increased exposure of Bcl-2 BH3 domain in mitochondria coated with misfolded SOD1

It has recently been proposed that mutant SOD1 damages mitochondria by inducing a conformational change in the anti-apoptotic protein Bcl-2 [382]. Specifically, the binding of mutant SOD1 to Bcl-2 results in its conversion into a pro-apoptotic protein due to exposure of the normally hidden BH3 domain. Using our flow cytometry assay, we performed simultaneous antibody labelling for misfolded SOD1 and the toxic BH3 domain of Bcl-2 on spinal cord mitochondria of $SOD1^{G93A}$ rats. Labelling for the BH3 domain of Bcl-2 was low in the total mitochondrial population as illustrated by a representative animal (**Fig. 5A,** 2.7 ± 0.5%, n=3),

However, analysis of B8H10$^{+}$ mitochondria demonstrated a 10-fold enrichment for the toxic BH3 domain of Bcl-2 (27.9 ± 3%) compared to B8H10$^{-}$ mitochondria which demonstrated negligible BH3 labelling (0.8 ± 0.3%) (**Fig. 5B, C**; $p<0.01$). Thus, spinal cord mitochondria coated with misfolded SOD1 are enriched for Bcl-2 protein in a toxic conformation.

### 3.4.7. B8H10 labels misfolded SOD1 within motor neurons prior to gliosis and clinical disease

In an effort to determine the cellular origin of the mitochondria detected by our flow cytometric assay, we performed immunofluorescent labelling with B8H10 of lumbar spinal cord sections of a similar time course of SOD1$^{G93A}$ rats. Here, B8H10 extensively labels motor neurons identified by ChAT staining starting at 14 weeks (**Fig. 6A**, *top row*), in agreement with previous work in mice [243]. Moreover, B8H10 labelling was evident prior to astrogliosis and microglial activation, as marked by IbaI and GFAP, respectively (**Fig. 6B**, **C**). Counts of lumbar motor neurons using cresyl violet staining (**Fig. 6D**) demonstrated a loss of 47% of motor neuron cell bodies at the symptomatic stage, corresponding to approximately 18.0 weeks (**Fig. 6E;** $p=0.0207$) but not at 14 and 15 weeks, time points at which elevated B8H10 staining is observed. Taken together, B8H10 deposition on motor neuron mitochondria occurs prior to key pathological features of disease, including motor neuron loss and glial activation.

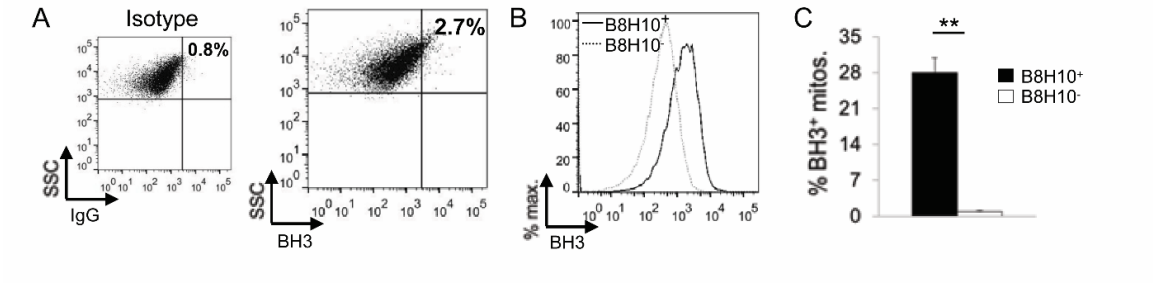


**Figure 5: Increased Bcl-2 BH3 domain exposure on mitochondria bearing misfolded SOD1.** A) Representative dot plot of spinal cord mitochondria from a symptomatic $SOD1^{G93A}$ rat labelled with a Bcl-2 antibody specific for the BH3 domain. The population labelling positive for exposure of the BH3 domain ($BH3^+$, 2.7 ± 0.5%, n=3), was assessed in comparison to the isotype control (0.8 ± 0.01%) and represented as mean ± SEM. B) Mitochondria were also labelled with the B8H10 antibody. A representative histogram reveals that the $B8H10^+$ (solid line) population has a higher amount of $BH3^+$ mitochondria compared to the $B8H10^-$ (dashed line) population. C) Quantification of $BH3^+$ mitochondria from $B8H10^+$ (black) and $B8H10^-$ (white) mitochondria, (mean ± SEM, n=3). ** $p< 0.01$.

### 3.4.8. Dysfunction of B8H10$^{+}$ mitochondrial subset in a second SOD1 model

To demonstrate that the reported observations are common in ALS pathogenesis, and not confined to the SOD1$^{G93A}$ rat model, we also examined a time course of *Lox*SOD1$^{G37R}$ mice. These mice develop nearly identical muscle atrophy, motor neuron loss, and gliosis but on an extended time span of ~12 months [265]. Using these mice, we demonstrate a similar time-dependent deposition of misfolded SOD1, as detected by B8H10, on the surface of SOD1$^{G37R}$ spinal cord mitochondria (**Fig. 7A**). Moreover, B8H10$^{+}$ labelling positively correlates with increased mitochondrial volume (**Fig. 7B, C**; $p<0.0001$) and excess superoxide production (**Fig. 7D**) to similar degrees as observed in SOD1$^{G93A}$ rats (FSC: 1.8-fold, MTG ΔMFI: 2.2-fold and% of MitoSOX Red$^{+}$ mitochondria: 1.5-fold), indicating that these are common features of mitochondrial damage in mutant SOD1 ALS models. Importantly, in *Lox*SOD1$^{G37R}$ mice, these changes occurred as early as 8 months, a point at which animals are clearly pre-symptomatic and lack any overt pathogenic changes (36). Due to mouse sample limitations, we were unable to assess mitochondrial polarization status. B8H10-reactive misfolded SOD1, and its ability to identify dysfunctional mitochondria, are a common feature of two ALS rodent models.

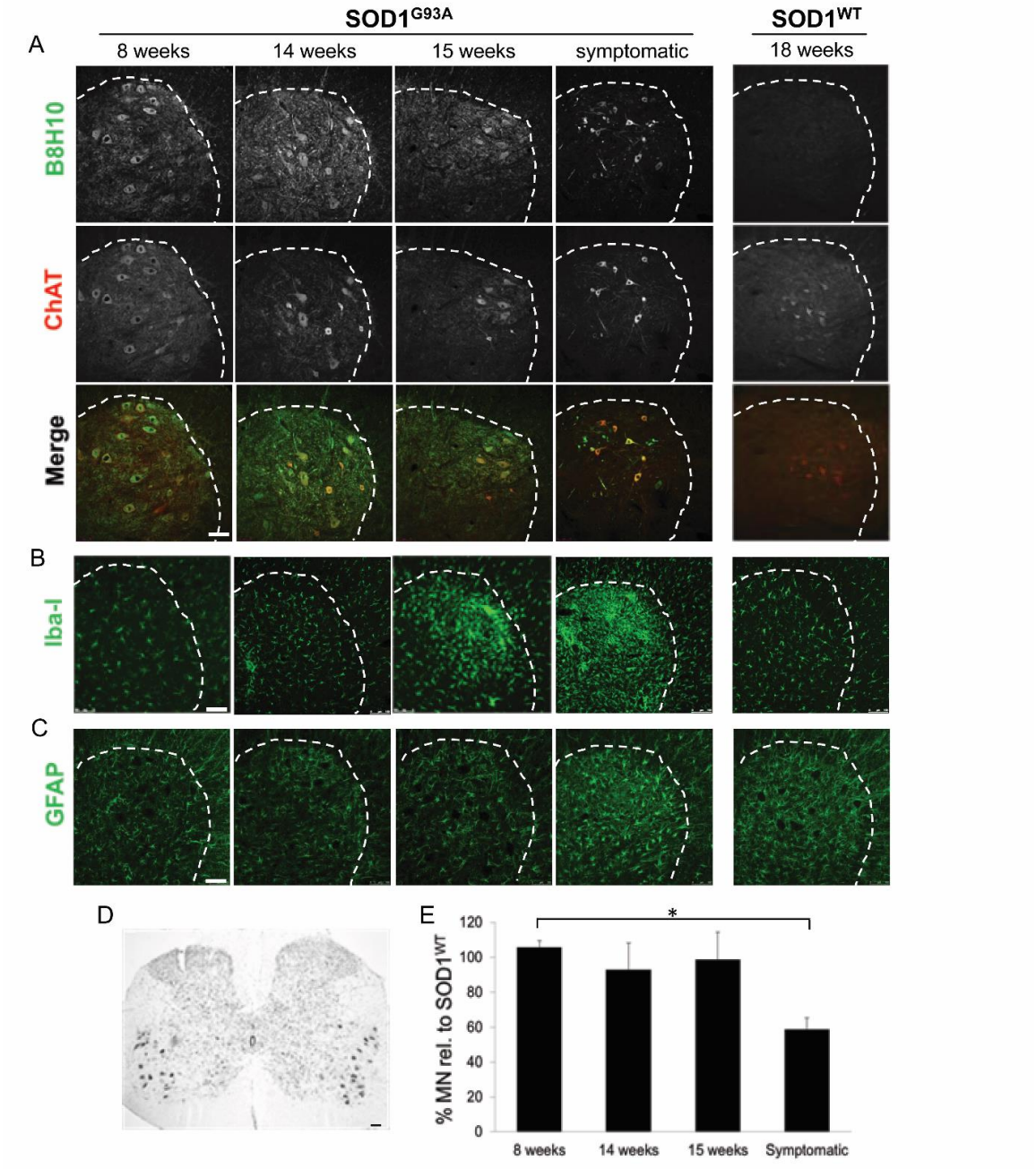


**Figure 6: Accumulation of misfolded SOD1 in motor neurons begins prior to gliosis and motor neuron loss.** Immunohistochemical analysis of SOD1$^{G93A}$ and SOD1$^{WT}$ rat spinal cords at different time points. Transverse sections of the lumbar spinal cord were stained and analyzed

accordingly. A) Sections were stained with anti-B8H10 (green) and co-labelled with ChAT (red) demonstrating presence of misfolded SOD1 in motor neurons beginning at 14 weeks. B) Sections were stained with anti-Iba-I (marker of macrophages/microglia) or C) anti-GFAP (astrocyte marker) to assess activation of microglia and astrocytes, respectively. D) Representative image of spinal cord sections stained with cresyl violet. E) Motor neurons in the anterior horn were counted and averaged per section (mean ± SEM, n=3-5 per group). Scale bar = 100 μm. * $p < 0.05$.

### 3.4.9. B8H10 immunoreactivity in ALS patient cells

Transformed lymphoblastoid cell lines derived from five ALS patients expressing four different SOD1 mutations (H48Q, D83G, G93V, and I113T) were analyzed on non-denaturing gels for the presence of misfolded SOD1. B8H10 positively identified misfolded SOD1 to differing extents in five patient cell lines while no signal was detected in cells derived from three healthy controls (**Fig. 8A**). Eight additional controls were screened to verify that the B8H10 signal was in fact due to misfolded mutant SOD1, and indeed no B8H10 reactivity was detected (**Fig. 8B**). We also analyzed ten sporadic ALS patient cells but, if B8H10-reactive misfolded SOD1 is present in these lines, it was below the level of detection (**Fig. 8C**). To assess if B8H10-reactive misfolded SOD1 was associated with mitochondria in this cell type, mitochondria were magnetically isolated and immunoblotted for the presence of misfolded SOD1 with B8H10. Magnetic bead isolation avoids any potential artefact from co-sedimenting aggregates. Indeed mitochondria from patients with SOD1 mutations labelled modestly for B8H10, while mitochondria isolated from a healthy individual did not (**Fig. 8D**). However, the amount of misfolded SOD1 on mitochondria appeared to be insufficient to induce any appreciable elevation in superoxide production when measured on the whole population (data not shown).

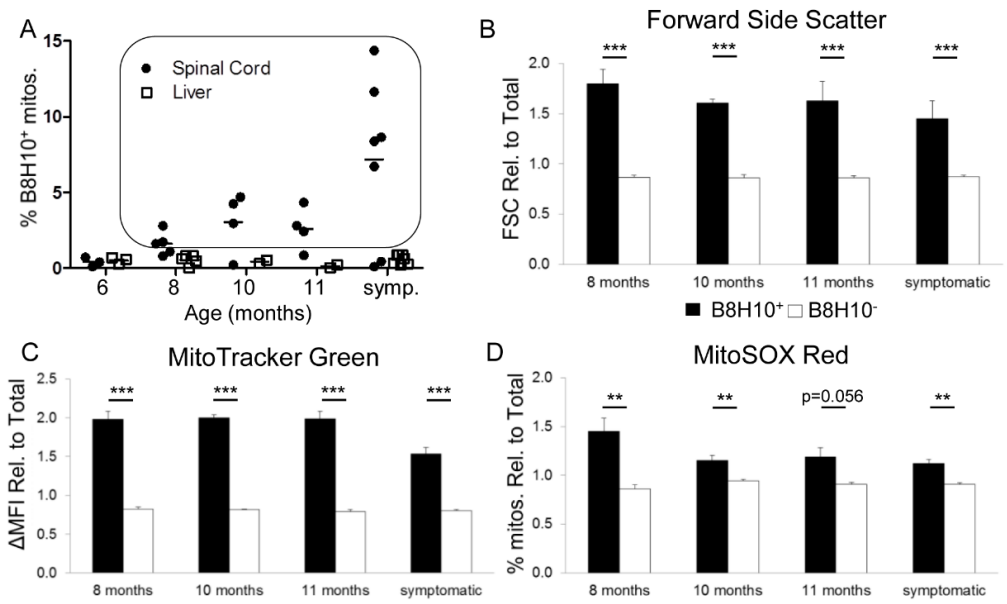


**Figure 7: Mitochondrial-associated misfolded SOD1 tracks with mitochondrial damage in SOD1$^{G37R}$ mouse model**. A) The number of spinal cord (black circle), but not liver (white square) mitochondria that label positive for B8H10 increases with age. Each dot represents an individual mouse. Animals with greater than 1% of mitochondria labelling positive for B8H10 (within black box) were included in the functional analysis. B) Quantification of the geometric mean of FSC of B8H10$^{+}$ mitochondria (black) and B8H10$^{-}$ mitochondria (white) relative to the total population. C) Quantification of ΔMFI of MTG of B8H10$^{+}$ mitochondria and B8H10$^{-}$ mitochondria relative to the total population. D) Quantification of the percentage of MitoSOX$^{+}$ mitochondria in each mitochondrial sub-population relative to the total population. * $p < 0.05$, ** $p < 0.01$, *** $p < 0.0001$.

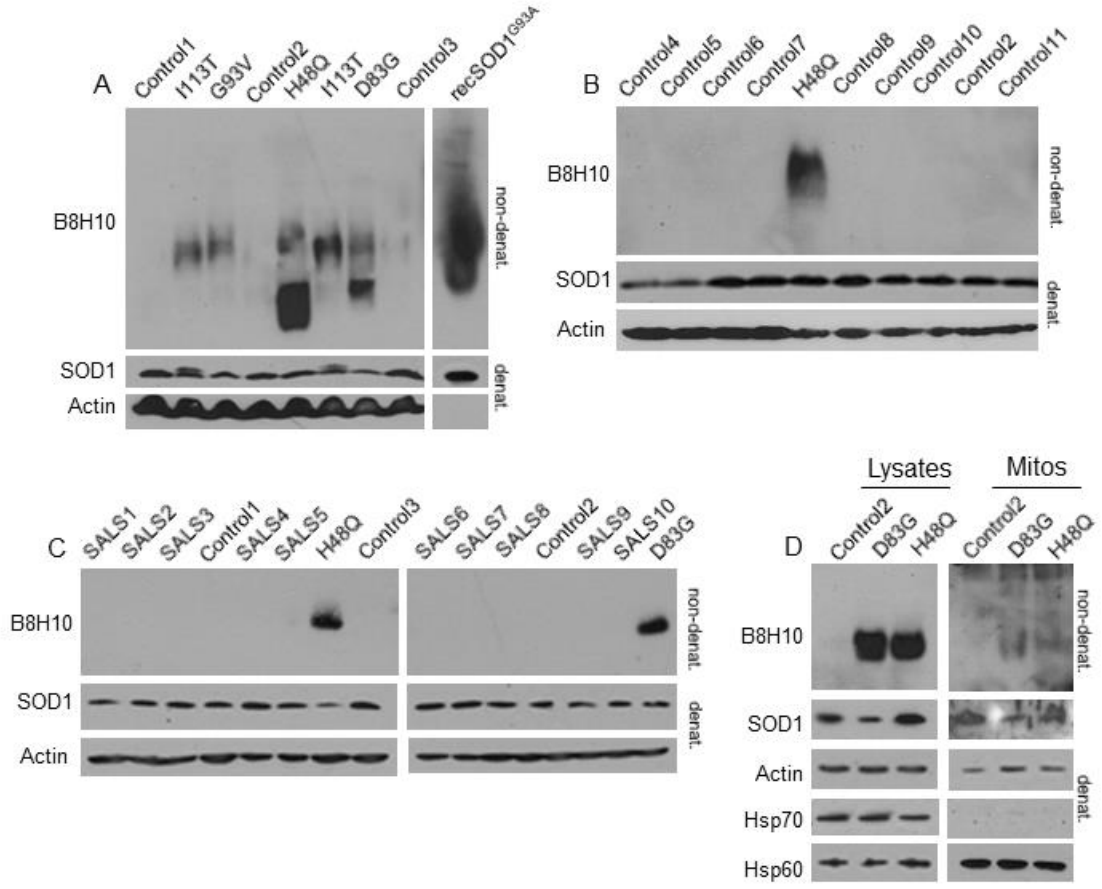


**Figure 8: Misfolded SOD1 detection in ALS patient cells.** Cell lysates were prepared from lymphoblastoid cell lines derived from healthy controls, non-ALS disease controls, sporadic ALS patients or familial ALS patients identified with SOD1 mutations and screened for B8H10-reactive SOD1. A) Non-denaturing gel of lysates from healthy controls (control1-3), and ALS patients identified with SOD1 mutations (H48Q, D83G, G93V, and I113T) were tested for reactivity with the B8H10 antibody targeted against misfolded SOD1. Recombinant SOD1$^{G93A}$ protein (100 ng) served as a positive control to verify detection of misfolded SOD1. *Bottom*: Denaturing gel blotted for total SOD1 and Actin served as loading controls. B) Healthy controls

(2) and non-ALS diseased controls (1 individual with insomnia, 2 individuals with obsessive compulsive disorder and 4 individuals with sleeping disorders) were screened for B8H10-reactive misfolded SOD1. *Bottom*: Denaturing gel blotted for total SOD1 and Actin served as loading controls. C) Sporadic ALS patients (SALS1-10) were screened for B8H10-reactive misfolded SOD1. Mutant SOD1 patients (H48Q and D83G) and three controls are included as positive and negative controls, respectively, for the B8H10 antibody. *Bottom:* Denaturing gel blotted for total SOD1 and Actin served as a loading control. D) Isolated mitochondria from one healthy control and two ALS patients carrying SOD1 mutations (D83G and H48Q) were probed for B8H10 reactivity on non-denaturing gels. *Bottom:* Denaturing gel blotted for total SOD1, Hsp70 and Hsp60 which serve as controls for the cytoplasmic and mitochondrial fractions respectively. Actin serves as a loading control.

Regardless, these data highlight that the association of misfolded SOD1 to mitochondria is central to ALS as it is found in both rodent models and human patient material.

### 3.5. Discussion

Our *ex vivo* analysis of $SOD1^{G93A}$ rat spinal cord mitochondria with surface bound misfolded SOD1 ($B8H10^{+}$) reveal several aspects of mitochondrial dysfunction that correlates positively with disease. Using a novel quantitative approach, we report that $B8H10^{+}$ mitochondria exhibit increased volume compared to their $B8H10^{-}$ counterparts, have elevated superoxide levels, and enhanced exposure of the toxic BH3 domain of Bcl-2. Increased mitochondrial volume could arise from either mitochondrial swelling or increased mitochondrial fusion. Our findings that mutant/misfolded SOD1 associates with increased mitochondria volume are in line with histological examination of the spinal cords of ALS patients [301] and mutant SOD1 transgenic animals [307, 309, 310, 434], where swollen and aggregated mitochondria have been observed. Similarly, neuron-like cell lines and primary motor neurons also exhibit swollen mitochondria following mutant SOD1 expression (8,40,41). In our previous studies, we found significant morphological changes of motor neuron mitochondria in both axons and cell bodies [310]. The significance of this increased volume/size is unclear but could be due to defects in ionic homeostasis causing mitochondrial swelling, altered fission/fusion dynamics causing larger mitochondria, or defective autophagy, resulting in the inability to clear large or swollen mitochondria.

In support of ionic homeostasis dysfunction, VDAC1 conductance is reportedly impaired by mutant SOD1, effectively disrupting normal ionic homeostasis [233]. However, it has also been reported that mutant SOD1 is associated with spinal cord mitochondria even in

the absence of VDAC1 [346]. Also, given that the genetic deletion of VDAC1 in the *Lox*SOD1$^{G37R}$ background yielded an accelerated disease phenotype, it is unclear how VDAC1 is a required mediator of misfolded SOD1 toxicity [233]. The model proposed by Israelson and colleagues predicts that altered VDAC conductance will decrease metabolites entering the mitochondria, resulting in decreased ATP synthesis and a depolarization of mitochondrial transmembrane potential [233]. However, we find mitochondrial transmembrane potential of isolated mitochondria to be unaffected by the presence of misfolded SOD1 (Fig. 4) and ATP synthesis is reported to be unchanged [346]. While there is clearly some ambiguity about the importance of VDAC in disease pathogenesis, it is noteworthy that in liver mitochondria, increased mitochondrial superoxide can be triggered by VDAC closure [435]. Moreover, VDAC has been shown to regulate the release of mitochondrial superoxide to the cytosol in certain cases [436, 437]. Additional experiments will be needed to resolve this issue.

A previous report using human neuroblastoma cells overexpressing various SOD1 mutations documented increased superoxide levels but the mechanisms involved were not identified [353]. From our analysis of mitochondria isolated from mutant SOD1 animal models, we find that misfolded SOD1 bearing mitochondria specifically produce very high levels of superoxide weeks before disease onset (Fig. 4 and 7). Mitochondria are the principle cellular generators of ROS and mitochondria are equipped with a mitochondrial superoxide dismutase (SOD2) to detoxify superoxide generated by mitochondria. While SOD2 can attenuate toxicity in cell culture [353], the role of SOD2 in mutant SOD1 mouse models is less clear [438]. However, the mitochondrial redox system has been strongly implicated in ALS. In cell culture, SOD1 mutant proteins were found to associate with mitochondria and causes a shift to an

oxidizing redox environment [347]. Recently, mutant SOD1 was shown to activate p66Shc, a protein involved in controlling mitochondrial redox in neuronal-like cells [439].

We also examined whether the presence of misfolded SOD1 on mitochondria correlated with the conversion of Bcl-2 to a toxic conformation. In our experiments, we demonstrate for the first time that a robust proportion of mitochondria bearing misfolded SOD1 exhibit positive labelling for the BH3 domain of Bcl-2. Although this is not a direct test of an interaction between Bcl-2 and misfolded SOD1, it is compatible with the view that exposure of Bcl-2's BH3 domain is deleterious to mitochondrial function [382], as we demonstrate that $B8H10^{+}$ mitochondria are functionally impaired compared to their $B8H10^{-}$ counterparts. Interestingly, *in vitro* experiments have shown that glutathione interacts with Bcl-2 in the BH3 groove, as BH3 mimetics disrupt this interaction [440]. BH3 mimetics also disrupt mitochondrial glutathione levels and decrease the ability of isolated mitochondria to import glutathione [440]. That we find both increased levels of the toxic BH3-exposed Bcl-2 conformer and increased superoxide suggests that misfolded SOD1 may cause an alteration in mitochondrial redox causing increased levels of superoxide *in vivo*.

For the first time we show *in vivo* that misfolded SOD1 association to mitochondria correlates positively with increased mitochondrial volume, superoxide production, and the presence of a toxic conformer of Bcl-2. Although our methods are currently unable to differentiate if misfolded SOD1 directly causes the damage or is recruited to mitochondria following damage, both scenarios are possible, and are currently under evaluation in our lab. For misfolded SOD1 as the cause, over expression of mutant SOD1 in cell culture has been shown to associate with mitochondria and cause increased ROS production [353].

We place the deposition of misfolded B8H10$^{+}$ SOD1 onto the mitochondrial outer membrane as early as 14 weeks in the SOD1$^{G93A}$ rat and 8 months in SOD1$^{G37R}$ mice, which is prior to disease onset. Our analysis of pathological hallmarks in the rat model shows that misfolded SOD1 protein is robustly detected within the motor neurons of the ventral spinal cord at time points prior to gliosis and significant motor neuron loss. Levels of mitochondrially associated misfolded SOD1 peak at the symptomatic stage, despite the loss of motor neurons, and decreased B8H10 immunoreactivity in spinal cord sections. This is consistent with a previous report in SOD1$^{G93A}$ mice where misfolded SOD1, as detected by the misfolded SOD1 specific antibody D3H5, was increased in spinal cord despite motor neuron loss [243]. This apparent paradox could be explained if the levels of misfolded SOD1 present in each individual cell increases over time, and this subsequently provokes misfolded SOD1 enrichment at the mitochondria. In support of this, it has been reported that that the level of human mutant SOD1 in the spinal cords of SOD1$^{G93A}$ rats increases in an age-dependent manner, peaking at end-stage [216]. Knowledge that mitochondrial damage occurs pre-symptomatically may be instrumental in deciding when misfolded SOD1 and/or mitochondrial-targeted therapeutics will be most efficacious. That diminution of B8H10-reactive SOD1 in the spinal cords of SOD1$^{G93A}$ mice following passive immunization with misfolded SOD1 antibody, clone D3H5, correlated positively with survival, suggests this form of misfolded SOD1 is intimately linked to the toxicity of mutant SOD1 [243]. We theorize that therapies aimed at decreasing B8H10-reactive misfolded could prevent or decrease its association with spinal cord mitochondria and subsequent mitochondrial damage.

Accumulating evidence suggests that misfolded SOD1 mediates ALS pathogenesis [243, 244]. However, the field fails to completely understand which biological pathways are disrupted

by the presence of these non-native SOD1 proteins. Our initial experiments guided us to select B8H10 for the mitochondrial function experiments, but also suggested that more than one form of misfolded SOD1 exists. This concept is supported by recent data from others [236, 408]. Here, using the $SOD1^{G93A}$ rat and $SOD1^{G37R}$ mouse model, we find B8H10-reactive misfolded SOD1 is associated with spinal cord mitochondria. In contrast, little C4F6-reactive SOD1 was detected in these same samples. Within our cohort, one symptomatic rat and two symptomatic mice exhibited mitochondria-associated B8H10-reactive misfolded SOD1 that was below our threshold. These outliers raise the question: if mitochondrial damage is central to disease, how can these animals which lack appreciable levels of misfolded SOD1 associated to the mitochondria, exhibit symptoms? We propose two possible hypotheses. First, mitochondrial damage may still be central to disease, if other conformers of misfolded SOD1 are also associated to mitochondria. Previous work has shown that at least three other misfolded SOD1 antibodies detect SOD1 at the mitochondria: SEDI [248], DSE2 [234], and A5C3 [310]. Alternately, there may be non-mitochondrial mechanisms of misfolded SOD1 toxicity. It has been demonstrated that the C4F6 antibody recognizes recombinant wild-type SOD1 oxidized by $H_2O_2$ [244]. In this same study, addition of oxidized wild-type SOD1 or mutant SOD1 altered axonal transport in a squid axoplasm model. Perfusion of the C4F6 antibody in this system corrected the axonal transport defect induced by oxidized/misfolded SOD1. Given this evidence, we feel it is likely that distinct SOD1 conformers may differentially influence cellular mechanisms. Specifically, B8H10-misfolded SOD1 links to mitochondrial-based modes of pathogenesis, while we propose that C4F6-misfolded SOD1 impacts axonal transport but not mitochondria.

Lastly, we detected B8H10-reactive misfolded SOD1 in patient-derived lymphoblasts, a cell type generally considered to be unaffected by disease. While the rationale of why misfolded SOD1 is detected in these cells is not readily apparent, it is consistent with work by others using the recently described MS785 antibody which demonstrates an altered SOD1 conformer [36] as well as another study indicating the presence of an over-oxidized SOD1 conformer [290] in these same cells. Combined with our data from ALS animal models, B8H10-reactive SOD1 is common to six different SOD1 mutations, emphasizing that this conformation of misfolded SOD1 may be especially relevant for SOD1-mediated toxicity. However, the amount of misfolded SOD1 detected on mitochondria from patient lymphoblasts was insufficient to induce any appreciable elevation in superoxide production when measured on the whole population raising the possibility that mitochondrial dysfunction and toxicity may be dependent on intrinsic cell type characteristics and/or the level of mitochondrial-associated misfolded SOD1. We speculate that long lived cells, such as motor neurons, may be predisposed to damage resulting from the association of misfolded SOD1 onto mitochondria, whereas rapidly turned over cells (e.g. cells in the liver) may not acquire sufficient levels of SOD1 association or are unaffected by such mitochondrial association (e.g. lymphoblast cells). Our data suggests this is plausible, given that the number of mitochondria carrying B8H10-reactive SOD1 increased with age in the animal models. As a final thought, while lymphoblasts may not be the appropriate cell type for mechanistic studies probing mitochondrial dysfunction in relation to misfolded SOD1, these cells are easily accessible and thus may offer a potentially useful way by which to monitor misfolded SOD1 levels, disease progression, efficacy of therapeutics and/or *a priori* selection of patients for particular clinical trials.

### 3.6. Materials and methods

*Animals:* SOD1$^{G93A}$ and SOD1$^{WT}$ transgenic rats and *Lox*SOD1$^{G37R}$ mice have been previously described [216, 265, 441]. In some experiments, non-transgenic littermates were used. SOD1$^{G93A}$ rats were monitored with biweekly weight measurements and observation. In order to limit the impact of genetic drift inherent to transgenic lines, all SOD1$^{G93A}$ rats used to breed the colony were maintained until end-stage in order to validate disease course and thus ensure that only progeny of animals which developed symptoms "on-time" were selected for subsequent breeding. Rats presenting with forelimb paralysis were eliminated from the colony and the study. Animals of both sexes were used. LoxG37R mice were also similarly followed and monitored for disease. Animals were treated in strict adherence with approved protocols from the CRCHUM Institutional Committee for the Protection of Animals and the Canadian Council on Animal Care (CCAC).

*Antibodies:* For Western Blot: human specific rabbit anti-SOD1 (Cell Signalling), rabbit anti-Cu/Zn SOD (Stressgen), mouse anti-VDAC1 (Calbiochem), mouse anti-Hsp70 (Chemicon) and mouse anti-Hsp60 (BD Biosciences) were used. For immunoprecipitation and native gels: misfolded SOD1 monoclonal antibody B8H10 (Medimabs and JP Julien lab), and misfolded SOD1 monoclonal antibody C4F6 (Medimabs) were employed. For flow cytometry, misfolded SOD1 monoclonal antibody B8H10 (Medimabs), mouse anti-IgG1 (BD Biosciences), rabbit anti-BH3 Bcl-2 antibody (Abgent) and rabbit IgG (Jackson ImmunoResearch) were purchased. For immunofluorescence, rabbit anti-IbaI (Wako) and rabbit anti-GFAP (Dako) were used.

*Flow cytometry of isolated mitochondria:* Spinal cord and liver mitochondria were isolated from mice and rats exactly as previously described [234]. Mitochondria (25 µg) were re-suspended in M Buffer (220 mM sucrose, 68 mM mannitol, 10 mM KCl, 5 mM $KH_2PO_4$, 2 mM

$MgCl_2$, 500 μM EGTA, 5 mM succinate, 2 μM rotenone, 10 mM HEPES pH 7.2, 0.1 % fatty acid-free BSA). For labeling with antibodies, mitochondria were first blocked with M buffer supplemented with 10% fatty acid-free BSA for 15 minutes at 4ºC. Mitochondria were then incubated with primary antibody for 30 minutes at 4ºC, washed once with M buffer, and then incubated with allyphycocyanin-conjugated fluorescent secondary antibody for 30 minutes at 4ºC. MitoTrackerGreen (MTG, 100 nM; Invitrogen) was used to confirm mitochondrial identity. Tetramethylrhodamine Methyl Ester (TMRM, 100 nM; Invitrogen) was used to assess mitochondria membrane potential ($\Delta\Psi_m$) and MitoSOX Red (MitoSOX, 5 uM; Invitrogen) to quantify mitochondrial superoxide. The protonophore carbonyl cyanide *m*-chlorophenyl hydrazone (CCCP, 100 μM; Sigma) was used as a control for $\Delta\Psi_m$ measurements, and the complex III inhibitor, Antimycin A (AA, 100 uM; Sigma) was used as a control for mitochondrial superoxide production. 100, 000 events were acquired on a LSR II flow cytometry (BD Biosciences). Mitochondria were gated according to light scatter, after doublets were excluded, then MTG staining and labelling with B8H10 were assessed. All flow cytometry data were analyzed with FlowJo (Treestar, Ashland, Oregon). Dyes and antibodies selected exhibited distinct spectral properties with minimal to no overlap. Where necessary, compensation was applied according to single-color control samples. CCCP and Antimycin A treated samples were included in every experiment to confirm that the dyes functioned as expected. An isotype control sample was also included in every experiment to ensure the specificity of the B8H10 antibody.

*Immunoprecipitation, immunoblotting, and native gel analysis:* Isolated mitochondria were solubilized and immunoprecipitated as previously described [234]. Samples for native gel analysis were prepared with 2X loading buffer (Invitrogen), separated by PAGE on 12% Tris-

Glycine Gels (Invitrogen) in running buffer (Invitrogen) and transferred to PVDF membrane (BioRad). Densitometry was performed with ImageJ. For denaturing gels, nitrocellulose was used.

*Immunofluorescence*. Animals were transcardially perfused with 4% phosphate-buffered paraformaldehyde (FD NeuroTechnologies). Tissues were subsequently dissected, post-fixed for 2 hours, cryoprotected, and then embedded in OCT (TissueTek). 30 μm floating spinal cord sections were cut from the lumbar region (L4-L6; corresponding to the lumbar enlargement) to make sure that all animals are adequately compared, and labelled with B8H10, Iba-I or GFAP, as previously described [243] or cresyl violet [442]. Immunofluorescent images were captured by confocal microscope (Leica SP5; 20x objective, 1.7 NA) and processed with Leica LAS AF software and/or PhotoshopCS4 (Adobe). Images of cresyl violet stained sections were captured on a Leica DM600B light microscope. Motor neurons, determined by size and location in ventral horn from twenty lumbar sections per animal were counted, spaced at 90μm intervals. 3-5 animals per group were evaluated.

*Patient cells:* Lymphocytes were isolated from peripheral blood samples using standard protocols and then immortalized with Epstein–Barr virus [443]. In all experiments, controls (four healthy donors, seven non-neurodegenerative donors (insomnia, sleeping disorders, obsessive-compulsive disorder), ten sporadic ALS, and mutant SOD1-ALS (H48Q, D83G, G93V, and two I113T) cells were thawed at the same time and cultured in Iscove's Modified Dulbecco's Medium supplemented with 10% FCS, 300 IU/mL penicillin, 300 μg/mL streptomycin, and 0.5% fungizone. Isolation of mitochondria from lymphoblasts was done using the Mitochondrial Isolation Kit (Miltenyi Biotec, Germany), as per the manufacturer's instructions. Protocols were approved by the ethics committee on human experimentation of the

Center Hospitalier de l'Université de Montréal. All patients gave written informed consent prior to collection of patient information and blood.

*Statistics:* Student's *t*-test was used to determine that B8H10 labelling of spinal cord mitochondria is significantly different from B8H10 labelling of liver mitochondria from $SOD1^{G93A}$ rats. A least square regression model was used to determine that time (age of animal) had an effect on misfolded SOD1 association to spinal cord, but not liver mitochondria in the $SOD1^{G93A}$ rat model. ANOVA was used to evaluate differences in $B8H10^{+}$ and $B8H10^{-}$ mitochondria subpopulations in rat and mouse models and motor neuron counts in 8 week and symptomatic rats. Student's *t*-test was also used to analyze differences in $B8H10^{+}$ and $B8H10^{-}$ mitochondrial subpopulation for BH3 labelling. * $p < 0.05$, ** $p < 0.01$ and *** $p < 0.0001$.

### 3.7. Acknowledgements

We thank C. Lobsiger, S. Boillée, P.A. Dion, H. McBride, and J. St-Pierre for valuable discussions; L. Hayward for baculoviruses, and A. Prat for access to the flow cytometer and confocal microscope. This work was supported by the Canadian Institutes of Health Research (CIHR) Neuromuscular Research Partnership, Canadian Foundation for Innovation, ALS Society of Canada, the Frick Foundation for ALS Research, CHUM Foundation, and Fonds de la Recherche en Santé du Québec (CVV). NA obtained a Donald Paty Career Development Award from the Multiple Sclerosis Society of Canada and both CVV and NA are Research Scholars of the Fonds de la Recherche en Santé du Québec and CIHR New Investigators. SP is supported by the Tim Noël Studentship from the ALS Society of Canada.

# Chapter 4

## ALS-linked misfolded SOD1 species have divergent impacts on mitochondria

Sarah Pickles, Sabrina Semmler, Helen R. Broom, Laurie Destroismaisons, Neil R. Cashman, Elizabeth Meiering, and Christine Vande Velde. ALS-linked misfolded SOD1 species have divergent impacts on mitochondria. In preparation for Acta Neuropathologica Communications.

### 4.1. Author contributions

Contribution: SP performed majority of experiments. SS isolated mitochondria for some experiments and collected tissue from rats for immunohistochemistry. HB produced recombinant SOD1 protein. LD assisted with *in vitro* mitochondrial binding assay. NC provided AMF7-63 antibody. EM provided recombinant SOD1 protein. SP analyzed data in consultation with NA and CVV. SP and CVV wrote the manuscript.

### 4.2. Abstract

Approximately 20% of familial ALS is caused by mutations in superoxide dismutase (*SOD1)*, which leads to misfolding of the SOD1 protein, resulting in a toxic gain of function. Several antibodies have been generated that are specific for the misfolded form of the protein, and have been used as therapeutics in pre-clinical models. Misfolded SOD1 selectively associates with spinal cord mitochondria in SOD1 rodent models. Using the $SOD1^{G93A}$ rat model, we found that SOD1 conformational antibodies AMF7-63 and DSE2-3H1 labeled a distinctive fibrillar network concentrated in the anterior horn; while A5C3, B8H10, C4F6 and D3H5 labeled motor neurons as well as puncta in the neuropil. There is a time-dependent accumulation of misfolded SOD1 at the surface of spinal cord mitochondria with AMF7-$63^{+}$ mitochondria having increased volume compared to B8H$10^{+}$ mitochondria. Furthermore, AMF7-63, DSE2-3H1 and B8H10 detect misfolded SOD1 incorporated into aggregates from spinal cord homogenates and isolated mitochondria, while C4F6-reactive misfolded SOD1 is absent. Mutant SOD1 lacking its metal cofactors has an increased binding affinity to naïve mitochondria and misfolded SOD1 antibodies B8H10 and DSE2-3H1 readily detect demetalated mutant and wild-type SOD1. Together, these data suggest that there exists more

than one non-native species of misfolded SOD1 that damage mitochondria to varying degrees. Conformational antibodies are invaluable tools to identify and characterize the continuum of misfolded SOD1 species with regards to biochemical characteristics and toxicity. This information is highly relevant to the further development of these reagents as therapeutics.

### 4.3. Introduction

The defining feature of the neurodegenerative disease Amyotrophic Lateral Sclerosis (ALS) is the loss of upper motor neurons in the cortex and lower motor neurons in the brain stem and spinal cord [20]. Loss of motor neurons leads to denervation resulting in muscle weakness, atrophy and eventual paralysis. Despite identification of the first gene linked to familial ALS (FALS), Superoxide Dismutase 1 (SOD1) [26], over twenty years ago, and the discovery of many more ALS genes since, the causes of motor neuron degeneration remain unknown.

Mutations in SOD1 account for 15 to 20% of all FALS cases, and approximately 3% of sporadic ALS (SALS) cases [37]. SOD1 mutations universally lead to conformation changes within the native protein structure, causing the acquisition of a toxic function [130]. Several antibodies have been developed to specifically target these altered conformations, termed misfolded SOD1 (reviewed in [33, 235]). Animals immunized with $SOD1^{G93A}$ protein lacking its metals (apo) generated antibodies named as A5C3, B8H10, C4F6, and D3H5. Other antibodies, such as DSE2-3H1, SEDI, USOD, and a series of polyclonal peptide antibodies produced by Forsberg and colleagues, were produced via immunization with peptides comprised of amino acids that are normally inaccessible in the well folded protein. All of these antibodies recognize epitopes that are exposed only when SOD1 adopts a non-native conformation induced

either by mutation, loss of its zinc cofactor, and/or oxidation [243, 244]. While many of these were developed with the intent to be potential therapeutics, these reagents have also become valuable tools with which to track the toxic form of SOD1. Misfolded SOD1 is detected predominantly within the motor neurons of ALS animal models [234, 243, 250, 310, 444]. In humans, various antibodies report on misfolded SOD1 in neurons of FALS patients as well as SALS patients, although this latter finding remains controversial [119, 240, 244, 246]. In pre-clinical research using mutant SOD1 animals, it is now appreciated that reducing misfolded SOD1 levels via immunization significantly increases survival [190, 243], providing additional support that misfolded SOD1 lies at the root of SOD1-mediated ALS [190, 243].

Despite consensus in the field that misfolded SOD1 is central to disease pathogenesis, it remains unknown how misfolded SOD1 causes motor neuron death. Misfolded SOD1 has been implicated in the induction of ER stress [36, 250], defective axonal transport [244], and mitochondrial dysfunction [233, 234, 310, 444] in SOD1 mediated ALS disease models. Multiple aspects of mitochondrial physiology are disrupted in mutant SOD1 cell culture and animal models including morphology [307, 309, 312], ATP generation [343], calcium handling [336], axonal transport [321] and protein import [346]. Interestingly, misfolded SOD1 directly associates with mitochondria derived from affected, but not unaffected tissues [234]. The selective association of misfolded SOD1 to spinal cord mitochondria has just recently been attributed to a lack of the putative chaperone macrophage migration inhibitory factor (MIF) in this tissue, and more specifically motor neurons.

Recent evidence suggests that multiple non-native/misfolded SOD1 species may exist [407, 408]. Consistent with this concept, we have previously reported that the B8H10 antibody detects misfolded protein in both cytosolic and mitochondrial fractions prepared from SOD1$^{G93A}$

spinal cords while the C4F6 antibody exclusively detects cytosolic misfolded SOD1 [444]. Other work in cultured cells made to overexpress mutant SOD1 indicates that the C4F6 antibody recognizes soluble mutant protein, whereas SEDI preferentially detects mutant SOD1 within inclusions [408]. Additionally, a series of polyclonal SOD1 peptide antibodies identify two different forms of SOD1 aggregates (or "strains") in mutant SOD1 mice based on epitope accessibility, with one such aggregate-type/strain correlating with an earlier age of onset [407]. Together these data suggest that multiple forms of misfolded SOD1 are possible.

We hypothesized that if more than one form of misfolded SOD1 exists, there may be conformer-specific differences in localization, potency and/or pathomechanistic consequences. Using a panel of misfolded SOD1 antibodies, we evaluated misfolded SOD1 localization, ability to induce mitochondrial toxicity and incorporation into aggregates. Herein, we report that the misfolded SOD1 antibody DSE2-3H1 labels motor neurons and robustly detects fibrils in the anterior horn of $SOD1^{G93A}$ spinal cords, a finding that is confirmed by a second independent antibody raised with the same immunogen (AMF7-63). Other misfolded SOD1 antibodies, A5C3, B8H10, C4F6 and D3H5 localize to motor neurons and numerous neuropil puncta. Despite their different labelling patterns within the spinal cord, both B8H10 and AMF7-63 antibodies immunolabel spinal cord mitochondria in a time-dependent manner. However, the finding of AMF7-63-reactive misfolded SOD1 at mitochondria correlates with a more severe dysregulation of mitochondrial volume.

## 4.4. Results

### 4.4.1. Misfolded SOD1 specific antibodies DSE2 and AMF7-63 detect fibrils in the spinal cord of SOD1$^{G93A}$ rats

Lumbar spinal sections of symptomatic SOD1$^{G93A}$ rats were labelled with a panel of misfolded SOD1 specific antibodies to evaluate whether multiple antibodies targeted to non-native/misfolded conformations of SOD1 yielded a universal pattern under identical conditions. In symptomatic SOD1$^{G93A}$ rats, all of the misfolded SOD1 specific antibodies tested (A5C3, B8H10, C4F6, D3H5, DSE2-3H1, and AMF7-63) labelled motor neurons as marked by choline acetyltransferase (ChAT) (**Fig. 1A**). Antibodies DSE2-3H1 (mouse monoclonal) and AMF7-63 (rabbit monoclonal) are raised against the same epitope located in the electrostatic loop (amino acids 125-142) of SOD1 which is normally inaccessible in the well-folded SOD1 structure [234]. In symptomatic animals, both antibodies intensely labelled the anterior horn albeit with varying affinities, with AMF7-63 demonstrating a more intense labelling (**Fig. 1A**). This is consistent with a $10^5$-fold enhanced affinity for the immunogenic peptide (N. Cashman, unpublished data). The labelling resembled a network of fibril-like structures, with some motor neuron soma being obviously labelled. In general, the fibrillar pattern detected by DSE2 and AMF7-63 was so robust, it was often difficult to discern individual motor neurons. These two antibodies also revealed a fibrillar network in pre-symptomatic animals (14 and 15 weeks old) (**Fig. 1B**). A similar pattern was also observed with SEDI, but since this antibody required antigen retrieval, while the other antibodies did not, we did not pursue this further (**Fig. S1A**). In contrast, fibrils were only occasionally detected in sections labelled with misfolded SOD1 antibodies A5C3, B8H10 and C4F6, but not D3H5, in pre-symptomatic as well as symptomatic animals. Instead, we noted that A5C3, B8H10, C4F6 and D3H5 antibodies homogenously labelled motor neuron soma, and this was accompanied by numerous small puncta observed

throughout the neuropil. As expected, none of the antibodies detected any signal in lumbar spinal cords of age-matched rats expressing comparable levels of human wild type SOD1 ($SOD1^{WT}$), thereby confirming antibody specificity, nor was there non-specific labelling in IgG controls or sections stained with secondary antibody alone (**Fig. S1B, C**). To determine if misfolded SOD1-positive fibrils reflected dendritic accumulations of misfolded SOD1, sections were co-labelled with AMF7-63 and the dendritic marker MAP2 (microtubule associated protein 2). However, no co-localization between AMF7-63 and MAP2 was detected, suggesting that misfolded SOD1 fibrils were not confined to dendrites (**Fig. 1C**). However, partial colocalization between ubiquitin and DSE2-3H1 and AMF7-63 was observed (**Fig. 1D**). These initial studies indicate that misfolded SOD1 antibodies can be broadly considered as two distinct groups: A5C3, B8H10, C4F6, and D3H5 which label motor neurons and numerous puncta throughout the neuropil; and AMF7-63 and DSE2-3H1 which also label motor neurons but also intensely reveal fibril-like structures. These data suggest that more than one type of misfolded SOD1 species may exist *in vivo*.

To determine if these seemingly different misfolded SOD1 conformations could co-exist within the same motor neuron, spinal cord sections were co-labelled with AMF7-63 and B8H10. A partial co-localization of these two antibodies within ChAT-positive motor neurons was frequently observed (**Fig. 1D**), suggesting that these antibodies recognize apparently distinct non-native SOD1 species within the same neurons. In addition, we observed neurons that labelled with AMF7-63 uniquely (i.e. void of B8H10), and vice versa.

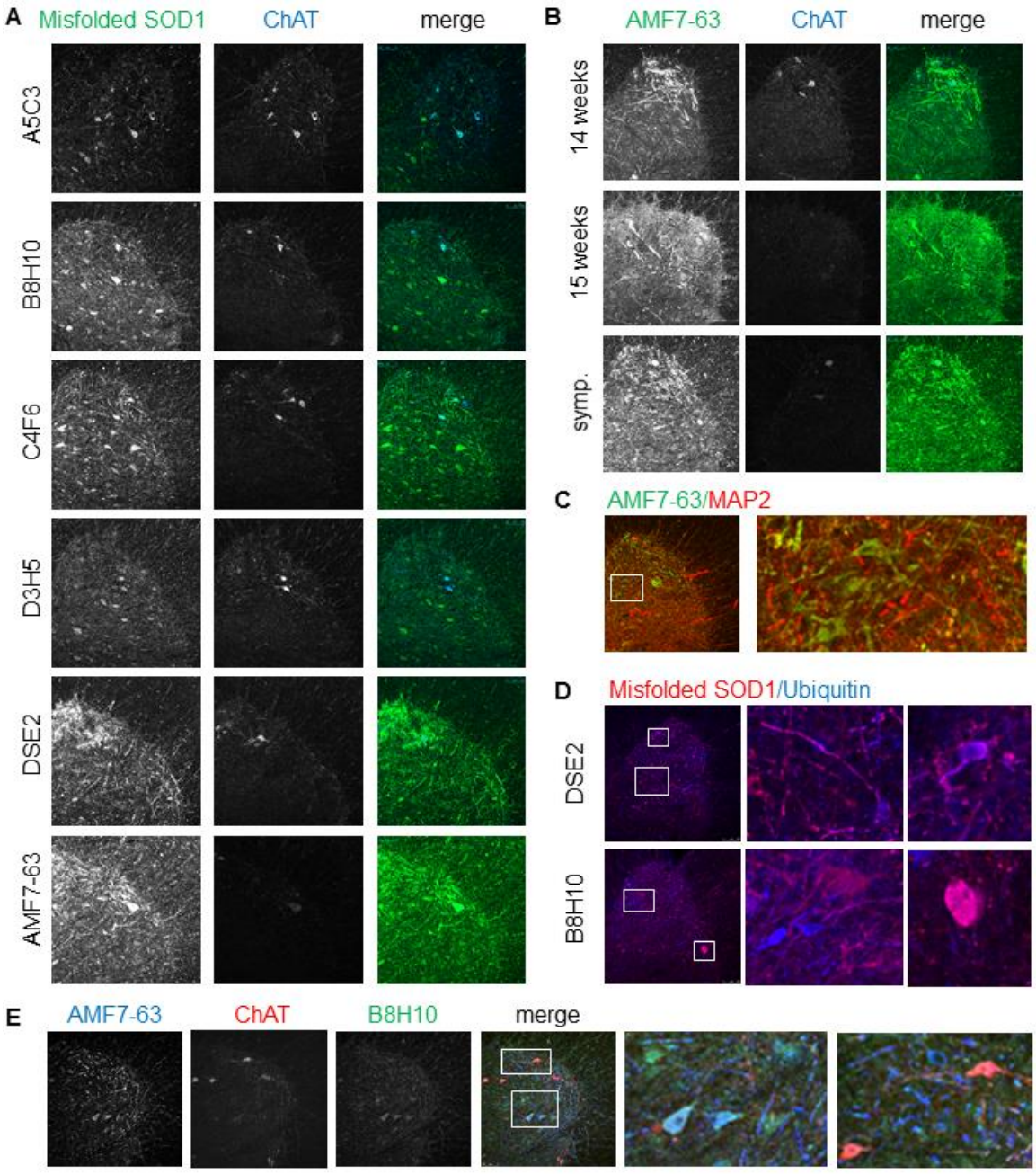


**Figure 1: Misfolded SOD1 antibodies have distinct labelling patterns in SOD1$^{G93A}$ rat spinal cords.** Immunohistochemistry for misfolded SOD1 in SOD1$^{G93A}$ lumbar spinal cords. A) Lumbar sections of a symptomatic SOD1$^{G93A}$ rat were stained with misfolded SOD1 specific antibodies A5C3, B8H10, C4F6, D3H5, DSE2-3H1 and AMF7-63 (green), and co-labelled with

ChAT (blue). B) The AMF7-63 antibody (green) detects fibrils in pre-symptomatic, 14 and 15 week, SOD1$^{G93A}$ rat spinal cords. Sections were co-labelled with ChAT (blue). C) Symptomatic SOD1$^{G93A}$ rats labeled with AMF7-63 (green) and MAP2 (red) or D) B8H10 and DSE2 (red) and ubiquitin (blue). E) Lumbar labeled with misfolded SOD1 antibodies AMF7-63 (blue), B8H10 (green), and co-labelled with ChAT (red). Two to three animals of each genotype were analyzed. Scale bar = 100 μM.

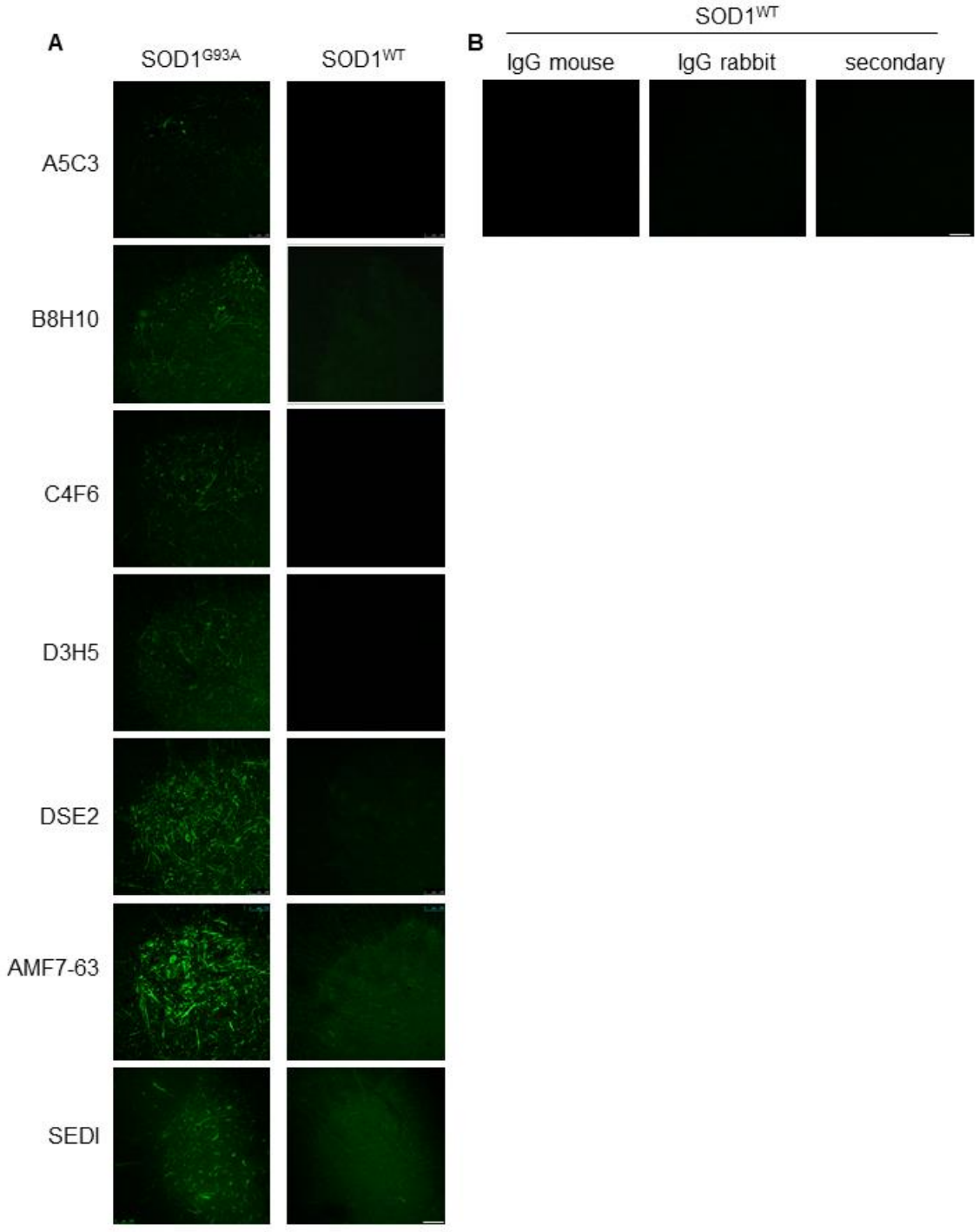


**SUPPLEMENTAL FIGURE 1: Misfolded SOD1 specific antibodies do not label SOD1$^{WT}$.**

A) Lumbar spinal cord sections of a symptomatic SOD1$^{G93A}$ rat and age-matched SOD1$^{WT}$ were

labelled with misfolded SOD1 specific antibodies A5C3, B8H10, C4F6, D3H5, DSE2-3H1 and AMF7-63 (green) to determine specificity of antibodies to misfolded SOD1. B) No non-specific labelling as determined by IgG controls (mouse and rabbit), or incubation with secondary antibody alone, was detected.

### 4.4.2. AMF7-63 detects misfolded SOD1$^{G93A}$ at the mitochondrial surface

Several misfolded SOD1 specific antibodies (DSE2-3H1, A5C3, B8H10, SEDI) recognize misfolded SOD1 protein deposited at the mitochondrial surface [233, 234, 248, 310, 444]. However, this is not a universally shared feature of misfolded SOD1 as conformers recognized by C4F6 are primarily cytosolic and little to no mitochondrial association [444]. Thus, we sought to determine if AMF7-63-reactive misfolded SOD1 also associates with mitochondria. Misfolded SOD1 antibodies A5C3, B8H10, DSE2-3H1 and AMF7-63 were used to immunoprecipitate misfolded SOD1 from spinal cord mitochondria isolated from symptomatic SOD1$^{G93A}$ animals (**Fig. 2A**). As previously published, B8H10 and DSE2-3H1-reactive SOD1 were robustly detected in mitochondrial fractions [234, 249, 444] (**Fig. 2A**). AMF7-63 detected similar amounts of misfolded SOD1 (**Fig. 2A**). A5C3, which we have previously demonstrated to label misfolded SOD1 on axonal mitochondria [234] also detected misfolded SOD1 within mitochondrial fractions, but to a lesser extent than the other antibodies (**Fig. 2A**). The specificity of the AMF7-63 antibody was confirmed by immunoprecipitation of spinal cord homogenates and isolated mitochondria from symptomatic SOD1$^{G93A}$ rats as well as age-matched SOD1$^{WT}$ rats. As expected, AMF7-63 immunoprecipitated misfolded SOD1 exclusively from SOD1$^{G93A}$ rat spinal cord homogenates and mitochondria, but not similar preparations from livers (**Fig. S2**). A non-specific band migrating just above SOD1 was also detected in all cases where the AMF7-63 antibody was used for immunoprecipitation, regardless of whether misfolded SOD1 was detected.

We wondered if the presence of AMF7-63-reactive misfolded SOD1 conformer negatively impacted mitochondrial function. To this end, we employed flow cytometric detection of isolated spinal cord mitochondria immunolabelled with the misfolded SOD1

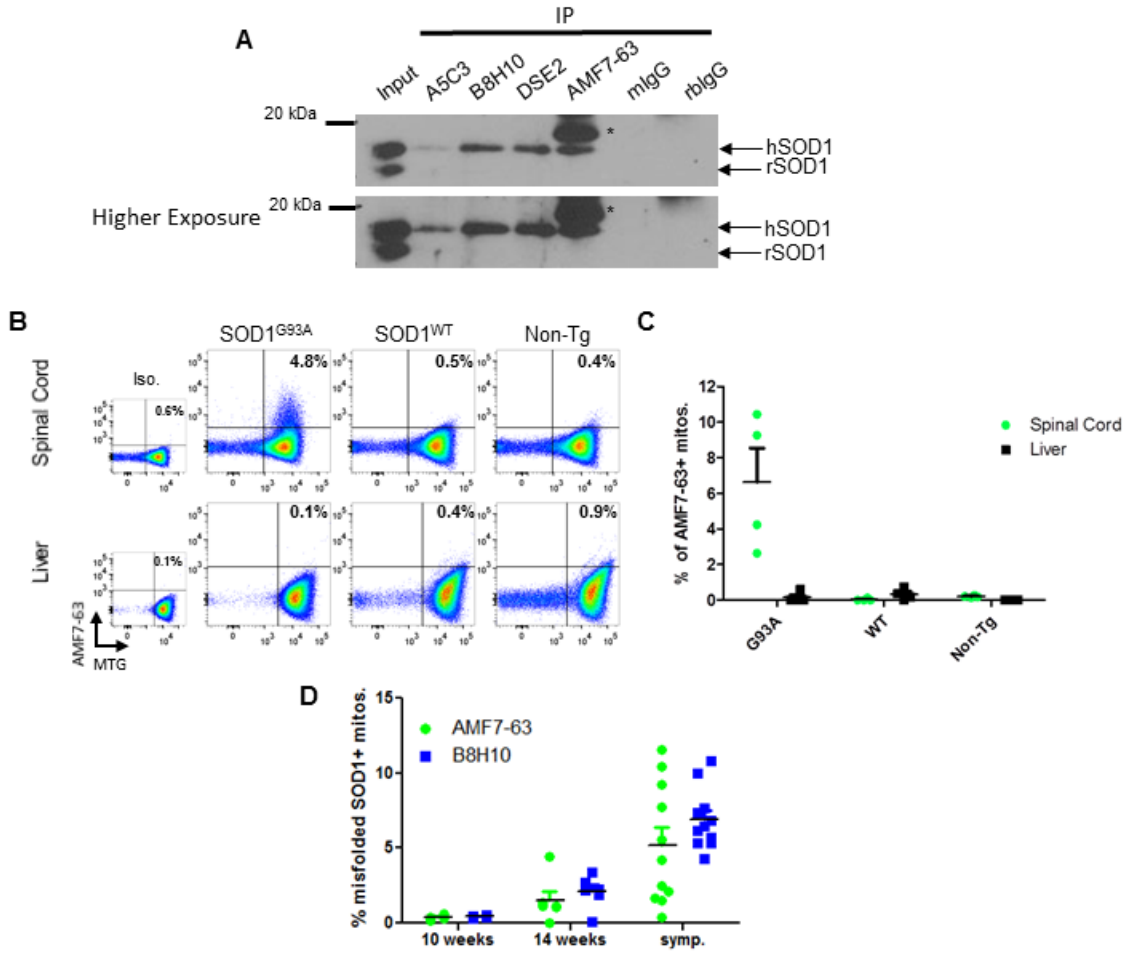


**Figure 2: B8H10 and AMF7-63 reactive misfolded SOD1 is present in SOD1$^{G93A}$ spinal mitochondrial fractions.** A) Immunoprecipitation for misfolded SOD1 in isolated SOD1$^{G93A}$ mitochondria with A5C3, B8H10, DSE2 3H1 and AMF7-63. Mouse (mIgG) and rabbit IgG (rbIgG) serve as controls. Input is 10 µg isolated mitochondria. Upper bands and lower bands correspond to human (hSOD1) and rat (rSOD1) SOD1, respectively. Immunoprecipitation with the AMF7-63 resulted in a non-specific band (*) just above human SOD1, regardless of misfolded SOD1 status. Experiment shown is representative of three independent trials. B) Immunolabelling of isolated spinal cord and liver mitochondria with misfolded SOD1 antibody

AMF7-63 from symptomatic $SOD1^{G93A}$ rats and controls (aged matched $SOD1^{WT}$ and non-transgenic rats) by flow cytometry. Misfolded SOD1 positive labelling is determined by comparing to isotype control (rabbit IgG for AMF7-63) of $SOD1^{G93A}$ sample. Percentage of misfolded $SOD1^{+}$ events is shown for each tissue and genotype in a representative sample. C) Quantification of AMF7-$63^{+}$ events in spinal cord (green circle) or liver (black square) of symptomatic $SOD1^{G93A}$ rats, and age- matched $SOD1^{WT}$ and non-transgenic rats. Data is represented as percent of misfolded AMF7-$63^{+}$ mitochondria (mean ± SEM), n=4 animals per genotype per tissue. D) Comparison of spinal cord mitochondrial labelling positive for AMF7-63 (green, circle) or B8H10 (blue, square) in pre-symptomatic (10 and 14 weeks) and symptomatic $SOD1^{G93A}$ rats by flow cytometry. Data is represented as percentage of misfolded $SOD1^{+}$ mitochondria (mean ± SEM), *n*=4-11 animals. * $P < 0.05$.

antibodies AMF7-63 and B8H10 [445]. Using early symptomatic SOD1$^{G93A}$ rats, we established that AMF7-63 preferentially detected misfolded SOD1 on isolated spinal cord mitochondria compared to liver, a tissue that is unaffected in ALS (**Fig. 2B**). Significantly more individual spinal cord mitochondria (as marked by the indicator dye MitoTracker Green, MTG) from SOD1$^{G93A}$ rats labelled for AMF7-63 (6.6 ± 1.9%) compared to SOD1$^{WT}$ (0.1 ± 0.03%) and non-transgenic (0.2 ± 0.03%) animals (**Fig. 2B, C**). As expected, AMF7-63-reactive misfolded SOD1 was barely detectable on liver mitochondria from any group (SOD1$^{G93A}$: 0.1 ± 0.1%; SOD1$^{WT}$: 0.3 ± 0.02%; non-transgenic: 0.1 ± 0.2%), confirming specificity of misfolded SOD1 for affected tissues ($P < 0.001$, $n$=4 animals per genotype) (**Fig. 2B, C**). Similarly, B8H10$^{+}$ mitochondria were robustly detected in mitochondrial preparations from symptomatic SOD1$^{G93A}$ spinal cords (6.1 ± 0.4%) but not SOD1$^{WT}$ (0.4 ± 0.2%) or non-transgenic cords (0.4 ± 0.1%) ($P < 0.0001$, $n$=3 animals per genotype) (**Fig. S3A, B**). There was no substantial B8H10 labelling of liver mitochondria from any of the models (**Fig. S3A, B**).

At an early symptomatic stage, both AMF7-63 and B8H10 antibodies detected misfolded SOD1 at the surface of spinal cord mitochondria. Thus, we asked whether there was a temporal difference in the accumulation of these two conformers. Spinal cord mitochondria from 10 and 14 week old SOD1$^{G93A}$ rats were processed for labelling with B8H10 and AMF7-63. While no mitochondrial signal for either antibody was detected at 10 weeks, comparable labelling was detected in mitochondria from 14 week animals (AMF7-63$^{+}$: 1.5 ± 0.6%; B8H10$^{+}$: 2.1 ± 0.5%). Higher proportions of mitochondria labelled for misfolded SOD1 at the early symptomatic stage, demonstrating a significant age-dependent accumulation of each misfolded SOD1 conformer at the mitochondrial surface ($P < 0.0001$). Comparison of the relative amounts

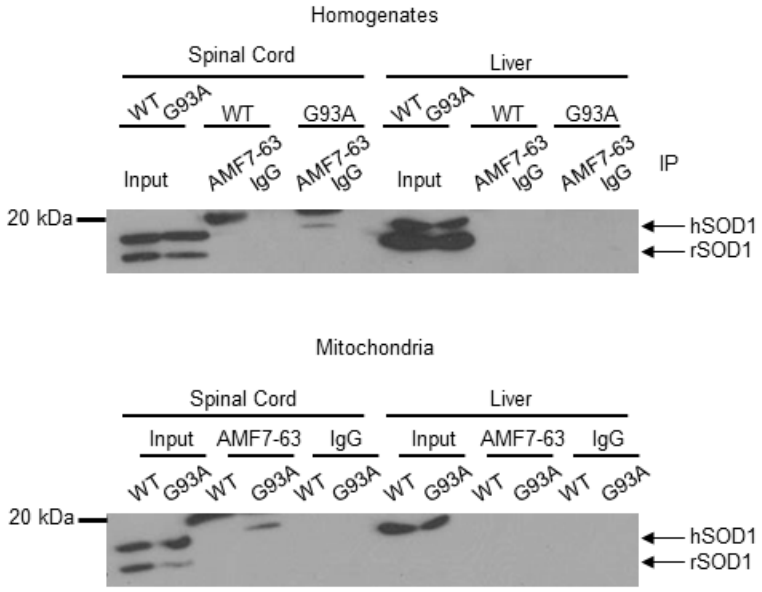


**SUPPLEMENTAL FIGURE 2: Misfolded SOD1 antibody AMF7-63 specifically identifies mutant SOD1 in spinal cord but not liver from SOD1$^{G93A}$ rats.** The capacity for misfolded SOD1 antibody to detect misfolded SOD1 in homogenates or isolated mitochondria from spinal cords and livers was assayed by immunoprecipitation. Rabbit IgG (IgG) serve as controls. Input is 10 μg of homogenate or isolated mitochondria. Upper bands and lower bands correspond to human (hSOD1) and rat (rSOD1) SOD1, respectively.

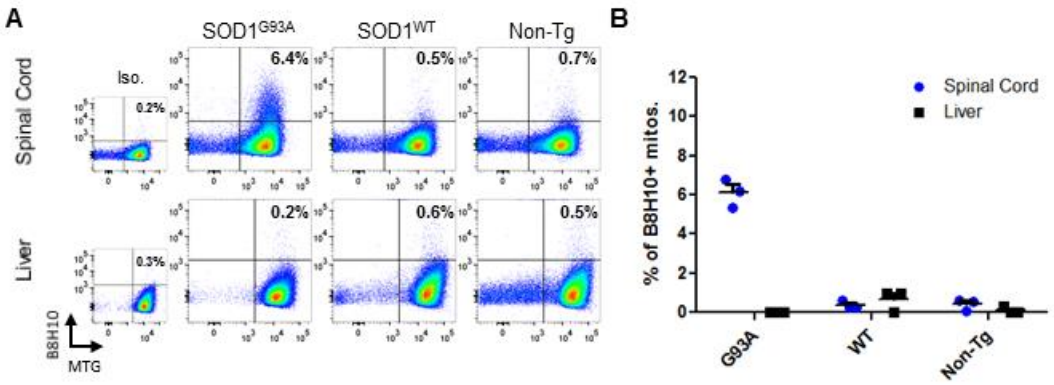


**SUPPLEMENTAL FIGURE 3: Misfolded SOD1 B8H10 specifically identifies misfolded SOD1 on the surface isolated mitochondria from spinal cord but not liver of SOD1$^{G93A}$ rats.** A) Immunolabelling of isolated spinal cord and liver mitochondria with misfolded SOD1 antibody B8H10 from symptomatic SOD1$^{G93A}$ rats and controls (age-matched SOD1$^{WT}$ and non-transgenic rats) by flow cytometry. Misfolded SOD1 positive labelling is determined by comparing to isotype control (mouse IgG1) of SOD1$^{G93A}$ sample. Percentage of misfolded SOD1$^{+}$ events is shown for each tissue and genotype in a representative sample. C) Quantification of B8H10$^{+}$ events in spinal cord (blue circles) or liver (black squares) of symptomatic SOD1$^{G93A}$ rats, and age- matched SOD1$^{WT}$ and non-transgenic rats. Data is represented as percent of misfolded B8H10$^{+}$ mitochondria (mean ± SEM). ** $P < 0.01$, $n$=3 animals per genotype per tissue.

of AMF7-63$^+$ (5.2 ± 1.1%) and B8H10$^+$ (6.9 ± 0.6%) subpopulations yielded no significant differences (**Fig. 2D**). Collectively, these data would argue that there is no preferential temporal accumulation of these two forms of non-native SOD1 conformers at the mitochondrial surface.

Given these latter data, one might argue that the antibodies are detecting the same conformer *in vivo*. Thus, to address this, we analyzed our data to determine if it was possible to detect B8H10-labelled mitochondria void of AMF7-63 labelling, and vice versa. By simultaneously immunolabelling isolated mitochondria with both AMF7-63 and B8H10, we were able to discern four distinct mitochondrial subpopulations: *i)* double negative (AMF7-63$^-$ B8H10$^-$); *ii)* AMF7-63 only (AMF7-63$^+$B8H10$^-$); *iii)* B8H10 only (AMF7-63$^-$B8H10$^+$); and *iv)* double positive (AMF7-63$^+$B8H10$^+$) (**Fig. 3A**). Therefore, the total AMF7-63$^+$ subpopulation consists of both B8H10$^+$ and B8H10$^-$ mitochondria. Indeed, 70 ± 4% of AMF7-63-coated mitochondria also labelled for B8H10 (**Fig. 3B**). Similarly, just under half of the B8H10$^+$ subpopulation also labelled for AMF7-63 (43 ± 8%) (**Fig. 3B**). That a proportion of mitochondria label positive with both misfolded SOD1 antibodies, while others label for only one conformer, suggests that AMF7-63 and B8H10 recognize distinct misfolded SOD1 species.

From 14 weeks to the early symptomatic stage, there was a significant time dependent increase in the percentage of misfolded SOD1 labelled mitochondria for all three misfolded SOD1$^+$ subpopulations ($P < 0.01$) (**Fig. 3C**). The relative amounts of the three subpopulations with surface-bound misfolded SOD1 revealed no significant differences between them at 14 weeks. Interestingly, between 14 weeks and the early symptomatic stage, the proportion of AMF7-63$^+$B8H10$^+$ and B8H10$^+$ mitochondrial subpopulations nearly doubled, whereas the AMF7-63$^+$ subpopulation remained roughly constant (**Fig. 3C**). At the latter time point, there is a significantly higher percentage of AMF7-63$^-$B8H10$^+$ than AMF7-63$^+$B8H10$^-$ mitochondria (*P*

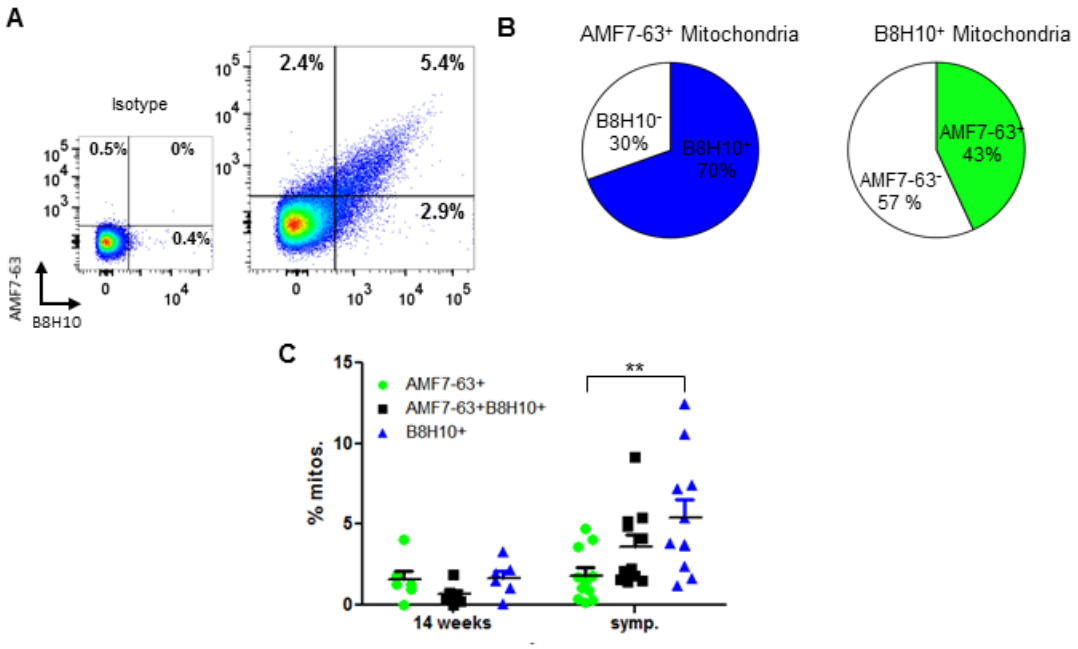


**Figure 3: Four distinct mitochondrial subpopulations revealed by simultaneously immunolabelling with AMF7-63 and B8H10 misfolded SOD1 antibodies**. A) Flow cytometric analysis of isolated spinal cord mitochondria from symptomatic SOD1$^{G93A}$ animals labelled with AMF7-63 and B8H10. Analysis only includes events previously gated for MTG staining (MTG$^{+}$). Percentage of misfolded SOD1$^{+}$ events is shown for each subpopulation in a representative experiment. B) Subdivision of AMF7-63$^{+}$ mitochondria into B8H10$^{+}$ (blue) and B8H10$^{-}$ (white) subpopulations and B8H10$^{+}$ mitochondria into AMF7-63$^{+}$ (green) and AMF7-63$^{-}$ (white) subpopulations. Data is represented as percentage of misfolded SOD1$^{+}$ mitochondria of that subcategory, *n*=11 animals. C) Quantification of AMF7-63$^{+}$ (green, circle), AMF7-63$^{+}$B8H10$^{+}$ (black, square) and B8H10$^{+}$ (blue, triangle) mitochondrial subpopulations from spinal cords of 14 week and early symptomatic SOD1$^{G93A}$ rats. Data is represented as percent of misfolded SOD1$^{+}$ mitochondria (mean ± SEM), *n*=4-11 animals per subpopulation. ** $P <$ 0.01.

< 0.01) (**Fig. 3C**). These data suggest there is a either preferential removal of the AMF7-$63^{+}$B8H10$^{-}$ subpopulation or disturbed removal/enhanced accumulation of B8H10-coated mitochondria.

### 4.4.3. Mitochondria with surface-bound AMF7-63-reactive SOD1 have an enlarged volume and produce increased amounts of superoxide

A distinct advantage of the flow cytometry based method to detect mitochondrially-associated misfolded SOD1 is that it permits the simultaneous coupling of fluorescent indicator dyes to report on mitochondrial function. Since a temporal difference in mitochondrial association between the two misfolded SOD1 conformers was not detected, we hypothesized that perhaps they may exhibit variable toxicity towards mitochondria. Thus, we evaluated select aspects of mitochondrial function in the AMF7-63$^{+}$ subpopulation. Mitochondrial size/volume was assessed by flow cytometry on the basis of the intensity of forward light scatter (FSC) of individual mitochondria [428, 446]. Quantification of the FSC normalized to the total population indicate that mitochondria bearing AMF7-63 reactive misfolded SOD1 from 14 week and early symptomatic SOD1$^{G93A}$ animals were significantly larger than non-coated mitochondria ($P <$ 0.001) (**Fig. 4A**). Intriguingly, the AMF7-63$^{+}$ subpopulation was also significantly larger than the B8H10$^{+}$ only subpopulation when animals began exhibiting early symptoms ($P < 0.0001$) (**Fig. 4A**).

MTG can be used not only to identify mitochondria, but also to report on mitochondrial volume. Specifically, dye uptake measured by the delta mean fluorescent intensity (ΔMFI) correlates with mitochondrial volume as the dye accumulates within mitochondria independent of the mitochondrial transmembrane potential [429]. In agreement with our FSC data, AMF7-63$^{+}$ and B8H10$^{+}$ subpopulations have a significantly higher ΔMFI compared to uncoated mitochondria at both time points (AMF7-63$^{+}$, $P < 0.0001$; B8H10$^{+}$, $P < 0.01$), with AMF7-63$^{+}$ mitochondria taking up more dye compared to B8H10$^{+}$ mitochondria ($P < 0.0001$) (**Fig. 4B**). Together, these data indicate that the association of AMF7-63-reactive misfolded SOD1 conformers with the mitochondrial surface correlates with enlarged mitochondria.

Superoxide is produced as a natural by-product at complex I and complex III of the electron transport chain during oxidative phosphorylation [352]. We evaluated the levels of mitochondrial superoxide produced by the AMF7-63$^{+}$ and B8H10$^{+}$ subpopulations using MitoSOX Red, a mitochondria specific superoxide indicator [430, 431]. Following normalization for size differences, the three mitochondrial subpopulations were significantly different at both time points ($P < 0.05$). Further comparison revealed that the AMF7-63$^{+}$ and B8H10+ subpopulations were not significantly different, only the AMF7-63$^{+}$ subpopulation was significant compared to the unlabelled subpopulations ($P < 0.05$). (**Fig. 4C**). These changes were independent of mitochondrial transmembrane potential ($\Delta\Psi_m$) which were unchanged between subpopulations (**Fig. 4D**). Taken together, these data suggest that there is variable mitochondrial damage associated with different conformers of misfolded SOD1. Specifically, AMF7-63-reactive misfolded SOD1 is associated with more severe deregulation of mitochondrial volume homeostasis, while superoxide production is equivalent to B8H10-coated mitochondria.

Since mitochondrial size/volume was significantly higher in AMF7-63$^{+}$ mitochondria compared to those bearing B8H10-reactive SOD1, we examined the AMF7-63$^{+}$ subpopulation in the absence of confounding B8H10$^{+}$ mitochondria. No significant differences were found between the three mitochondrial subpopulations, although mitochondria with AMF7-63 on their surface had a trend toward increased volume (**Fig. 4E, F**).

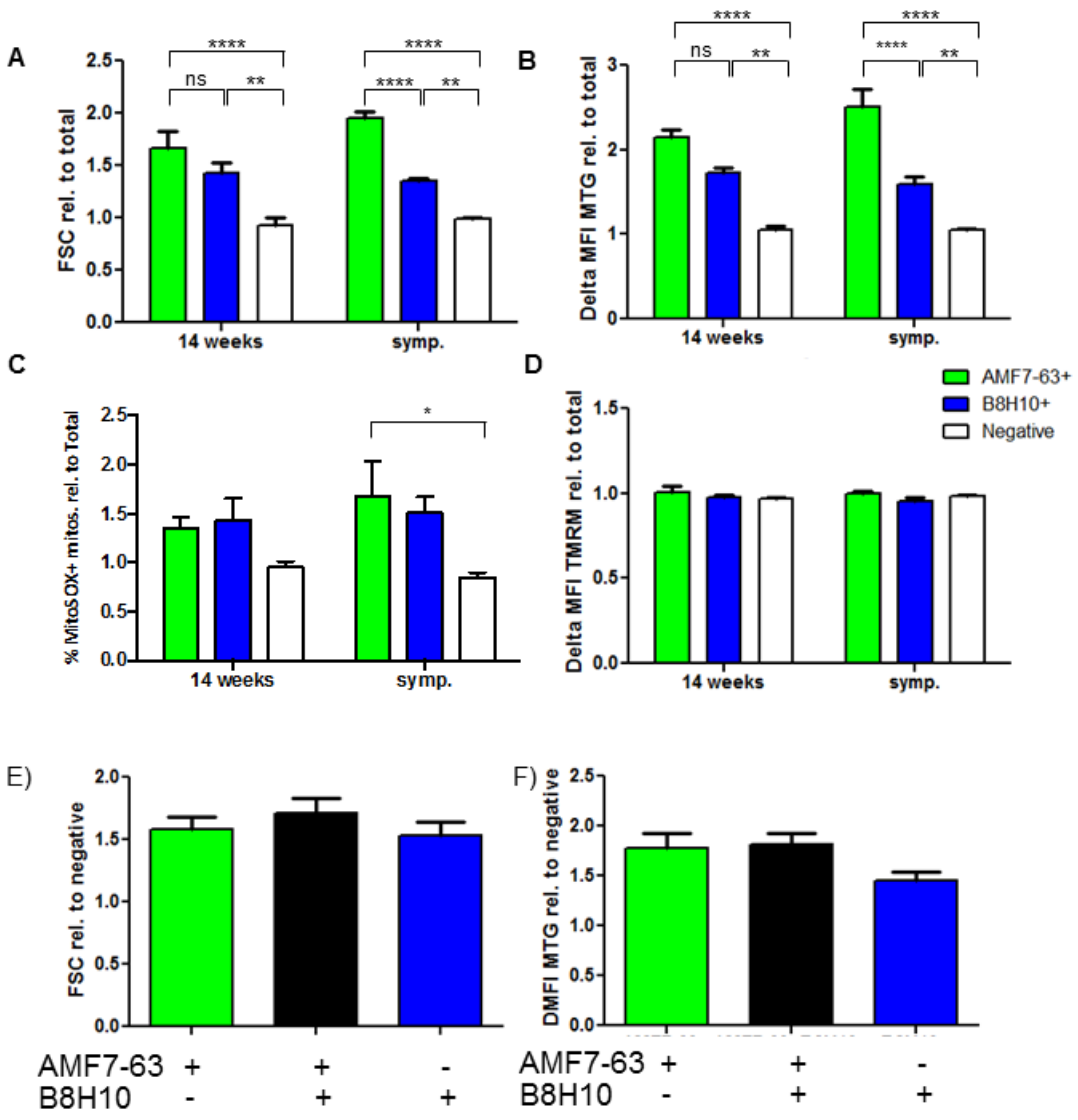


**Figure 4: Presence of AMF7-63 reactive misfolded SOD1 at mitochondrial surface coincides with increased mitochondrial volume.** Flow cytometric analysis of isolated spinal cord mitochondria from 14 week and early symptomatic SOD1$^{G93A}$ rats labelled with misfolded SOD1 specific antibodies AMF7-63 and B8H10. Analysis includes only events previously gated for MTG staining (MTG$^{+}$). A) Quantification of the geometric mean of FSC of AMF7-63$^{+}$

(green) B8H10$^{+}$ (blue) and negative (white) mitochondrial subpopulations relative to total population in 14 week and symptomatic SOD1$^{G93A}$ rats. B) Quantification of delta mean fluorescent intensity (ΔMFI) of MTG staining of mitochondrial sub-populations relative to total population. C) Quantification of percentage of MitoSOX$^{+}$ mitochondria from mitochondrial subpopulations relative to total population. Each subpopulation was normalized for MTG staining. D) Quantification of ΔMFI of TMRM staining of mitochondrial subpopulations relative to total population and normalized to size/MTG. *n*=4-5 animals per time point. E) Quantification of the geometric mean of FSC of AMF7-63$^{+}$ (green), AMF7-63$^{+}$B8H10$^{+}$ (black) and B8H10$^{+}$ (blue) mitochondrial subpopulations relative to negative (AMF7-63$^{-}$B8H10$^{-}$) subpopulation. F) Quantification of geometric mean of delta mean fluorescent intensity (ΔMFI) of MTG staining of misfolded SOD1$^{+}$ subpopulations relative to negative subpopulation. n=4-5 animals per time point. Not significant (ns), * $P < 0.05$, ** $P < 0.01$, **** $P < 0.0001$.

### 4.4.4. Misfolded SOD1 conformers are present in mitochondrial aggregates

Given that B8H10 and AMF7-63-reactive misfolded SOD1 disturbed mitochondrial volume to varying degrees, we speculated this may be attributed to differences in biochemical properties. Certain misfolded SOD1 specific antibodies are reported to detect aggregates/inclusions [407, 408], therefore we examined the incorporation of misfolded SOD1 into aggregates in both total spinal cord homogenates and isolated mitochondrial fractions. A size exclusion filter assay, which retains proteinaceous aggregates larger than 200 nm on a cellulose acetate membrane [178], was performed on homogenates and isolated mitochondria from spinal cords of pre-symptomatic (10 week) and early symptomatic $SOD1^{G93A}$ rats as well as age-matched $SOD1^{WT}$ animals. Given that this assay is performed in non-denaturing conditions, we reasoned that the misfolded SOD1 conformational antibodies should retain their specificity. In agreement with this, misfolded SOD1 antibodies B8H10, DSE2-3H1 and AMF7-63 preferentially labelled homogenates of $SOD1^{G93A}$ spinal cords but not controls (**Fig. 5A**). Moreover, these three antibodies demonstrated more intense immunoreactivity for mitochondrial samples (which were enriched via buoyant density so as to eliminate artefact from co-pelleting aggregates) (**Fig. 5A**). Furthermore, the formation of aggregates was disease/age-dependent, with robust labelling of homogenates and isolated mitochondria from early symptomatic animals, but little to no labelling at 10 weeks. Note, the C4F6 antibody did not detect aggregates in homogenates or isolated mitochondria at any age (**Fig. 5A**), consistent with reports by others that C4F6 recognizes soluble misfolded SOD1 [236, 408]. Western blots confirm equivalent SOD1 expression between samples (**Fig. 5B**). These results suggest that

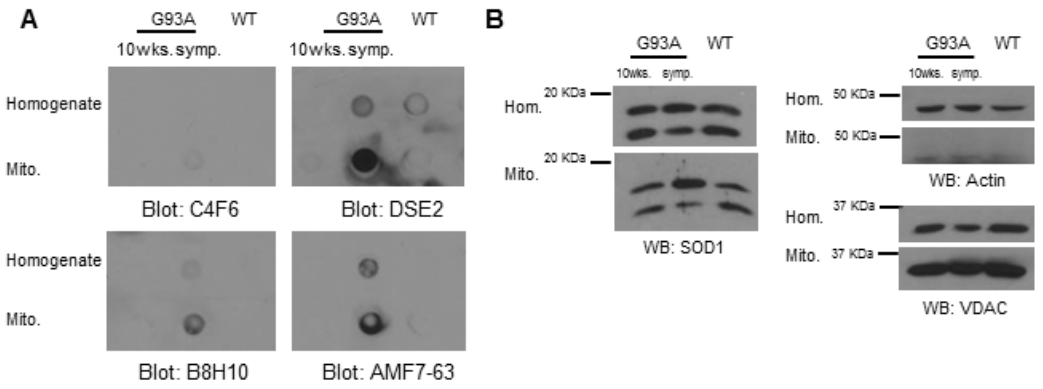


**Figure 5: AMF7-63 and B8H10 antibodies detect misfolded SOD1 in spinal cord aggregates.** A) Size exclusion filter-trap assay of homogenates or isolated mitochondria from spinal cords of pre-symptomatic (10 week) and symptomatic $SOD1^{G93A}$ rats or age-matched $SOD1^{WT}$ controls, blotted for misfolded SOD1 specific antibodies B8H10, DSE2-3H1, AMF7-63 and C4F6. Data is representative of three independent trials. B) Homogenates and isolated mitochondria immunoblotted for SOD1 to verify expression levels. Actin and VDAC serve as loading controls.

distinct misfolded SOD1 conformers recognized by B8H10, DSE2-3H1, and AMF7-63, but not C4F6, are enriched at spinal cord mitochondria.

### 4.4.5. Preferential recognition of demetalated and reduced recombinant SOD1

To determine if the misfolded SOD1 specific antibodies have a particular affinity to certain gross perturbations in SOD1 structure, demetalation, aggregation or reduction of the intra-molecular disulfide bond, recombinant wild-type and various SOD1 mutants (G93A, G85R, and A4V) were spotted onto a nitrocellulose membrane and blotted with misfolded SOD1 antibodies B8H10 and AMF7-63 under native conditions. SOD1 proteins that were properly folded in a native structure have both copper and zinc bound as well as an intact (oxidized) disulfide bond between Cys57 and Cys146, and are referred to as holo SOD1. Extended incubation of this protein in ambient conditions can generate aggregated holo protein. Note, recombinant holo $SOD1^{WT}$ does not aggregate, and thus buffer (Buf) was applied to the membrane at that position. Protein lacking both metal cofactors is referred to as apo SOD1. A reduced apo form of the protein also lacks the crucial Cys57-Cys146 disulfide bond. Regardless of genotype, both AMF7-63 and B8H10 had an increased preference for apo and apo reduced proteins (**Fig. 6A**). Fully denatured protein served as a positive control.

To determine if apo SOD1 mutants had a preferential association with isolated mitochondria, we performed an *in vitro* mitochondrial binding assay. Briefly, recombinant human SOD1 proteins were incubated with non-transgenic spinal cord mitochondria, and after washing away unbound protein, mitochondria were recovered and analyzed by western blot for the presence of human SOD1. Recombinant $SOD1^{G93A}$ protein showed an increased binding to mitochondria compared to $SOD1^{WT}$ protein. Treatment with EDTA, to chelate the metal

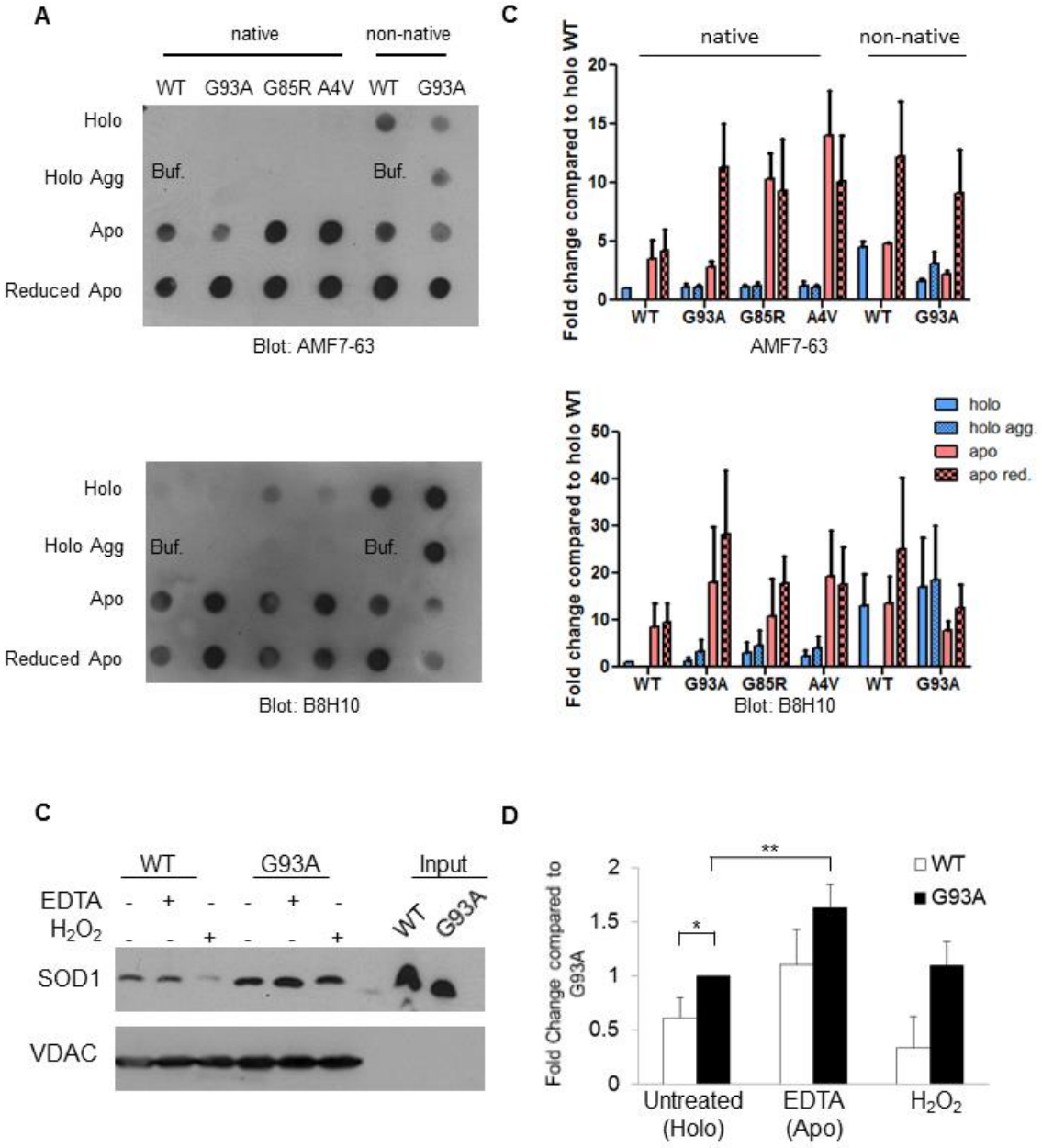
A
native
non-native
WT G93A G85R A4V WT G93A
Holo
Holo Agg
Apo
Reduced Apo
Buf.
Buf.
Blot: AMF7-63
Holo
Holo Agg
Apo
Reduced Apo
Buf.
Buf.
Blot: B8H10
C
native
non-native
Fold change compared to holo WT
WT G93A G85R A4V WT G93A
AMF7-63
holo
holo agg.
apo
apo red.
Fold change compared to holo WT
WT G93A G85R A4V WT G93A
Blot: B8H10
C
WT
G93A
Input
EDTA
H2O2
WT
G93A
SOD1
VDAC
D
Fold Change compared to G93A
WT
G93A
*
**
Untreated (Holo)
EDTA (Apo)
H2O2

**Figure 6: Misfolded SOD1 specific antibodies show preferential avidity for demetalated (apo) SOD1.** A) Recombinant SOD1 proteins (WT, G93A, G85R and A4V) were produced (1) with its full complement of metals (holo); (2) with its full complement of metals and aggregated (holo agg); (3) lacking metals (apo); and (4) lacking metals and a reduced Cys57-Cys146 disulfide bond (apo reduced) were spotted onto nitrocellulose and probed for misfolded SOD1 with AMF7-63 (*top*) and B8H10 (*bottom*). *Left:* Quantification of dot blots, data represented as fold change normalized to holo wild-type (WT) SOD1, and expressed as mean +/ SEM), n=3-4 replicates. B) *In vitro* mitochondrial binding assay. Recombinant $SOD^{WT}$ (white) and $SOD1^{G93A}$ (black) was incubated with spinal cord mitochondria from a non-transgenic rat, washed and subjected to analysis by western blot. Recombinant SOD1 was either left untreated or incubated with EDTA or $H_2O_2$ before addition to mitochondria. *Left:* Quantification normalized to $SOD1^{G93A}$ binding. * $P < 0.05$, ** $P < 0.01$, $n$=5.

cofactors of SOD1, resulted in significantly increased binding of $SOD1^{G93A}$ (**Fig. 6B, C**). $SOD1^{WT}$ displayed a trend toward increased binging to mitochondrial following treatment with EDTA (**Fig. 6B, C**). Treatment with hydrogen peroxide, previously published to oxidize SOD1 [244], did not significantly affect the ability of either recombinant wild-type or mutant SOD1 to associate with mitochondria (**Fig. 6B, C**). Taken together, misfolded SOD1 antibodies B8H10 and AMF7-63 preferentially detect apo and apo/reduced misfolded SOD1, and this form of mutant SOD1 has an increased association with mitochondria *in vitro*.

## 4.5 Discussion

### 4.5.1. Misfolded SOD1 specific antibodies recognize distinct non-native SOD1 confomers

Misfolded SOD1 antibodies partition into distinct patterns with A5C3, B8H10, C4F6 and D3H5 antibodies predominantly labelling misfolded SOD1 in motor neurons and numerous puncta within the neuropil. In contrast, the DSE2-3H1 and AMF7-63 antibodies labelled an extensive fibrillar network, within which motor neurons were often visualized. Fibrils are a subset of aggregates composed of β-sheets observed in many neurodegenerative diseases [182, 447]. Whether SOD1 forms fibrils in SOD1-mediated FALS cases, remains controversial [119, 183]. However, inclusions found in the spinal cords of SOD1 animal models contain fibrils that stain positive for Thioflavin T, a fluorescent molecule that fluoresces upon binding to β-sheets [152, 184]. Interestingly, fibrils have the propensity to seed aggregation *in vitro* [447], and apo reduced wild-type and mutant SOD1 readily form fibrils *in vitro* [152]. The C-terminal segment of SOD1 including residues 147-153, was previously identified to accelerate fibril formation of wild-type and mutant SOD1 lacking metal cofactors *in vitro* [188]. The epitope for the misfolded SOD1 specific antibodies AMF7-63 and DSE2-3H1 (residues 125-142) is adjacent to this fibril

forming segment, and thus is concordant with our observation that these antibodies robustly recognize fibrillized misfolded SOD1 protein. The epitope for the misfolded SOD1 antibody SEDI (residues 143-153) wholly encompasses this fibril forming segment. Indeed, fibrils were detected when antigen retrieval was used. However, the SEDI antibody does not detect fibrils in patient material, as evidenced by a lack of labelling of serial sections with Thioflavin T or Congo Red (another molecule that detects fibrils) [119].

The A5C3, B8H10, C4F6, and D3H5 antibodies exhibit a distinctly different pattern from DSE2-3H1 and AMF7-63. Despite their similarity, evidence is emerging that there are differences. For example, A5C3 and B8H10-misfolded SOD1 localize to mitochondria whereas as C4F6 does not. These data would seem to suggest that misfolded SOD1 specific antibodies recognize distinct misfolded SOD1 species. That B8H10 and AMF7-63 only partially co-localized in some neurons, but also individually labelled other neurons strongly supports that there are indeed multiple non-native misfolded SOD1 conformers *in vivo*, and that the available antibodies are capable of differentiating them.

### 5.5.2. AMF7-63-reactive misfolded SOD1 correlates with increased mitochondrial size/volume

That several misfolded SOD1-reactive conformers converge at the mitochondria highlights mitochondrial dysfunction as an important disease mechanism in ALS. To date, misfolded SOD1 antibodies SEDI [248], DSE2-3H1 [233, 234], A5C3 [234] and B8H10 [444] detect misfolded SOD1 at the surface of spinal cord mitochondria. In this report, we now add the AMF7-63 antibody to this list. In a single spinal cord, AMF7-63- and B8H10-reactive misfolded SOD1 conformers were detected both separately and together on distinct mitochondrial subpopulations.

AMF7-63$^+$ mitochondria have increased size/volume compared to B8H10$^+$ mitochondria, and exhibit a trend toward elevated superoxide production. However, separation into distinct subpopulations, AMF7-63$^+$, AMF7-63$^+$B8H10$^+$, or B8H10$^+$ mitochondria yielded no significant differences between the groups in terms of mitochondrial size/volume, although AMF7-63$^+$ and AMF7-63$^+$B8H10$^+$ showed a trend toward increased volume. That the AMF7-63$^+$ and B8H10$^+$ mitochondrial subpopulations demonstrate differences in mitochondrial size/volume suggest that these antibodies recognize distinct misfolded species that elicit disparate degrees of damage, with AMF7-63 reactive misfolded SOD1 correlating with increased potency. The misfolded SOD1 antibody DSE2 has been shown to interact with VDAC1 [233], a mitochondrial outer membrane protein important for ionic homeostasis [448]. Recombinant mutant SOD1 inhibits VDAC1 conductance in a reconstituted lipid bilayer [233]. Another group, not focusing on misfolded SOD1, reports that the interaction of mutant SOD1 and Bcl-2 and corresponding exposure of pro-apoptotic BH3 domain is necessary for Bcl-2 to alter VDAC permeability [350]. It remains unknown whether misfolded (DSE2-3H1 or B8H10 reactive) interact with Bcl-2. However, B8H10-reactive misfolded SOD1 and the pro-apoptotic form of Bcl-2 preferentially accumulate on the same mitochondria, but this is not indicative of a direct interaction. Furthermore, a portion of B8H10$^+$ mitochondria also contain AMF7-63-reactive SOD1 on their surface. Therefore, DSE2-3H1-reactive SOD1 could have an increased association with the pro-apoptotic Bcl-2/VDAC complex, resulting in altered mitochondrial ionic homeostasis. Future knowledge of the interactome of each misfolded SOD1 conformer may provide insight into the differential toxicity exhibited between AMF7-63 and B8H10-reactive misfolded SOD1.

We speculated that AMF7-63-reactive misfolded SOD1 may be prone to aggregation, as fibrils are composed of insoluble, ordered oligomeric chains [449]. However, both B8H10 and AMF7-63 labelled aggregates in spinal cord homogenates and isolated mitochondria. Therefore, the increases in mitochondrial size/volume elicited by AMF7-63-reactive misfolded SOD1 cannot be due solely to its participation in aggregates at the mitochondrial surface. We cannot exclude the possibility that AMF7-63-reactive misfolded SOD1 is included in aggregates of differing size/properties compared to the B8H10-reactive conformer. Nor can we exclude the possibility that the solubility of these two forms of misfolded SOD1 may differ so as to account for the increased toxicity. C4F6-reactive misfolded SOD1 is not detected in aggregates by this assay, consistent with reports that this antibody recognizes a soluble form of misfolded SOD1 [193, 408].

There is considerable debate over whether SOD1 monomers [190], oligomers [191] or large aggregates [192] mediate toxicity. A caveat to these studies is they have focused on cytosolic SOD1. Mitochondria are vulnerable to proteotoxic stress [450], particularly aggregated protein [451] and thus, have developed multiple layers of quality control mechanisms to combat this form of stress [452]. Mutant SOD1 has been reported to form aggregates in the matrix of brain mitochondria from ALS animal models [372] and at the surface of mitochondria of cells over-expressing mutant SOD1 [385]. Whether these internal- or surface-localized aggregates contain misfolded SOD1 or cause mitochondrial dysfunction was not determined. However, several recent studies suggest that aggregated SOD1 can perturb mitochondrial membrane integrity *in vitro* [377, 378].

### 5.5.3. Demetalated SOD1 is preferentially detected by misfolded SOD1 antibodies AMF7-63 and B8H10

Although broadly considered as a cytosolic protein, a small portion of SOD1 is localized to the mitochondrial intermembrane space (IMS) in normal physiological conditions [122]. In order for SOD1 to be imported into mitochondria, it must be in its apo reduced form [366]. Given this, a pool of apo SOD1 at the mitochondrial surface is expected. Interestingly, in our *in vitro* mitochondrial binding assay, apo SOD1 readily associated with the outer mitochondrial membrane. Import of mitochondrial substrates is slowed in spinal cord mitochondria from $SOD1^{G93A}$ [346], and the regulation of mutant SOD1s import into mitochondria is altered [369], therefore apo mutant SOD1 on route to the IMS may be accumulating at the outer mitochondrial membrane and disturbing normal mitochondrial physiology. Both AMF7-63 and B8H10 detected recombinant apo and apo reduced SOD1 more readily than recombinant holo and holo aggregated SOD1. Detection had no dependence on mutational status as wild-type and mutant SOD1 (A4V, G85R, G93A) were equally labelled. Conversely, DSE2-3H1 and AMF7-63 were generated by immunizing animals with a C-terminal fragment of SOD1 (residues 125-142), which is localized to the electrostatic loop [234], implying that exposure of this epitope occurs when SOD1 lacks its metal cofactors. Indeed, apo SOD1 has reduced structural stability when lacking its metals [153, 161].

## 5.6. Conclusion

Conformational antibodies targeted to misfolded SOD1 show promise not only as therapeutics for ALS, but also as valuable tools with which to probe the mechanisms of misfolded SOD1 toxicity. These antibodies have revealed that multiple non-native species of misfolded SOD1 exist to contribute to motor neuron degeneration, possibly via distinct

mechanisms [453, 454]. Our study further supports this premise and highlights that variable potency/toxicity of different SOD1 species is possible. This finding may have profound implications for therapeutics aimed at neutralizing misfolded SOD1.

### 5.7. Materials and methods

*Animals:* $SOD1^{G93A}$ and $SOD1^{WT}$ transgenic rats have been previously described [216, 441]. Non-transgenic littermates were used in some experiments. Early symptomatic is defined as animals that have a noticeable gait defect, hopping or limping. Both male and female rats were used. Animals were treated in strict adherence with approved protocols from the CRCHUM Institutional Committee for the Protection of Animals and the Canadian Council on Animal Care (CCAC).

*Antibodies:* Rabbit anti-Cu/Zn SOD (Enzo Life Sciences), rabbit anti-SOD1 (Cell Signalling), mouse anti-VDAC1 (Calbiochem), mouse anti-actin (MP Biomedicals), were used for immunoblots. Mouse anti-misfolded SOD1 monoclonal antibodies D3H5 (generously provided by Dr. J-P Julien), A5C3, B8H10 and C4F6 (Medimabs), DSE2-3H1, rabbit anti-misfolded SOD1 monoclonal antibody AMF7-63 and rabbit polyclonal antibody SEDI (generously provided by Dr. J. Robertson) were used for blotting, immunofluorescence and flow cytometry. Mouse and rabbit IgG (Jackson Immunoresearch Labs) and mouse anti-IgG1 (BD Biosciences) were used as controls. Goat anti-mouse allophycocyanin-conjugated (BD Pharmingen), goat anti-rabbit PE (eBioscience) and goat anti-rabbit PE-Cy7-conjugated (Santa Cruz) secondary antibodies were used for flow cytometry studies. For immunofluorescence, goat anti-ChAT (Millipore), mouse anti- MAP2 (Sigma), rabbit anti-GFAP (Dako), and rabbit anti-ubiquitin (Dako) were used.

*Flow cytometry of isolated mitochondria:* Spinal cord and liver mitochondria were isolated from mice and rats [234], and prepared for analysis by flow cytometry exactly as previously described [444, 445].

*Immunoprecipitation, and immunoblotting:* Isolated mitochondria were solubilized and immunoprecipitated as previously described [234]. Briefly, 50 μg of mitochondria was incubated with 15 μL Protein G magnetic beads (Invitrogen), overnight at 4 degrees with rotation. Protein G beads were previously incubated with misfolded SOD1 antibody, as per manufacturer's instructions. Immunoprecipitated proteins were eluted from the beads in 2.5X Laemmli sample buffer and electrophoresed on 15 % Tris-Glycine gels, and subsequently transferred to nitrocellulose.

*Immunofluorescence*. Animals and sections were prepared as previously described [444]. Sections were labelled with anti-misfolded SOD1 antibodies, as previously described [444]. Briefly, sections were washed 10 minutes at room temperature in PBS, then permeabilized for 10 minutes at room temperature in PBS with 0.4 % TX-100. Sections were blocked with 2 % normal donkey serum (Sigma), 2 % bovine serum albumin (Sigma), in 0.4 % TX-100/PBS for 1 hour at room temperature. Primary antibodies were incubated overnight at 4 degrees in blocking solution. Appropriate secondary antibodies were added in blocking solution for 1 hour at room temperature and subsequently mounted, using ProLong anti-fade reagent (Invitrogen). Immunofluorescent images were captured by confocal microscope (Leica SP5; 20x objective, 1.7 NA) and processed with Leica LAS AF software and/or PhotoshopCS4 (Adobe).

*Filter-trap assay:* 20 μg of spinal cord homogenates or isolated spinal cord mitochondria in PBS were filtered onto 0.22 μM cellulose acetate membrane (GE Healthcare), for 1 hour at room temperature, using the Bio-Dot Microfiltration Apparatus (Bio-Rad). Wells were washed

twice with PBS, the membrane was removed from the apparatus and then blocked 1 hour at room temperature and immunoblotted with misfolded SOD1 antibodies. Isolated mitochondria for these experiments were prepared by a method in which mitochondria were floated to their buoyant density as to avoid any possible co-sedimentation with aggregates, as previously described [234].

*Dot Blot of recombinant SOD1 protein:* 1 μg of recombinant SOD1 protein, produced as previously described [455, 456], in TBS (20 mM Tris, 500 mM NaCl, 1mM EDTA pH 7.5) was filtered onto nitrocellulose membrane (BioRad), for 1 hour at room temperature using the Bio-Dot Microfiltration Apparatus (Bio-Rad). Wells were washed twice with TBS, and the membrane was removed from the apparatus and blocked in TBS-T (as above plus 0.05 % Tween-20) with 1 % bovine serum albumin (BSA) for 30 minutes at room temperature, and immunoblotted with misfolded SOD1 antibodies. Primary and secondary antibodies were incubated in blocking buffer. For non-native samples, 5 % v/v BME, and 0.5% v/v SDS was added, and samples were heat denatured by incubation for 5 minutes at 95 degrees Celsius.

*In vitro mitochondrial binding assay:* 50 μg of isolated spinal cord mitochondria (2μg/μL) from non-transgenic rats were incubated with 3 μM baculovirus-produced $SOD1^{WT}$ and $SOD1^{G93A}$ recombinant protein, purified as previously described [156], for 20 minutes at 37 degrees in HB Buffer (210 mM Mannitol, 70 mM Sucrose, 10 mM Tris pH 7.5, 1 mM EDTA) [156]. Mitochondria were washed once with HB buffer and then re-suspended in HB and 4X Laemmli sample buffer and subjected to SDS-PAGE and immunoblotted with an antibody to human SOD1 (Cell Signaling). To determine if modification of SOD1 structure would alter its binding to the mitochondrial surface, the protein was incubated with 5.5 mM EDTA or 10 mM hydrogen peroxide in PBS overnight at 4 degrees or room temperature, respectively, with

protease inhibitors (Roche). EDTA and hydrogen peroxide were removed and replaced by PBS by dialysis with Slide-A-Lyzer Mini dialysis devices (Pierce). Untreated samples were treated equivalently.

*Statistics:* Two-way ANOVA was used to determine the interaction between groups and time for percentage of misfolded $SOD1^+$ mitochondrial subpopulations over time and differences in AMF7-$63^+$, B8H$10^+$, and negative mitochondrial subpopulations over time. Sidak's multiple comparison test was used to determine differences between misfolded $SOD1^+$ groups. One-way ANOVA was used to determine differences in AMF7-$63^+$, AMF7-$63^+$B8H$10^+$ and B8H$10^+$ subpopulations. * $P < 0.05$, ** $P < 0.01$ *** $P < 0.001$, **** $P < 0.0001$.

## 5.8. Acknowledgements

We thank L. Hayward, J.P. Julien, and J. Robertson for sharing of reagents, A. Prat for access to the flow cytometer and confocal microscope, and G.A. Rouleau for his contribution to baculovirus protein production. This work was supported by the Canadian Foundation for Innovation, ALS Society of Canada, and the Frick Foundation for ALS Research (CVV). CVV and NA are CIHR New Investigators. SP was partially supported by the Tim Noël Studentship from the ALS Society of Canada.

# 5. Discussion

## 5.1. Misfolded SOD1, Bcl-2 and VDAC1

SOD1$^{G93A}$ rats accumulate B8H10-reactive misfolded SOD1 on the surface of spinal cord, but not liver mitochondria. The timing of B8H10-reactive deposition occurs just prior to symptoms, and before other hallmarks of disease [444]. Mitochondria with B8H10-reactive misfolded SOD1 on their surface have an increased volume, produce elevated levels of superoxide and have augmented levels of the pro-apoptotic form of Bcl-2 compared to mitochondria without misfolded SOD1 [444]. Misfolded SOD1 specific antibody DSE2 interacts with the voltage dependent anion channel 1 (VDAC1) and *in vitro* functional studies demonstrate that recombinant mutant SOD1, but not wild-type SOD1, decreases VDAC1 conductance in a reconstituted lipid bilayer. Although not focusing on misfolded SOD1, another group shows the interaction of mutant SOD1 with Bcl-2 is upstream of the altered VDAC1 permeability, therefore the conformational change of Bcl-2 induced by mutant SOD1 mediates toxicity and mitochondrial dysfunction [350]. B8H10-reactive misfolded SOD1 and the pro-apoptotic form of Bcl-2 accumulate on the same mitochondria, which have altered volume homeostasis and elevated superoxide levels [444]. VDAC1 has been shown to regulate both mitochondrial ionic hemostasis and the release of superoxide to the cytosol [436, 437, 448]. Taken together, this indirectly places misfolded SOD1, Bcl-2, and VDAC1 in the same complex at the mitochondrial surface, causing decreased outer membrane permeability to ADP (shown in [233, 350]), increased superoxide production (shown in [444] and proposed in [406]), as well as other possible downstream consequences such as decreased ATP production and increased calcium signaling (proposed in [406]). Whether VDAC1 and Bcl-2 interact with B8H10-

reactive misfolded SOD1 remains to be established. An argument against toxicity arising solely from a complex of misfolded SOD1/Bcl-2/VDAC1 is that $SOD1^{G37R}$ mice have an accelerated disease course and shortened survival when bred on a VDAC1 null background [233]. The authors state that further loss of VDAC1 conductance could sensitize mitochondria to SOD1-induced mitochondrial damage as well as to other mechanisms of disease [233]. To prove if this complex is disease relevant *in vivo,* mutant SOD1 mice could be immunized with the exon 2 peptide to determine if disease onset is delayed and survival extended. In addition to survival, evaluation of the interaction of BH3 exposed Bcl-2 confomer with VDAC1, ADP accumulation in mitochondria, and misfolded SOD1 (B8H10 and DSE2-reactive) accumulation at mitochondria will indicate the importance of this putative complex in disease.

### 5.2. Selective accumulation of misfolded SOD1 in tissue and cells

The B8H10 antibody detects misfolded SOD1 in lymphoblastoid cells from five FALS patients with four different SOD1 mutations, but not healthy controls, disease controls, or sporadic ALS patients [444]. Likewise, MS758-reactive misfolded SOD1 is detected in 14 FALS patients with 11 different SOD1 mutations [36]. However, evidence from SOD1 animal models indicates that misfolded SOD1 is selectively present in affected tissues [248], and is enriched in ventral versus dorsal spinal cord [236]. Why then is misfolded SOD1 found in patient lymphoblasts? It remains possible it is an artifact due to immortalization of these cell lines, as misfolded SOD1 has not yet been reported in peripheral blood drawn from ALS patients or animal models. However, it also suggests that all cell types have the capacity to produce misfolded SOD1. These results are consistent with oxidized wild-type SOD1 found in SALS

patient lymphoblasts [290]. Very little B8H10-reactive misfolded SOD1 is associated with isolated mitochondria from FALS patient lymphoblasts, and superoxide levels and mitochondrial transmembrane potential are comparable to controls [444]. Perhaps SOD1 association with mitochondria and subsequent toxicity depends on intrinsic cell-type specific factors. In fact, a recent publication identified the chaperone, MIF which inhibits the association of misfolded SOD1 with mitochondria [249]. MIF levels are abundant in liver, but not spinal cord cytosol. Perhaps MIF is not highly expressed in lymphoblasts thereby causing accumulation of misfolded SOD1. Alternatively, other motor neuron specific characteristics, such as their long-lived nature, may predispose these cells to increased association of misfolded SOD1 as opposed to cells in the liver, which are rapidly turned over.

### 5.3. A continuum of misfolded SOD1 species

Recent evidence suggests there are multiple misfolded SOD1 species, with distinct localizations, biochemical properties and disease mechanisms. Misfolded SOD1 specific antibodies may provide us the unique opportunity to tease out these differences and determine which misfolded SOD1 species contribute to disease. C4F6-reactive misfolded SOD1 is absent from spinal cord mitochondrial fractions [444], whereas B8H10, A5C3, DSE2, and a novel antibody with the same epitope as DSE2, AMF7-63 all readily detect non-native/misfolded SOD1 in these same mitochondrial fractions (**Chp. 4**). Therefore, C4F6-reactive misfolded SOD1 cannot contribute to mitochondrial dysfunction in ALS. Rather, evidence suggests that it is involved in disruption of axonal transport [244]. These results imply that misfolded SOD1

specific antibodies detect misfolded SOD1 conformations that have unique properties, such as association to spinal cord mitochondria.

AMF7-63-reactive misfolded SOD1, like B8H10, preferentially associates with isolated spinal cord, but not liver mitochondria (**Chp. 4**). Interestingly, a subpopulation of mitochondria have both B8H10 and AMF7-63-reactive misfolded SOD1 deposited on their surface. B8H10 and AMF7-63-reactive SOD1 segregated onto distinct mitochondrial subpopulations (**Chp. 4**). The presence of AMF7-63-reactive misfolded SOD1 on the mitochondria, regardless of the co-occurrence of B8H10-reactive misfolded SOD1, correlated with a larger mitochondrial volume and a trend towards enhanced superoxide production, compared to mitochondria with only B8H10-reactive misfolded SOD1. These results suggest that there are at least two distinct non-overlapping forms of misfolded SOD1 associated to the mitochondrial OMM, and indicate that individual forms of misfolded SOD1 may have distinct potencies.

Returning to the hypothesis that the misfolded SOD1/Bcl-2/VDAC1 complex is an important agent of mitochondrial damage, could AMF7-63-reactive misfolded SOD1 preferentially interact with Bcl-2 and VDAC1 versus B8H10-reactive misfolded SOD1? DSE2-reactive misfolded SOD1 is a known interactor of VDAC1, and the AMF7-63 misfolded SOD1 antibody recognizes the same epitope as the DSE2 antibody [233]. $B8H10^{+}$ mitochondria have increased levels of BH3-exposed Bcl-2 on their surface [444], although this does not prove a direct interaction. $B8H10^{+}$, BH3-exposed $Bcl\text{-}2^{+}$ mitochondria may also be $AMF7\text{-}63^{+}$, although this remains to be confirmed. Alternatively, unidentified protein interacting partners of AMF7-63 or B8H10-reactive misfolded SOD1 at the mitochondrial surface could mediate differential potencies.

Université de Montréal

Cette thèse intitulée:

# Uncovering the role of misfolded SOD1 in the pathogenesis of Amyotrophic Lateral Sclerosis

Présentée par
Sarah Pickles

a été évaluée par un jury composé des personnes suivantes:

Dr. Luis Rokeach, Président rapporteur

Dr. Christine Vande Velde, Directeur de recherché

Dr. Christopher Rose, Membre du jury

Dr. Daryl Bosco, Examinateur externe

Dr. Jean-Claude Labbé, Représentant du doyen

mitochondria accounted for its inability to modify disease course in SOD1 mouse models. Monitoring misfolded SOD1 association to mitochondria following treatment of SOD1 mouse models with misfolded SOD1 antibodies or ASO will provide evidence that mitochondrial damage is crucial for disease.

Collectively, multiple lines of evidence suggest that misfolded SOD1 assumes a spectrum of non-native conformations. Furthermore, these disparate misfolded SOD1 confomers may have different biochemical properties, localization, interacting partners, and participate in diverse disease mechanisms. C4F6-reactive misfolded SOD1 alters axonal transport [244], MS758-reactive misfolded SOD1 is linked to ER stress [36] and B8H10-reactive and now AMF7-63-reactive misfolded SOD1 correlate with mitochondrial damage (**Chp. 3-4**). Misfolded SOD1 antibodies are effective tools to differentiate misfolded SOD1 confomers and decipher common versus unique properties between misfolded SOD1 species. Do other misfolded SOD1 conformers known to associate with mitochondria, SEDI [248] and A5C3-reactive misfolded SOD1 [310], cause comparable damage and exhibit the same toxicity? Moreover, does misfolded SOD1 mediate other impairments in mitochondrial function, calcium handling, import, axonal transport, or ATP production? Categorizing the mitochondrial damage associated with each misfolded SOD1 confomer is of importance, but the ultimate goal is elucidating the mechanisms behind misfolded SOD1 toxicity. To that end, characterizing the misfolded SOD1 interactome for each misfolded SOD1 confomers would provide candidates to investigate. In addition, this approach could provide potential therapeutic targets aimed at reducing misfolded SOD1 association to mitochondria and ensuing mitochondrial damage.

### 5.4. Deficient mitochondrial import of SOD1

Metal deficient, apo SOD1, is structurally destabilized [152], readily forms fibrils [188] and is preferentially recognized by misfolded SOD1 specific antibodies B8H10 and AMF7-63 (**Chp. 4**). To be imported into mitochondria, SOD1 must be in its apo form [110, 152]. Metal depleted mutant SOD1 binds spinal cord mitochondria with greater affinity than mutant holo SOD1 (**Chp. 4**). SOD1 destined for mitochondrial import is synthesized as a polypeptide, and requires Hsp90/Hsp70 to supply the unfolded unmodified protein for import [458]. Given decreases in mitochondrial import in the $SOD1^{G93A}$ rat model [346] and that mutant SOD1 has altered regulation of import in neuronal cell lines [369], it is tempting to speculate that apo mutant SOD1 on route to the IMS is instead trapped at the OMM, either through aberrant protein interactions, including, but not limited to Lysyl-tRNA synthestase [385], Bcl-2 [374], MITOL [383] and/or VDAC [233] or by direct interaction with the lipids in the membrane [377, 378]. When in contact with lipid membranes apo SOD1 aggregates [459]. SOD1 aggregates and fibrils seed further fibrillation of natively folded SOD1 [295]. Therefore, apo SOD1 deposition at the mitochondrial OMM could lead to a feed-forward cascade of aggregation. Indeed, B8H10 and AMF7-63-reactive misfolded SOD1 are present in mitochondrial aggregates (**Chp. 4**). In addition to this seeding effect, CCS import and therefore SOD1 import is controlled by respiratory chain activity. Blocking complex III with Antimycin A results in increased mitochondrial localization of both CCS, and mutant SOD1 [369]. Defects in mitochondrial respiration have been documented in mutant SOD1 models [343-345], although not usually at complex III. Decreased respiration could drive mitochondrial import of SOD1, and increased retention of misfolded SOD1 at the mitochondrial surface, leading to more damaged

mitochondria. In support of this, the percentage of mitochondria with misfolded SOD1 on their surface increases with age in SOD1$^{G93A}$ rats, peaking when animals are symptomatic [444].

### 5.5 Relevance of misfolded SOD1 specific antibodies B8H10 and AMF7-63 in ALS

Both misfolded SOD1 specific antibodies, B8H10 and AMF7-63, detect a toxic form of mutant SOD1 that associates with damaged mitochondria in SOD1 rodent models, thus emphasizing their relevance in ALS pathogenesis (**Chp. 3-4**). Future efforts should aim to further characterize both B8H10 and AMF7-63-reactive misfolded SOD1 in terms of sub-cellular localization, mechanism(s) of toxicity and biochemical properties. Determining if B8H10 or AMF7-63-reactive misfolded SOD1 interact with other organelles would provide insight into what cellular process are specifically affected by these SOD1 species. Ultimately knowing what pathways are disrupted will aid in identify therapeutic targets. Furthermore, determining the biochemical properties, solubility, propensity to oligomerize or aggregate and protein interactors of specific misfolded SOD1 species may provide beneficial for the design of small molecule inhibitors of misfolded SOD1.

B8H10-reactive misfolded SOD1 was identified in lymphoblasts from five SOD1-linked FALS cases suggesting this form of misfolded SOD1 is relevant in human disease (**Chp.3**). The presence of AMF7-63-reactive misfolded in SOD1-mediated cases FALS cases should be evaluated to determine if this form of misfolded SOD1 is also implicated in human disease. The presence and relative abundance of both B8H10 and AMF7-63-reactive misfolded should be evaluated in spinal cords collected post-mortem from SOD1-linked FALS patient as well as iPSC derived motor neurons, to determine how common each of these misfolded SOD1 species are. Although B8H10-ractive misfolded SOD1 was not identified in lymphoblasts from SALS patients (**Chp. 3**), determining whether either B8H10 or AMF7-63 antibodies detect misfolded SOD1 in spinal cord tissue from SALS cases would be informative. Furthermore it could provide insight into whether SOD1 in relevant to SALS.

To date, no study has demonstrated that treatment with either B8H10 or AMF7-63 antibodies will provide any therapeutic benefit *in vivo*. Therefore a priority in future studies should be to treat SOD1 mouse models with B8H10 and AMF7-63 and evaluate survival, motor neuron preservation, attenuation of gliosis, neuromuscular junction innervation as well as association of misfolded SOD1 to mitochondria and mitochondrial damage. Given that both B8H10 and AMF7-63-reactive misfolded SOD1 are linked to damaged mitochondria (**Chp. 3-4**) and that reduction of B8H10-reactive misfolded SOD1 levels correlated with increased survival following treatment with another misfolded SOD1 antibody, it is likely these antibodies will also prove to be therapeutically viable. Multiple lines of evidence suggest that there are multiple species of misfolded SOD1 (**Chp.4**) [407, 408] perhaps necessitating reduction of many species of misfolded SOD1. Immunization with a cocktail of misfolded SOD1 antibodies targeting diverse SOD1 species with differing biochemical properties and mechanisms of toxicity may be more efficacious than treating with a single antibody. Proof of this hypothesis could be easily evaluated in SOD1 rodent models by comparing survival times and various makers of disease in animal immunized with one antibody (just B8H10 or AMF7-63) versus animals immunized with a combination of both antibodies (B8H10 and AMF7-63). Results presented in this thesis are summarized in **Figure 1**.

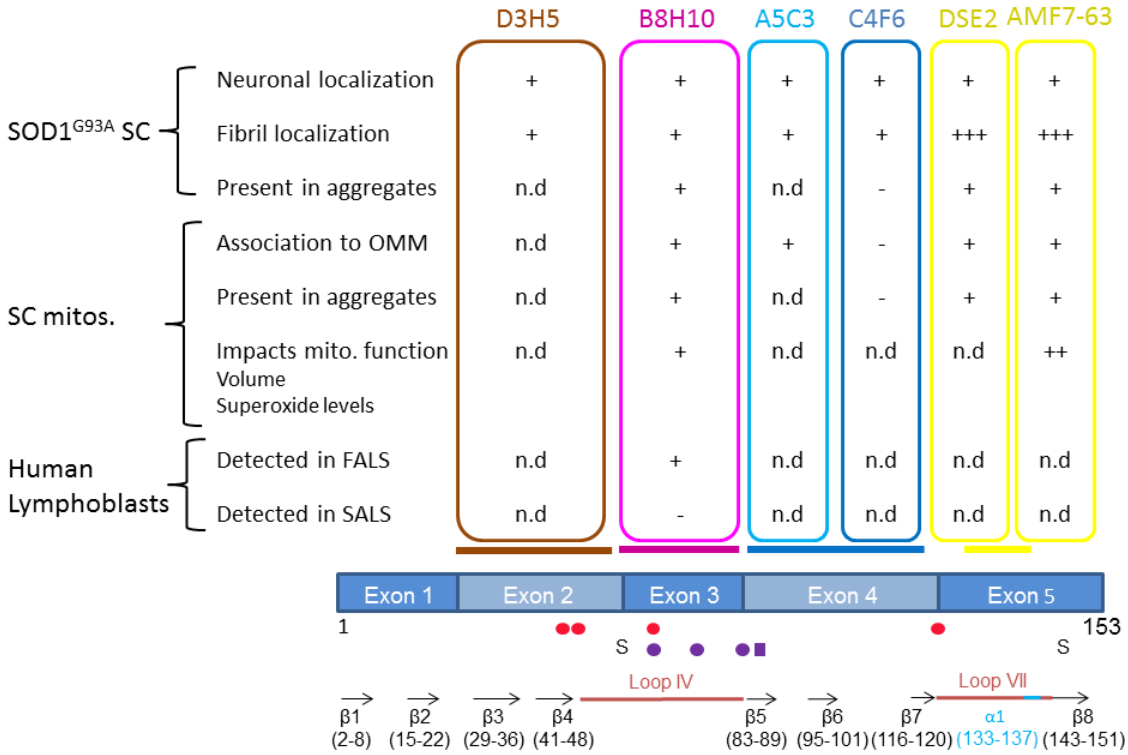


**Figure 1: Summary of findings**. Adapted from Pickles *et al*., 2012 [235]. Epitopes recognized by misfolded SOD1 antibodies used in this these mapped onto the SOD1 structure. Structural features are as indicated: β-strand (black), loops (pink), α helix (blue), disulfide bonds between Cys57 and Cys146 (S), copper-binding residues His46, His48, His63 His120 (red circles) and zinc-binding residues His63, His71, His80 and Asp83 (His, purple circles and Asp, purple square). SC, spinal cord OMM, outer mitochondrial membrane; +, positive finding; -, negative finding; n.d, not determined.

### 5.6. A mitochondrial (mito)-centric view of ALS

Mitochondria disturbances are a prominent feature of SOD1-mediated FALS, and likely SALS as well [290, 342, 351]. Evidence from non-SOD1 mediated FALS models suggests that mitochondria may also be relevant. It is tempting to speculate that mitochondrial dysfunction contributes to all ALS.

#### 5.6.1. Transactive response DNA binding protein 43 kDa

Although TDP-43 has a predominantly nuclear localization, it is also found in anterior horn neuron mitochondria of SALS patients as well as controls, signifying a role for TDP-43 in both normal physiology and in ALS pathology [460]. TDP-43 co-localizes with mitochondrial targeted fluorescent protein in axons and dendrites of rats over-expressing wild-type or mutant TDP-43, and both endogenous TDP-43 and exogenous TDP-43 is present in mitochondrial fractions from NSC-34 cells [461, 462]. It remains to be determined in which mitochondrial sub compartment TDP-43 is located.

Examination of tissue from several rodent models expressing wild-type or mutant TDP-43 reveals clusters of mitochondrial aggregates with altered morphology, including disorganization of cristae and vacuolization [463-467]. These abnormalities are also evident in cell culture models [462, 468]. TDP-$43^{WT}$ transgenic mice have increased levels of mitochondrial fission proteins, Fis1, and phosphorylated Drp-1, and decreased levels of Mfn1 [464, 465]. Reduction in mitochondria at the NMJ are observed in TDP-$43^{WT}$ mice, indicative

of deficits in mitochondrial transport [463]. Indeed, mitochondrial transport is compromised in the sciatic nerves of TDP-43$^{A315T}$ mice [469], with retrograde transport affected first, followed by anterograde transport [321]. Transport defects are accompanied by decreased mitochondrial length and mitochondrial clustering [321]. TDP-43$^{A315T}$ mice were compared to non-transgenic littermates, rather than mice expressing wild-type TDP-43, therefore the results should be interpreted with some caution as over-expression of wild-type TDP-43 can cause deleterious effects [470]. Mitochondrial transport dynamics are also altered in rat motor neurons expressing mutant and wild-type TDP-43, more so with mutant expression, and when levels of TDP-43 are depleted [461]. However, another study finds no difference in mitochondrial transport in mouse cortical neurons expressing wild-type or mutant TDP-43 [471]. Mitochondrial transport defects could be cell type specific as previously documented in cases of SOD1-mediated transport defects [320].

Wild-type and mutant TDP-43 expression in NSC-34 cells is linked to bioenergetics defects [467, 468], decreased membrane potential [462, 468], and increased reactive oxygen species production [462]. In yeast, TDP-43 expression causes peri-mitochondrial aggregated foci of TDP-43, which correlate with cytotoxicity [472]. Decreasing mitochondrial respiration genetically and pharmacologically improves cell survival, while increasing mitochondrial respiration decreased cell survival, implying mitochondrial respiration is linked to cell death possibly through ROS production [472]. One study tenuously linked TDP-43 and mitophagy, the selective removal of mitochondria by an autophagy like process, based on the observation that LC3-phosphatidylethanolamine conjugate (LC3-II) levels, a marker of the autophagosome, are increased in mitochondrial fractions of cells expressing TDP-43 [462]. TDP-43 binds Parkin mRNA [58, 462] and SALS patient motor neurons with cytoplasmic TDP-43 inclusions have

reduced levels of Parkin [69]. Moreover, Parkin ubiquitinates TDP-43 [473], thus providing evidence of a functional interaction between TDP-43 and Parkin. The link to mitophagy remains unknown, but it is possible TDP-43 modulates Parkin in the cytoplasm and/or at the mitochondrial surface. Interestingly, C-terminal fragments of TDP-43, commonly localized to TDP-43 positive inclusions in ALS patients, localize to mitochondria and lead to alterations in morphology, increased ROS production and defective mitophagy [462]. As many of these defects can be attributed to both wild-type and mutant TDP-43 expression, it is difficult to assess their relevance to disease. It is possible that many of the observed mitochondrial defects are simply artifacts of TDP-43 over-expression. Studies exploring the physiological role of TDP-43 with regards to mitochondria functional are required to dissect its true relevance. Few studies have examined mitochondrial function when TDP-43 levels are depleted, and this approach could begin to unravel whether TDP-43 is required for normal mitochondrial function. Nevertheless, it is possible that depletion of TDP-43 from the nucleus and accumulation in the cytoplasm causes a toxic gain of function of which the mitochondria are a possible target.

### 5.6.2. Vesicle–associated membrane protein-associated protein B

ALS associated VAPB mutation P56S disrupts anterograde transport of mitochondria via disruption of the interaction between mitochondrial motor proteins and tubulin as a consequence of increased cytosolic calcium [474]. VAPB interacts with the OMM protein. protein tyrosine phosphatase-interacting protein-51 (PTP1P51) at the mitochondria and mitochondria-associated membranes (MAMs) [475]. MAMs are domains where the mitochondrial outer membrane and the ER are in close proximity and actively held together by

tethering complexes [476]. These domains are important for phospholipid transfer and calcium signalling [476]. The PTPIP51-VAPB interaction regulates the formation of MAMs and mutant VAPB disrupts mitochondrial calcium uptake following release from the ER. Importantly, TDP-43 modulates this interaction [475, 477].

### 5.6.3. Fused in sarcoma

Transgenic rats over-expressing $FUS^{R521C}$ have aggregated and damaged spinal cord mitochondria. The lack of an appropriate control ($FUS^{WT}$ transgenic rats) makes it difficult to determine if these observed mitochondrial morphological defects can be specifically attributed to mutant FUS expression [478]. Expression of mutant FUS in motor neurons of dissociated mouse spinal cord cultures results in shorter mitochondria compared to wild-type FUS [479]. Despite hints that mutant FUS could impact mitochondrial functions it has yet to be fully characterized.

### 5.6.4. Valosin-containing protein

VCP, also known as p97 is implicated in ALS, but was first known to cause Inclusion body myopathy with early-onset Paget disease and frontotemporal dementia (IBMPFD). VCP is a member of the AAA+-ATPase protein family and has diverse functions including, but not limited to autophagy, vesicle transport, endoplasmic-reticulum-associated protein degradation

(ERAD) and of relevance here, mitochondria quality control [480]. VCP functions in the outer mitochondrial membrane associated degradation (OMMAD) by ensuring ubiquitinated proteins are brought to the proteasome [481]. VCP is linked to mitophagy, as it is recruited to depolarized mitochondria to remove Parkin-ubiquitinated Mfn1 and Mfn2 from the mitochondrial surface for degradation by the proteasome [482, 483]. Mitophagy is inhibited in mouse embryonic fibroblasts expressing either a disease associated mutant or an inactive mutant of VCP, leading to the accumulation of aggregated mitochondria [483]. Fibroblasts from patients with VCP mutations have decreased membrane potential, increased ROS production, and decreased ATP levels [484], as well as increased levels of glycolysis [485].

### 5.6.5. Optineurin

*OPTN* mutations were first identified in primary open-angle glaucoma (POAG) [486], and only later associated with ALS [92]. Optineurin is an autophagy receptor and is therefore able to bind both ubiquitin and LC3. Recently, Optineurin has been linked to mitophagy. Optineurin is recruited in a Parkin-dependent manner to damaged mitochondria [487]. At the mitochondria, Optineurin interacts with ubiquitinated proteins to recruit LC3 and form the autophagomsome [487]. Decreasing Optineurin levels inhibits the recruitment of LC3 thereby inhibiting mitochondrial degradation. This phenotype can be rescued by expressing wild-type Optineurin, but not mutations associated with ALS [487].

### 5.6.6. p62/Sequestosome 1 (p62/SQSTM1)

p62 also interacts with ubiquitinated proteins and LC3, functioning in protein degradation through both the proteasome and autophagy [488]. Several mutations in p62 are reported in FALS and SALS cases [489]. p62 is connected to mitophagy, and likely serves to cluster mitochondria, following Parkin-dependent recruitment to damaged mitochondria [490, 491]. In addition to involvement in mitophagy, p62 is linked to mitochondria in non-stressed conditions. MEFs depleted of p62 have fragmented mitochondria, decreased mitochondrial transmembrane potential, and decreased ATP production, attributed to decreased import of the mitochondrial transcription factor TFAM [492].

### 5.6.7. Coiled-coil helix coiled-coil helix domain 10

Mutations in *CHCHD10* are found in ALS as well as FTD, cerebellar ataxia and mitochondrial myopathy [96, 493-496]. *CHCHD10* is a nuclear-encoded mitochondrial protein of unknown function that resides in the IMS of mitochondria [96]. Although several ALS genes (*SOD1, TARDP, FUS, VCP, OPTN, VABP*, p62) are reported to disturb mitochondrial function, this is the first *bona fide* mitochondrial localized (but nuclear encoded) ALS gene, therefore reaffirming the importance of a mitochondrial contribution to ALS pathogenesis. Indeed, expression of mutant CHCHD10 in HeLa cells causes mitochondrial fragmentation and cristae disorganization [96]. Determining the exact function of CHCHD10 and how mutations cause disease will be an important area of future research. Members of the CHCHD protein family are also linked to mitochondria. CHCHD3 localizes to the IM, facing the IMS, and knock-down in HeLa cells causes mitochondrial fragmentation by modulation of Opa1 and Drp1 levels. In

addition, lack of CHCHD3 decreases respiration leading to diminution of ATP production, and disorganization of cristae [497]. Furthermore, CHCHD3 interacts with both Opa1 and Mitofilin [498, 499], two proteins involved in cristae formation [315]. Interestingly, CHCHD3 is imported into mitochondria and is properly folded by interaction with Mia40, the same protein that mediates SOD1 mitochondrial import [498]. If CHCHD10 also interacts with Mia40 for proper folding and retention within the IMS, it is possible that mutations cause its improper localization or regulation [500]. However, mislocalization due to pathological mutations has yet to be reported [96]. Proteomic analysis of NSC-34 cells expressing $SOD1^{G93A}$ reveal CHCHD3 is down regulated [501], perhaps indicative of a direct or indirect interaction of SOD1 with CHCHD proteins or involvement in a common pathway. CHCHD6 also interacts with Mitofilin [499], and knock-down causes defects in cristae morphology and decreased ATP production [502]. Finally, CHCHD2 is associated with Parkinson's disease [503]. Functional studies reveal it participates in mitochondrial respiration [504, 505], and is a negative regulator of apoptosis through interaction with Bcl-xL [506].

### 5.7. Novel avenues of research

Several mechanisms of mitochondrial dysfunction are recapitulated in other genetic models of ALS, morphological alterations, bioenergetics dysfunction, mitochondrial transport and calcium handling defects. However, several novel mechanisms of mitochondrial dysfunction not previously identified in SOD1 mediated FALS have been linked to other mutations, including mitochondria-ER connection via MAMs (also linked to calcium handling), and

mitophagy. Perhaps mutant/misfolded SOD1 is also involved in these pathways and negatively regulates various aspects of mitochondrial physiology.

### 5.7.2. Mitochondria-associated membranes

Given misfolded SOD1s penchant for association with membranes of both the mitochondria [233, 234, 248, 310, 444] and likely the ER [248, 249], it is reasonable to predict that misfolded SOD1 also localizes to MAMs. Two reported protein interactors of mutant/misfolded SOD1 are MAM proteins, VDAC1 [507], and MITOL [508], therefore strengthening a possible link between misfolded SOD1 and MAMS. VDAC1 dysfunction in ALS has already been documented to result in decreased levels of ADP [233, 350]. VDAC1 also regulates calcium influx from the ER into the mitochondria [509], therefore SOD1 mediated decreases in VDAC1 conductance could be hypothesized to limit mitochondrial calcium buffering. Whether VDAC does indeed cause mitochondrial calcium handling defects has yet to be evaluated in the context of ALS.

In vitro, MITOL ubiquitinates SOD1 to facilitate its proteosomal degradation. While this remains to be confirmed *in vivo*, it is also known that MITOL ubiquitinates Mfn2 so as to mediate Mfn2 oligomerization, which is crucial for mitochondrial-ER tethering and therefore MAM formation [508]. We can speculate that MAM formation is disturbed in ALS and evaluate whether there are differences in expression of MAM proteins in SOD1 models. If indeed misfolded SOD1 is present at MAMs, does it interact with other resident MAM proteins? Furthermore, it remains untested whether MAM functions, such as calcium handling and lipid synthesis are disturbed in ALS models. Addition of misfolded SOD1 antibodies to restore MAM

structure and function would be a valuable experiment that would be highly suggestive that misfolded negatively impacts MAMs. With regards to calcium handling it may be difficult to dissect the contribution from mitochondria versus MAMs. In fact, it could be possible that mitochondrial attributed calcium handling defects may be partially caused by altered function of MAMs. MAM function is reportedly increased in cells derived from Alzheimer Disease patients and well as post-mortem brain tissue [510, 511]. Of interest, MAMs may also play a role in ER-stress and autophagy, two pathways strongly implicated in ALS pathogenesis [512, 513].

### 5.7.3. Mitophagy

Mitophagy is the selective removal of mitochondria by autophagosomes [514]. This pathway was originally described in the elimination of depolarized mitochondria involving the accumulation of PTEN-induced putative kinase 1 (PINK1) on the mitochondrial outer membrane. Parkin is recruited to the mitochondria and is phosphorylated by PINK1 thereby activating its E3 ubiquitin ligase activity. Once activated, Parkin ubiquitinates various mitochondrial substrates (Mfn1, Mfn2 and VDAC1) for both ubiquitin mediated proteasome degradation and autophagosome recruitment. Autophagosomes are then brought to the lysosome to be degraded [514].

Three ALS-linked proteins, Optineurin, VCP and p62 are implicated in various aspects of mitophagy. TDP-43 damaged mitochondria could be a substrate for mitophagy, however the link is less well established. Surprisingly, mitophagy in the context of SOD1-mediated mitochondrial damage has not yet been investigated. Multiple lines of evidence indicate that

mitochondria are damaged in ALS. Why then are they not eliminated by mitophagy? Failure or inefficiency of the mitophagy system may result in the accumulation of damaged mitochondria that are observed in $SOD1^{G93A}$ rats (**Chp. 3-4**). Furthermore, if mitochondrial damage is unavoidable, augmenting mitophagy could be another viable approach to target mitochondrial-mediated damage involved in ALS.

Levels of PINK1 are increased in $SOD1^{G93A}$ mouse spinal cord motor neurons [515], but decreased PINK1 mRNA levels are documented in muscles in the same model, as well as in human SALS muscle tissue [516]. Accumulation of PINK1, and LC3-II on the surface of crude mitochondria is increased in human neuronal cells expressing mutant SOD1 when compared to wild-type SOD1 [318], indicating mitochondria exposed to mutant SOD1 could be a substrate for mitophagy. Unfortunately, this study did not investigate Parkin recruitment, or clearance of damaged mitochondria. Increased levels of LC3-II are documented in ALS animal models [517, 518], as well as the presence of lysosomes and autolysosomes surrounding mitochondria [519]. p62 levels increase with age in $SOD1^{G93A}$ mouse spinal cord, and p62 along with ubiquitinated SOD1 are found in spinal cord aggregates [520]. Mutant SOD1 interacts with p62 and this interaction facilitates the formation of aggregates which are engulfed by autophagosomes [521]. p62 is a proposed adaptor for the autophagosome formation in mitophagy [522], although the autophagosome can form independently of p62 [490, 491]. Collectively, these results suggest activation of mitophagy in ALS, yet it also indicates autophagy as a whole is upregulated in SOD1 animal models, consistent with many recent reports [523]. The classical paradigm of mitophagy involves recognition of depolarized mitochondria, which is not consistently reported in mutant SOD1-mediated mitochondrial damage. However, mitophagy is activated by other forms of damage, including increased ROS production [524], mitochondrial (mt) DNA

mutations [525], and misfolded protein in mitochondria [526]. Increased ROS production and misfolded proteins are widely documented in mutant SOD1 models, whereas a consensus on whether mutant SOD1 causes increased mitochondrial (mt) DNA mutations has yet to emerge [527-530]. Nevertheless, damaged mitochondria observed in SOD1 models are likely a substrate for mitophagy.

Further studies should determine if mitophagic flux is disturbed in ALS, and if so at what point in the pathway. Do disturbances in mitochondrial import [346] seen in ALS rat models affect PINK1 accumulation on mitochondria? An aberrant interaction between misfolded SOD1 and PINK1 at the mitochondrial surface could lead to decreased removal of mitochondria by mitophagy. In the same vein, misfolded SOD1 could also interact with Parkin. This interaction could be deleterious in both the cytosol and at the mitochondrial surface, in the former case leading to decreased recruitment of Parkin to mitochondria, and in the latter affecting ubiquitination and recruitment of autophagosome. Autophagosome recruitment could also be affected by misfolded SOD1 interacting with p62 or LC3-II. Furthermore, increased p62 and LC3-II levels could be indicative of an increased autophagic response to compensate for decreased targeted removal of damaged mitochondria.

Mitophagy in neurons is less straightforward than in immortalized cell lines, has distinct kinetics [531] and only affects a subset of mitochondria [524] so as to not completely deplete neurons of their main source of energy. Interestingly, PINK1 and Parkin activation lead to the degradation of Miro, an adaptor protein important for mitochondrial transport, and arrest of mitochondria in axons. It is possible that the mitochondrial transport defects (both anterograde

and retrograde) in mutant SOD1 models is due to PINK1/Parkin mediated halting of mitochondrial movement.

### 5.7.4. Mitochondrial unfolded protein response ($UPR^{mt}$)

Mitochondria are vulnerable to proteotoxicity due to exposure to high amounts of ROS that can disturb protein folding, structure, and cause mtDNA mutations. Furthermore the electron transport chain is formed of both nuclear and mitochondrial subunits which must be assembled in precise stoichiometries as to not leave orphaned subunits [532]. For these reasons, mitochondria have developed an unfolded protein response ($UPR^{mt}$) analogous to that of the cytoplasm and ER, which when activated causes increased expression of mitochondrial chaperones and proteases. This pathway is extensively characterized in *C. elegans*. The accumulation of unfolded proteins in the mitochondria results in cleavage of these proteins into peptides by the mitochondrial matrix protease ClpP. Peptides are exported out of the mitochondria by HAF-1, and signal to the transcription factor activating transcription factor associated with stress-1 (ATFS-1). ATFS-1 has both a mitochondrial targeting sequence, and a nuclear localization sequence. Under basal conditions, ATFS-1 is imported into mitochondria and degraded by another matrix protease, Lon. During stress, a portion of ATFS-1 fails to be imported into mitochondria, and translocates to the nucleus where it activates other transcription factors, which upregulate the expression of mitochondrial chaperones and proteases [532].

The mammalian $UPR^{mt}$ is not as thoroughly characterized, but misfolded protein accumulation in the mitochondrial matrix results in an up regulation of mitochondrial chaperones and proteases, via the transcription factor CHOP. CHOP is activated by c-Jun N-

terminal kinases (JNK activation) of c-Jun. A distinct $UPR^{mt}$ for misfolded proteins in the IMS involves AKT phosphorylation and activation of estrogen receptor α (ERα), which increases levels of IMS protease Htra2, the chaperone Nuclear respiratory factor-1 (NRF1), as well as the proteasome [532]. The signalling mechanism of how unfolded proteins in the matrix are sensed and transmitted remains unknown, and no mammalian counterpart for ATFS-1 has yet been found.

$UPR^{mt}$ has yet to be studied in the context of ALS, yet several lines of evidence provide the rationale that mutant/misfolded SOD1 at the mitochondria could activate $UPR^{mt}$. Mutant SOD1 targeted to the mitochondria matrix causes cytochrome C release, leading to apoptosis and death in N2a cells [533]. $UPR^{mt}$ was not assessed directly in this study and except for one report, SOD1 is not known to localize to the matrix. Nonetheless, mutant SOD1 in the matrix does lead to mitochondrial stress. Mitochondrial import is decreased in mitochondria from $SOD1^{G93A}$ rats, compared to $SOD1^{WT}$ rats [346]. In *C. elegans* decreased mitochondria import results in ATSF-1 nuclear localization and activation of gene expression to cope with mitochondrial stress. This is reminiscent of accumulation of PINK1 on the mitochondrial surface, due to decreased import leading to mitophagy. Decreased mitochondrial import may be a common mechanism by which mitochondria cope with stress or damage [534]. Gene expression profiling of iPSC-derived motor neurons from FALS patients reveals approximately 60% of the genes most down regulated are related to mitochondrial function [306]. Gene ontology analysis, demonstrates mitochondrial respiration and translation as pathways that are significantly down regulated [306]. A decrease in translation by treatment with cyclohexamide is protective to yeast during mitochondrial dysfunction [535]. Furthermore, decreased mitochondrial translation by knock down of mitochondrial ribosomal protein S5 (Mrps5)

activates the UPR$^{mt}$, by causing a mitochondria-nuclear protein imbalance [536]. Taken together, the data suggests that the balance of cytosolic and mitochondrial translation is tightly regulated. If not, UPR$^{mt}$ is activated. Alternatively, if mitochondria are damaged, decreased cytosolic translation is beneficial by relieving the stress of incorporating newly synthesized nuclear-encoded mitochondrial proteins into an already taxed organelle. At present, attenuation of mitochondrial translation is not implicated in the UPR$^{mt}$ response, as it is in the UPR$^{ER}$ [532]. The same study that showed mitochondrial ribosomal genes downregulated in mutant SOD1 motor neuron derived iPSCs also found that markers of UPR$^{ER}$ were upregulated [306]. Traditionally, the ER and mitochondrial act as discrete organelles and their respective unfolded protein response are specific and not co-activated [532]. However, with the discovery of an actual physical interactions between the ER and mitochondria, MAMs, the field is rethinking possible cross regulation between the ER and mitochondria. In fact, PERK may mediate signaling through CHOP to both the ER and mitochondria, providing a possible connection between both mitochondria and ER unfolded protein responses [537]. Mitochondria from SOD1 FALS patient motor neurons derived from iPSCs are dysfunctional and have decreased expression of genes involved in mitochondrial translation, implicating possible activation of UPR$^{mt}$, although this was not examined directly. Lastly, UPR$^{mt}$ is activated by depletion of mtDNA, deletions in electron transport genes [538], accumulation of misfolded proteins, inhibition of mitochondrial proteases and altered mitochondrial translation [536]. Mutant SOD1 has already been shown to cause accumulation of misfolded proteins in mitochondria, may cause mtDNA mutations, and leads to upregulation of ROS.

Whether mutant/misfolded SOD1 activates the UPR$^{mt}$ should be verified in *C.elegans* models, mammalian cells, and in iPSC-derived motor neurons. Up regulation of mitochondrial

chaperones and proteases is an appropriate readout of $UPR^{mt}$ activation. The focus should be on the IMS protease Htra2, as SOD1 localizes to the IMS. At present, it is not known how SOD1 (wild-type or mutant) is cleared from the mitochondrial interior. The expression of IMS localized SOD1 upon over-expression or knock-down should be evaluated to determine if Htra2 is the protease responsible for mitochondrial SOD1 degradation.

The combined evidence that matrix or IMS targeted mutant SOD1 causes mitochondrial damage, mitochondrial import is decreased in ALS animals models, and mitochondria ribosomal proteins and likely mitochondrial translation is down regulated in FALS patient motor neuron derived iPSCs, strongly implicates that the $UPR^{mt}$ is triggered in these model systems. A systematic investigation could reveal mechanistic insights into how mutant SOD1 damages mitochondria.

### 5.8. Mitochondria in SALS

Mitochondrial morphological abnormalities, bioenergetics defects and various forms of mitochondrial damage have been documented in SALS post-mortem tissue or cells [290, 342, 351]. However, until recently, the field has lacked an appropriate model to thoroughly interrogate mitochondrial dysfunction in SALS. With the development of iPSC-derived motor neurons, screening for disturbances in mitochondrial morphology, bioenergetics, protein import, axonal transport, calcium handling, MAM formation or function, mitophagy, $UPR^{mt}$, and vulnerability to mitochondrial stress, compared to cells from healthy controls or isogenic/gene-edited controls should be undertaken. These studies would provide clear answers as to whether

mitochondrial dysfunction is a common disease mechanism, relevant to the most abundant disease type, sporadic ALS.

# Conclusion

ALS is a devastating disease for both patients and their caregivers. To date, there is no treatment that significantly prolongs the lifespan of patients, despite countless clinical trials. A better understanding of why specifically motor neurons succumb to degeneration and the mechanisms leading to their death, would greatly improve the development of targeted clinical interventions. A portion of ALS cases are linked to mutations in *SOD1*, leading to misfolding of this protein. It is increasingly appreciated that misfolded SOD1 mediates toxicity in SOD1-mediated FALS. Thus several conformational antibodies that specifically detect misfolded SOD1 have been generated. We have shown that several of these antibodies detect misfolded SOD1 localized to spinal cord mitochondria, and more precisely to motor neuron mitochondria.

In an effort to determine how the presence of misfolded SOD1 at the mitochondrial surface impacts mitochondrial function in ALS rodent models, we developed a novel flow cytometric method. This method allowed us to identify two mitochondrial subpopulations, based on immunolabelling with the misfolded SOD1 specific antibody, B8H10. The decision to select this antibody was based on previous findings that decreased levels of B8H10 were associated with increased survival in SOD1 mouse models, following immunization with another misfolded SOD1 antibody [243]. B8H10-reactive misfolded SOD1 accumulates on $SOD1^{G93A}$ rat spinal cord mitochondria beginning at 14 weeks, just prior to disease onset, and reaches highest levels when rats become symptomatic. $B8H10^{+}$ mitochondria are of larger volume and produce more superoxide compared to $B8H10^{-}$ counterparts. In addition, the presence of B8H10-reactive misfolded SOD1 at mitochondria correlates with increased levels of the pro-apoptotic, BH3 domain-exposed form of Bcl-2. Pre-symptomatic deposition of misfolded SOD1

at the mitochondria, and increased mitochondrial volume and elevated superoxide levels are recapitulated in the SOD1$^{G37R}$ mouse model. Collectively, these results indicate that B8H10-reactive misfolded SOD1 tracks with mitochondrial damage. B8H10-reactive misfolded SOD1 is detected in lymphoblastoid cells derived from ALS patients with *SOD1* mutations, but not SALS patients or controls. Together these results indicate B8H10-reactive misfolded SOD1 is a common feature of both ALS rodent models and human disease.

From this study we also observe B8H10, but not C4F6-reactive misfolded SOD1 in mitochondrial fractions, suggesting differing localization of misfolded SOD1 species. Similarly, a report from another group comparing the SEDI and C4F6 antibody reactivities in a cell culture model of mutant SOD1 expression suggest different misfolded SOD1 species may have different biochemical characteristics [408]. The SEDI antibody detects misfolded SOD1 in insoluble inclusions whereas the C4F6 antibody recognizes soluble misfolded SOD1 [408]. Exposure of certain SOD1 epitopes as recognized by a series of SOD1 peptide antibodies identified different strains of SOD1 aggregates in SOD1 mouse models [407]. One such strain was suggested to have enhanced toxicity as increased amounts of this form of SOD1 aggregate correlated with earlier time of onset and a faster disease progression [407]. Together, these data indicate there are multiple forms of misfolded SOD1 species that can be differentiated based on binding to different misfolded SOD1 antibodies. In an effort to better characterize misfolded SOD1 species, we used a panel of misfolded SOD1 antibodies to label SOD1$^{G93A}$ spinal cord sections. Misfolded SOD1 antibodies DSE2 and AMF7-63, both targeted to the same of epitope of SOD1, labeled motor neurons as well as fibrils in the anterior horn. Misfolded SOD1 antibodies A5C3, B8H10, C4F6 and D3H5, all raised against apo SOD1$^{G93A}$ protein, predominantly labeled motor neurons and puncta in the neuropil. Interestingly, double labelling

with AMF7-63 and B8H10 antibodies yielded a partial co-localization, again suggestive of two distinct species of misfolded SOD1. With the exception of C4F6, all of the misfolded SOD1 antibodies indicated a pool of misfolded SOD1 is localized to the surface of spinal cord mitochondria. Immunolabelling and flow cytometric analysis of spinal cord mitochondria with both AMF7-63 and B8H10 antibodies revealed AMF7-63$^{+}$ mitochondria had a larger mitochondrial volume, but similar superoxide levels compared to the B8H10$^{+}$ subpopulation, implying that these antibodies recognize separate misfolded SOD1 species, with differing toxicities. Analysis of subpopulations of just AMF7-63$^{+}$, B8H10$^{+}$ or mitochondria with both misfolded SOD1 species, AMF7-63$^{+}$B8H10$^{+}$ yielded no volume difference, although mitochondria with AMF7-63-misfolded SOD1 on their surface had a trend toward increased volume. The presence of AMF7-63 alone on mitochondria cannot directly be linked to increased mitochondrial volume. Both AMF7-63 and B8H10-misfolded SOD1 are found in mitochondrial aggregates and partially co-localize with ubiquitin in SOD1$^{G93A}$ rat spinal cords. Differences in mitochondrial volume cannot be explained by incorporation of diverse misfolded species into aggregates. Alternatively, the size of misfolded SOD1 aggregates, solubility of misfolded SOD1 species, or interacting partners of different misfolded SOD1 species may account for altered potencies. All of these elements should be investigated to better understand the differences between misfolded SOD1 species.

Taken together, multiple misfolded SOD1 species converge at the mitochondria, and two such species correlate with increased mitochondria volume and superoxide levels. Future efforts should be aimed at characterizing if other misfolded species localize to the mitochondria and if they are also associated with damage. In the current set of studies, we have focused on mitochondrial volume, superoxide production and transmembrane potential, however mutant

SOD1 has been linked to many other aspects of mitochondrial dysfunction which have yet to be examined in mitochondria coated with misfolded SOD1. In addition, understanding the mechanisms of how misfolded SOD1 exerts its toxic effects at the mitochondria could potentially lead to targets for future therapies.

Mitochondria have been implicated in non-SOD1 mediated FALS, as well as SALS, demonstrating the universality of mitochondria dysfunction in ALS. The protein products of the ALS-linked genes, TDP-43, VCP, p62, OPTN, VAPB and CHCHD10 have implicated new aspects of mitochondrial function in disease, including MAMs and mitophagy, which have yet to be explored in the context of SOD1 mutations. Finally, it is hoped that fully understanding the various pathways regulating mitochondrial physiology will provide crucial information for the development of viable therapeutics for ALS.

# Bibliography


1. Rowland, L.P., *How amyotrophic lateral sclerosis got its name: the clinical-pathologic genius of Jean-Martin Charcot*. Arch Neurol, 2001. **58**(3): p. 512-5.
2. Chio, A., et al., *Global epidemiology of amyotrophic lateral sclerosis: a systematic review of the published literature*. Neuroepidemiology., 2013. **41**(2): p. 118-30. doi: 10.1159/000351153. Epub 2013 Jul 11.
3. Marangi, G. and B.J. Traynor, *Genetic causes of amyotrophic lateral sclerosis: New genetic analysis methodologies entailing new opportunities and challenges*. Brain Res, 2014.
4. Logroscino, G., et al., *Incidence of amyotrophic lateral sclerosis in Europe*. J Neurol Neurosurg Psychiatry., 2010. **81**(4): p. 385-90. doi: 10.1136/jnnp.2009.183525. Epub 2009 Aug 25.
5. Turner, M.R., et al., *Young-onset amyotrophic lateral sclerosis: historical and other observations*. Brain., 2012. **135**(Pt 9): p. 2883-91. doi: 10.1093/brain/aws144. Epub 2012 Jun 1.
6. Kiernan, M.C., et al., *Amyotrophic lateral sclerosis*. Lancet., 2011. **377**(9769): p. 942-55. doi: 10.1016/S0140-6736(10)61156-7. Epub 2011 Feb 4.
7. Alonso, A., et al., *Incidence and lifetime risk of motor neuron disease in the United Kingdom: a population-based study*. Eur J Neurol, 2009. **16**(6): p. 745-51.
8. Chio, A., et al., *Prognostic factors in ALS: A critical review*. Amyotroph Lateral Scler, 2009. **10**(5-6): p. 310-23.
9. Wijesekera, L.C. and P.N. Leigh, *Amyotrophic lateral sclerosis*. Orphanet J Rare Dis, 2009. **4**: p. 3.
10. Leblond, C.S., et al., *Dissection of genetic factors associated with amyotrophic lateral sclerosis*. Exp Neurol, 2014. **262 Pt B**: p. 91-101.
11. Byrne, S., et al., *Cognitive and clinical characteristics of patients with amyotrophic lateral sclerosis carrying a C9orf72 repeat expansion: a population-based cohort study*. Lancet Neurol, 2012. **11**(3): p. 232-40.
12. Al-Chalabi, A. and O. Hardiman, *The epidemiology of ALS: a conspiracy of genes, environment and time*. Nat Rev Neurol, 2013. **9**(11): p. 617-28.
13. Scarmeas, N., et al., *Premorbid weight, body mass, and varsity athletics in ALS*. Neurology, 2002. **59**(5): p. 773-5.
14. Sutedja, N.A., et al., *Exposure to chemicals and metals and risk of amyotrophic lateral sclerosis: a systematic review*. Amyotroph Lateral Scler, 2009. **10**(5-6): p. 302-9.
15. Beghi, E., et al., *Amyotrophic lateral sclerosis, physical exercise, trauma and sports: results of a population-based pilot case-control study*. Amyotroph Lateral Scler, 2010. **11**(3): p. 289-92.
16. Van Langenhove, T., J. van der Zee, and C. Van Broeckhoven, *The molecular basis of the frontotemporal lobar degeneration-amyotrophic lateral sclerosis spectrum*. Ann Med, 2012. **44**(8): p. 817-28.
17. Sieben, A., et al., *The genetics and neuropathology of frontotemporal lobar degeneration*. Acta Neuropathol, 2012. **124**(3): p. 353-72.

18. Ringholz, G.M., et al., *Prevalence and patterns of cognitive impairment in sporadic ALS*. Neurology, 2005. **65**(4): p. 586-90.
19. Byrne, S., et al., *Aggregation of neurologic and neuropsychiatric disease in amyotrophic lateral sclerosis kindreds: a population-based case-control cohort study of familial and sporadic amyotrophic lateral sclerosis*. Ann Neurol, 2013. **74**(5): p. 699-708.
20. Harms, M.B. and R.H. Baloh, *Clinical neurogenetics: amyotrophic lateral sclerosis*. Neurol Clin, 2013. **31**(4): p. 929-50.
21. Kiernan, M.C., et al., *Amyotrophic lateral sclerosis*. Lancet, 2011. **377**(9769): p. 942-55.
22. Simon, N.G., et al., *Quantifying disease progression in amyotrophic lateral sclerosis*. Ann Neurol, 2014. **76**(5): p. 643-57.
23. Brockington, A., et al., *Unravelling the enigma of selective vulnerability in neurodegeneration: motor neurons resistant to degeneration in ALS show distinct gene expression characteristics and decreased susceptibility to excitotoxicity*. Acta Neuropathol, 2013. **125**(1): p. 95-109.
24. Kinsley, L. and T. Siddique, *Amyotrophic Lateral Sclerosis Overview*, in *GeneReviews(R)*, R.A. Pagon, et al., Editors. 1993, University of Washington, Seattle

University of Washington, Seattle. All rights reserved.: Seattle (WA).
25. Gordon, P.H., *Amyotrophic Lateral Sclerosis: An update for 2013 Clinical Features, Pathophysiology, Management and Therapeutic Trials*. Aging Dis, 2013. **4**(5): p. 295-310.
26. Rosen, D.R., et al., *Mutations in Cu/Zn superoxide dismutase gene are associated with familial amyotrophic lateral sclerosis*. Nature, 1993. **362**(6415): p. 59-62.
27. McCord, J.M. and I. Fridovich, *Superoxide dismutase. An enzymic function for erythrocuprein (hemocuprein)*. J Biol Chem, 1969. **244**(22): p. 6049-55.
28. Abel, O., et al., *ALSoD: A user-friendly online bioinformatics tool for amyotrophic lateral sclerosis genetics*. Hum Mutat, 2012. **33**(9): p. 1345-51.
29. Saccon, R.A., et al., *Is SOD1 loss of function involved in amyotrophic lateral sclerosis?* Brain, 2013. **136**(Pt 8): p. 2342-58.
30. Felbecker, A., et al., *Four familial ALS pedigrees discordant for two SOD1 mutations: are all SOD1 mutations pathogenic?* J Neurol Neurosurg Psychiatry, 2010. **81**(5): p. 572-7.
31. Cleveland, D.W. and J.D. Rothstein, *From Charcot to Lou Gehrig: deciphering selective motor neuron death in ALS*. Nat Rev Neurosci, 2001. **2**(11): p. 806-19.
32. Pratt, A.J., et al., *Aggregation propensities of superoxide dismutase G93 hotspot mutants mirror ALS clinical phenotypes*. Proc Natl Acad Sci U S A, 2014. **111**(43): p. E4568-76.
33. Rotunno, M.S. and D.A. Bosco, *An emerging role for misfolded wild-type SOD1 in sporadic ALS pathogenesis*. Front Cell Neurosci, 2013. **7**: p. 253.
34. Al-Chalabi, A., et al., *Recessive amyotrophic lateral sclerosis families with the D90A SOD1 mutation share a common founder: evidence for a linked protective factor*. Hum Mol Genet, 1998. **7**(13): p. 2045-50.
35. Renton, A.E., et al., *A hexanucleotide repeat expansion in C9ORF72 is the cause of chromosome 9p21-linked ALS-FTD*. Neuron, 2011. **72**(2): p. 257-68.

36. Fujisawa, T., et al., *A novel monoclonal antibody reveals a conformational alteration shared by amyotrophic lateral sclerosis-linked SOD1 mutants*. Ann Neurol, 2012. **72**(5): p. 739-49.
37. Renton, A.E., A. Chio, and B.J. Traynor, *State of play in amyotrophic lateral sclerosis genetics*. Nat Neurosci, 2014. **17**(1): p. 17-23.
38. Bennion Callister, J. and S.M. Pickering-Brown, *Pathogenesis/genetics of frontotemporal dementia and how it relates to ALS*. Exp Neurol, 2014. **262 Pt B**: p. 84-90.
39. Camu, W., et al., *Genetics of familial ALS and consequences for diagnosis. French ALS Research Group*. J Neurol Sci, 1999. **165 Suppl 1**: p. S21-6.
40. Cudkowicz, M.E., et al., *Epidemiology of mutations in superoxide dismutase in amyotrophic lateral sclerosis*. Ann Neurol, 1997. **41**(2): p. 210-21.
41. Del Grande, A., et al., *D11Y SOD1 mutation and benign ALS: a consistent genotype-phenotype correlation*. J Neurol Sci, 2011. **309**(1-2): p. 31-3.
42. Neumann, M., et al., *Ubiquitinated TDP-43 in frontotemporal lobar degeneration and amyotrophic lateral sclerosis*. Science, 2006. **314**(5796): p. 130-3.
43. Sreedharan, J., et al., *TDP-43 mutations in familial and sporadic amyotrophic lateral sclerosis*. Science, 2008. **319**(5870): p. 1668-72.
44. Kabashi, E., et al., *TARDBP mutations in individuals with sporadic and familial amyotrophic lateral sclerosis*. Nat Genet, 2008. **40**(5): p. 572-4.
45. Gitcho, M.A., et al., *TDP-43 A315T mutation in familial motor neuron disease*. Ann Neurol, 2008. **63**(4): p. 535-8.
46. Lattante, S., G.A. Rouleau, and E. Kabashi, *TARDBP and FUS mutations associated with amyotrophic lateral sclerosis: summary and update*. Hum Mutat, 2013. **34**(6): p. 812-26.
47. Ou, S.H., et al., *Cloning and characterization of a novel cellular protein, TDP-43, that binds to human immunodeficiency virus type 1 TAR DNA sequence motifs*. J Virol, 1995. **69**(6): p. 3584-96.
48. Cohen, T.J., et al., *An acetylation switch controls TDP-43 function and aggregation propensity*. Nat Commun, 2015. **6**: p. 5845.
49. Ling, S.C., M. Polymenidou, and D.W. Cleveland, *Converging mechanisms in ALS and FTD: disrupted RNA and protein homeostasis*. Neuron, 2013. **79**(3): p. 416-38.
50. King, O.D., A.D. Gitler, and J. Shorter, *The tip of the iceberg: RNA-binding proteins with prion-like domains in neurodegenerative disease*. Brain Res, 2012. **1462**: p. 61-80.
51. Da Cruz, S. and D.W. Cleveland, *Understanding the role of TDP-43 and FUS/TLS in ALS and beyond*. Curr Opin Neurobiol, 2011. **21**(6): p. 904-19.
52. Budini, M., et al., *TDP-43 loss of cellular function through aggregation requires additional structural determinants beyond its C-terminal Q/N prion-like domain*. Hum Mol Genet, 2015. **24**(1): p. 9-20.
53. Chang, C.K., et al., *The N-terminus of TDP-43 promotes its oligomerization and enhances DNA binding affinity*. Biochem Biophys Res Commun, 2012. **425**(2): p. 219-24.
54. Qin, H., et al., *TDP-43 N terminus encodes a novel ubiquitin-like fold and its unfolded form in equilibrium that can be shifted by binding to ssDNA*. Proc Natl Acad Sci U S A, 2014. **111**(52): p. 18619-24.

55. Zhang, Y.J., et al., *The dual functions of the extreme N-terminus of TDP-43 in regulating its biological activity and inclusion formation*. Hum Mol Genet, 2013. **22**(15): p. 3112-22.
56. Buratti, E., et al., *Nuclear factor TDP-43 and SR proteins promote in vitro and in vivo CFTR exon 9 skipping*. Embo j, 2001. **20**(7): p. 1774-84.
57. Mercado, P.A., et al., *Depletion of TDP 43 overrides the need for exonic and intronic splicing enhancers in the human apoA-II gene*. Nucleic Acids Res, 2005. **33**(18): p. 6000-10.
58. Polymenidou, M., et al., *Long pre-mRNA depletion and RNA missplicing contribute to neuronal vulnerability from loss of TDP-43*. Nat Neurosci, 2011. **14**(4): p. 459-68.
59. Igaz, L.M., et al., *Dysregulation of the ALS-associated gene TDP-43 leads to neuronal death and degeneration in mice*. J Clin Invest, 2011. **121**(2): p. 726-38.
60. Swarup, V., et al., *Pathological hallmarks of amyotrophic lateral sclerosis/frontotemporal lobar degeneration in transgenic mice produced with TDP-43 genomic fragments*. Brain, 2011. **134**(Pt 9): p. 2610-26.
61. Wils, H., et al., *TDP-43 transgenic mice develop spastic paralysis and neuronal inclusions characteristic of ALS and frontotemporal lobar degeneration*. Proc Natl Acad Sci U S A, 2010. **107**(8): p. 3858-63.
62. Avendano-Vazquez, S.E., et al., *Autoregulation of TDP-43 mRNA levels involves interplay between transcription, splicing, and alternative polyA site selection*. Genes Dev, 2012. **26**(15): p. 1679-84.
63. Kwiatkowski, T.J., Jr., et al., *Mutations in the FUS/TLS gene on chromosome 16 cause familial amyotrophic lateral sclerosis*. Science, 2009. **323**(5918): p. 1205-8.
64. Vance, C., et al., *Mutations in FUS, an RNA processing protein, cause familial amyotrophic lateral sclerosis type 6*. Science, 2009. **323**(5918): p. 1208-11.
65. Rabbitts, T.H., et al., *Fusion of the dominant negative transcription regulator CHOP with a novel gene FUS by translocation t(12;16) in malignant liposarcoma*. Nat Genet, 1993. **4**(2): p. 175-80.
66. Iko, Y., et al., *Domain architectures and characterization of an RNA-binding protein, TLS*. J Biol Chem, 2004. **279**(43): p. 44834-40.
67. Deng, H., K. Gao, and J. Jankovic, *The role of FUS gene variants in neurodegenerative diseases*. Nat Rev Neurol, 2014. **10**(6): p. 337-48.
68. Zinszner, H., et al., *TLS (FUS) binds RNA in vivo and engages in nucleo-cytoplasmic shuttling*. J Cell Sci, 1997. **110 ( Pt 15)**: p. 1741-50.
69. Lagier-Tourenne, C., et al., *Divergent roles of ALS-linked proteins FUS/TLS and TDP-43 intersect in processing long pre-mRNAs*. Nat Neurosci, 2012. **15**(11): p. 1488-97.
70. Broustal, O., et al., *FUS mutations in frontotemporal lobar degeneration with amyotrophic lateral sclerosis*. J Alzheimers Dis, 2010. **22**(3): p. 765-9.
71. Merner, N.D., et al., *Exome sequencing identifies FUS mutations as a cause of essential tremor*. Am J Hum Genet, 2012. **91**(2): p. 313-9.
72. Van Langenhove, T., et al., *Genetic contribution of FUS to frontotemporal lobar degeneration*. Neurology, 2010. **74**(5): p. 366-71.
73. Blair, I.P., et al., *FUS mutations in amyotrophic lateral sclerosis: clinical, pathological, neurophysiological and genetic analysis*. J Neurol Neurosurg Psychiatry, 2010. **81**(6): p. 639-45.

74. Millecamps, S., et al., *SOD1, ANG, VAPB, TARDBP, and FUS mutations in familial amyotrophic lateral sclerosis: genotype-phenotype correlations*. J Med Genet, 2010. **47**(8): p. 554-60.
75. DeJesus-Hernandez, M., et al., *Expanded GGGGCC hexanucleotide repeat in noncoding region of C9ORF72 causes chromosome 9p-linked FTD and ALS*. Neuron, 2011. **72**(2): p. 245-56.
76. Majounie, E., et al., *Frequency of the C9orf72 hexanucleotide repeat expansion in patients with amyotrophic lateral sclerosis and frontotemporal dementia: a cross-sectional study*. Lancet Neurol, 2012. **11**(4): p. 323-30.
77. Budworth, H. and C.T. McMurray, *A brief history of triplet repeat diseases*. Methods Mol Biol, 2013. **1010**: p. 3-17.
78. van Blitterswijk, M., et al., *Association between repeat sizes and clinical and pathological characteristics in carriers of C9ORF72 repeat expansions (Xpansize-72): a cross-sectional cohort study*. Lancet Neurol, 2013. **12**(10): p. 978-88.
79. Nordin, A., et al., *Extensive size variability of the GGGGCC expansion in C9orf72 in both neuronal and non-neuronal tissues in 18 patients with ALS or FTD*. Hum Mol Genet, 2015.
80. Cooper-Knock, J., P.J. Shaw, and J. Kirby, *The widening spectrum of C9ORF72-related disease; genotype/phenotype correlations and potential modifiers of clinical phenotype*. Acta Neuropathol, 2014. **127**(3): p. 333-45.
81. Levine, T.P., et al., *The product of C9orf72, a gene strongly implicated in neurodegeneration, is structurally related to DENN Rab-GEFs*. Bioinformatics, 2013. **29**(4): p. 499-503.
82. Marat, A.L., H. Dokainish, and P.S. McPherson, *DENN domain proteins: regulators of Rab GTPases*. J Biol Chem, 2011. **286**(16): p. 13791-800.
83. Farg, M.A., et al., *C9ORF72, implicated in amytrophic lateral sclerosis and frontotemporal dementia, regulates endosomal trafficking*. Hum Mol Genet, 2014. **23**(13): p. 3579-95.
84. Ciura, S., et al., *Loss of function of C9orf72 causes motor deficits in a zebrafish model of amyotrophic lateral sclerosis*. Ann Neurol, 2013. **74**(2): p. 180-7.
85. Therrien, M., et al., *Deletion of C9ORF72 results in motor neuron degeneration and stress sensitivity in C. elegans*. PLoS One, 2013. **8**(12): p. e83450.
86. Pearson, C.E., *Repeat associated non-ATG translation initiation: one DNA, two transcripts, seven reading frames, potentially nine toxic entities!* PLoS Genet, 2011. **7**(3): p. e1002018.
87. Donnelly, C.J., et al., *RNA toxicity from the ALS/FTD C9ORF72 expansion is mitigated by antisense intervention*. Neuron, 2013. **80**(2): p. 415-28.
88. Zu, T., et al., *RAN proteins and RNA foci from antisense transcripts in C9ORF72 ALS and frontotemporal dementia*. Proc Natl Acad Sci U S A, 2013. **110**(51): p. E4968-77.
89. Belzil, V.V., T.F. Gendron, and L. Petrucelli, *RNA-mediated toxicity in neurodegenerative disease*. Mol Cell Neurosci, 2013. **56**: p. 406-19.
90. Gendron, T.F., et al., *Antisense transcripts of the expanded C9ORF72 hexanucleotide repeat form nuclear RNA foci and undergo repeat-associated non-ATG translation in c9FTD/ALS*. Acta Neuropathol, 2013. **126**(6): p. 829-44.

91. Wen, X., et al., *Antisense proline-arginine RAN dipeptides linked to C9ORF72-ALS/FTD form toxic nuclear aggregates that initiate in vitro and in vivo neuronal death*. Neuron, 2014. **84**(6): p. 1213-25.
92. Maruyama, H., et al., *Mutations of optineurin in amyotrophic lateral sclerosis*. Nature, 2010. **465**(7295): p. 223-6.
93. Johnson, J.O., et al., *Exome sequencing reveals VCP mutations as a cause of familial ALS*. Neuron, 2010. **68**(5): p. 857-64.
94. Deng, H.X., et al., *Mutations in UBQLN2 cause dominant X-linked juvenile and adult-onset ALS and ALS/dementia*. Nature, 2011. **477**(7363): p. 211-5.
95. Mitchell, J., et al., *Familial amyotrophic lateral sclerosis is associated with a mutation in D-amino acid oxidase*. Proc Natl Acad Sci U S A, 2010. **107**(16): p. 7556-61.
96. Bannwarth, S., et al., *A mitochondrial origin for frontotemporal dementia and amyotrophic lateral sclerosis through CHCHD10 involvement*. Brain, 2014. **137**(Pt 8): p. 2329-45.
97. Johnson, J.O., et al., *Mutations in the Matrin 3 gene cause familial amyotrophic lateral sclerosis*. Nat Neurosci., 2014. **17**(5): p. 664-6. doi: 10.1038/nn.3688. Epub 2014 Mar 30.
98. Cirulli, E.T., et al., *Exome sequencing in amyotrophic lateral sclerosis identifies risk genes and pathways*. Science, 2015. **347**(6229): p. 1436-1441.
99. Ronemus, M., et al., *The role of de novo mutations in the genetics of autism spectrum disorders*. Nat Rev Genet, 2014. **15**(2): p. 133-41.
100. Veltman, J.A. and H.G. Brunner, *De novo mutations in human genetic disease*. Nat Rev Genet, 2012. **13**(8): p. 565-75.
101. Alexander, M.D., et al., "*True*" *sporadic ALS associated with a novel SOD-1 mutation*. Ann Neurol, 2002. **52**(5): p. 680-3.
102. Calvo, A., et al., *De novo nonsense mutation of the FUS gene in an apparently familial amyotrophic lateral sclerosis case*. Neurobiol Aging, 2014. **35**(6): p. 1513.e7-11.
103. Chio, A., et al., *A de novo missense mutation of the FUS gene in a "true" sporadic ALS case*. Neurobiol Aging, 2011. **32**(3): p. 553.e23-6.
104. DeJesus-Hernandez, M., et al., *De novo truncating FUS gene mutation as a cause of sporadic amyotrophic lateral sclerosis*. Hum Mutat, 2010. **31**(5): p. E1377-89.
105. Kim, Y.E., et al., *De novoFUS mutations in 2 Korean patients with sporadic amyotrophic lateral sclerosis*. Neurobiol Aging, 2014.
106. Zou, Z.Y., et al., *De novo FUS gene mutations are associated with juvenile-onset sporadic amyotrophic lateral sclerosis in China*. Neurobiol Aging, 2013. **34**(4): p. 1312.e1-8.
107. Chesi, A., et al., *Exome sequencing to identify de novo mutations in sporadic ALS trios*. Nat Neurosci, 2013. **16**(7): p. 851-5.
108. Keller, M.F., et al., *Genome-wide analysis of the heritability of amyotrophic lateral sclerosis*. JAMA Neurol, 2014. **71**(9): p. 1123-34.
109. Elden, A.C., et al., *Ataxin-2 intermediate-length polyglutamine expansions are associated with increased risk for ALS*. Nature, 2010. **466**(7310): p. 1069-75.
110. Sheng, Y., et al., *SOD1 aggregation and ALS: role of metallation states and disulfide status*. Curr Top Med Chem, 2012. **12**(22): p. 2560-72.
111. Xiao, S., J. McLean, and J. Robertson, *Neuronal intermediate filaments and ALS: a new look at an old question*. Biochim Biophys Acta, 2006. **1762**(11-12): p. 1001-12.

112. Shibata, N., et al., *Intense superoxide dismutase-1 immunoreactivity in intracytoplasmic hyaline inclusions of familial amyotrophic lateral sclerosis with posterior column involvement*. J Neuropathol Exp Neurol, 1996. **55**(4): p. 481-90.
113. Neumann, M., et al., *Abundant FUS-immunoreactive pathology in neuronal intermediate filament inclusion disease*. Acta Neuropathol, 2009. **118**(5): p. 605-16.
114. Al-Sarraj, S., et al., *p62 positive, TDP-43 negative, neuronal cytoplasmic and intranuclear inclusions in the cerebellum and hippocampus define the pathology of C9orf72-linked FTLD and MND/ALS*. Acta Neuropathol, 2011. **122**(6): p. 691-702.
115. Ajroud-Driss, S. and T. Siddique, *Sporadic and hereditary amyotrophic lateral sclerosis (ALS)*. Biochim Biophys Acta, 2015. **1852**(4): p. 679-684.
116. Shibata, N., et al., *Immunohistochemical study on superoxide dismutases in spinal cords from autopsied patients with amyotrophic lateral sclerosis*. Dev Neurosci, 1996. **18**(5-6): p. 492-8.
117. Shibata, N., et al., *Cu/Zn superoxide dismutase-like immunoreactivity in Lewy body-like inclusions of sporadic amyotrophic lateral sclerosis*. Neurosci Lett, 1994. **179**(1-2): p. 149-52.
118. Mackenzie, I.R., et al., *Pathological TDP-43 distinguishes sporadic amyotrophic lateral sclerosis from amyotrophic lateral sclerosis with SOD1 mutations*. Ann Neurol, 2007. **61**(5): p. 427-34.
119. Kerman, A., et al., *Amyotrophic lateral sclerosis is a non-amyloid disease in which extensive misfolding of SOD1 is unique to the familial form*. Acta Neuropathol, 2010. **119**(3): p. 335-44.
120. Wang, J., G. Xu, and D.R. Borchelt, *Mapping superoxide dismutase 1 domains of non-native interaction: roles of intra- and intermolecular disulfide bonding in aggregation*. J Neurochem, 2006. **96**(5): p. 1277-88.
121. Crapo, J.D., et al., *Copper,zinc superoxide dismutase is primarily a cytosolic protein in human cells*. Proc Natl Acad Sci U S A, 1992. **89**(21): p. 10405-9.
122. Weisiger, R.A. and I. Fridovich, *Mitochondrial superoxide simutase. Site of synthesis and intramitochondrial localization*. J Biol Chem, 1973. **248**(13): p. 4793-6.
123. Gertz, B., M. Wong, and L.J. Martin, *Nuclear localization of human SOD1 and mutant SOD1-specific disruption of survival motor neuron protein complex in transgenic amyotrophic lateral sclerosis mice*. J Neuropathol Exp Neurol, 2012. **71**(2): p. 162-77.
124. Islinger, M., et al., *Hitchhiking of Cu/Zn superoxide dismutase to peroxisomes--evidence for a natural piggyback import mechanism in mammals*. Traffic, 2009. **10**(11): p. 1711-21.
125. Urushitani, M., et al., *The endoplasmic reticulum-Golgi pathway is a target for translocation and aggregation of mutant superoxide dismutase linked to ALS*. Faseb j, 2008. **22**(7): p. 2476-87.
126. Pardo, C.A., et al., *Superoxide dismutase is an abundant component in cell bodies, dendrites, and axons of motor neurons and in a subset of other neurons*. Proc Natl Acad Sci U S A, 1995. **92**(4): p. 954-8.
127. Fukai, T. and M. Ushio-Fukai, *Superoxide dismutases: role in redox signaling, vascular function, and diseases*. Antioxid Redox Signal, 2011. **15**(6): p. 1583-606.
128. Borchelt, D.R., et al., *Superoxide dismutase 1 with mutations linked to familial amyotrophic lateral sclerosis possesses significant activity*. Proc Natl Acad Sci U S A, 1994. **91**(17): p. 8292-6.

129. Reaume, A.G., et al., *Motor neurons in Cu/Zn superoxide dismutase-deficient mice develop normally but exhibit enhanced cell death after axonal injury*. Nat Genet, 1996. **13**(1): p. 43-7.
130. Gurney, M.E., et al., *Motor neuron degeneration in mice that express a human Cu,Zn superoxide dismutase mutation*. Science, 1994. **264**(5166): p. 1772-5.
131. Kondo, T., et al., *Reduction of CuZn-superoxide dismutase activity exacerbates neuronal cell injury and edema formation after transient focal cerebral ischemia*. J Neurosci, 1997. **17**(11): p. 4180-9.
132. Lu, L., et al., *Mutant Cu/Zn-superoxide dismutase associated with amyotrophic lateral sclerosis destabilizes vascular endothelial growth factor mRNA and downregulates its expression*. J Neurosci, 2007. **27**(30): p. 7929-38.
133. Ge, W.W., et al., *Mutant copper-zinc superoxide dismutase binds to and destabilizes human low molecular weight neurofilament mRNA*. J Biol Chem, 2005. **280**(1): p. 118-24.
134. Chen, H., et al., *Modeling ALS with iPSCs reveals that mutant SOD1 misregulates neurofilament balance in motor neurons*. Cell Stem Cell, 2014. **14**(6): p. 796-809.
135. Tsang, C.K., et al., *Superoxide dismutase 1 acts as a nuclear transcription factor to regulate oxidative stress resistance*. Nat Commun, 2014. **5**: p. 3446.
136. Reddi, A.R. and V.C. Culotta, *SOD1 integrates signals from oxygen and glucose to repress respiration*. Cell, 2013. **152**(1-2): p. 224-35.
137. Banci, L., et al., *Human superoxide dismutase 1 (hSOD1) maturation through interaction with human copper chaperone for SOD1 (hCCS)*. Proc Natl Acad Sci U S A, 2012. **109**(34): p. 13555-60.
138. Carroll, M.C., et al., *Mechanisms for activating Cu- and Zn-containing superoxide dismutase in the absence of the CCS Cu chaperone*. Proc Natl Acad Sci U S A, 2004. **101**(16): p. 5964-9.
139. Brown, N.M., et al., *Oxygen and the copper chaperone CCS regulate posttranslational activation of Cu,Zn superoxide dismutase*. Proc Natl Acad Sci U S A, 2004. **101**(15): p. 5518-23.
140. Furukawa, Y. and T.V. O'Halloran, *Posttranslational modifications in Cu,Zn-superoxide dismutase and mutations associated with amyotrophic lateral sclerosis*. Antioxid Redox Signal, 2006. **8**(5-6): p. 847-67.
141. Bruns, C.K. and R.R. Kopito, *Impaired post-translational folding of familial ALS-linked Cu, Zn superoxide dismutase mutants*. Embo j, 2007. **26**(3): p. 855-66.
142. Mulligan, V.K. and A. Chakrabartty, *Protein misfolding in the late-onset neurodegenerative diseases: common themes and the unique case of amyotrophic lateral sclerosis*. Proteins, 2013. **81**(8): p. 1285-303.
143. Lepock, J.R., *Measurement of protein stability and protein denaturation in cells using differential scanning calorimetry*. Methods, 2005. **35**(2): p. 117-25.
144. Forman, H.J. and I. Fridovich, *Superoxide dismutase: a comparison of rate constants*. Arch Biochem Biophys, 1973. **158**(1): p. 396-400.
145. Bartnikas, T.B. and J.D. Gitlin, *Mechanisms of biosynthesis of mammalian copper/zinc superoxide dismutase*. J Biol Chem, 2003. **278**(35): p. 33602-8.
146. Ratovitski, T., et al., *Variation in the biochemical/biophysical properties of mutant superoxide dismutase 1 enzymes and the rate of disease progression in familial amyotrophic lateral sclerosis kindreds*. Hum Mol Genet, 1999. **8**(8): p. 1451-60.

147. Valentine, J.S., P.A. Doucette, and S. Zittin Potter, *Copper-zinc superoxide dismutase and amyotrophic lateral sclerosis*. Annu Rev Biochem, 2005. **74**: p. 563-93.
148. Arnesano, F., et al., *The unusually stable quaternary structure of human Cu,Zn-superoxide dismutase 1 is controlled by both metal occupancy and disulfide status*. J Biol Chem, 2004. **279**(46): p. 47998-8003.
149. Tiwari, A. and L.J. Hayward, *Familial amyotrophic lateral sclerosis mutants of copper/zinc superoxide dismutase are susceptible to disulfide reduction*. J Biol Chem, 2003. **278**(8): p. 5984-92.
150. Lindberg, M.J., et al., *Folding of human superoxide dismutase: disulfide reduction prevents dimerization and produces marginally stable monomers*. Proc Natl Acad Sci U S A, 2004. **101**(45): p. 15893-8.
151. Doucette, P.A., et al., *Dissociation of human copper-zinc superoxide dismutase dimers using chaotrope and reductant. Insights into the molecular basis for dimer stability*. J Biol Chem, 2004. **279**(52): p. 54558-66.
152. Furukawa, Y., et al., *Complete loss of post-translational modifications triggers fibrillar aggregation of SOD1 in the familial form of amyotrophic lateral sclerosis*. J Biol Chem, 2008. **283**(35): p. 24167-76.
153. Lindberg, M.J., L. Tibell, and M. Oliveberg, *Common denominator of Cu/Zn superoxide dismutase mutants associated with amyotrophic lateral sclerosis: decreased stability of the apo state*. Proc Natl Acad Sci U S A, 2002. **99**(26): p. 16607-12.
154. Rodriguez, J.A., et al., *Destabilization of apoprotein is insufficient to explain Cu,Zn-superoxide dismutase-linked ALS pathogenesis*. Proc Natl Acad Sci U S A, 2005. **102**(30): p. 10516-21.
155. Bowling, A.C., et al., *Superoxide dismutase concentration and activity in familial amyotrophic lateral sclerosis*. J Neurochem, 1995. **64**(5): p. 2366-9.
156. Hayward, L.J., et al., *Decreased metallation and activity in subsets of mutant superoxide dismutases associated with familial amyotrophic lateral sclerosis*. J Biol Chem, 2002. **277**(18): p. 15923-31.
157. Cao, X., et al., *Structures of the G85R variant of SOD1 in familial amyotrophic lateral sclerosis*. J Biol Chem, 2008. **283**(23): p. 16169-77.
158. Elam, J.S., et al., *Amyloid-like filaments and water-filled nanotubes formed by SOD1 mutant proteins linked to familial ALS*. Nat Struct Biol, 2003. **10**(6): p. 461-7.
159. Galaleldeen, A., et al., *Structural and biophysical properties of metal-free pathogenic SOD1 mutants A4V and G93A*. Arch Biochem Biophys, 2009. **492**(1-2): p. 40-7.
160. Hart, P.J., et al., *Subunit asymmetry in the three-dimensional structure of a human CuZnSOD mutant found in familial amyotrophic lateral sclerosis*. Protein Sci, 1998. **7**(3): p. 545-55.
161. Furukawa, Y. and T.V. O'Halloran, *Amyotrophic lateral sclerosis mutations have the greatest destabilizing effect on the apo- and reduced form of SOD1, leading to unfolding and oxidative aggregation*. J Biol Chem, 2005. **280**(17): p. 17266-74.
162. Lelie, H.L., et al., *Copper and zinc metallation status of copper-zinc superoxide dismutase from amyotrophic lateral sclerosis transgenic mice*. J Biol Chem, 2011. **286**(4): p. 2795-806.
163. Luchinat, E., et al., *In-cell NMR reveals potential precursor of toxic species from SOD1 fALS mutants*. Nat Commun, 2014. **5**: p. 5502.

164. Leal, S.S., et al., *Aberrant zinc binding to immature conformers of metal-free copper-zinc superoxide dismutase triggers amorphous aggregation*. Metallomics, 2015. **7**(2): p. 333-46.
165. Oztug Durer, Z.A., et al., *Loss of metal ions, disulfide reduction and mutations related to familial ALS promote formation of amyloid-like aggregates from superoxide dismutase*. PLoS One, 2009. **4**(3): p. e5004.
166. Pollari, E., et al., *The role of oxidative stress in degeneration of the neuromuscular junction in amyotrophic lateral sclerosis*. Front Cell Neurosci, 2014. **8**: p. 131.
167. Beal, M.F., et al., *Increased 3-nitrotyrosine in both sporadic and familial amyotrophic lateral sclerosis*. Ann Neurol, 1997. **42**(4): p. 644-54.
168. Ferrante, R.J., et al., *Evidence of increased oxidative damage in both sporadic and familial amyotrophic lateral sclerosis*. J Neurochem, 1997. **69**(5): p. 2064-74.
169. Andrus, P.K., et al., *Protein oxidative damage in a transgenic mouse model of familial amyotrophic lateral sclerosis*. J Neurochem, 1998. **71**(5): p. 2041-8.
170. Rakhit, R., et al., *Oxidation-induced misfolding and aggregation of superoxide dismutase and its implications for amyotrophic lateral sclerosis*. J Biol Chem, 2002. **277**(49): p. 47551-6.
171. Mulligan, V.K., et al., *Early steps in oxidation-induced SOD1 misfolding: implications for non-amyloid protein aggregation in familial ALS*. J Mol Biol, 2012. **421**(4-5): p. 631-52.
172. Rakhit, R., et al., *Monomeric Cu,Zn-superoxide dismutase is a common misfolding intermediate in the oxidation models of sporadic and familial amyotrophic lateral sclerosis*. J Biol Chem, 2004. **279**(15): p. 15499-504.
173. Mulligan, V.K., et al., *Denaturational stress induces formation of zinc-deficient monomers of Cu,Zn superoxide dismutase: implications for pathogenesis in amyotrophic lateral sclerosis*. J Mol Biol, 2008. **383**(2): p. 424-36.
174. Rumfeldt, J.A., J.R. Lepock, and E.M. Meiering, *Unfolding and folding kinetics of amyotrophic lateral sclerosis-associated mutant Cu,Zn superoxide dismutases*. J Mol Biol, 2009. **385**(1): p. 278-98.
175. Bruijn, L.I., et al., *Aggregation and motor neuron toxicity of an ALS-linked SOD1 mutant independent from wild-type SOD1*. Science, 1998. **281**(5384): p. 1851-4.
176. Johnston, J.A., et al., *Formation of high molecular weight complexes of mutant Cu, Zn-superoxide dismutase in a mouse model for familial amyotrophic lateral sclerosis*. Proc Natl Acad Sci U S A, 2000. **97**(23): p. 12571-6.
177. Jonsson, P.A., et al., *Minute quantities of misfolded mutant superoxide dismutase-1 cause amyotrophic lateral sclerosis*. Brain, 2004. **127**(Pt 1): p. 73-88.
178. Wang, J., G. Xu, and D.R. Borchelt, *High molecular weight complexes of mutant superoxide dismutase 1: age-dependent and tissue-specific accumulation*. Neurobiol Dis, 2002. **9**(2): p. 139-48.
179. Watanabe, M., et al., *Histological evidence of protein aggregation in mutant SOD1 transgenic mice and in amyotrophic lateral sclerosis neural tissues*. Neurobiol Dis, 2001. **8**(6): p. 933-41.
180. Westermark, P., et al., *Amyloid fibril protein nomenclature -- 2002*. Amyloid, 2002. **9**(3): p. 197-200.

181. Harper, J.D. and P.T. Lansbury, Jr., *Models of amyloid seeding in Alzheimer's disease and scrapie: mechanistic truths and physiological consequences of the time-dependent solubility of amyloid proteins*. Annu Rev Biochem, 1997. **66**: p. 385-407.
182. Zerovnik, E., et al., *Mechanisms of amyloid fibril formation--focus on domain-swapping*. Febs j, 2011. **278**(13): p. 2263-82.
183. Kato, S., et al., *New consensus research on neuropathological aspects of familial amyotrophic lateral sclerosis with superoxide dismutase 1 (SOD1) gene mutations: inclusions containing SOD1 in neurons and astrocytes*. Amyotroph Lateral Scler Other Motor Neuron Disord, 2000. **1**(3): p. 163-84.
184. Wang, J., et al., *Fibrillar inclusions and motor neuron degeneration in transgenic mice expressing superoxide dismutase 1 with a disrupted copper-binding site*. Neurobiol Dis, 2002. **10**(2): p. 128-38.
185. Chattopadhyay, M., et al., *Initiation and elongation in fibrillation of ALS-linked superoxide dismutase*. Proc Natl Acad Sci U S A, 2008. **105**(48): p. 18663-8.
186. Strange, R.W., et al., *The structure of holo and metal-deficient wild-type human Cu, Zn superoxide dismutase and its relevance to familial amyotrophic lateral sclerosis*. J Mol Biol, 2003. **328**(4): p. 877-91.
187. Seetharaman, S.V., et al., *Disrupted zinc-binding sites in structures of pathogenic SOD1 variants D124V and H80R*. Biochemistry, 2010. **49**(27): p. 5714-25.
188. Ivanova, M.I., et al., *Aggregation-triggering segments of SOD1 fibril formation support a common pathway for familial and sporadic ALS*. Proc Natl Acad Sci U S A, 2014. **111**(1): p. 197-201.
189. Furukawa, Y., et al., *Mutation-dependent polymorphism of Cu,Zn-superoxide dismutase aggregates in the familial form of amyotrophic lateral sclerosis*. J Biol Chem, 2010. **285**(29): p. 22221-31.
190. Liu, H.N., et al., *Targeting of monomer/misfolded SOD1 as a therapeutic strategy for amyotrophic lateral sclerosis*. J Neurosci, 2012. **32**(26): p. 8791-9.
191. Redler, R.L., et al., *Non-native soluble oligomers of Cu/Zn superoxide dismutase (SOD1) contain a conformational epitope linked to cytotoxicity in amyotrophic lateral sclerosis (ALS)*. Biochemistry, 2014. **53**(14): p. 2423-32.
192. Matsumoto, G., et al., *Structural properties and neuronal toxicity of amyotrophic lateral sclerosis-associated Cu/Zn superoxide dismutase 1 aggregates*. J Cell Biol, 2005. **171**(1): p. 75-85.
193. Brotherton, T.E., Y. Li, and J.D. Glass, *Cellular toxicity of mutant SOD1 protein is linked to an easily soluble, non-aggregated form in vitro*. Neurobiol Dis, 2013. **49**: p. 49-56.
194. Seetharaman, S.V., et al., *Immature copper-zinc superoxide dismutase and familial amyotrophic lateral sclerosis*. Exp Biol Med (Maywood), 2009. **234**(10): p. 1140-54.
195. Abdolvahabi, A., et al., *Arresting Amyloid with Coulomb's Law: Acetylation of ALS-Linked SOD1 by Aspirin Impedes Aggregation*. Biophys J, 2015. **108**(5): p. 1199-212.
196. Redler, R.L., et al., *Glutathionylation at Cys-111 induces dissociation of wild type and FALS mutant SOD1 dimers*. Biochemistry, 2011. **50**(32): p. 7057-66.
197. Wilcox, K.C., et al., *Modifications of superoxide dismutase (SOD1) in human erythrocytes: a possible role in amyotrophic lateral sclerosis*. J Biol Chem, 2009. **284**(20): p. 13940-7.

198. Hilgarth, R.S., et al., *Regulation and function of SUMO modification*. J Biol Chem, 2004. **279**(52): p. 53899-902.
199. Fei, E., et al., *SUMO-1 modification increases human SOD1 stability and aggregation*. Biochem Biophys Res Commun, 2006. **347**(2): p. 406-12.
200. Niikura, T., Y. Kita, and Y. Abe, *SUMO3 modification accelerates the aggregation of ALS-linked SOD1 mutants*. PLoS One, 2014. **9**(6): p. e101080.
201. Basso, M., et al., *Insoluble mutant SOD1 is partly oligoubiquitinated in amyotrophic lateral sclerosis mice*. J Biol Chem, 2006. **281**(44): p. 33325-35.
202. Mishra, A., et al., *E6-AP association promotes SOD1 aggresomes degradation and suppresses toxicity*. Neurobiol Aging, 2013. **34**(4): p. 1310.e11-23.
203. Niwa, J., et al., *Dorfin ubiquitylates mutant SOD1 and prevents mutant SOD1-mediated neurotoxicity*. J Biol Chem, 2002. **277**(39): p. 36793-8.
204. Miyazaki, K., et al., *NEDL1, a novel ubiquitin-protein isopeptide ligase for dishevelled-1, targets mutant superoxide dismutase-1*. J Biol Chem, 2004. **279**(12): p. 11327-35.
205. Ying, Z., et al., *Gp78, an ER associated E3, promotes SOD1 and ataxin-3 degradation*. Hum Mol Genet, 2009. **18**(22): p. 4268-81.
206. Turner, B.J. and K. Talbot, *Transgenics, toxicity and therapeutics in rodent models of mutant SOD1-mediated familial ALS*. Prog Neurobiol, 2008. **85**(1): p. 94-134.
207. Deng, H.X., et al., *Conversion to the amyotrophic lateral sclerosis phenotype is associated with intermolecular linked insoluble aggregates of SOD1 in mitochondria*. Proc Natl Acad Sci U S A, 2006. **103**(18): p. 7142-7.
208. Wong, P.C., et al., *An adverse property of a familial ALS-linked SOD1 mutation causes motor neuron disease characterized by vacuolar degeneration of mitochondria*. Neuron, 1995. **14**(6): p. 1105-16.
209. Wang, J., et al., *Copper-binding-site-null SOD1 causes ALS in transgenic mice: aggregates of non-native SOD1 delineate a common feature*. Hum Mol Genet, 2003. **12**(21): p. 2753-64.
210. Chang-Hong, R., et al., *Neuroprotective effect of oxidized galectin-1 in a transgenic mouse model of amyotrophic lateral sclerosis*. Exp Neurol, 2005. **194**(1): p. 203-11.
211. Bruijn, L.I., et al., *ALS-linked SOD1 mutant G85R mediates damage to astrocytes and promotes rapidly progressive disease with SOD1-containing inclusions*. Neuron, 1997. **18**(2): p. 327-38.
212. Tobisawa, S., et al., *Mutant SOD1 linked to familial amyotrophic lateral sclerosis, but not wild-type SOD1, induces ER stress in COS7 cells and transgenic mice*. Biochem Biophys Res Commun, 2003. **303**(2): p. 496-503.
213. Ripps, M.E., et al., *Transgenic mice expressing an altered murine superoxide dismutase gene provide an animal model of amyotrophic lateral sclerosis*. Proc Natl Acad Sci U S A, 1995. **92**(3): p. 689-93.
214. Jonsson, P.A., et al., *Motor neuron disease in mice expressing the wild type-like D90A mutant superoxide dismutase-1*. J Neuropathol Exp Neurol, 2006. **65**(12): p. 1126-36.
215. Wang, J., et al., *Somatodendritic accumulation of misfolded SOD1-L126Z in motor neurons mediates degeneration: alphaB-crystallin modulates aggregation*. Hum Mol Genet, 2005. **14**(16): p. 2335-47.

216. Howland, D.S., et al., *Focal loss of the glutamate transporter EAAT2 in a transgenic rat model of SOD1 mutant-mediated amyotrophic lateral sclerosis (ALS)*. Proc Natl Acad Sci U S A, 2002. **99**(3): p. 1604-9.
217. Nagai, M., et al., *Rats expressing human cytosolic copper-zinc superoxide dismutase transgenes with amyotrophic lateral sclerosis: associated mutations develop motor neuron disease*. J Neurosci, 2001. **21**(23): p. 9246-54.
218. Fischer, L.R., et al., *Amyotrophic lateral sclerosis is a distal axonopathy: evidence in mice and man*. Exp Neurol, 2004. **185**(2): p. 232-40.
219. Mourelatos, Z., et al., *The Golgi apparatus of spinal cord motor neurons in transgenic mice expressing mutant Cu,Zn superoxide dismutase becomes fragmented in early, preclinical stages of the disease*. Proc Natl Acad Sci U S A, 1996. **93**(11): p. 5472-7.
220. Bendotti, C., et al., *Early vacuolization and mitochondrial damage in motor neurons of FALS mice are not associated with apoptosis or with changes in cytochrome oxidase histochemical reactivity*. J Neurol Sci, 2001. **191**(1-2): p. 25-33.
221. Vinsant, S., et al., *Characterization of early pathogenesis in the SOD1(G93A) mouse model of ALS: part II, results and discussion*. Brain Behav, 2013. **3**(4): p. 431-57.
222. Hall, E.D., J.A. Oostveen, and M.E. Gurney, *Relationship of microglial and astrocytic activation to disease onset and progression in a transgenic model of familial ALS*. Glia, 1998. **23**(3): p. 249-56.
223. Matsumoto, A., et al., *Disease progression of human SOD1 (G93A) transgenic ALS model rats*. J Neurosci Res, 2006. **83**(1): p. 119-33.
224. Thomsen, G.M., et al., *Delayed disease onset and extended survival in the SOD1G93A rat model of amyotrophic lateral sclerosis after suppression of mutant SOD1 in the motor cortex*. J Neurosci, 2014. **34**(47): p. 15587-600.
225. Herbik, M.A., et al., *Maintenance of the rat transgenic model of familial amyotrophic lateral sclerosis expressing human SOD1G93A mutation*. Folia Neuropathol, 2006. **44**(3): p. 149-53.
226. Lemmens, R., et al., *Overexpression of mutant superoxide dismutase 1 causes a motor axonopathy in the zebrafish*. Hum Mol Genet, 2007. **16**(19): p. 2359-65.
227. Ramesh, T., et al., *A genetic model of amyotrophic lateral sclerosis in zebrafish displays phenotypic hallmarks of motoneuron disease*. Dis Model Mech, 2010. **3**(9-10): p. 652-62.
228. Watson, M.R., et al., *A drosophila model for amyotrophic lateral sclerosis reveals motor neuron damage by human SOD1*. J Biol Chem, 2008. **283**(36): p. 24972-81.
229. Wang, J., et al., *An ALS-linked mutant SOD1 produces a locomotor defect associated with aggregation and synaptic dysfunction when expressed in neurons of Caenorhabditis elegans*. PLoS Genet, 2009. **5**(1): p. e1000350.
230. Gidalevitz, T., et al., *Destabilizing protein polymorphisms in the genetic background direct phenotypic expression of mutant SOD1 toxicity*. PLoS Genet, 2009. **5**(3): p. e1000399.
231. Bendotti, C. and M.T. Carri, *Lessons from models of SOD1-linked familial ALS*. Trends Mol Med, 2004. **10**(8): p. 393-400.
232. Grad, L.I., et al., *Intermolecular transmission of superoxide dismutase 1 misfolding in living cells*. Proc Natl Acad Sci U S A, 2011. **108**(39): p. 16398-403.
233. Israelson, A., et al., *Misfolded mutant SOD1 directly inhibits VDAC1 conductance in a mouse model of inherited ALS*. Neuron, 2010. **67**(4): p. 575-87.

234. Vande Velde, C., et al., *Selective association of misfolded ALS-linked mutant SOD1 with the cytoplasmic face of mitochondria*. Proc Natl Acad Sci U S A, 2008. **105**(10): p. 4022-7.
235. Pickles, S. and C. Vande Velde, *Misfolded SOD1 and ALS: zeroing in on mitochondria*. Amyotroph Lateral Scler, 2012. **13**(4): p. 333-40.
236. Brotherton, T.E., et al., *Localization of a toxic form of superoxide dismutase 1 protein to pathologically affected tissues in familial ALS*. Proc Natl Acad Sci U S A, 2012. **109**(14): p. 5505-10.
237. Grad, L.I., et al., *Exosome-dependent and independent mechanisms are involved in prion-like transmission of propagated Cu/Zn superoxide dismutase misfolding*. Prion, 2014. **8**(5): p. 331-5.
238. Pokrishevsky, E., et al., *Aberrant localization of FUS and TDP43 is associated with misfolding of SOD1 in amyotrophic lateral sclerosis*. PLoS One, 2012. **7**(4): p. e35050.
239. Sabado, J., et al., *Immunodetection of disease-associated conformers of mutant cu/zn superoxide dismutase 1 selectively expressed in degenerating neurons in amyotrophic lateral sclerosis*. J Neuropathol Exp Neurol, 2013. **72**(7): p. 646-61.
240. Forsberg, K., et al., *Novel antibodies reveal inclusions containing non-native SOD1 in sporadic ALS patients*. PLoS One, 2010. **5**(7): p. e11552.
241. Rakhit, R. and A. Chakrabartty, *Structure, folding, and misfolding of Cu,Zn superoxide dismutase in amyotrophic lateral sclerosis*. Biochim Biophys Acta, 2006. **1762**(11-12): p. 1025-37.
242. Sabado, J., et al., *Accumulation of misfolded SOD1 in dorsal root ganglion degenerating proprioceptive sensory neurons of transgenic mice with amyotrophic lateral sclerosis*. Biomed Res Int, 2014. **2014**: p. 852163.
243. Gros-Louis, F., et al., *Intracerebroventricular infusion of monoclonal antibody or its derived Fab fragment against misfolded forms of SOD1 mutant delays mortality in a mouse model of ALS*. J Neurochem, 2010. **113**(5): p. 1188-99.
244. Bosco, D.A., et al., *Wild-type and mutant SOD1 share an aberrant conformation and a common pathogenic pathway in ALS*. Nat Neurosci, 2010. **13**(11): p. 1396-403.
245. Morfini, G.A., et al., *Inhibition of fast axonal transport by pathogenic SOD1 involves activation of p38 MAP kinase*. PLoS One, 2013. **8**(6): p. e65235.
246. Ayers, J.I., et al., *Conformational specificity of the C4F6 SOD1 antibody; low frequency of reactivity in sporadic ALS cases*. Acta Neuropathol Commun, 2014. **2**: p. 55.
247. Rotunno, M.S., et al., *Identification of a misfolded region in superoxide dismutase 1 that is exposed in amyotrophic lateral sclerosis*. J Biol Chem, 2014. **289**(41): p. 28527-38.
248. Rakhit, R., et al., *An immunological epitope selective for pathological monomer-misfolded SOD1 in ALS*. Nat Med, 2007. **13**(6): p. 754-9.
249. Israelson, A., et al., *Macrophage Migration Inhibitory Factor as a Chaperone Inhibiting Accumulation of Misfolded SOD1*. Neuron, 2015.
250. Saxena, S., et al., *Neuroprotection through excitability and mTOR required in ALS motoneurons to delay disease and extend survival*. Neuron, 2013. **80**(1): p. 80-96.
251. Saxena, S., E. Cabuy, and P. Caroni, *A role for motoneuron subtype-selective ER stress in disease manifestations of FALS mice*. Nat Neurosci, 2009. **12**(5): p. 627-36.

252. Homma, K., et al., *SOD1 as a molecular switch for initiating the homeostatic ER stress response under zinc deficiency*. Mol Cell, 2013. **52**(1): p. 75-86.
253. Kanning, K.C., A. Kaplan, and C.E. Henderson, *Motor neuron diversity in development and disease*. Annu Rev Neurosci, 2010. **33**: p. 409-40.
254. Dengler, R., et al., *Amyotrophic lateral sclerosis: macro-EMG and twitch forces of single motor units*. Muscle Nerve, 1990. **13**(6): p. 545-50.
255. Urushitani, M., S.A. Ezzi, and J.P. Julien, *Therapeutic effects of immunization with mutant superoxide dismutase in mice models of amyotrophic lateral sclerosis*. Proc Natl Acad Sci U S A, 2007. **104**(7): p. 2495-500.
256. Patel, P., J.P. Julien, and J. Kriz, *Early-stage treatment with withaferin a reduces levels of misfolded superoxide dismutase 1 and extends lifespan in a mouse model of amyotrophic lateral sclerosis*. Neurotherapeutics, 2015. **12**(1): p. 217-33.
257. Wainger, B.J., et al., *Intrinsic membrane hyperexcitability of amyotrophic lateral sclerosis patient-derived motor neurons*. Cell Rep, 2014. **7**(1): p. 1-11.
258. Jaarsma, D., et al., *Neuron-specific expression of mutant superoxide dismutase is sufficient to induce amyotrophic lateral sclerosis in transgenic mice*. J Neurosci, 2008. **28**(9): p. 2075-88.
259. Lino, M.M., C. Schneider, and P. Caroni, *Accumulation of SOD1 mutants in postnatal motoneurons does not cause motoneuron pathology or motoneuron disease*. J Neurosci, 2002. **22**(12): p. 4825-32.
260. Pramatarova, A., et al., *Neuron-specific expression of mutant superoxide dismutase 1 in transgenic mice does not lead to motor impairment*. J Neurosci, 2001. **21**(10): p. 3369-74.
261. Gong, Y.H., et al., *Restricted expression of G86R Cu/Zn superoxide dismutase in astrocytes results in astrocytosis but does not cause motoneuron degeneration*. J Neurosci, 2000. **20**(2): p. 660-5.
262. Clement, A.M., et al., *Wild-type nonneuronal cells extend survival of SOD1 mutant motor neurons in ALS mice*. Science, 2003. **302**(5642): p. 113-7.
263. Boillee, S., C. Vande Velde, and D.W. Cleveland, *ALS: a disease of motor neurons and their nonneuronal neighbors*. Neuron, 2006. **52**(1): p. 39-59.
264. Ilieva, H., M. Polymenidou, and D.W. Cleveland, *Non-cell autonomous toxicity in neurodegenerative disorders: ALS and beyond*. J Cell Biol, 2009. **187**(6): p. 761-72.
265. Boillee, S., et al., *Onset and progression in inherited ALS determined by motor neurons and microglia*. Science, 2006. **312**(5778): p. 1389-92.
266. Kang, S.H., et al., *Degeneration and impaired regeneration of gray matter oligodendrocytes in amyotrophic lateral sclerosis*. Nat Neurosci, 2013. **16**(5): p. 571-9.
267. Yamanaka, K., et al., *Astrocytes as determinants of disease progression in inherited amyotrophic lateral sclerosis*. Nat Neurosci, 2008. **11**(3): p. 251-3.
268. Lobsiger, C.S., et al., *Schwann cells expressing dismutase active mutant SOD1 unexpectedly slow disease progression in ALS mice*. Proc Natl Acad Sci U S A, 2009. **106**(11): p. 4465-70.
269. Zhong, Z., et al., *Activated protein C therapy slows ALS-like disease in mice by transcriptionally inhibiting SOD1 in motor neurons and microglia cells*. J Clin Invest, 2009. **119**(11): p. 3437-49.

270. Miller, T.M., et al., *Gene transfer demonstrates that muscle is not a primary target for non-cell-autonomous toxicity in familial amyotrophic lateral sclerosis*. Proc Natl Acad Sci U S A, 2006. **103**(51): p. 19546-51.
271. Rezai-Zadeh, K., D. Gate, and T. Town, *CNS infiltration of peripheral immune cells: D-Day for neurodegenerative disease?* J Neuroimmune Pharmacol, 2009. **4**(4): p. 462-75.
272. Alexianu, M.E., M. Kozovska, and S.H. Appel, *Immune reactivity in a mouse model of familial ALS correlates with disease progression*. Neurology, 2001. **57**(7): p. 1282-9.
273. Beers, D.R., et al., *CD4+ T cells support glial neuroprotection, slow disease progression, and modify glial morphology in an animal model of inherited ALS*. Proc Natl Acad Sci U S A, 2008. **105**(40): p. 15558-63.
274. Chiu, I.M., et al., *T lymphocytes potentiate endogenous neuroprotective inflammation in a mouse model of ALS*. Proc Natl Acad Sci U S A, 2008. **105**(46): p. 17913-8.
275. Banerjee, R., et al., *Adaptive immune neuroprotection in G93A-SOD1 amyotrophic lateral sclerosis mice*. PLoS One, 2008. **3**(7): p. e2740.
276. Beers, D.R., et al., *Endogenous regulatory T lymphocytes ameliorate amyotrophic lateral sclerosis in mice and correlate with disease progression in patients with amyotrophic lateral sclerosis*. Brain, 2011. **134**(Pt 5): p. 1293-314.
277. Arbour, D., et al., *Early and persistent abnormal decoding by glial cells at the neuromuscular junction in an ALS model*. J Neurosci, 2015. **35**(2): p. 688-706.
278. Xiao, Q., et al., *Mutant SOD1(G93A) microglia are more neurotoxic relative to wild-type microglia*. J Neurochem, 2007. **102**(6): p. 2008-19.
279. Zhao, W., et al., *Extracellular mutant SOD1 induces microglial-mediated motoneuron injury*. Glia, 2010. **58**(2): p. 231-43.
280. Zhao, W., et al., *Regulatory T lymphocytes from ALS mice suppress microglia and effector T lymphocytes through different cytokine-mediated mechanisms*. Neurobiol Dis, 2012. **48**(3): p. 418-28.
281. Zhao, W., et al., *Protective effects of an anti-inflammatory cytokine, interleukin-4, on motoneuron toxicity induced by activated microglia*. J Neurochem, 2006. **99**(4): p. 1176-87.
282. Nagai, M., et al., *Astrocytes expressing ALS-linked mutated SOD1 release factors selectively toxic to motor neurons*. Nat Neurosci, 2007. **10**(5): p. 615-22.
283. Marchetto, M.C., et al., *Non-cell-autonomous effect of human SOD1 G37R astrocytes on motor neurons derived from human embryonic stem cells*. Cell Stem Cell, 2008. **3**(6): p. 649-57.
284. Di Giorgio, F.P., et al., *Human embryonic stem cell-derived motor neurons are sensitive to the toxic effect of glial cells carrying an ALS-causing mutation*. Cell Stem Cell, 2008. **3**(6): p. 637-48.
285. Haidet-Phillips, A.M., et al., *Astrocytes from familial and sporadic ALS patients are toxic to motor neurons*. Nat Biotechnol, 2011. **29**(9): p. 824-8.
286. Re, D.B., et al., *Necroptosis drives motor neuron death in models of both sporadic and familial ALS*. Neuron, 2014. **81**(5): p. 1001-8.
287. Banci, L., et al., *Metal-free superoxide dismutase forms soluble oligomers under physiological conditions: a possible general mechanism for familial ALS*. Proc Natl Acad Sci U S A, 2007. **104**(27): p. 11263-7.

288. Takeuchi, S., et al., *Induction of protective immunity by vaccination with wild-type apo superoxide dismutase 1 in mutant SOD1 transgenic mice*. J Neuropathol Exp Neurol, 2010. **69**(10): p. 1044-56.
289. Ezzi, S.A., M. Urushitani, and J.P. Julien, *Wild-type superoxide dismutase acquires binding and toxic properties of ALS-linked mutant forms through oxidation*. J Neurochem, 2007. **102**(1): p. 170-8.
290. Guareschi, S., et al., *An over-oxidized form of superoxide dismutase found in sporadic amyotrophic lateral sclerosis with bulbar onset shares a toxic mechanism with mutant SOD1*. Proc Natl Acad Sci U S A, 2012. **109**(13): p. 5074-9.
291. Fujiwara, N., et al., *Oxidative modification to cysteine sulfonic acid of Cys111 in human copper-zinc superoxide dismutase*. J Biol Chem, 2007. **282**(49): p. 35933-44.
292. Nagano, S., et al., *A cysteine residue affects the conformational state and neuronal toxicity of mutant SOD1 in mice - Relevance to the pathogenesis of ALS*. Hum Mol Genet, 2015.
293. Grad, L.I., et al., *Intercellular propagated misfolding of wild-type Cu/Zn superoxide dismutase occurs via exosome-dependent and -independent mechanisms*. Proc Natl Acad Sci U S A, 2014. **111**(9): p. 3620-5.
294. Prusiner, S.B., *Biology and genetics of prions causing neurodegeneration*. Annu Rev Genet, 2013. **47**: p. 601-23.
295. Chia, R., et al., *Superoxide dismutase 1 and tgSOD1 mouse spinal cord seed fibrils, suggesting a propagative cell death mechanism in amyotrophic lateral sclerosis*. PLoS One, 2010. **5**(5): p. e10627.
296. Ayers, J.I., et al., *Experimental transmissibility of mutant SOD1 motor neuron disease*. Acta Neuropathol, 2014. **128**(6): p. 791-803.
297. Munch, C., J. O'Brien, and A. Bertolotti, *Prion-like propagation of mutant superoxide dismutase-1 misfolding in neuronal cells*. Proc Natl Acad Sci U S A, 2011. **108**(9): p. 3548-53.
298. Urushitani, M., et al., *Chromogranin-mediated secretion of mutant superoxide dismutase proteins linked to amyotrophic lateral sclerosis*. Nat Neurosci, 2006. **9**(1): p. 108-18.
299. Ezzi, S.A., et al., *Neuronal over-expression of chromogranin A accelerates disease onset in a mouse model of ALS*. J Neurochem, 2010. **115**(5): p. 1102-11.
300. Knott, A.B., et al., *Mitochondrial fragmentation in neurodegeneration*. Nat Rev Neurosci, 2008. **9**(7): p. 505-18.
301. Sasaki, S. and M. Iwata, *Mitochondrial alterations in the spinal cord of patients with sporadic amyotrophic lateral sclerosis*. J Neuropathol Exp Neurol, 2007. **66**(1): p. 10-6.
302. Sasaki, S. and M. Iwata, *Dendritic synapses of anterior horn neurons in amyotrophic lateral sclerosis: an ultrastructural study*. Acta Neuropathol, 1996. **91**(3): p. 278-83.
303. Hirano, A., et al., *Fine structural study of neurofibrillary changes in a family with amyotrophic lateral sclerosis*. J Neuropathol Exp Neurol, 1984. **43**(5): p. 471-80.
304. Sasaki, S. and M. Iwata, *Ultrastructural change of synapses of Betz cells in patients with amyotrophic lateral sclerosis*. Neurosci Lett, 1999. **268**(1): p. 29-32.
305. Sasaki, S., Y. Horie, and M. Iwata, *Mitochondrial alterations in dorsal root ganglion cells in sporadic amyotrophic lateral sclerosis*. Acta Neuropathol, 2007. **114**(6): p. 633-9.

306. Kiskinis, E., et al., *Pathways disrupted in human ALS motor neurons identified through genetic correction of mutant SOD1*. Cell Stem Cell, 2014. **14**(6): p. 781-95.
307. Dal Canto, M.C. and M.E. Gurney, *Development of central nervous system pathology in a murine transgenic model of human amyotrophic lateral sclerosis*. Am J Pathol, 1994. **145**(6): p. 1271-9.
308. Doi, K., et al., *Mitochondrial changes in motor neurons of homozygotes of leucine 126 TT deletion SOD1 transgenic mice*. Neuropathology, 2008. **28**(3): p. 269-76.
309. Higgins, C.M., C. Jung, and Z. Xu, *ALS-associated mutant SOD1G93A causes mitochondrial vacuolation by expansion of the intermembrane space and by involvement of SOD1 aggregation and peroxisomes*. BMC Neurosci, 2003. **4**: p. 16.
310. Vande Velde, C., et al., *Misfolded SOD1 associated with motor neuron mitochondria alters mitochondrial shape and distribution prior to clinical onset*. PLoS One, 2011. **6**(7): p. 11.
311. Arai, T., et al., *TDP-43 is a component of ubiquitin-positive tau-negative inclusions in frontotemporal lobar degeneration and amyotrophic lateral sclerosis*. Biochem Biophys Res Commun, 2006. **351**(3): p. 602-11.
312. Kong, J. and Z. Xu, *Massive mitochondrial degeneration in motor neurons triggers the onset of amyotrophic lateral sclerosis in mice expressing a mutant SOD1*. J Neurosci, 1998. **18**(9): p. 3241-50.
313. Sasaki, S., et al., *Ultrastructural study of mitochondria in the spinal cord of transgenic mice with a G93A mutant SOD1 gene*. Acta Neuropathol, 2004. **107**(5): p. 461-74.
314. Lee, Y.J., et al., *Roles of the mammalian mitochondrial fission and fusion mediators Fis1, Drp1, and Opa1 in apoptosis*. Mol Biol Cell, 2004. **15**(11): p. 5001-11.
315. Zick, M., R. Rabl, and A.S. Reichert, *Cristae formation-linking ultrastructure and function of mitochondria*. Biochim Biophys Acta, 2009. **1793**(1): p. 5-19.
316. Menzies, F.M., et al., *Mitochondrial dysfunction in a cell culture model of familial amyotrophic lateral sclerosis*. Brain, 2002. **125**(Pt 7): p. 1522-33.
317. Magrane, J., et al., *Mutant SOD1 in neuronal mitochondria causes toxicity and mitochondrial dynamics abnormalities*. Hum Mol Genet, 2009. **18**(23): p. 4552-64.
318. Ferri, A., et al., *Glutaredoxin 2 prevents aggregation of mutant SOD1 in mitochondria and abolishes its toxicity*. Hum Mol Genet, 2010. **19**(22): p. 4529-42.
319. Liu, W., et al., *Mitochondrial fusion and fission proteins expression dynamically change in a murine model of amyotrophic lateral sclerosis*. Curr Neurovasc Res, 2013. **10**(3): p. 222-30.
320. Magrane, J., et al., *Mitochondrial dynamics and bioenergetic dysfunction is associated with synaptic alterations in mutant SOD1 motor neurons*. J Neurosci, 2012. **32**(1): p. 229-42.
321. Magrane, J., et al., *Abnormal mitochondrial transport and morphology are common pathological denominators in SOD1 and TDP43 ALS mouse models*. Hum Mol Genet, 2014. **23**(6): p. 1413-24.
322. Williamson, T.L. and D.W. Cleveland, *Slowing of axonal transport is a very early event in the toxicity of ALS-linked SOD1 mutants to motor neurons*. Nat Neurosci, 1999. **2**(1): p. 50-6.
323. Zhang, B., et al., *Neurofilaments and orthograde transport are reduced in ventral root axons of transgenic mice that express human SOD1 with a G93A mutation*. J Cell Biol, 1997. **139**(5): p. 1307-15.

324. Sotelo-Silveira, J.R., et al., *Axonal mitochondrial clusters containing mutant SOD1 in transgenic models of ALS*. Antioxid Redox Signal, 2009. **11**(7): p. 1535-45.
325. De Vos, K.J., et al., *Familial amyotrophic lateral sclerosis-linked SOD1 mutants perturb fast axonal transport to reduce axonal mitochondria content*. Hum Mol Genet, 2007. **16**(22): p. 2720-8.
326. Song, W., et al., *Mutant SOD1G93A triggers mitochondrial fragmentation in spinal cord motor neurons: neuroprotection by SIRT3 and PGC-1alpha*. Neurobiol Dis, 2013. **51**: p. 72-81.
327. Bilsland, L.G., et al., *Deficits in axonal transport precede ALS symptoms in vivo*. Proc Natl Acad Sci U S A, 2010. **107**(47): p. 20523-8.
328. Zhu, Y.B. and Z.H. Sheng, *Increased axonal mitochondrial mobility does not slow amyotrophic lateral sclerosis (ALS)-like disease in mutant SOD1 mice*. J Biol Chem, 2011. **286**(26): p. 23432-40.
329. Marinkovic, P., et al., *Axonal transport deficits and degeneration can evolve independently in mouse models of amyotrophic lateral sclerosis*. Proc Natl Acad Sci U S A, 2012. **109**(11): p. 4296-301.
330. Clapham, D.E., *Calcium signaling*. Cell, 1995. **80**(2): p. 259-68.
331. Jaiswal, M.K., et al., *Impairment of mitochondrial calcium handling in a mtSOD1 cell culture model of motoneuron disease*. BMC Neurosci, 2009. **10**: p. 64.
332. Damiano, M., et al., *Neural mitochondrial Ca2+ capacity impairment precedes the onset of motor symptoms in G93A Cu/Zn-superoxide dismutase mutant mice*. J Neurochem, 2006. **96**(5): p. 1349-61.
333. Fuchs, A., et al., *Selective mitochondrial Ca2+ uptake deficit in disease endstage vulnerable motoneurons of the SOD1G93A mouse model of amyotrophic lateral sclerosis*. J Physiol, 2013. **591**(Pt 10): p. 2723-45.
334. Jaiswal, M.K. and B.U. Keller, *Cu/Zn superoxide dismutase typical for familial amyotrophic lateral sclerosis increases the vulnerability of mitochondria and perturbs Ca2+ homeostasis in SOD1G93A mice*. Mol Pharmacol, 2009. **75**(3): p. 478-89.
335. Zhou, J., et al., *Hyperactive intracellular calcium signaling associated with localized mitochondrial defects in skeletal muscle of an animal model of amyotrophic lateral sclerosis*. J Biol Chem, 2010. **285**(1): p. 705-12.
336. Tradewell, M.L., et al., *Calcium dysregulation, mitochondrial pathology and protein aggregation in a culture model of amyotrophic lateral sclerosis: mechanistic relationship and differential sensitivity to intervention*. Neurobiol Dis, 2011. **42**(3): p. 265-75.
337. Elrod, J.W., et al., *Cyclophilin D controls mitochondrial pore-dependent Ca(2+) exchange, metabolic flexibility, and propensity for heart failure in mice*. J Clin Invest, 2010. **120**(10): p. 3680-7.
338. Martin, L.J., et al., *The mitochondrial permeability transition pore in motor neurons: involvement in the pathobiology of ALS mice*. Exp Neurol, 2009. **218**(2): p. 333-46.
339. Kim, H.J., et al., *The mitochondrial calcium regulator cyclophilin D is an essential component of oestrogen-mediated neuroprotection in amyotrophic lateral sclerosis*. Brain, 2012. **135**(Pt 9): p. 2865-74.
340. Parone, P.A., et al., *Enhancing mitochondrial calcium buffering capacity reduces aggregation of misfolded SOD1 and motor neuron cell death without extending*

*survival in mouse models of inherited amyotrophic lateral sclerosis*. J Neurosci, 2013. **33**(11): p. 4657-71.
341. Issartel, J.P., et al., *The ATP synthase (F0-F1) complex in oxidative phosphorylation*. Experientia, 1992. **48**(4): p. 351-62.
342. Ghiasi, P., et al., *Mitochondrial complex I deficiency and ATP/ADP ratio in lymphocytes of amyotrophic lateral sclerosis patients*. Neurol Res, 2012. **34**(3): p. 297-303.
343. Mattiazzi, M., et al., *Mutated human SOD1 causes dysfunction of oxidative phosphorylation in mitochondria of transgenic mice*. J Biol Chem, 2002. **277**(33): p. 29626-33.
344. Jung, C., C.M. Higgins, and Z. Xu, *A quantitative histochemical assay for activities of mitochondrial electron transport chain complexes in mouse spinal cord sections*. J Neurosci Methods, 2002. **114**(2): p. 165-72.
345. Kirkinezos, I.G., et al., *Cytochrome c association with the inner mitochondrial membrane is impaired in the CNS of G93A-SOD1 mice*. J Neurosci, 2005. **25**(1): p. 164-72.
346. Li, Q., et al., *ALS-linked mutant superoxide dismutase 1 (SOD1) alters mitochondrial protein composition and decreases protein import*. Proc Natl Acad Sci U S A, 2010. **107**(49): p. 21146-51.
347. Ferri, A., et al., *Familial ALS-superoxide dismutases associate with mitochondria and shift their redox potentials*. Proc Natl Acad Sci U S A, 2006. **103**(37): p. 13860-5.
348. Nguyen, K.T., et al., *The Psi(m) depolarization that accompanies mitochondrial Ca2+ uptake is greater in mutant SOD1 than in wild-type mouse motor terminals*. Proc Natl Acad Sci U S A, 2009. **106**(6): p. 2007-11.
349. Rizzardini, M., et al., *Low levels of ALS-linked Cu/Zn superoxide dismutase increase the production of reactive oxygen species and cause mitochondrial damage and death in motor neuron-like cells*. J Neurol Sci, 2005. **232**(1-2): p. 95-103.
350. Tan, W., et al., *Small peptides against the mutant SOD1/Bcl-2 toxic mitochondrial complex restore mitochondrial function and cell viability in mutant SOD1-mediated ALS*. J Neurosci, 2013. **33**(28): p. 11588-98.
351. Kirk, K., et al., *Bioenergetic markers in skin fibroblasts of sporadic amyotrophic lateral sclerosis and progressive lateral sclerosis patients*. Ann Neurol, 2014. **76**(4): p. 620-4.
352. Xu, X. and E.A. Arriaga, *Qualitative determination of superoxide release at both sides of the mitochondrial inner membrane by capillary electrophoretic analysis of the oxidation products of triphenylphosphonium hydroethidine*. Free Radic Biol Med, 2009. **46**(7): p. 905-13.
353. Zimmerman, M.C., L.W. Oberley, and S.W. Flanagan, *Mutant SOD1-induced neuronal toxicity is mediated by increased mitochondrial superoxide levels*. J Neurochem, 2007. **102**(3): p. 609-18.
354. Panov, A., et al., *Respiration and ROS production in brain and spinal cord mitochondria of transgenic rats with mutant G93a Cu/Zn-superoxide dismutase gene*. Neurobiol Dis, 2011. **44**(1): p. 53-62.
355. Hall, E.D., et al., *Relationship of oxygen radical-induced lipid peroxidative damage to disease onset and progression in a transgenic model of familial ALS*. J Neurosci Res, 1998. **53**(1): p. 66-77.

356. Liu, D., et al., *The roles of free radicals in amyotrophic lateral sclerosis: reactive oxygen species and elevated oxidation of protein, DNA, and membrane phospholipids*. Faseb j, 1999. **13**(15): p. 2318-28.
357. Warita, H., et al., *Oxidative damage to mitochondrial DNA in spinal motoneurons of transgenic ALS mice*. Brain Res Mol Brain Res, 2001. **89**(1-2): p. 147-52.
358. Cassina, P., et al., *Mitochondrial dysfunction in SOD1G93A-bearing astrocytes promotes motor neuron degeneration: prevention by mitochondrial-targeted antioxidants*. J Neurosci, 2008. **28**(16): p. 4115-22.
359. Bilsland, L.G., et al., *Expression of mutant SOD1 in astrocytes induces functional deficits in motoneuron mitochondria*. J Neurochem, 2008. **107**(5): p. 1271-83.
360. Sherratt, H.S., *Mitochondria: structure and function*. Rev Neurol (Paris), 1991. **147**(6-7): p. 417-30.
361. Higgins, C.M., et al., *Mutant Cu, Zn superoxide dismutase that causes motoneuron degeneration is present in mitochondria in the CNS*. J Neurosci, 2002. **22**(6).
362. Jaarsma, D., et al., *CuZn superoxide dismutase (SOD1) accumulates in vacuolated mitochondria in transgenic mice expressing amyotrophic lateral sclerosis-linked SOD1 mutations*. Acta Neuropathol, 2001. **102**(4): p. 293-305.
363. Okado-Matsumoto, A. and I. Fridovich, *Subcellular distribution of superoxide dismutases (SOD) in rat liver: Cu,Zn-SOD in mitochondria*. J Biol Chem, 2001. **276**(42): p. 38388-93.
364. Sturtz, L.A., et al., *A fraction of yeast Cu,Zn-superoxide dismutase and its metallochaperone, CCS, localize to the intermembrane space of mitochondria. A physiological role for SOD1 in guarding against mitochondrial oxidative damage*. J Biol Chem, 2001. **276**(41): p. 38084-9.
365. Kawamata, H. and G. Manfredi, *Import, maturation, and function of SOD1 and its copper chaperone CCS in the mitochondrial intermembrane space*. Antioxid Redox Signal, 2010. **13**(9): p. 1375-84.
366. Field, L.S., et al., *Factors controlling the uptake of yeast copper/zinc superoxide dismutase into mitochondria*. J Biol Chem, 2003. **278**(30): p. 28052-9.
367. Herrmann, J.M. and R. Kohl, *Catch me if you can! Oxidative protein trapping in the intermembrane space of mitochondria*. J Cell Biol, 2007. **176**(5): p. 559-63.
368. Fischer, M. and J. Riemer, *The mitochondrial disulfide relay system: roles in oxidative protein folding and beyond*. Int J Cell Biol, 2013. **2013**: p. 742923.
369. Kawamata, H. and G. Manfredi, *Different regulation of wild-type and mutant Cu,Zn superoxide dismutase localization in mammalian mitochondria*. Hum Mol Genet, 2008. **17**(21): p. 3303-17.
370. Cozzolino, M., et al., *Oligomerization of mutant SOD1 in mitochondria of motoneuronal cells drives mitochondrial damage and cell toxicity*. Antioxid Redox Signal, 2009. **11**(7): p. 1547-58.
371. Igoudjil, A., et al., *In vivo pathogenic role of mutant SOD1 localized in the mitochondrial intermembrane space*. J Neurosci, 2011. **31**(44): p. 15826-37.
372. Vijayvergiya, C., et al., *Mutant superoxide dismutase 1 forms aggregates in the brain mitochondrial matrix of amyotrophic lateral sclerosis mice*. J Neurosci, 2005. **25**(10): p. 2463-70.
373. Liu, J., et al., *Toxicity of familial ALS-linked SOD1 mutants from selective recruitment to spinal mitochondria*. Neuron, 2004. **43**(1): p. 5-17.

374. Pasinelli, P., et al., *Amyotrophic lateral sclerosis-associated SOD1 mutant proteins bind and aggregate with Bcl-2 in spinal cord mitochondria*. Neuron, 2004. **43**(1): p. 19-30.
375. Allen, M.J., et al., *Mutant SOD1 forms ion channel: Implications for ALS pathophysiology*. Neurobiol Dis, 2011.
376. Shirwany, N.A., et al., *The amyloid beta ion channel hypothesis of Alzheimer's disease*. Neuropsychiatr Dis Treat, 2007. **3**(5): p. 597-612.
377. Salehi, M., et al., *Mitochondrial membrane disruption by aggregation products of ALS-causing superoxide dismutase-1 mutants*. Int J Biol Macromol, 2015. **75c**: p. 290-297.
378. Oladzad Abbasabadi, A., et al., *Disruption of mitochondrial membrane integrity induced by amyloid aggregates arising from variants of SOD1*. Int J Biol Macromol, 2013. **61**: p. 212-7.
379. Chng, C.P. and R.W. Strange, *Lipid-associated aggregate formation of superoxide dismutase-1 is initiated by membrane-targeting loops*. Proteins, 2014. **82**(11): p. 3194-209.
380. Lim, L., X. Lee, and J. Song, *Mechanism for transforming cytosolic SOD1 into integral membrane proteins of organelles by ALS-causing mutations*. Biochim Biophys Acta, 2015. **1848**(1 Pt A): p. 1-7.
381. Mazumder, P., J.E. Suk, and T.S. Ulmer, *Insight into alpha-synuclein plasticity and misfolding from differential micelle binding*. J Phys Chem B, 2013. **117**(39): p. 11448-59.
382. Pedrini, S., et al., *ALS-linked mutant SOD1 damages mitochondria by promoting conformational changes in Bcl-2*. Hum Mol Genet, 2010. **19**(15): p. 2974-86.
383. Yonashiro, R., et al., *Mitochondrial ubiquitin ligase MITOL ubiquitinates mutant SOD1 and attenuates mutant SOD1-induced reactive oxygen species generation*. Mol Biol Cell, 2009. **20**(21): p. 4524-30.
384. Kunst, C.B., et al., *Mutations in SOD1 associated with amyotrophic lateral sclerosis cause novel protein interactions*. Nat Genet, 1997. **15**(1): p. 91-4.
385. Kawamata, H., et al., *Lysyl-tRNA synthetase is a target for mutant SOD1 toxicity in mitochondria*. J Biol Chem, 2008. **283**(42): p. 28321-8.
386. Pehar, M., et al., *Mitochondria-targeted catalase reverts the neurotoxicity of hSOD1G(9)(3)A astrocytes without extending the survival of ALS-linked mutant hSOD1 mice*. PLoS One, 2014. **9**(7): p. e103438.
387. Miquel, E., et al., *Modulation of astrocytic mitochondrial function by dichloroacetate improves survival and motor performance in inherited amyotrophic lateral sclerosis*. PLoS One, 2012. **7**(4): p. e34776.
388. Da Cruz, S., et al., *Elevated PGC-1alpha activity sustains mitochondrial biogenesis and muscle function without extending survival in a mouse model of inherited ALS*. Cell Metab, 2012. **15**(5): p. 778-86.
389. Cetin, H., et al., *Epidemiology of amyotrophic lateral sclerosis and effect of riluzole on disease course*. Neuroepidemiology, 2015. **44**(1): p. 6-15.
390. Thomsen, G.M., et al., *The past, present and future of stem cell clinical trials for ALS*. Exp Neurol, 2014. **262 Pt B**: p. 127-37.

391. Vucic, S., J.D. Rothstein, and M.C. Kiernan, *Advances in treating amyotrophic lateral sclerosis: insights from pathophysiological studies*. Trends Neurosci, 2014. **37**(8): p. 433-42.
392. Bucchia, M., et al., *Therapeutic Development in Amyotrophic Lateral Sclerosis*. Clin Ther, 2015.
393. Boucherie, C., et al., *Chimerization of astroglial population in the lumbar spinal cord after mesenchymal stem cell transplantation prolongs survival in a rat model of amyotrophic lateral sclerosis*. J Neurosci Res, 2009. **87**(9): p. 2034-46.
394. Xu, L., et al., *Human neural stem cell grafts in the spinal cord of SOD1 transgenic rats: differentiation and structural integration into the segmental motor circuitry*. J Comp Neurol, 2009. **514**(4): p. 297-309.
395. Karussis, D., et al., *Safety and immunological effects of mesenchymal stem cell transplantation in patients with multiple sclerosis and amyotrophic lateral sclerosis*. Arch Neurol, 2010. **67**(10): p. 1187-94.
396. Mazzini, L., et al., *Mesenchymal stem cell transplantation in amyotrophic lateral sclerosis: A Phase I clinical trial*. Exp Neurol, 2010. **223**(1): p. 229-37.
397. Glass, J.D., et al., *Lumbar intraspinal injection of neural stem cells in patients with amyotrophic lateral sclerosis: results of a phase I trial in 12 patients*. Stem Cells, 2012. **30**(6): p. 1144-51.
398. Kim, C., H.C. Lee, and J.J. Sung, *Amyotrophic lateral sclerosis - cell based therapy and novel therapeutic development*. Exp Neurobiol, 2014. **23**(3): p. 207-14.
399. Bennett, C.F. and E.E. Swayze, *RNA targeting therapeutics: molecular mechanisms of antisense oligonucleotides as a therapeutic platform*. Annu Rev Pharmacol Toxicol, 2010. **50**: p. 259-93.
400. Lagier-Tourenne, C., et al., *Targeted degradation of sense and antisense C9orf72 RNA foci as therapy for ALS and frontotemporal degeneration*. Proc Natl Acad Sci U S A, 2013. **110**(47): p. E4530-9.
401. Foust, K.D., et al., *Therapeutic AAV9-mediated suppression of mutant SOD1 slows disease progression and extends survival in models of inherited ALS*. Mol Ther, 2013. **21**(12): p. 2148-59.
402. Raoul, C., et al., *Lentiviral-mediated silencing of SOD1 through RNA interference retards disease onset and progression in a mouse model of ALS*. Nat Med, 2005. **11**(4): p. 423-8.
403. Wang, H., et al., *Widespread spinal cord transduction by intrathecal injection of rAAV delivers efficacious RNAi therapy for amyotrophic lateral sclerosis*. Hum Mol Genet, 2014. **23**(3): p. 668-81.
404. Miller, T.M., et al., *An antisense oligonucleotide against SOD1 delivered intrathecally for patients with SOD1 familial amyotrophic lateral sclerosis: a phase 1, randomised, first-in-man study*. Lancet Neurol, 2013. **12**(5): p. 435-42.
405. Patel, P., et al., *Adeno-associated virus-mediated delivery of a recombinant single-chain antibody against misfolded superoxide dismutase for treatment of amyotrophic lateral sclerosis*. Mol Ther, 2014. **22**(3): p. 498-510.
406. Tan, W., P. Pasinelli, and D. Trotti, *Role of mitochondria in mutant SOD1 linked amyotrophic lateral sclerosis*. Biochim Biophys Acta, 2014. **1842**(8): p. 1295-301.
407. Bergh, J., et al., *Structural and kinetic analysis of protein-aggregate strains in vivo using binary epitope mapping*. Proc Natl Acad Sci U S A, 2015. **112**(14): p. 4489-94.

408. Prudencio, M. and D.R. Borchelt, *Superoxide dismutase 1 encoding mutations linked to ALS adopts a spectrum of misfolded states*. Mol Neurodegener, 2011. **6**: p. 77.
409. Itoh K, N.K., Iijima M, Sesaki H., *Mitochondrial dynamics in neurodegeneration*. Trends Cell Biol., 2013. **23**(2): p. 64-71. doi: 10.1016/j.tcb.2012.10.006. Epub 2012 Nov 16.
410. Zorov DB, K.E., Juhaszova M, Sollott SJ., *Examining intracellular organelle function using fluorescent probes: from animalcules to quantum dots*. Circ Res., 2004. **95**(3): p. 239-52.
411. Vande Velde C, M.T., Cashman NR, Cleveland DW., *Selective association of misfolded ALS-linked mutant SOD1 with the cytoplasmic face of mitochondria*. Proc Natl Acad Sci U S A., 2008. **105**(10): p. 4022-7. doi: 10.1073/pnas.0712209105. Epub 2008 Feb 22.
412. Loew LM, T.R., Carrington W, Fay FS., *Imaging in five dimensions: time-dependent membrane potentials in individual mitochondria*. Biophys J, 1993. **65**(6): p. 2396-407.
413. Perry, S.W., et al., *Mitochondrial membrane potential probes and the proton gradient: a practical usage guide*. Biotechniques., 2011. **50**(2): p. 98-115. doi: 10.2144/000113610.
414. Xu X, A.E., *Qualitative determination of superoxide release at both sides of the mitochondrial inner membrane by capillary electrophoretic analysis of the oxidation products of triphenylphosphonium hydroethidine*. Free Radic Biol Med., 2009. **46**(7): p. 905-13. doi: 10.1016/j.freeradbiomed.2008.12.019. Epub 2009 Jan 7.
415. Otera H, I.N., Mihara K., *New insights into the function and regulation of mitochondrial fission*. Biochim Biophys Acta., 2013. **1833**(5): p. 1256-68. doi: 10.1016/j.bbamcr.2013.02.002. Epub 2013 Feb 20.
416. Olga Martins de Brito, L.S., *Mitofusin 2 tethers endoplasmic reticulum to mitochondria*. Nature., 2008. **456**(7222): p. 605-10. doi: 10.1038/nature07534.
417. Wikstrom JD, T.G., Shirihai OS., *What can mitochondrial heterogeneity tell us about mitochondrial dynamics and autophagy?* Int J Biochem Cell Biol, 2009. **41**(10): p. 1914-27. doi: 10.1016/j.biocel.2009.06.006. Epub 2009 Jun 21.
418. Pickles S, D.L., Peyrard SL, Cadot S, Rouleau GA, Brown RH Jr, Julien JP, Arbour N, Vande Velde C., *Mitochondrial damage revealed by immunoselection for ALS-linked misfolded SOD1*. Hum Mol Genet., 2013. **22**(19): p. 3947-59. doi: 10.1093/hmg/ddt249. Epub 2013 Jun 4.
419. Frank S, G.B., Bergmann-Leitner ES, Leitner WW, Robert EG, Catez F, Smith CL, Youle RJ., *The role of dynamin-related protein 1, a mediator of mitochondrial fission, in apoptosis*. Dev Cell., 2001. **1**(4): p. 515-25.
420. West AP, B.I., Rahner C, Woo DK, Erdjument-Bromage H, Tempst P, Walsh MC, Choi Y, Shadel GS, Ghosh S., *TLR signalling augments macrophage bactericidal activity through mitochondrial ROS*. Nature., 2011. **472**(7344): p. 476-80. doi: 10.1038/nature09973.
421. Abad MF, D.B.G., Magalhães PJ, Filippin L, Pozzan T., *Mitochondrial pH monitored by a new engineered green fluorescent protein mutant*. J Biol Chem., 2004. **279**(12): p. 11521-9. Epub 2003 Dec 30.
422. Murphy AN, B.D., Cortopassi G, Wang E, Fiskum G., *Bcl-2 potentiates the maximal calcium uptake capacity of neural cell mitochondria*. Proc Natl Acad Sci U S A, 1996. **93**(18): p. 9893-8.

423. Tantama M, M.-F.J., Mongeon R, Yellen G., *Imaging energy status in live cells with a fluorescent biosensor of the intracellular ATP-to-ADP ratio*. Nat Commun, 2013. **4:2550.**(doi): p. 10.1038/ncomms3550.
424. Sasaki, S. and M. Iwata, *Impairment of fast axonal transport in the proximal axons of anterior horn neurons in amyotrophic lateral sclerosis*. Neurology, 1996. **47**(2): p. 535-40.
425. Browne, S.E., et al., *Metabolic dysfunction in familial, but not sporadic, amyotrophic lateral sclerosis*. J Neurochem, 1998. **71**(1): p. 281-7.
426. Lobsiger, C.S., S. Boillee, and D.W. Cleveland, *Toxicity from different SOD1 mutants dysregulates the complement system and the neuronal regenerative response in ALS motor neurons*. Proc Natl Acad Sci U S A, 2007. **104**(18): p. 7319-26.
427. Kowaltowski, A.J., et al., *Effect of Bcl-2 overexpression on mitochondrial structure and function*. J Biol Chem, 2002. **277**(45): p. 42802-7.
428. Mullaney, P.F. and P.N. Dean, *Cell sizing: a small-angle light-scattering method for sizing particles of low relative refractive index*. Appl Opt, 1969. **8**(11): p. 2361-2.
429. Metivier, D., et al., *Cytofluorometric detection of mitochondrial alterations in early CD95/Fas/APO-1-triggered apoptosis of Jurkat T lymphoma cells. Comparison of seven mitochondrion-specific fluorochromes*. Immunol Lett, 1998. **61**(2-3): p. 157-63.
430. Mukhopadhyay, P., et al., *Simple quantitative detection of mitochondrial superoxide production in live cells*. Biochem Biophys Res Commun, 2007. **358**(1): p. 203-8.
431. Robinson, K.M., et al., *Selective fluorescent imaging of superoxide in vivo using ethidium-based probes*. Proc Natl Acad Sci U S A, 2006. **103**(41): p. 15038-43.
432. Loew, L.M., et al., *Imaging in five dimensions: time-dependent membrane potentials in individual mitochondria*. Biophys J, 1993. **65**(6): p. 2396-407.
433. Carriedo, S.G., et al., *AMPA exposures induce mitochondrial Ca(2+) overload and ROS generation in spinal motor neurons in vitro*. J Neurosci, 2000. **20**(1): p. 240-50.
434. Sasaki, S., et al., *Impairment of axonal transport in the axon hillock and the initial segment of anterior horn neurons in transgenic mice with a G93A mutant SOD1 gene*. Acta Neuropathol, 2005. **110**(1): p. 48-56.
435. Tikunov, A., et al., *Closure of VDAC causes oxidative stress and accelerates the Ca(2+)-induced mitochondrial permeability transition in rat liver mitochondria*. Arch Biochem Biophys, 2010. **495**(2): p. 174-81.
436. Han, D., et al., *Voltage-dependent anion channels control the release of the superoxide anion from mitochondria to cytosol*. J Biol Chem, 2003. **278**(8): p. 5557-63.
437. Lustgarten, M.S., et al., *Complex I generated, mitochondrial matrix-directed superoxide is released from the mitochondria through voltage dependent anion channels*. Biochem Biophys Res Commun, 2012. **422**(3): p. 515-21.
438. Muller, F.L., et al., *MnSOD deficiency has a differential effect on disease progression in two different ALS mutant mouse models*. Muscle Nerve, 2008. **38**(3): p. 1173-83.
439. Pesaresi, M.G., et al., *Mitochondrial redox signalling by p66Shc mediates ALS-like disease through Rac1 inactivation*. Hum Mol Genet, 2011. **20**(21): p. 4196-208.
440. Zimmermann, A.K., et al., *Glutathione binding to the Bcl-2 homology-3 domain groove: a molecular basis for Bcl-2 antioxidant function at mitochondria*. J Biol Chem, 2007. **282**(40): p. 29296-304.

441. Chan, P.H., et al., *Overexpression of SOD1 in transgenic rats protects vulnerable neurons against ischemic damage after global cerebral ischemia and reperfusion*. J Neurosci, 1998. **18**(20): p. 8292-9.
442. Vande Velde, C., et al., *The neuroprotective factor Wlds does not attenuate mutant SOD1-mediated motor neuron disease*. Neuromolecular Med, 2004. **5**(3): p. 193-203.
443. Pramatarova, A., et al., *Identification of new mutations in the Cu/Zn superoxide dismutase gene of patients with familial amyotrophic lateral sclerosis*. Am J Hum Genet, 1995. **56**(3): p. 592-6.
444. Pickles, S., et al., *Mitochondrial damage revealed by immunoselection for ALS-linked misfolded SOD1*. Hum Mol Genet, 2013. **22**(19): p. 3947-59.
445. Pickles, S., N. Arbour, and C. Vande Velde, *Immunodetection of outer membrane proteins by flow cytometry of isolated mitochondria*. J Vis Exp, 2014(91): p. 51887.
446. Chen, Y. and G.W. Dorn, 2nd, *PINK1-phosphorylated mitofusin 2 is a Parkin receptor for culling damaged mitochondria*. Science, 2013. **340**(6131): p. 471-5.
447. Westermark, P., *Aspects on human amyloid forms and their fibril polypeptides*. Febs j, 2005. **272**(23): p. 5942-9.
448. Shoshan-Barmatz, V. and M. Golan, *Mitochondrial VDAC1: function in cell life and death and a target for cancer therapy*. Curr Med Chem, 2012. **19**(5): p. 714-35.
449. Rambaran, R.N. and L.C. Serpell, *Amyloid fibrils: abnormal protein assembly*. Prion, 2008. **2**(3): p. 112-7.
450. Martinelli, P. and E.I. Rugarli, *Emerging roles of mitochondrial proteases in neurodegeneration*. Biochim Biophys Acta, 2010. **1797**(1): p. 1-10.
451. Hashimoto, M., et al., *Role of protein aggregation in mitochondrial dysfunction and neurodegeneration in Alzheimer's and Parkinson's diseases*. Neuromolecular Med, 2003. **4**(1-2): p. 21-36.
452. Baker, M.J., T. Tatsuta, and T. Langer, *Quality control of mitochondrial proteostasis*. Cold Spring Harb Perspect Biol, 2011. **3**(7).
453. Pickles, S. and C. Vande Velde, *Misfolded SOD1 and ALS: Zeroing in on mitochondria*. Amyotroph.Lateral.Scler., 2012.
454. Prudencio, M. and D.R. Borchelt, *Superoxide dismutase 1 encoding mutations linked to ALS adopts a spectrum of misfolded states*. Mol.Neurodegener., 2011. **6**: p. 77.
455. Vassall, K.A., et al., *Equilibrium thermodynamic analysis of amyotrophic lateral sclerosis-associated mutant apo Cu,Zn superoxide dismutases*. Biochemistry, 2006. **45**(23): p. 7366-79.
456. Vassall, K.A., et al., *Decreased stability and increased formation of soluble aggregates by immature superoxide dismutase do not account for disease severity in ALS*. Proc Natl Acad Sci U S A, 2011. **108**(6): p. 2210-5.
457. Brown, H.H. and D.R. Borchelt, *Analysis of mutant SOD1 electrophoretic mobility by Blue Native gel electrophoresis; evidence for soluble multimeric assemblies*. PLoS One, 2014. **9**(8): p. e104583.
458. Young, J.C., et al., *Pathways of chaperone-mediated protein folding in the cytosol*. Nat Rev Mol Cell Biol, 2004. **5**(10): p. 781-91.
459. Choi, I., et al., *Lipid molecules induce the cytotoxic aggregation of Cu/Zn superoxide dismutase with structurally disordered regions*. Biochim Biophys Acta, 2011. **1812**(1): p. 41-8.

460. Sasaki, S., et al., *Alterations in subcellular localization of TDP-43 immunoreactivity in the anterior horns in sporadic amyotrophic lateral sclerosis*. Neurosci Lett, 2010. **478**(2): p. 72-6.
461. Wang, W., et al., *The ALS disease-associated mutant TDP-43 impairs mitochondrial dynamics and function in motor neurons*. Hum Mol Genet, 2013. **22**(23): p. 4706-19.
462. Hong, K., et al., *Full-length TDP-43 and its C-terminal fragments activate mitophagy in NSC34 cell line*. Neurosci Lett, 2012. **530**(2): p. 144-9.
463. Shan, X., et al., *Altered distributions of Gemini of coiled bodies and mitochondria in motor neurons of TDP-43 transgenic mice*. Proc Natl Acad Sci U S A, 2010. **107**(37): p. 16325-30.
464. Xu, Y.F., et al., *Wild-type human TDP-43 expression causes TDP-43 phosphorylation, mitochondrial aggregation, motor deficits, and early mortality in transgenic mice*. J Neurosci, 2010. **30**(32): p. 10851-9.
465. Xu, Y.F., et al., *Expression of mutant TDP-43 induces neuronal dysfunction in transgenic mice*. Mol Neurodegener, 2011. **6**: p. 73.
466. Janssens, J., et al., *Overexpression of ALS-associated p.M337V human TDP-43 in mice worsens disease features compared to wild-type human TDP-43 mice*. Mol Neurobiol, 2013. **48**(1): p. 22-35.
467. Stribl, C., et al., *Mitochondrial dysfunction and decrease in body weight of a transgenic knock-in mouse model for TDP-43*. J Biol Chem, 2014. **289**(15): p. 10769-84.
468. Lu, J., et al., *Mitochondrial dysfunction in human TDP-43 transfected NSC34 cell lines and the protective effect of dimethoxy curcumin*. Brain Res Bull, 2012. **89**(5-6): p. 185-90.
469. Wegorzewska, I., et al., *TDP-43 mutant transgenic mice develop features of ALS and frontotemporal lobar degeneration*. Proc Natl Acad Sci U S A, 2009. **106**(44): p. 18809-14.
470. Ash, P.E., et al., *Neurotoxic effects of TDP-43 overexpression in C. elegans*. Hum Mol Genet, 2010. **19**(16): p. 3206-18.
471. Alami, N.H., et al., *Axonal transport of TDP-43 mRNA granules is impaired by ALS-causing mutations*. Neuron, 2014. **81**(3): p. 536-43.
472. Braun, R.J., et al., *Neurotoxic 43-kDa TAR DNA-binding protein (TDP-43) triggers mitochondrion-dependent programmed cell death in yeast*. J Biol Chem, 2011. **286**(22): p. 19958-72.
473. Hebron, M.L., et al., *Parkin ubiquitinates Tar-DNA binding protein-43 (TDP-43) and promotes its cytosolic accumulation via interaction with histone deacetylase 6 (HDAC6)*. J Biol Chem, 2013. **288**(6): p. 4103-15.
474. Morotz, G.M., et al., *Amyotrophic lateral sclerosis-associated mutant VAPBP56S perturbs calcium homeostasis to disrupt axonal transport of mitochondria*. Hum Mol Genet, 2012. **21**(9): p. 1979-88.
475. De Vos, K.J., et al., *VAPB interacts with the mitochondrial protein PTPIP51 to regulate calcium homeostasis*. Hum Mol Genet, 2012. **21**(6): p. 1299-311.
476. van Vliet, A.R., T. Verfaillie, and P. Agostinis, *New functions of mitochondria associated membranes in cellular signaling*. Biochim Biophys Acta, 2014. **1843**(10): p. 2253-62.

477. Stoica, R., et al., *ER-mitochondria associations are regulated by the VAPB-PTPIP51 interaction and are disrupted by ALS/FTD-associated TDP-43*. Nat Commun, 2014. **5**: p. 3996.
478. Huang, C., et al., *FUS transgenic rats develop the phenotypes of amyotrophic lateral sclerosis and frontotemporal lobar degeneration*. PLoS Genet, 2011. **7**(3): p. e1002011.
479. Tradewell, M.L., et al., *Arginine methylation by PRMT1 regulates nuclear-cytoplasmic localization and toxicity of FUS/TLS harbouring ALS-linked mutations*. Hum Mol Genet, 2012. **21**(1): p. 136-49.
480. Majcher, V., et al., *Autophagy receptor defects and ALS-FTLD*. Mol Cell Neurosci, 2015.
481. Heo, J.M., et al., *A stress-responsive system for mitochondrial protein degradation*. Mol Cell, 2010. **40**(3): p. 465-80.
482. Tanaka, A., et al., *Proteasome and p97 mediate mitophagy and degradation of mitofusins induced by Parkin*. J Cell Biol, 2010. **191**(7): p. 1367-80.
483. Kim, N.C., et al., *VCP is essential for mitochondrial quality control by PINK1/Parkin and this function is impaired by VCP mutations*. Neuron, 2013. **78**(1): p. 65-80.
484. Bartolome, F., et al., *Pathogenic VCP mutations induce mitochondrial uncoupling and reduced ATP levels*. Neuron, 2013. **78**(1): p. 57-64.
485. Nalbandian, A., et al., *In vitro studies in VCP-associated multisystem proteinopathy suggest altered mitochondrial bioenergetics*. Mitochondrion, 2015. **22**: p. 1-8.
486. Sarfarazi, M. and T. Rezaie, *Optineurin in primary open angle glaucoma*. Ophthalmol Clin North Am, 2003. **16**(4): p. 529-41.
487. Wong, Y.C. and E.L. Holzbaur, *Optineurin is an autophagy receptor for damaged mitochondria in parkin-mediated mitophagy that is disrupted by an ALS-linked mutation*. Proc Natl Acad Sci U S A, 2014. **111**(42): p. E4439-48.
488. Moscat, J. and M.T. Diaz-Meco, *p62: a versatile multitasker takes on cancer*. Trends Biochem Sci, 2012. **37**(6): p. 230-6.
489. Fecto, F., et al., *SQSTM1 mutations in familial and sporadic amyotrophic lateral sclerosis*. Arch Neurol, 2011. **68**(11): p. 1440-6.
490. Narendra, D., et al., *p62/SQSTM1 is required for Parkin-induced mitochondrial clustering but not mitophagy; VDAC1 is dispensable for both*. Autophagy, 2010. **6**(8): p. 1090-106.
491. Okatsu, K., et al., *p62/SQSTM1 cooperates with Parkin for perinuclear clustering of depolarized mitochondria*. Genes Cells, 2010. **15**(8): p. 887-900.
492. Seibenhener, M.L., et al., *A role for sequestosome 1/p62 in mitochondrial dynamics, import and genome integrity*. Biochim Biophys Acta, 2013. **1833**(3): p. 452-9.
493. Ajroud-Driss, S., et al., *Mutation in the novel nuclear-encoded mitochondrial protein CHCHD10 in a family with autosomal dominant mitochondrial myopathy*. Neurogenetics, 2015. **16**(1): p. 1-9.
494. Chio, A., et al., *CHCH10 mutations in an Italian cohort of familial and sporadic amyotrophic lateral sclerosis patients*. Neurobiol Aging, 2015.
495. Ronchi, D., et al., *CHCHD10 mutations in Italian patients with sporadic amyotrophic lateral sclerosis*. Brain, 2015.

496. Chaussenot, A., et al., *Screening of CHCHD10 in a French cohort confirms the involvement of this gene in frontotemporal dementia with amyotrophic lateral sclerosis patients*. Neurobiol Aging, 2014. **35**(12): p. 2884.e1-4.
497. Darshi, M., et al., *ChChd3, an inner mitochondrial membrane protein, is essential for maintaining crista integrity and mitochondrial function*. J Biol Chem, 2011. **286**(4): p. 2918-32.
498. Darshi, M., et al., *Targeting and import mechanism of coiled-coil helix coiled-coil helix domain-containing protein 3 (ChChd3) into the mitochondrial intermembrane space*. J Biol Chem, 2012. **287**(47): p. 39480-91.
499. Xie, J., et al., *The mitochondrial inner membrane protein mitofilin exists as a complex with SAM50, metaxins 1 and 2, coiled-coil-helix coiled-coil-helix domain-containing protein 3 and 6 and DnaJC11*. FEBS Lett, 2007. **581**(18): p. 3545-9.
500. Cozzolino, M., et al., *Mitochondrial dynamism and the pathogenesis of Amyotrophic Lateral Sclerosis*. Front Cell Neurosci, 2015. **9**: p. 31.
501. Fukada, K., et al., *Mitochondrial proteomic analysis of a cell line model of familial amyotrophic lateral sclerosis*. Mol Cell Proteomics, 2004. **3**(12): p. 1211-23.
502. An, J., et al., *CHCM1/CHCHD6, novel mitochondrial protein linked to regulation of mitofilin and mitochondrial cristae morphology*. J Biol Chem, 2012. **287**(10): p. 7411-26.
503. Funayama, M., et al., *CHCHD2 mutations in autosomal dominant late-onset Parkinson's disease: a genome-wide linkage and sequencing study*. Lancet Neurol, 2015. **14**(3): p. 274-82.
504. Aras, S., et al., *MNRR1 (formerly CHCHD2) is a bi-organellar regulator of mitochondrial metabolism*. Mitochondrion, 2015. **20**: p. 43-51.
505. Wei, Y., et al., *CHCHD2 is Co-amplified with EGFR in NSCLC and Regulates Mitochondrial Function and Cell Migration*. Mol Cancer Res, 2015.
506. Liu, Y., et al., *CHCHD2 inhibits apoptosis by interacting with Bcl-x L to regulate Bax activation*. Cell Death Differ, 2014.
507. Szabadkai, G., et al., *Chaperone-mediated coupling of endoplasmic reticulum and mitochondrial Ca2+ channels*. J Cell Biol, 2006. **175**(6): p. 901-11.
508. Sugiura, A., et al., *MITOL regulates endoplasmic reticulum-mitochondria contacts via Mitofusin2*. Mol Cell, 2013. **51**(1): p. 20-34.
509. Hajnoczky, G., G. Csordas, and M. Yi, *Old players in a new role: mitochondria-associated membranes, VDAC, and ryanodine receptors as contributors to calcium signal propagation from endoplasmic reticulum to the mitochondria*. Cell Calcium, 2002. **32**(5-6): p. 363-77.
510. Area-Gomez, E., et al., *Upregulated function of mitochondria-associated ER membranes in Alzheimer disease*. Embo j, 2012. **31**(21): p. 4106-23.
511. Hedskog, L., et al., *Modulation of the endoplasmic reticulum-mitochondria interface in Alzheimer's disease and related models*. Proc Natl Acad Sci U S A, 2013. **110**(19): p. 7916-21.
512. Hamasaki, M., et al., *Autophagosomes form at ER-mitochondria contact sites*. Nature, 2013. **495**(7441): p. 389-93.
513. Malhotra, J.D. and R.J. Kaufman, *ER stress and its functional link to mitochondria: role in cell survival and death*. Cold Spring Harb Perspect Biol, 2011. **3**(9): p. a004424.

514. Pickrell, A.M. and R.J. Youle, *The roles of PINK1, parkin, and mitochondrial fidelity in Parkinson's disease*. Neuron, 2015. **85**(2): p. 257-73.
515. Morimoto, N., et al., *Induction of parkinsonism-related proteins in the spinal motor neurons of transgenic mouse carrying a mutant SOD1 gene*. J Neurosci Res, 2010. **88**(8): p. 1804-11.
516. Knippenberg, S., et al., *Altered expression of DJ-1 and PINK1 in sporadic ALS and in the SOD1(G93A) ALS mouse model*. J Neuropathol Exp Neurol, 2013. **72**(11): p. 1052-61.
517. Li, L., X. Zhang, and W. Le, *Altered macroautophagy in the spinal cord of SOD1 mutant mice*. Autophagy, 2008. **4**(3): p. 290-3.
518. Morimoto, N., et al., *Increased autophagy in transgenic mice with a G93A mutant SOD1 gene*. Brain Res, 2007. **1167**: p. 112-7.
519. Sasaki, S., *Autophagy in spinal cord motor neurons in sporadic amyotrophic lateral sclerosis*. J Neuropathol Exp Neurol, 2011. **70**(5): p. 349-59.
520. Gal, J., et al., *p62 accumulates and enhances aggregate formation in model systems of familial amyotrophic lateral sclerosis*. J Biol Chem, 2007. **282**(15): p. 11068-77.
521. Gal, J., et al., *Sequestosome 1/p62 links familial ALS mutant SOD1 to LC3 via an ubiquitin-independent mechanism*. J Neurochem, 2009. **111**(4): p. 1062-73.
522. Geisler, S., et al., *PINK1/Parkin-mediated mitophagy is dependent on VDAC1 and p62/SQSTM1*. Nat Cell Biol, 2010. **12**(2): p. 119-31.
523. Song, C.Y., et al., *Autophagy and Its Comprehensive Impact on ALS*. Int J Neurosci, 2012. **122**(12): p. 695-703.
524. Ashrafi, G., et al., *Mitophagy of damaged mitochondria occurs locally in distal neuronal axons and requires PINK1 and Parkin*. J Cell Biol, 2014. **206**(5): p. 655-70.
525. Suen, D.F., et al., *Parkin overexpression selects against a deleterious mtDNA mutation in heteroplasmic cybrid cells*. Proc Natl Acad Sci U S A, 2010. **107**(26): p. 11835-40.
526. Jin, S.M. and R.J. Youle, *The accumulation of misfolded proteins in the mitochondrial matrix is sensed by PINK1 to induce PARK2/Parkin-mediated mitophagy of polarized mitochondria*. Autophagy, 2013. **9**(11): p. 1750-7.
527. Artuso, L., et al., *Mitochondrial genome aberrations in skeletal muscle of patients with motor neuron disease*. Amyotroph Lateral Scler Frontotemporal Degener, 2013. **14**(4): p. 261-6.
528. Gajewski, C.D., et al., *Mitochondrial DNA from platelets of sporadic ALS patients restores normal respiratory functions in rho(0) cells*. Exp Neurol, 2003. **179**(2): p. 229-35.
529. Ingram, C.J., et al., *Analysis of European case-control studies suggests that common inherited variation in mitochondrial DNA is not involved in susceptibility to amyotrophic lateral sclerosis*. Amyotroph Lateral Scler, 2012. **13**(4): p. 341-6.
530. Keeney, P.M. and J.P. Bennett, Jr., *ALS spinal neurons show varied and reduced mtDNA gene copy numbers and increased mtDNA gene deletions*. Mol Neurodegener, 2010. **5**: p. 21.
531. Cai, Q., et al., *Spatial parkin translocation and degradation of damaged mitochondria via mitophagy in live cortical neurons*. Curr Biol, 2012. **22**(6): p. 545-52.
532. Pellegrino, M.W., A.M. Nargund, and C.M. Haynes, *Signaling the mitochondrial unfolded protein response*. Biochim Biophys Acta, 2013. **1833**(2): p. 410-6.

533. Takeuchi, H., et al., *Mitochondrial localization of mutant superoxide dismutase 1 triggers caspase-dependent cell death in a cellular model of familial amyotrophic lateral sclerosis*. J Biol Chem, 2002. **277**(52): p. 50966-72.
534. Haynes, C.M., C.J. Fiorese, and Y.F. Lin, *Evaluating and responding to mitochondrial dysfunction: the mitochondrial unfolded-protein response and beyond*. Trends Cell Biol, 2013. **23**(7): p. 311-8.
535. Wang, X., et al., *Reduced cytosolic protein synthesis suppresses mitochondrial degeneration*. Nat Cell Biol, 2008. **10**(9): p. 1090-7.
536. Houtkooper, R.H., et al., *Mitonuclear protein imbalance as a conserved longevity mechanism*. Nature, 2013. **497**(7450): p. 451-7.
537. Rainbolt, T.K., J.M. Saunders, and R.L. Wiseman, *Stress-responsive regulation of mitochondria through the ER unfolded protein response*. Trends Endocrinol Metab, 2014. **25**(10): p. 528-37.
538. Durieux, J., S. Wolff, and A. Dillin, *The cell-non-autonomous nature of electron transport chain-mediated longevity*. Cell, 2011. **144**(1): p. 79-91.

# Annex 1 :

# Misfolded SOD1 and ALS: zeroing in on mitochondria

Pickles, S., Vande Velde, C. Misfolded SOD1 and ALS: zeroing in on mitochondria. Amyotroph Lateral Scler., 2012 June; 13(4): 333-40.

*Amyotrophic Lateral Sclerosis*, 2012; Early Online, 1–8

informa
healthcare

**REVIEW ARTICLE**

# Misfolded SOD1 and ALS: Zeroing in on mitochondria

SARAH PICKLES & CHRISTINE VANDE VELDE

*Centre d'excellence en neuromique de l'Université de Montréal, Centre de recherche du CHUM (CRCHUM) and Departments of Medicine and Biochemistry, Université de Montréal, Montréal, QC, Canada*



**Abstract**
Mutations in SOD1, causative for a subset of familial ALS cases, are associated with the formation of non-normal SOD1 conformers. Recent studies have defined this pool of SOD1 as misfolded and new antibodies have been developed to selectively detect misfolded SOD1 in vivo and in vitro. We will review these new tools and expand on the evidence demonstrating mitochondria as a common intersecting point for misfolded SOD1.

**Key words:** *ALS, mitochondria, misfolded SOD1, antibodies, motor neuron*

## Introduction

While the majority of ALS cases do not have an obvious genetic cause, 10% of all cases are dominantly inherited and referred to as familial. Of these familial ALS cases, a proportion is due to mutations in the gene encoding superoxide dismutase-1 (SOD1). More than 150 mutations in SOD1 have been identified as causative for ALS (http://alsod.iop.kcl.ac.uk). This large number of mutations, mostly single amino acid substitutions, is exceptional as the protein is comprised of only 153 amino acids. Some mutations (e.g. SOD1-G85R) significantly alter the structure of the protein causing a loss of dismutase activity, while others yield a protein with dismutase activity at or exceeding wild-type levels (e.g. SOD1-G93A and SOD1-G37R). It is now appreciated that SOD1 mutations cause ALS by an unknown toxic gain of function (1,2). While many pathways have been proposed (reviewed recently by (3)), no consensus has emerged. In recent years, it has been recognized that a subset of SOD1 molecules either does not fold properly or fails to retain their normal structure. Collectively, the field refers to these alternate conformations of SOD1 as misfolded and, generally speaking, are considered to be equivalent. In an effort to study these non-normal potentially noxious SOD1 species, many groups have developed antibodies designed to specifically detect misfolded SOD1. With these tools, the field has gained some insights as to how and where mutant SOD1 exerts its toxicity. Moreover, some of these very same tools have demonstrated potential to be utilized as vaccines for ALS. This review summarizes these recently developed reagents and focuses on how mitochondria are a target for misfolded SOD1 toxicity.

## Antibodies to misfolded SOD1

SOD1-containing inclusions have long been a prominent point of discussion in cellular and rodent models of SOD1-mediated ALS (4–6). Furthermore, there have been several in vitro studies using recombinant SOD1 protein aimed at dissecting the folding and maturation pathway(s) of SOD1 so as to define the process by which these inclusions arise (7–10). Whether detected by immunohistochemistry, immunoblotting or physical chemistry methods in vivo or in vitro, it is now appreciated that mutations in SOD1 increase the propensity for misfolded species of SOD1 to accumulate during the disease process (5). In the past few years, several new antibodies have been developed to specifically recognize misfolded SOD1, a term that is meant to represent alternative conformers of SOD1 that have escaped the normal maturation process and are suspected to be important to ALS pathogenesis (Figure 1).

Correspondence: C. Vande Velde, CHUM Research Centre, Université de Montréal 1560 rue Sherbrooke Est, Montréal, Canada H2L 4M1. Fax: 514 412 7602. E-mail: [redacted]

*(Received 25 July 2011; accepted 5 December 2011)*

ISSN 1748-2968 print/ISSN 1471-180X online © 2012 Informa Healthcare
DOI: 10.3109/17482968.2012.648645

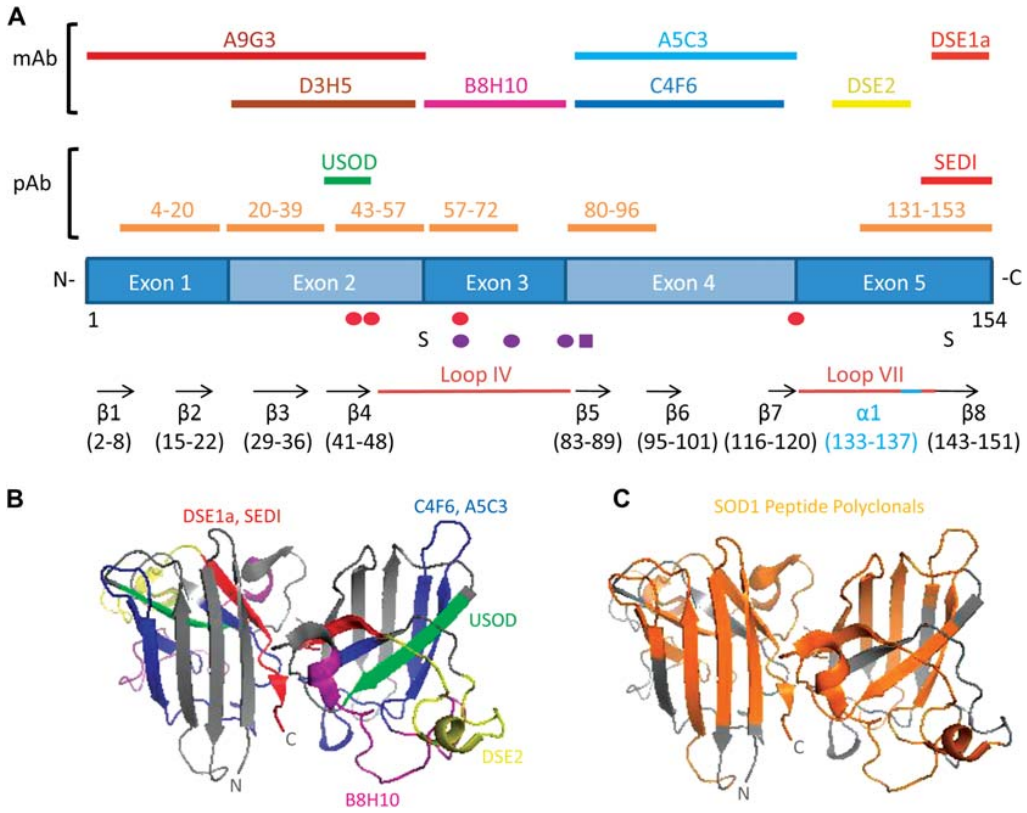


Figure 1. Antibodies recognizing misfolded SOD1 conformers. (A) Epitopes recognized by the various antibodies for detection of misfolded SOD1 antibodies are mapped to the SOD1 structure: A9G3 (burgundy), D3H5 (brown), USOD (green), B8H10 (purple), A5C3 and C4F6 (blue), DSE2 (yellow), SEDI (red), DSE1a (light red) and SOD1 peptide antibodies (orange). Features of the SOD1 structure are indicated as a linear diagram: β strands (black), loops (pink), alpha helix (light blue), disulphide bond mediated by Cys57 and Cys146 (S), copper-binding residues His46, His48, His63 and His120 (red circles) and zinc-binding residues His63, His71, His80 and Asp83 (purple circles and square). (B and C) Three dimensional reconstructions of the SOD1 homodimer (PDB: 2C9V) showing the locations of some of the misfolded SOD1 antibodies. Metals have been omitted for clarity.

*SEDI*

The SEDI antibody, a polyclonal antibody raised against an epitope that is normally inaccessible in the homodimer, was the first antibody developed to detect a misfolded conformation of SOD1 (11). The SEDI antibody is targeted to residues 143−151 of human SOD1 within the dimer interface. Specifically, using in vitro assays SEDI positively detects recombinant SOD1 protein denatured with urea or oxidized via hydrogen peroxide (11). However, due to the location of the epitope within the dimer interface, SEDI is unable to distinguish misfolded SOD1 independent of monomeric forms of SOD1. This is an interesting caveat given that that metal-deficient (apo) monomeric SOD1 could itself be toxic since apoSOD1 is now considered as a precursor to aggregate formation (12−14). Nevertheless, immunoprecipitation and immunohistochemistry with the SEDI antibody provided the first demonstration that misfolded SOD1 was present in the spinal cords of pre-symptomatic mutant SOD1 mice (11). By immunohistochemistry, SEDI labels SOD1 aggregates within motor neurons and axons of SOD1 transgenic mice (11) and within the hyaline conglomerate inclusions found in spinal neurons of SOD1-mediated (but not non-SOD1) familial ALS patients (15).

*USOD*

A second polyclonal antibody targeted to unfolded SOD1, and thus referred to as USOD, was raised against residues 42 − 48 located within the hydrophobic core of the protein and includes two of the four histidine residues required to coordinate copper binding (16). USOD recognizes only highly unfolded SOD1 molecules, as the epitope is not accessible in the dimer or monomer. ELISA assays demonstrate the specificity of USOD for unfolded, demetallated SOD1 but not for folded, metallated SOD1 (16). Like SEDI, USOD also labels large inclusions within the spinal cord motor neurons of familial SOD1 ALS cases (16).

*Peptide polyclonals*

A series of polyclonal antibodies raised against several small peptides spanning nearly the entire SOD1 structure have also been developed. These SOD1 peptide antibodies are referred to by their location

in SOD1: residues 4 – 20, 24 – 39, 43 – 57, 57 – 72, 80 – 96 and 131 – 153 (17). In addition, the Marklund group has developed the apoSOD1 antibody using denatured and demetallated SOD1 as immunogen (18). All of these antibodies have been shown to be specific for misfolded/denatured SOD1 in vivo, by either immunohistochemistry, ELISA or immunoblotting of human ALS patient samples (17,18). Collectively, the development of polyclonal antibodies directed to non-native SOD1 conformers has been an important step in the proof-of-principle that non-native or misfolded forms of SOD1 exist and can be uniquely detected.

*Monoclonals*

In order to further the field towards possible diagnostic and/or future therapeutics premised on misfolded SOD1, the development of additional tools was needed. The Disease Specific Epitope monoclonal antibody, referred to as DSE2, detects misfolded SOD1 in the spinal cords and motor neurons of various transgenic mutant SOD1 rodent models (19,20). DSE2 was raised against amino acids 125 – 142 within the electrostatic loop which has increased flexibility in the context of the mutant protein (21). Importantly, this epitope is normally inaccessible in well-folded SOD1 (21). Recently, a new antibody DSE1a, targeted to residues 145 – 151 of the SOD1 dimer interface, similar to the SEDI epitope except with a cysteic acid replacing Cys146, was described (22).

Additional monoclonal antibodies were raised against human apoSOD1-G93A recombinant protein (23). Characterization of these reagents revealed that each clone possesses a varying affinity for different SOD1 mutations, highlighting the potential that each antibody may react with a different conformation of misfolded SOD1 (23) – a point we will revisit later. Building on earlier data demonstrating extracellular secretion of mutant SOD1 (24) and an active immunization approach to remove extracellular SOD1 (25), the Julien group furthered their hypothesis using these reagents in a passive immunization approach. Specifically, SOD1-G93A mice passively immunized with D3H5, which maps to exon 2, at clinical onset (85 days) extended survival by six days (23). Earlier and longer treatments with D3H5 yielded a nine-day extension of life span demonstrating potential dose dependence. Importantly, immunization with these antibodies resulted in a decrease in the abundance of misfolded SOD1 as detected with another of these antibodies, B8H10 targeted to exon 3, and correlated well with a trend (however, not significant) towards preservation of L5 motor axons and neuromuscular junctions, compared to sham controls (23). Notably, the correlation of reduced misfolded SOD1 load and improved motor neuron survival and function is reminiscent of an active immunization approach in SOD1-G37R mice vaccinated with metal-free human SOD1-G93A protein. Here, the misfolded SOD1 monoclonal antibody, C4F6, raised against SOD1-G93A and mapping to residues 80 – 118 encoded by exon 4 (26), was used to show that the burden of misfolded SOD1 but not total SOD1 levels, were reduced in vaccinated SOD1-G37R mice (25). Collectively, these data provide support to the concept that the generation of misfolded SOD1 is an important element in ALS pathogenesis. Finally, it is curious that passive immunization with another antibody in the panel (A5C3) that also maps to exon 4, did not yield a significant extension in survival (23). It remains unknown whether this antibody failed to extend survival because it was unable to reduce levels of misfolded SOD1 like D3H5, or because it reduced the levels of a benign or less toxic species of misfolded SOD1. This observation raises again the notion that perhaps not all misfolded SOD1 conformations are the same and/or that misfolded SOD1 proteins are not of equal toxicity.

*Other*

Finally, and unexpectedly, an antibody for the $P2X_4$ adenosine triphosphate receptor recognizes a low molecular weight protein in the SOD1-G93A transgenic mice (27). Mass spectrometry and biochemical characterization identified this protein species as SOD1 and immunohistochemistry suggested that this protein was preferentially present in neurons, but not glial cells, of mutant SOD1 mice (27). Most interestingly, intracerebral injection of this presumably misfolded SOD1 species isolated with the $P2X_4$ antibody into mouse brains caused robust microglial and astrocytic activation, both features of ALS pathology (27). If the injected SOD1 was indeed pure of any contaminant, this work is then actually a novel demonstration that misfolded SOD1 is toxic in vivo. Inspection of the sequences of SOD1 and $P2X_4$ reveals that residues 34 – 53 of SOD1 (residing in the hydrophobic core and thus buried in native SOD1) bear a high similarity to the $P2X_4$ immunizing peptide. Interestingly, this region includes the epitope for USOD.

## Misfolded SOD1 without mutations?

One of the most exciting findings in ALS research is the realization that wild-type human SOD1 (SOD1-WT) may play a role in ALS pathogenesis. The first suggestion of this came from cell culture experiments where neuroblastoma cells were made to transiently express SOD1-WT and then treated with hydrogen peroxide (28). Here, oxidized SOD1-WT was both ubiquitinated and associated with chaperone proteins, just as is observed for mutant SOD1 (28). Moreover, SOD1-WT oxidized in vitro and then added to motor neurons cultures was found to induce toxicity equivalent to SOD1-G93A (28). This was the first evidence that the SOD1-WT, if

misfolded, could exert toxicity equivalent to mutant SOD1. Since then, additional experiments have demonstrated that metal-depleted SOD1-WT is well detected by immunoprecipitation with D3H5, providing evidence that the structure of demetallated SOD1-WT mimics that of mutant SOD1 (23). Most recently, Bosco et al. confirmed that oxidation of SOD1-WT with hydrogen peroxide induced a misfolded conformation of SOD1 that was readily detectable by C4F6 (26). Additional characterization of this misfolded SOD1 species determined it to be oxidized at Cys111, a free cysteine residue located at the surface of SOD1, that is known to be readily oxidized in vitro as well as in SOD1 mice (26,29). Previous studies indicate that Cys111 plays an important role in stabilizing the SOD1 protein (29,30). C4F6 recognizes exon 4 of SOD1-G93A, which is home to both the G93A mutation and Cys111. Together, the G93A mutation and the oxidation of Cys111 create an alternate conformation for which C4F6 has a robust affinity (26). That oxidized/misfolded SOD1-WT may participate in disease pathogenesis was demonstrated in an in vitro transport assay where oxidized/misfolded recombinant SOD1-WT or SOD1 protein isolated directly from sporadic ALS patient spinal cords inhibited the axonal transport of membrane-bound vesicles in giant squid axoplasm. Significantly, this effect was completely reversed by perfusing C4F6 into the assay (26).

C4F6 detects misfolded SOD1 within spinal cord motor neurons of approximately 40% of the sporadic ALS patients examined, with a complete absence of signal in both neurological controls and non-SOD1 familial ALS cases (26). It remains to be demonstrated if C4F6 labels SOD1-mediated familial ALS cases. However, other studies using either SEDI or USOD have failed to detect misfolded SOD1 in sporadic ALS cases by either immunohistochemistry or immunoprecipitation (15,16). This apparent contradiction may be due to technical differences in the fixation and/or processing of patient tissue, as has been suggested (26), or could reflect the possibility that more than one conformer of misfolded SOD1 exists. To that end, A9G3, another antibody produced by Julien et al. and mapping to exons 1 and 2 of SOD1, does not detect misfolded SOD1 in the same sporadic ALS case demonstrating robust C4F6 reactivity (26). In a separate study using the full panel of Marklund's polyclonal SOD1 peptide antibodies described earlier, SOD1 inclusions were positively detected within the soma of motor neurons of sporadic and familial ALS cases, as well as some spinal bulbar muscular atrophy (SBMA) patients, by both immunohistochemistry and immunoblot (17). However, SOD1 immunoreactive material was also found in a few neurological and non-neurological control patients, making it difficult to be definitive in this study (17). Nevertheless, the idea to use a panel of antibodies that collectively span 80% of SOD1 sequence is a strength to this study, as it increases the likelihood to detect multiple non-native SOD1 conformations. Additional studies using the various misfolded SOD1 antibodies on the same tissue are required to more fully evaluate this possibility, and more patients need to be examined to establish the frequency of misfolded SOD1 in sporadic ALS. Moreover, data acquired with C4F6 highlights that misfolded SOD1 may also exist in a soluble form, whereas SEDI and USOD seem to preferentially label inclusions, which are presumably insoluble. However, at present we summarize that misfolded SOD1 has been detected in sporadic ALS patients with the following antibodies: SOD1 peptide polyclonals and C4F6, but not with A9G3, SEDI or USOD (Table I). That SOD1-WT exists in a misfolded conformation (which is shared by mutant SOD1) in sporadic ALS validates the utility of the SOD1 models both for dissection of disease mechanisms and for therapeutic development with wide applicability to the majority of ALS cases. Future studies to understand ALS pathogenesis should be focused on identifying those mechanisms impacted by misfolded SOD1 conformers.

## Mitochondria: a target of misfolded SOD1

The evidence presented above demonstrates that misfolded SOD1 can exist in non-native conformations, resulting from improper folding (due to mutation) or aberrant post-translational modifications (oxidation). From these seminal observations, several questions ensue. Which conformation(s) of misfolded SOD1 confers a toxic gain of function? Alternatively, is there a continuum of toxic SOD1 structures? Also, if there is more than one misfolded SOD1 species, do they act on the same mechanism?

Table I. Summary of misfolded SOD1 antibodies in post mortem human tissue.

| | Familial ALS | | | |
|---|---|---|---|---|
| Antibody | SOD1 | Non-SOD1 | Sporadic ALS | Controls |
| SEDI | Yes, 5 cases (IHC, IP) | No, 1 case (IHC, IP) | No, 13 cases (IHC, IP) | No, 4 cases (IHC, IP) |
| USOD | Yes (IHC) | n.d. | No | No |
| SOD1 peptides | Yes (IHC) | Yes (IHC) | Yes, 29 cases (IHC) | Yes, 2/44 cases with SBMA (IHC) |
| C4F6 | n.d. | No, 1 case (IHC) | Yes, 5/9 cases (IHC) | No, 17 cases (IHC) |
| A9G3 | n.d. | n.d. | No, 1 case (IHC) | n.d. |

n.d.: not determined; IHC: immunohistochemistry; IP: immunoprecipitation.

In an effort to answer some of these questions, we present recent work identifying mitochondria as a target of misfolded SOD1.

SOD1 is considered to be a primarily cytosolic protein. However, it has long been known that a small portion of SOD1 is found to be localized within mitochondria in certain tissues (31). Several studies have now reported mutant SOD1 to be associated with mitochondria derived from spinal cords of both mutant SOD1 mice and SOD1-mediated familial ALS samples (19,32 – 34). An important refinement to this observation is the demonstration that misfolded SOD1 has a preferential affinity for mitochondria, as demonstrated by multiple antibodies, which we will elaborate upon here.

Using the SEDI antibody, misfolded SOD1 was detected in fractions enriched for spinal cord, but not liver, mitochondria isolated from all three main SOD1 models (SOD1-G37R, SOD1-G85R, and SOD1-G93A) (11). The relative amount of misfolded SOD1 was particularly prominent in SOD1-G85R spinal cords. This mitochondrial associated SOD1 was absent at pre-symptomatic ages and in age-matched SOD1-WT animals expressing SOD1 at comparable levels. The localization of misfolded SOD1 to spinal cord mitochondria was independently verified using the DSE2 antibody (19). Here, misfolded SOD1 was uniquely associated with spinal cord mitochondria, but not other membranes from the same tissue in several transgenic SOD1 animals including SOD1-G85R and SOD1-G127X mice and SOD1-G93A and SOD1-H46R rats (19). Moreover, the claim of specific misfolded SOD1 association with mitochondria, rather than non-specific copelleting as had been previously proposed (35), was strengthened due to the use of buoyant density centrifugation in which mitochondria are enriched via floatation upwards through a gradient to their buoyant density, rather than downward pelleting. This work also further defined that misfolded SOD1 is associated with the cytoplasmic face of the mitochondrial outer membrane with alkali-sensitivity properties similar to an integral membrane protein (19). It should be mentioned here that while SOD1 has also been reported to be localized to the intermembrane space, (as expected) (36), matrix (34), and inner membrane (37), these studies did not focus on misfolded SOD1. Importantly, this study demonstrated that the mitochondrial association of misfolded SOD1 is a common property in SOD1-mediated ALS rodent models. Moreover, the amount of mitochondrial-associated misfolded SOD1 was similar in all models examined despite broad variability in overall transgene expression levels, suggesting the possibility that there is a potential limiting factor to this association (19).

So what is the limiting factor? Is there an outer mitochondrial protein, for example, that is in limited supply and for which misfolded SOD1 has a particular affinity? To this end, several groups have reported mitochondrial proteins that interact with mutant SOD1, including VDAC1 (20), Bcl-2 (33,38), MITOL (39), and mito-KARS (40). Of this list, an interaction with misfolded SOD1, as detected by DSE2, has been demonstrated only for VDAC1 (voltage dependent anion channel 1), a mitochondrial outer membrane protein important for the movement of metabolites across the outer membrane (20). The interaction with the anti-apoptotic outer membrane protein Bcl-2 is potentially interesting, since Bcl-2 can modulate VDAC1 function (41 – 43). Moreover, while both wild-type and mutant SOD1 can interact with Bcl-2, only the mutant protein induces a conformational change in Bcl-2 (38). The interaction between mutant SOD1 and MITOL, an E3 ubiquitin ligase anchored in the outer membrane that can directly ubiquitinate SOD1, was demonstrated in a neuronal cell culture model but remains to be confirmed in vivo (39). Finally, while Bcl-2, MITOL, and VDAC1 are all outer mitochondrial proteins, mito-KARS (mitochondrial lysyl-tRNA synthetase) is an enzyme required for protein translation that is localized internally to mitochondria, so its significance remains unclear. Much work remains to identify novel interacting partners of misfolded SOD1 at the mitochondrial surface, and to confirm the relevance of previously characterized partners in ALS pathology.

In vitro functional studies convincingly demonstrate that the conductance properties of VDAC1 in spinal cord mitochondria are reduced in the presence of recombinant mutant SOD1 (20). While this protein was not pre-treated so as to intentionally yield misfolded protein, ADP uptake into mitochondria was reduced, and similar results were obtained with mitochondria from symptomatic SOD1-G93A rats (20). Collectively, these experiments suggest that VDAC1 function is impaired by the presence of misfolded SOD1 and mediates its toxicity. Surprisingly, however, SOD1-G93A with a genetic deletion of VDAC1 accelerated disease onset and shortened survival (20). Clearly, these results demonstrate that misfolded SOD1 at the mitochondrial outer membrane can have deleterious functional consequences relevant to disease initiation and/or progression, but additional mechanisms are expected. Furthermore, that a large amount of mitochondrially associated SOD1 persists in the spinal cords of SOD1-G93A on a VDAC1-null background (44) suggests that additional targets and mechanisms impacted by misfolded SOD1 at the mitochondrial surface remain to be identified.

At present, there are few studies that have reported on mitochondria uniquely within the motor neurons. However, mitochondrial function is frequently considered to be intimately linked to mitochondrial morphology. To this end, we have recently reported on the morphology and distribution of motor neuron mitochondria in mutant SOD1 mice using a new transgenic reporter mouse, Hb9-MitoEGFP (45).

These mice have motor neuron-restricted expression of mitochondrially targeted EGFP. Using these mice, into which two different SOD1 mutations were introduced (SOD1-G37R and SOD1-G85R), we demonstrated that A5C3 detected misfolded SOD1 on motor neuron mitochondria in both animal models concurrent with the development of symptoms. A5C3 immunoreactivity was especially noted to be colocalized with axonal mitochondria of spinal cord axonal exit zones, descending tracts, and L5 ventral roots (45). The finding of misfolded SOD1 within motor neurons in this study is consistent with reports of misfolded SOD1 detected in spinal motor neurons, as early as 30 days and throughout disease progression in the SOD1-G93A mouse model with DSE2, A5C3 and D3H5 (20,23). Moreover, colocalization with misfolded SOD1 to the mitochondria indicates that this organelle may play a particularly important role in motor neuron susceptibility to ALS.

Motor neuron mitochondrial morphology is altered in SOD1 mutants compared to controls. In short, mitochondria distribution within the motor neuron axon was markedly altered in SOD1-G37R mice, with major mitochondrial accumulations at distinct locations along the peripheral extending axon (45), similar to what has been reported in teased fibre preparations from SOD1-G93A mice (46). Mitochondria from SOD1-G37R mice were increasingly rounded, whereas mitochondria from SOD1-G85R mice were more tubular and elongated as early as six months, which is a full six months before disease manifests (45). These results demonstrate that misfolded SOD1 is localized to motor neuron mitochondria in vivo and mitochondrial morphology and connectivity is affected early within the course of the disease. Whether these morphological changes are due to impairment of the fission/fusion machinery remains to be determined.

Mitochondria have largely been accepted as one of the possible targets of mutant SOD1, but there is no consensus on how mitochondria are affected. The challenge is to identify what other functional defects, besides VDAC1 conductance and mitochondrial morphology, are caused by the presence of misfolded SOD1. Various aspects of mitochondrial dysfunction have been reported in ALS including mitochondria respiration (47,48), reactive oxygen species production (49), calcium handling (50,51), protein import (44), and pro-apoptotic Bcl-2 conformational changes (38). Further evaluation of these pathways and others, with a focus on assaying only those mitochondria coated with misfolded SOD1, would be beneficial to dissecting out the mechanisms impacted in ALS. Given that the forced localization of mutant SOD1 within the mitochondrial intermembrane space (and anchored to the inner membrane via fusion with the transmembrane domain of mitofilin) was insufficient to recapitulate ALS-like disease in rodents (52), a focus on surface accumulated misfolded SOD1 is appropriate. In addition, developing strategies to block the interaction of misfolded SOD1 with mitochondria (e.g. antibodies, blocking peptides) would be useful to assess the role of misfolded SOD1 as a driving force in ALS pathogenesis and/or be of therapeutic interest. We have recently validated B8H10 to label mitochondria, as detected by flow cytometry (Pickles & Vande Velde, unpublished). Thus, misfolded SOD1 at the mitochondrial surface can be detected by antibodies directed to exons 3 – 5 (Table II). Further studies are required to determine if mitochondrially associated SOD1 can be recognized by antibodies targeted to exons 1 and 2 and/or define a mitochondrial interacting domain.

## Conclusion

Antibodies developed for the recognition of misfolded SOD1 have ushered in a new area of ALS research. To date four different antibodies (SEDI, DSE2, A5C3 and B8H10), by three methods (immunoprecipitation, immunofluorescence and flow cytometry) have shown that misfolded SOD1 is indeed localized to the mitochondrial outer membrane, and consequently affects key aspects of mitochondrial biology, conductance and morphology. It is an interesting time to reflect on our definition of misfolded SOD1. As stated earlier, we collectively

Table II. Summary of misfolded SOD1 association with mitochondria.

| Misfolded SOD1 antibody | Method | SOD1 Mutation | Reference |
|---|---|---|---|
| SEDI | Immunoprecipitation | G93A<br>G85R | (11) |
| DSE2 | Immunoprecipitation<br>Immunohistochemistry | G93A<br>G37R<br>H46R<br>G85R<br>G127X<br>G37R | (19,20)<br>(20) |
| A5C3 | Immunohistochemistry | G37R<br>G85R | (45) |
| B8H10 | Immunoprecipitation &<br>Flow cytometry | G93A<br>G37R | Pickles & Vande Velde, unpublished |

refer to non-native or alternate conformations of SOD1 as misfolded and the field largely considers them to all be equivalent. However, this assumption may be flawed. To date, we have no evidence that the term 'misfolded SOD1' refers to a single species. It remains possible that some conformations may prove to be more toxic than others or alternatively toxic via different mechanisms. Moreover, the data summarized here suggest that perhaps multiple conformers do exist within a spectrum of toxic potency. Using the tools that are now available, there are many outstanding questions to be explored. Which SOD1 conformers are toxic? What is the origin and timing of noxious misfolded SOD1? At what level do these misfolded species elicit damage and motor neuron death? Also, going one step further, which of the collection of misfolded SOD1 antibodies detects the most toxic conformer(s) and thus is most useful for elucidating the mechanisms of SOD1 toxicity and the development of therapeutics? The current data, incorporating our new knowledge of misfolded SOD1, which we now know to be a component of both familial and sporadic disease, points once again to mitochondria as an important convergence point in ALS pathogenesis.

## Acknowledgements

The authors thank D. Bosco (U. Massachusetts) and J.-P. Julien (U. Laval) for sharing unpublished epitope information for D3H5 and B8H10, and S. Boillée (INSERM) for critical discussions. SP is supported by the Tim Noël Studentship from the ALS Society of Canada. The CVV laboratory has been supported by the ALS Society of Canada, CIHR, CFI, CRCHUM, FRSQ and MDA. CVV is a Research Scholar of the FRSQ.

***Declaration of interest:*** The authors report no conflicts of interest. The authors alone are responsible for the content and writing of the paper.

## References

1. Bruijn LI, Houseweart MK, Kato S, Anderson KL, Anderson SD, Ohama E, et al. Aggregation and motor neuron toxicity of an ALS-linked SOD1 mutant independent from wild-type SOD1. Science. 1998;281:1851–4.
2. Wong PC, Pardo CA, Borchelt DR, Lee MK, Copeland NG, Jenkins NA, et al. An adverse property of a familial ALS-linked SOD1 mutation causes motor neuron disease characterized by vacuolar degeneration of mitochondria. Neuron. 1995;14:1105–16.
3. Ilieva H, Polymenidou M, Cleveland DW. Non-cell autonomous toxicity in neurodegenerative disorders: ALS and beyond. J Cell Biol. 2009;187:761–72.
4. Durham HD, Roy J, Dong L, Figlewicz DA. Aggregation of mutant Cu/Zn superoxide dismutase proteins in a culture model of ALS. J Neuropathol Exp Neurol. 1997;56:523–30.
5. Prudencio M, Hart PJ, Borchelt DR, Andersen PM. Variation in aggregation propensities among ALS-associated variants of SOD1: correlation to human disease. Hum Mol Genet. 2009;18:3217–26.
6. Karch CM, Prudencio M, Winkler DD, Hart PJ, Borchelt DR. Role of mutant SOD1 disulphide oxidation and aggregation in the pathogenesis of familial ALS. Proc Natl Acad Sci U S A. 2009;106:7774–9.
7. Rakhit R, Crow JP, Lepock JR, Kondejewski LH, Cashman NR, Chakrabartty A. Monomeric Cu/Zn superoxide dismutase is a common misfolding intermediate in the oxidation models of sporadic and familial amyotrophic lateral sclerosis. J Biol Chem. 2004;279:15499–504.
8. Furukawa Y, O'Halloran TV. Amyotrophic lateral sclerosis mutations have the greatest destabilizing effect on the apo- and reduced form of SOD1, leading to unfolding and oxidative aggregation. J Biol Chem. 2005;280:17266–74.
9. Ip P, Mulligan VK, Chakrabartty A. ALS-causing SOD1 mutations promote production of copper-deficient misfolded species. J Mol Biol. 2011;409:839–52.
10. Vassall KA, Stubbs HR, Primmer HA, Tong MS, Sullivan SM, Sobering R, et al. Decreased stability and increased formation of soluble aggregates by immature superoxide dismutase do not account for disease severity in ALS. Proc Natl Acad Sci U S A. 2011;108:2210–5.
11. Rakhit R, Robertson J, Vande Velde C, Horne P, Ruth DM, Griffin J, et al. An immunological epitope selective for pathological monomer-misfolded SOD1 in ALS. Nat Med. 2007;13:754–9.
12. Khare SD, Dokholyan NV. Common dynamical signatures of familial amyotrophic lateral sclerosis-associated structurally diverse Cu/Zn superoxide dismutase mutants. Proc Natl Acad Sci U S A. 2006;103:3147–52.
13. Rumfeldt JA, Lepock JR, Meiering EM. Unfolding and folding kinetics of amyotrophic lateral sclerosis-associated mutant Cu/Zn superoxide dismutases. J Mol Biol. 2009;385:278–98.
14. Mulligan VK, Kerman A, Ho S, Chakrabartty A. Denaturational stress induces formation of zinc-deficient monomers of Cu/Zn superoxide dismutase: implications for pathogenesis in amyotrophic lateral sclerosis. J Mol Biol. 2008;383:424–36.
15. Liu HN, Sanelli T, Horne P, Pioro EP, Strong MJ, Rogaeva E, et al. Lack of evidence of monomer/misfolded superoxide dismutase-1 in sporadic amyotrophic lateral sclerosis. Ann Neurol. 2009;66:75–80.
16. Kerman A, Liu HN, Croul S, Bilbao J, Rogaeva E, Zinman L, et al. Amyotrophic lateral sclerosis is a non-amyloid disease in which extensive misfolding of SOD1 is unique to the familial form. Acta Neuropathol. 2010;119:335–44.
17. Forsberg K, Jonsson PA, Andersen PM, Bergemalm D, Graffmo KS, Hultdin M, et al. Novel antibodies reveal inclusions containing non-native SOD1 in sporadic ALS patients. PLoS One. 2010;5:e11552.
18. Zetterstrom P, Andersen PM, Brannstrom T, Marklund SL. Misfolded superoxide dismutase-1 in CSF from amyotrophic lateral sclerosis patients. J Neurochem. 2011;117:91–9.
19. Vande Velde C, Miller TM, Cashman NR, Cleveland DW. Selective association of misfolded ALS-linked mutant SOD1 with the cytoplasmic face of mitochondria. Proc Natl Acad Sci U S A. 2008;105:4022–7.
20. Israelson A, Arbel N, Da Cruz S, Ilieva H, Yamanaka K, Shoshan-Barmatz V, et al. Misfolded mutant SOD1 directly inhibits VDAC1 conductance in a mouse model of inherited ALS. Neuron. 2010;67:575–87.
21. Strange RW, Yong CW, Smith W, Hasnain SS. Molecular dynamics using atomic-resolution structure reveal structural fluctuations that may lead to polymerization of human Cu/Zn superoxide dismutase. Proc Natl Acad Sci U S A. 2007;104:10040–4.
22. Grad LI, Guest WC, Yanai A, Pokrishevsky E, O'Neill MA, Gibbs E, et al. Intermolecular transmission of superoxide dismutase-1 misfolding in living cells. Proc Natl Acad Sci U S A. 2011;108:16398–403.

23. Gros-Louis F, Soucy G, Lariviere R, Julien JP. Intracerebroventricular infusion of monoclonal antibody or its derived Fab fragment against misfolded forms of SOD1 mutant delays mortality in a mouse model of ALS. J Neurochem. 2010; 113:1188–99.
24. Urushitani M, Sik A, Sakurai T, Nukina N, Takahashi R, Julien JP. Chromogranin-mediated secretion of mutant superoxide dismutase proteins linked to amyotrophic lateral sclerosis. Nat Neurosci. 2006;9:108–18.
25. Urushitani M, Ezzi SA, Julien JP. Therapeutic effects of immunization with mutant superoxide dismutase in mice models of amyotrophic lateral sclerosis. Proc Natl Acad Sci U S A. 2007;104:2495–500.
26. Bosco DA, Morfini G, Karabacak NM, Song Y, Gros-Louis F, Pasinelli P, et al. Wild-type and mutant SOD1 share an aberrant conformation and a common pathogenic pathway in ALS. Nat Neurosci. 2010;13:1396–1403.
27. Hernandez S, Casanovas A, Piedrafita L, Tarabal O, Esquerda JE. Neurotoxic species of misfolded SOD1-G93A recognized by antibodies against the P2X4 subunit of the ATP receptor accumulate in damaged neurons of transgenic animal models of amyotrophic lateral sclerosis. J Neuropathol Exp Neurol. 2010;69:176–87.
28. Ezzi SA, Urushitani M, Julien JP. Wild-type superoxide dismutase acquires binding and toxic properties of ALS-linked mutant forms through oxidation. J Neurochem. 2007;102: 170–8.
29. Fujiwara N, Nakano M, Kato S, Yoshihara D, Ookawara T, Eguchi H, et al. Oxidative modification to cysteine sulphonic acid of Cys111 in human copper-zinc superoxide dismutase. J Biol Chem. 2007;282:35933–44.
30. Watanabe S, Nagano S, Duce J, Kiaei M, Li QX, Tucker SM, et al. Increased affinity for copper mediated by cysteine 111 in forms of mutant superoxide dismutase-1 linked to amyotrophic lateral sclerosis. Free Radic Biol Med. 2007;42: 1534–42.
31. Okado-Matsumoto A, Fridovich I. Subcellular distribution of superoxide dismutases (SOD) in rat liver: Cu/Zn SOD in mitochondria. J Biol Chem. 2001;276:38388–93.
32. Liu J, Lillo C, Jonsson PA, Vande Velde C, Ward CM, Miller TM, et al. Toxicity of familial ALS-linked SOD1 mutants from selective recruitment to spinal mitochondria. Neuron. 2004;43:5–17.
33. Pasinelli P, Belford ME, Lennon N, Bacskai BJ, Hyman BT, Trotti D, et al. Amyotrophic lateral sclerosis-associated SOD1 mutant proteins bind and aggregate with Bcl-2 in spinal cord mitochondria. Neuron. 2004;43:19–30.
34. Vijayvergiya C, Beal MF, Buck J, Manfredi G. Mutant superoxide dismutase-1 forms aggregates in the brain mitochondrial matrix of amyotrophic lateral sclerosis mice. J Neurosci. 2005;25:2463–70.
35. Bergemalm D, Jonsson PA, Graffmo KS, Andersen PM, Brannstrom T, Rehnmark A, et al. Overloading of stable and exclusion of unstable human superoxide dismutase-1 variants in mitochondria of murine amyotrophic lateral sclerosis models. J Neurosci. 2006;26:4147–54.
36. Goldsteins G, Keksa-Goldsteine V, Ahtoniemi T, Jaronen M, Arens E, Akerman K, et al. Deleterious role of superoxide dismutase in the mitochondrial intermembrane space. J Biol Chem. 2008;283:8446–52.
37. Ahtoniemi T, Jaronen M, Keksa-Goldsteine V, Goldsteins G, Koistinaho J. Mutant SOD1 from spinal cord of G93A rats is destabilized and binds to inner mitochondrial membrane. Neurobiol Dis. 2008;32:479–85.
38. Pedrini S, Sau D, Guareschi S, Bogush M, Brown RH Jr, Naniche N, et al. ALS-linked mutant SOD1 damages mitochondria by promoting conformational changes in Bcl-2. Genet. 2010;19:2974–86.
39. Yonashiro R, Sugiura A, Miyachi M, Fukuda T, Matsushita N, Inatome R, et al. Mitochondrial ubiquitin ligase MITOL ubiquitinates mutant SOD1 and attenuates mutant SOD1-induced reactive oxygen species generation. Mol Biol Cell. 2009;20:4524–30.
40. Kawamata H, Magrane J, Kunst C, King MP, Manfredi G. Lysyl-tRNA synthetase is a target for mutant SOD1 toxicity in mitochondria. J Biol Chem. 2008;283:28321–8.
41. Tsujimoto Y, Shimizu S. VDAC regulation by the Bcl-2 family of proteins. Cell Death Differ. 2000;7:1174–81.
42. Shimizu S, Narita M, Tsujimoto Y. Bcl-2 family proteins regulate the release of apoptogenic cytochrome c by the mitochondrial channel VDAC. Nature. 1999;399:483–7.
43. Arbel N, Shoshan-Barmatz V. Voltage-dependent anion channel 1-based peptides interact with Bcl-2 to prevent antiapoptotic activity. J Biol Chem. 2010;285:6053–62.
44. Li Q, Vande Velde C, Israelson A, Xie J, Bailey AO, Dong MQ, et al. ALS-linked mutant superoxide dismutase-1 (SOD1) alters mitochondrial protein composition and decreases protein import. Proc Natl Acad Sci U S A. 2010;107:21146–51.
45. Vande Velde C, McDonald KK, Boukhedimi Y, McAlonis-Downes M, Lobsiger CS, Bel Hadj S, et al. Misfolded SOD1 associated with motor neuron mitochondria alters mitochondrial shape and distribution prior to clinical onset. PLoS One. 2011;6:e22031.
46. Sotelo-Silveira JR, Lepanto P, Elizondo MV, Horjales S, Palacios F, Martinez PL, et al. Axonal mitochondrial clusters containing mutant SOD1 in transgenic models of ALS. Antioxid Redox Signal. 2009;11:1535–45.
47. Mattiazzi M, D'Aurelio M, Gajewski CD, Martushova K, Kiaei M, Beal MF, et al. Mutated human SOD1 causes dysfunction of oxidative phosphorylation in mitochondria of transgenic mice. J Biol Chem. 2002;277:29626–33.
48. Jung C, Higgins CM, Xu Z. Mitochondrial electron transport chain complex dysfunction in a transgenic mouse model for amyotrophic lateral sclerosis. J Neurochem. 2002;83: 535–45.
49. Panov AV, Kubalik N, Zinchenko N, Ridings DM, Radoff DA, Hemendinger R, et al. Metabolic and functional differences between brain and spinal cord mitochondria underlie different predisposition to pathology. Am J Physiol Regul Integr Comp Physiol. 2011;300:R844–54.
50. Damiano M, Starkov AA, Petri S, Kipiani K, Kiaei M, Mattiazzi M, et al. Neural mitochondrial $Ca^{2+}$ capacity impairment precedes the onset of motor symptoms in G93A Cu/Zn superoxide dismutase mutant mice. J Neurochem. 2006;96:1349–61.
51. Tradewell ML, Cooper LA, Minotti S, Durham HD. Calcium dysregulation, mitochondrial pathology and protein aggregation in a culture model of amyotrophic lateral sclerosis: mechanistic relationship and differential sensitivity to intervention. Neurobiol Dis. 2011;42:265–75.
52. Igoudjil A, Magrane J, Fischer LR, Kim HJ, Hervias I, Dumont M, et al. In vivo pathogenic role of mutant SOD1 localized in the mitochondrial intermembrane space. J Neurosci. 2011;31:15826–37.

# Annex 2

## Endo-MitoEGFP mice: a novel transgenic mouse with fluorescently marked mitochondria in microvascular endothelial cells

Pickles, S., Cadieux-Dion, M., Alvarez, JI., Lécuyer, MA., Peyrard, SL., Destroismaisons, L., St-Onge, L., Terouz, S., Cossette, P., Prat, A., Vande Velde, C. Endo-MitoEGFP mice: a novel transgenic mouse with fluorescently marked mitochondria in microvascular endothelial cells. PLoS One, 2013 September 3; 8 (9): e74603.

OPEN ACCESS Freely available online

PLOS ONE

# Endo-MitoEGFP Mice: A Novel Transgenic Mouse with Fluorescently Marked Mitochondria in Microvascular Endothelial Cells

**Sarah Pickles[1,2], Maxime Cadieux-Dion[1], Jorge I. Alvarez[1], Marc-Andre Lécuyer[1], Sarah L. Peyrard[1], Laurie Destroismaisons[1], Lydia St-Onge[1], Simone Terouz[1], Patrick Cossette[1,3], Alexandre Prat[1,3], Christine Vande Velde[1,3*]**

**1** Centre d'Excellence en Neuromique de l'Université de Montréal, Centre de Recherche du Centre Hospitalier de l'Université de Montréal (CRCHUM), Université de Montréal, Montréal, Quebec, Canada, **2** Department of Biochemistry, Université de Montréal, Montréal, Quebec, Canada, **3** Department of Medicine, Université de Montréal, Montréal, Quebec, Canada

## Abstract

Blood vessel-specific fluorescent transgenic mice are excellent tools to study the development of the vasculature and angiogenic processes. There is growing interest in the biological processes relevant to endothelial cells but limited tools exist to selectively evaluate subcellular functions of this cell type *in vivo*. Here, we report a novel transgenic animal model that expresses mitochondrially targeted enhanced green fluorescent protein (EGFP) via the Hb9 promoter, a homeobox transcription factor with limited known involvement in the vasculature. Random integration of the transgene, containing the entire mouse Hb9 promoter, was found to be expressed in a variety of vascularised tissues. Further inspection revealed that Mito-EGFP localizes to the endothelial cells (ECs) of a subset of microvascular blood vessels, especially in the central nervous system (CNS), heart, spleen, thymus, lymph nodes and skin. We demonstrate the utility of this novel transgenic mouse, named Endo-MitoEGFP, in the detection, imaging, and isolation of microvascular ECs and evaluation of EC mitochondrial function isolated from adult animals. These transgenic mice will be useful to studies of ECs in development, physiology, and pathology.

**Citation:** Pickles S, Cadieux-Dion M, Alvarez JI, Lécuyer M-A, Peyrard SL, et al. (2013) Endo-MitoEGFP Mice: A Novel Transgenic Mouse with Fluorescently Marked Mitochondria in Microvascular Endothelial Cells. PLoS ONE 8(9): e74603. doi:10.1371/journal.pone.0074603

**Editor:** Stefan Liebner, Institute of Neurology (Edinger-Institute), Germany

**Received** March 21, 2013; **Accepted** August 5, 2013; **Published** September 3, 2013



**Funding:** This work was supported by the Canadian Institutes of Health Research Neuromuscular Research Partnership, Muscular Dystrophy Association, CHUM Research Center, Canadian Foundation for Innovation, and Fonds de la Recherche du Québec-Santé (FRQS) (all to CVV). AP is a Senior Research Scholars of FRQS, respectively. CVV is a CIHR New Investigator. SP and MDC are supported by the Tim Noël Studentship from the ALS Society of Canada and the Réseau de Médecine Génétique Appliquée du FRQS, respectively. The funders had no role in study design, data collection and analysis, decision to publish, or preparation of the manuscript.

**Competing interests:** The authors have declared that no competing interests exist.

* E-mail: [redacted]

## Introduction

Transgenic reporter mice are important tools to study biological processes. Fluorescent transgenic mice have been previously developed to study blood vessels (*Tie2*-GFP) [1] and the lymphatic system (*Prox1*-GFP) [2]. A recent description of *Prox1*-GFP mice, a homeobox transcription factor that has widespread CNS expression [3], was also found to have unique expression in the lymphatic system and was excluded from blood vascular endothelial cells [2]. These models allow for studies *in vivo*, as well as the possibility for cell isolation. The current paradigm to achieve cell-specific expression of a reporter protein uses transcription factors, many coming from the homeobox family. Indeed, these transcription factors often serve as cell fate markers, however our understanding of their expression and regulation in development or in adult tissues is not complete. In fact many homeobox proteins with "neuronal restricted" expression have been found to also be expressed in other tissues and cell types [4–6].

In the current report, transgenic mice with a novel vasculature expression pattern were created by random integration of cDNA encoding mitochondrially targeted EGFP under the control of the homeobox transcription factor *Hb9*, a well-established specification factor for motor neurons. Mitochondrial localization of EGFP was achieved via the inclusion of the mitochondrial targeting sequence of a subunit of the electron transport chain fused to EGFP. We provide immunofluorescent, immunoblot and flow cytometric analysis of these mice, establishing unexpectedly, the expression of EGFP within ECs of vessels and have aptly named these mice Endo-

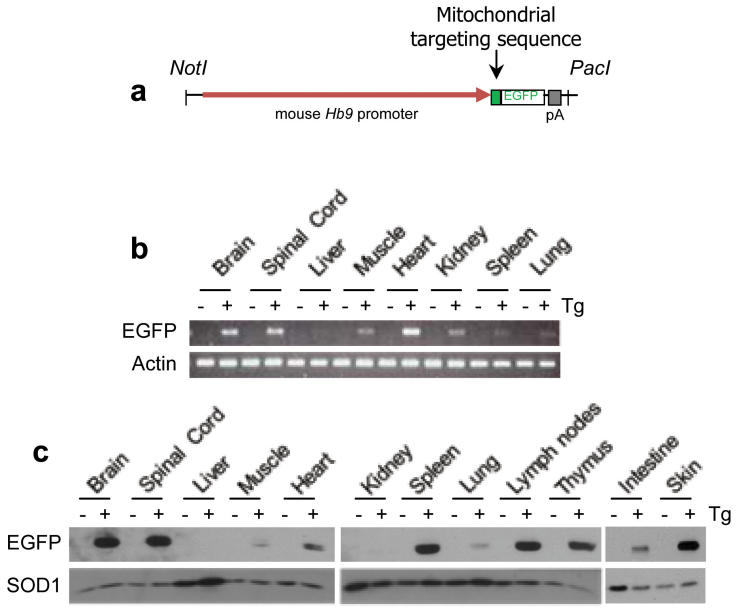


**Figure 1. EGFP expression is not restricted to central nervous system, but is also expressed in vascularized tissues.** (A) Schematic of p*Hb9*-MitoEGFP transgenic construct, with mitochondrial targeting sequence of Cytochrome *c* Oxidase subunit VIII. (B) RT-PCR of EGFP mRNA from a panel of tissues of transgenic (+) and non-transgenic littermates (-). Actin serves as a loading control. (C) EGFP protein levels detected via immunoblotting in a panel of tissues isolated from transgenic (+) and non-transgenic littermates (-). SOD1 serves as a loading control. *n*=3-4 animals.

doi: 10.1371/journal.pone.0074603.g001

MitoEGFP. We propose that the Hb9 promoter has come under altered or previously uncharacterized regulation during random integration of the transgene, leading to a novel expression pattern. We predict that the isolation and evaluation of mitochondrial function from ECs will be greatly aided by the use of the Endo-MitoEGFP transgenic model. Moreover, this model provides a unique opportunity to study the contribution of mitochondria to EC development, normal physiology, and in pathological conditions. Our data demonstrate the experimental usefulness of this novel transgenic model.

## Results and Discussion

A transgene encoding mitochondrially targeted EGFP (MitoEGFP) expressed from the promoter of the mouse homeobox transcription factor Hb9 was introduced via pronuclear injection and randomly integrated into the mouse genome as expected (Figure **1A**). Hb9 is typically expressed in post-mitotic motor neurons of the spinal cord during development, is required for the maintenance of motor neuron identity, and as such, is well regarded as a marker for motor neurons [7,8]. During the initial characterization of founder mice which genotyped positively for the transgene, it was noted that while several founders had the expected motor neuron-restricted expression of EGFP-labelled mitochondria [9], one founder exhibited a unique expression profile which extended beyond the central nervous system (CNS). Specifically, transgene mRNA was detected at high levels in brain, spinal cord, and heart with lesser amounts detectable in gastrocnemius muscle, kidney, spleen and lung and was largely absent in liver (Figure **1B**). Evaluation of EGFP protein levels revealed a similar pattern with the highest levels detected in the brain, spinal cord, spleen, lymph nodes, thymus and skin (Figure **1C**). Modest EGFP expression was detected in muscle, heart, lung, and intestine, but was absent by immunoblot in liver and kidney (Figure **1C**).

To determine the cell type in which EGFP protein was expressed, we examined native EGFP expression in a panel of tissues via confocal microscopy. During embryogenesis, EGFP expression was detected in the motor cortical strip and spinal cord, as expected for Hb9 (Figure **2A**). However, in adult mouse spinal cord EGFP expression was absent from motor neurons and other spinal neurons, as evidenced by the lack of co-localization of EGFP with NeuN or unphosphorylated neurofilament (SMI32), pan-neuronal and motor neuron markers, respectively (Figure **2B, 2C**). EGFP expression was also absent from astrocytes as marked with the astrocytic marker GFAP (Figure **2D**). During this initial analysis, we noted that EGFP was expressed in a speckled pattern within filamentous looking structures resembling blood vessels. Given the high level of EGFP expression in the brain, heart and spleen we examined these tissues and determined that this pattern was reminiscent of the vascular endothelium (Figure **2E**). Co-labelling with caveolin, the vessel matrix protein laminin and EC marker p120-catenin [10,11], demonstrated EGFP localization to the vasculature/ECs in the brain (Figure

**2F–H**). EGFP was primarily localized to small parenchymal vessels, mainly capillaries, with only modest labelling of larger vessels and was undetectable in the ECs lining the arteries and larger meningeal vessels.

To further prove that EGFP expression was restricted to ECs, splenic ECs were isolated from transgenic animals and labelled with fluorescently conjugated PECAM-1 antibody and analyzed by flow cytometry. PECAM-1 is expressed at the surface of ECs and is a well-recognized EC marker [12]. Two distinct cell populations were identified based on light scattering properties and ECs were identified by their larger size and positive cell surface labelling for PECAM-1 (Figure **3A**). Within the splenic EC population, 81.3 ± 5.8% stained positive for PECAM-1 and 74.0 ± 10.5% of these cells also expressed EGFP (Figure **3B**), indicating that a majority of ECs within the spleen express EGFP. While the analysis of brain ECs by flow cytometry was not possible due to low EC yields from brain, we did observe that EGFP was enriched in brain EC fractions as demonstrated by immunoblotting for the junctional protein p120 [13] (Figure **3C**).

In order to verify that EGFP protein was targeted to mitochondria as expected, mitochondria were isolated from brain, spinal cord and spleen via differential centrifugation. As expected, EGFP was predominately localized to fractions enriched for mitochondria in all tissues examined (Figure **4A**). SOD1 and VDAC serve as markers for the cytosolic and mitochondrial fractions, respectively. EGFP expression in spleen mitochondria was also examined by flow cytometry. Spleen homogenates, containing every cell in the spleen including endothelial cells, were processed for mitochondrial isolation. Mitochondria were initially selected based on size, as reflected by forward and side light scatter (FSC, SSC), and positive labelling with the mitochondria specific dye MitoTracker Red (MTR) (Figure **4B**). An average of 83.5 ± 4.7% of the total events collected were $MTR^+$, and thus mitochondria. Of these, 16.5 ± 4.1% of these events exhibited EGFP expression (Figure **4B**). To demonstrate the utility of this model for the evaluation of endothelial mitochondrial function, isolated spleen mitochondria were labelled with fluorescent indicator dyes reporting on different aspects of mitochondrial function by flow cytometry, and mitochondria that expressed EGFP were selected for evaluation (Figure **4C**). [In these experiments, mitochondrial identity was confirmed in a separate sample using MitoTracker Green, a dye that selectively accumulates in mitochondria (data not shown)]. The separation of charge across the mitochondrial inner membrane, referred to as the mitochondrial transmembrane potential ($\Delta\Psi_m$) is generated by the pumping of hydrogen atoms out of the matrix by members of the electron transport chain. This proton gradient is essential for the production of ATP, and thus serves as an excellent way to evaluate mitochondrial function. The fluorescent dye Tetramethylrhodamine, methyl ester (TMRM) is selectively taken up by mitochondria in proportion to the mitochondrial transmembrane potential. In our experiments, nearly all $EGFP^+$ spleen mitochondria are $TMRM^+$ (89.6 ± 0.8%), as expected for healthy mitochondria (Figure **4D**). $EGFP^+$ mitochondria also responded characteristically to Carbonyl cyanide *m*-chlorophenyl hydrazone (CCCP), a protonophore that allows the hydrogen ions to pass freely across the inner mitochondrial membrane, thereby collapsing the electrochemical gradient, causing depolarization and a corresponding decrease in TMRM fluorescence. Experimentally, this is reflected in a decreased percentage of mitochondria (43.0 ± 4.0%) falling within the gate previously determined by TMRM staining (Figure **4D**). The mitochondrial transmembrane potential of $EGFP^+$ mitochondria was not significantly different from $EGFP^-$ mitochondria within the same sample or from non-transgenic littermate controls. Similarly, the response to CCCP was unaltered by the presence of EGFP (data not shown).

Mitochondria normally produce superoxide as a by-product of oxidative phosphorylation. Mitochondrial superoxide can be specifically measured with MitoSOX Red, which produces a red fluorescent signal when oxidized. As expected, $EGFP^+$ mitochondria produce superoxide (66.5 ± 2.7% fall within the predetermined gate). An increased proportion of mitochondria label positively with MitoSox Red when mitochondria are treated with the complex III inhibitor antimycin A (AA; 75.2 ± 1.4%) (Figure **4E**). As was observed above, a comparison of superoxide production of $EGFP^+$ mitochondria and $EGFP^-$ mitochondria from non-transgenic littermate controls revealed no statistically significant difference (data not shown). Taken together, these mice represent a novel tool with which to evaluate key functional features of endothelial mitochondria isolated from vascularised tissues.

Hb9 is a well described homeobox transcription factor best characterized for its role in motor neuron development and in axonal pathfinding for a subset of neurons [7,14,15]. This promoter has been extensively used to generate motor neuron restricted EGFP expression in other transgenic models including mice, fly, zebrafish and chick [7,14]. During the characterization of a similarly intended transgenic line [9], we serendipitously generated the Endo-MitoEGFP model, where expression of EGFP within mitochondria was absent from the intended cell type but presented with a novel microvascular pattern consistent with expression within a subset of endothelial cells. Although Hb9 is often considered exclusively as a marker of motor neurons, it is well published that Hb9 is widely expressed in the endoderm during development which gives rise to the respiratory and digestive tubes. Furthermore, Hb9 is essential for early differentiation of the dorsal gut epithelium into pancreatic tissue and is also detected in differentiated beta cells [16,17]. An early characterization of the Hb9 transcript in human tissues reported expression in colon, small intestine, pancreas, lymphoid tissues and a range of hematopoetic cell lines [18]. Interestingly, Hb9 expression is also well reported in human bone marrow, especially in $CD34^+$ cells, and it becomes downregulated following differentiation [18,19]. Therefore, expression of Hb9 is not solely restricted to motor neurons and is more broadly expressed in other tissues during development and adulthood.

The mechanism(s) which regulate Hb9 expression are not fully understood, especially in non-motor neuron cell types [20]. Interestingly, Hb9 expression was increased 12.5 fold in primary human endothelial cells derived from umbilical vein following treatment with the pro-angiogenic sulfated steroid,

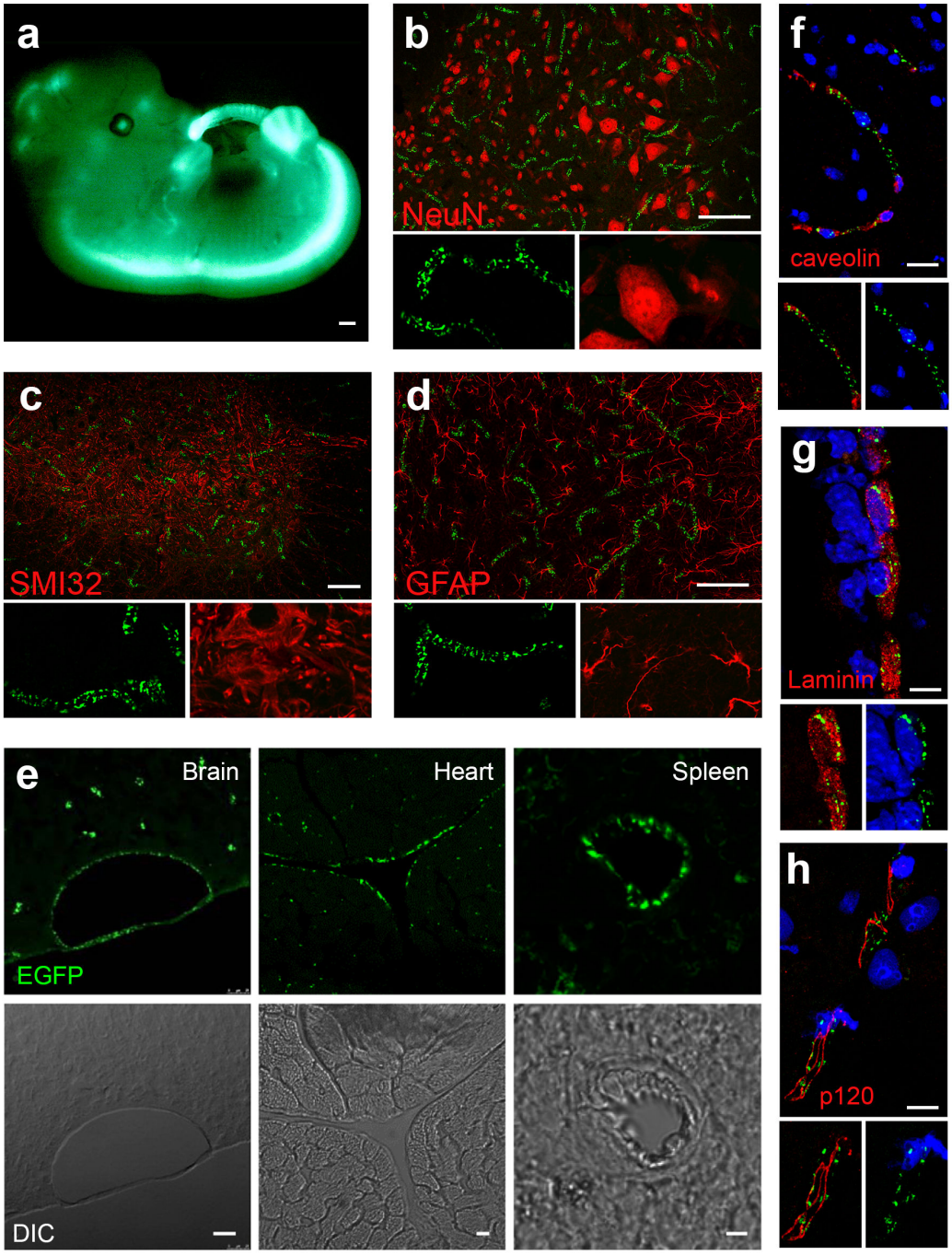


**Figure 2. EGFP is expressed in endothelial cells (EC) of blood vessels.** (A) Low power magnification of 12.5 day old embryo. Scale bar represents 250 µm. High power magnifications of lumbar spinal cord sections showing expression of EGFP (*green*) does not co-localize with (B) NeuN (*red*), a pan-neuronal marker. (C) unphosphorylated neurofilament, SMI32 (*red*), a motor neuron marker or (D) expression of the astrocyte marker GFAP (*red*). Scale bar represents 75 µm. (E) Higher power magnifications of brain (*left*), heart (*middle*) and spleen (*right*) sections, showing EGFP expression (*green*) and transmitted light (*DIC*). Scale bar represents 25, 10 and 5 µm for the brain, heart, and spleen, respectively. Brain sections showing expression of EGFP (*green*), and (F) EC marker caveolin (red), (G) matrix marker laminin (*red*) and (H) junctional protein p120 (*red*). Nuclei are marked by TOPRO-3 (blue). Scale bar represents 15 µm (F and G) and 105 µm (H). *n*=2 animals.

doi: 10.1371/journal.pone.0074603.g002

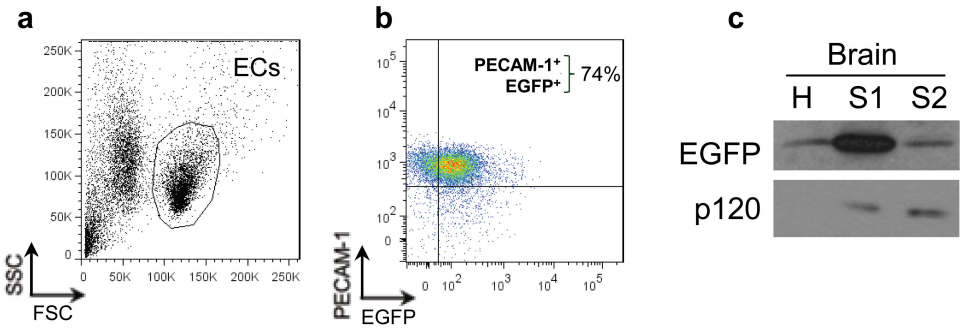


Pickles *et al*. Figure 3

**Figure 3. EGFP expression is detected in ECs via flow cytometry.** (A) Representative dot plot of ECs isolated from spleens of transgenic mice. The EC population was selected based on size and labelling with PECAM-1. (B) The majority of splenic ECs express EGFP and PECAM-1. (C) Western blot of brains homogenates (H), as well as soluble (S1) and insoluble (S2) fractions from lysates of ECs isolated from CNS vessels of transgenic animals and immunoblotted for EGFP and p120. *n*=3 animals.

doi: 10.1371/journal.pone.0074603.g003

sokotrasterol, suggesting a novel role for Hb9 in endothelial cell sprouting and/or angiogenesis [21]. In addition, it is noteworthy that the development of the vascular and neuronal systems are closely coupled in their genesis and branching/path formation [22–24]. In fact, the vascular and nervous systems are the first tissue systems specified during development [24]. The coordinated and concomitant expression of a variety of homeobox factors is required for angiogenesis in the CNS [22]. Homeobox factors are also required for formation of the cardiovascular and lymphatic system. For example, several genes in the HOX gene cluster including HOXA5, HOXA11, HOXB1, HOXB7, and HOXC9, are expressed during the development of the cardiac system; and Prx1 is involved in both cardiac and lymphatic tissue development [4]. In fact, arteries follow the path of nerves in embryonic limb skin, due to expression of VEGF in peripheral nerves and Schwann cells which induces arterial marker expression in endothelial cells [25]. Ablation of peripheral nerves due to genetic deletion of Neurogenin 1 and 2 yields defects in artery branching [25]. Isl1, another homeobox protein is also involved in the specification and maintenance of neuronal identities (especially motor neurons) [26], is now also well known to be expressed during development in the second heart field, giving rise to key structures within the heart [5,6]. In addition, embryonic stem cells expressing Isl1 *in vitro* can differentiate into cardiac progenitors as well as endothelial cells [27], leading to speculation that the expression of this transcription factor may be more widespread than previously believed [28]. Indeed, a careful characterization of Isl1 reporter mice led to the discovery that Isl1 cells are present in the endothelium of the aorta and in umbilical vessels [28]. Taken together, these studies demonstrate the connection between homeobox transcription factors, the development of the vasculature and endothelial cells. We propose here that random integration of the Hb9 promoter in the Endo-MitoEGFP mouse has come under novel or previously uncharacterized regulation leading to expression in a subset of ECs within a variety of vascularized tissues. We speculate that like Isl1 and other homeobox transcription factors, Hb9 may play a dual role in motor neuron identity and development of the vascular system.

## Conclusions

In summary, we report the development of Endo-MitoEGFP mice which feature mitochondrial-restricted expression of EGFP in microvascular ECs. These mice will be instrumental in examining the role and function of mitochondria in EC development, normal adult physiology, and potentially in certain pathologies such as arthrosclerosis, diabetes, multiple sclerosis, Alzheimer's disease, and amyotrophic lateral sclerosis.

## Materials and Methods

### Generation of transgenic mice

Animals used in this study were treated in strict accordance to a protocol (N08001CVsr) approved by the Centre de Recherche du Centre Hospitalier de l'Universite de Montreal (CRCHUM) Institutional Committee for the Protection of Animals which follows national standards as outlined by the Canadian Council on Animal Care (CCAC). The transgenic vector p*Hb9*-MitoEGFP was generated by introducing the mitochondrial targeting sequence of Cytochrome *c* Oxidase subunit VIII into p*Hb9*-EGFP (Dr. Sam Pfaff, Salk Institute) via standard cloning techniques. Transgenic founders (from F1 C57Bl/6 parental mice) were generated by pronuclear injection of a 10 kb NotI-PacI fragment containing p*Hb9*-MitoEGFP. Five

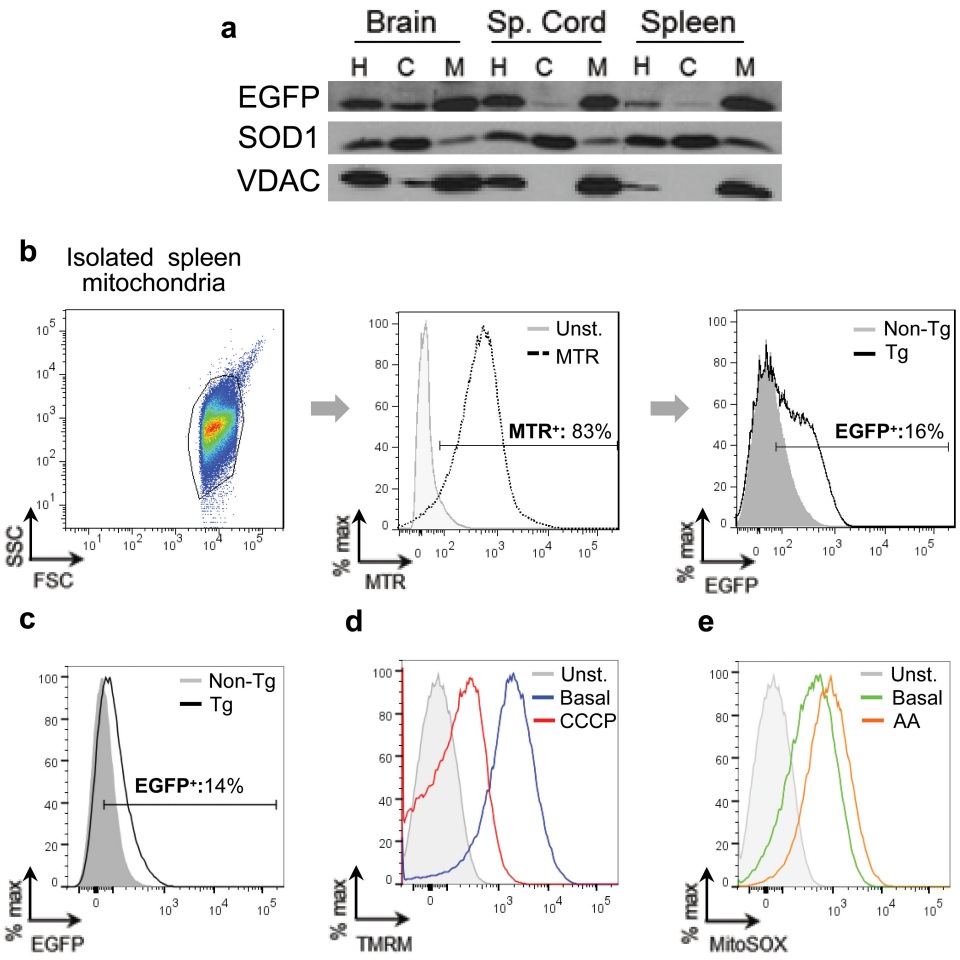


**Figure 4. EGFP is expressed within mitochondria.** (A) Homogenates (H), cytosolic protein (C) and purified mitochondria (M) were collected from the brain, spinal cord and spleen of transgenic mice and probed for EGFP via immunoblot. SOD1 and VDAC serve as controls for cytosol and mitochondria, respectively. (B) Mitochondria were isolated from the spleens of transgenic and non-transgenic mice. *Left*: Mitochondria were gated according to their light scattering properties (forward scatter, FSC; side scatter, SSC). *Middle*: Gated mitochondria were stained with MitoTracker Red (MTR, black, dashed) and compared to unstained (grey, shaded) mitochondria. *Right*: MTR$^+$ mitochondria from transgenic (black, unshaded) and non-transgenic (grey, shaded) mice were analyzed for EGFP expression. Data presented is representative of three independent experiments. (C) Mitochondria from transgenic (black, unshaded), and non-transgenic (grey, shaded) mice were analyzed for EGFP expression. (D) The transmembrane potential of EGFP$^+$ mitochondria was assayed using TMRM. Mitochondria were left, unstained (grey, filled), treated with TMRM, basal conditions (blue), or treated with the protonophore CCCP (red). (E) Mitochondrial superoxide production of EGFP$^+$ mitochondria, was assayed using MitoSOX Red. Mitochondria were left, unstained (grey, filled), treated with MitoSOX Red under basal conditions (green), or treated with the complex III inhibitor Antimycin A (orange). C, D, E are from the same sample and are representative of three independent experiments.

doi: 10.1371/journal.pone.0074603.g004

founders were identified via PCR, one of which gave a staining pattern that resembled the vasculature. These mice, referred to as Endo-MitoEGFP, were backcrossed with C57Bl/6 for eight generations with each generation yielding a consistent expression pattern. Genotyping was done via PCR, using the following primers: 5'-TCTTCTTCAAGGACGACGGCAACT-3' and 5'-CCTTGATGCCGTTCTTCTGCTTGT-3', as previously described [9]. Mice with the expected motor neuron-restricted transgene expression have been published elsewhere [9]. Animals were treated in accordance with Canadian Council for Animal Care (CCAC) and the Centre de recherche du Centre hospitalier de l'Université de Montréal (CRCHUM) guidelines.

### RT-PCR

RNA was extracted using the RNAeasy kit (Qiagen) and reverse transcribed with QuantiTect (Qiagen). Resulting cDNA was processed for standard PCR using the following primer sets: EGFP 5C: 5'-TCTTCTTCAAGGACGACGGCAACT-3'; EGFP 3C: 5'-CCTTGATGCCGTTCTTCTGCTTGT-3'; β-actin exon 5 F: 5'-CGTTGGCATCCACGAAACTA-3'; β-actin exon 6 R: 5'-AGTACTTGCGCTCAGGAGGA-3'.

### Immunoblotting

Adult mice were euthanized with isofluorane and then transcardially perfused with cold PBS prior to tissue collection. Tissues were homogenized in 5 volumes of lysis buffer (50 mM Tris pH 7.5, 1 mM EDTA, 150 mM NaCl, 1% NP-40, 1% SDS, and protease inhibitors). Cleared tissue lysates (25µg), isolated brain ECs (10µg) or mitochondrial and cytosolic fractions were subjected to SDS-PAGE and immunoblotted with an in-house polyclonal anti-EGFP antibody generated against the full-length protein (Covance), SOD1 (Stressgen), VDAC (Calbiochem) and p120 (BD Biosciences).

### Immunofluorescence

Animals were transcardially perfused with 4% phosphate-buffered paraformaldehyde (FD NeuroTechnologies). Tissues were subsequently dissected, post-fixed for 2 hours, cryoprotected, and then embedded in OCT (TissueTek). Ten micron sections collected directly on slides were blocked with 3% BSA in 0.2% Triton X-100/PBS, labelled with, SMI32 (Covance), NeuN (Millipore), GFAP (DAKO) diluted in blocking buffer. Antibodies were visualized via fluorescently conjugated anti-mouse or anti-rabbit secondary antibodies (Texas Red; Jackson Immunochemicals). Stainings for caveolin (Santa Cruz), laminin (DakoCyomation), and p120 (Santa Cruz) were done on sections from PBS-perfused mice. Slides were fixed with cold ethanol prior to immunolabelling. Coverslips were sealed using ProLong Antifade reagent (Invitrogen) and analyzed with a confocal microscope (Leica SP5; 63x oil, 1.7 NA) and processed with Leica LAS AF software and/or Photoshop CS4 (Adobe).

### Isolation of splenic and brain ECs

Transgenic animals were processed as previously described to isolate spleen and CNS vessels [13]. Briefly, tissues were dissected, minced and homogenized. Homogenates were washed with Hanks Balanced Salt Solution (HBSS) and centrifuged in 30% dextran (Sigma) at 4 000 x *g* for 30 min. For brains, the myelin layer was discarded and the pellet containing the ECs was washed and processed for western blot. Cells were lysed in 10 mM HEPES, 100 mM NaCl, 2 mM EDTA, 1% Triton X-100, pH 7.4 with protease inhibitors, using a 21G needle. Soluble proteins (S1) were obtained by collecting the supernatant after centrifugation at 15 000 x *g*. Insoluble fractions (S2) were resuspended in buffer with 1% SDS, sonicated, and then centrifuged at 15 000 x *g*. For spleens the pellet which contains vascular components was washed in HBSS and processed for flow cytometry.

### Isolation of mitochondria

For western blotting, mitochondria were isolated exactly as previously described [29]. For flow cytometry, mitochondria were isolated from spleen homogenates via differential centrifugation (17 000 x *g*) in homogenizing buffer (HB: 210 mM Mannitol, 70 mM Sucrose, 10 mM Tris, 1 mM EDTA, pH 7.5).

### Flow cytometry

Splenic ECs were labelled for expression of PECAM-1 at the cell surface with monoclonal PECAM-1 APC (BD Bioscience) or isotype control in FACS Buffer (1% Fetal Bovine Serum, 0.1% sodium azide in PBS). EC's were first gated according to size by light scattering properties (FSC/SSC), then PECAM-1 and EGFP expression were examined. Mitochondria (25 µg) were labelled with MitoTrackerRed (MTR, 100 nM; Invitrogen) to confirm mitochondrial identity in HB Buffer. Native EGFP fluorescence was detected without antibody. For mitochondrial functional assays, mitochondria (25 µg) were incubated in M Buffer (220 mM sucrose, 68 mM mannitol, 10 mM KCl, 5 mM $KH_2PO_4$, 2 mM $MgCl_2$, 500 µM EGTA, 5 mM succinate, 2 µM rotenone, 10 mM HEPES pH 7.2, 0.1% fatty acid-free BSA). Tetramethylrhodamine Methyl Ester (TMRM, 100 nM; Invitrogen) was used to assess mitochondrial transmembrane potential ($\Delta\Psi_m$) and MitoSOX Red (MitoSOX, 5 µM; Invitrogen) to quantify mitochondrial superoxide levels. The protonophore carbonyl cyanide *m*-chlorophenyl hydrazone (CCCP, 100 µM; Sigma) was used as a control for $\Delta\Psi_m$ measurements, and the complex III inhibitor, Antimycin A (AA, 100 µM; Sigma) was used as a control for mitochondrial superoxide production. Mitochondria were gated according to light scatter, after doublets were excluded, then $EGFP^+$ events were selected, and levels of TMRM and MitoSOX Red were evaluated. Dyes and antibodies selected exhibited distinct spectral properties with minimal to no overlap. Where necessary, compensation was applied according to single-color control samples. ECs and mitochondrial samples were processed on a LSR II flow cytometer (BD Biosciences). All flow cytometry data was analyzed with FlowJo (Treestar, Ashland, OR).

## Acknowledgements

We thank D.W. Cleveland for his support in the early stages of this work, N. Arbour for help with flow cytometric analysis, and S. Bel Hadj for technical assistance.

## Author Contributions

Conceived and designed the experiments: SP PC AP CVV. Performed the experiments: SP MCD JIA MAL SLP LSO LD ST CVV. Analyzed the data: SP JIA PC AP CVV. Wrote the manuscript: SP CVV.

## References


1. Motoike T, Loughna S, Perens E, Roman BL, Liao W et al. (2000) Universal GFP reporter for the study of vascular development. Genesis 28: 75-81. doi:10.1002/1526-968X(200010)28:2<75::AID-GENE50>3.0.CO;2-S[pii]. PubMed: 11064424.
2. Choi I, Chung HK, Ramu S, Lee HN, Kim KE et al. (2011) Visualization of lymphatic vessels by Prox1-promoter directed GFP reporter in a bacterial artificial chromosome-based transgenic mouse. Blood 117: 362-365. doi:10.1182/blood-2010-07-298562. PubMed: 20962325. blood-2010-07-298562 . PII . doi:10.1182/blood-2010-07-298562
3. Gong S, Zheng C, Doughty ML, Losos K, Didkovsky N et al. (2003) A gene expression atlas of the central nervous system based on bacterial artificial chromosomes. Nature 425: 917-925. doi:10.1038/nature02033. PubMed: 14586460. nature02033 . PII.
4. Gorski DH, Patel CV, Walsh K (1993) Homeobox transcription factor regulation in the cardiovascular system. Trends Cardiovasc Med 3: 184-190. doi:10.1016/1050-1738(93)90004-P. PubMed: 21244931. 1050-1738(93)90004-P . PII . doi:10.1016/1050-1738(93)90004-P
5. Sun Y, Liang X, Najafi N, Cass M, Lin L et al. (2007) Islet 1 is expressed in distinct cardiovascular lineages, including pacemaker and coronary vascular cells. Dev Biol 304: 286-296. doi:10.1016/j.ydbio.2006.12.048. PubMed: 17258700. 06)01503-X. PII.
6. Cai CL, Liang X, Shi Y, Chu PH, Pfaff SL et al. (2003) Isl1 identifies a cardiac progenitor population that proliferates prior to differentiation and contributes a majority of cells to the heart. Dev Cell 5: 877-889. doi:10.1016/S1534-5807(03)00363-0. PubMed: 14667410. S1534580703003630 . PII.
7. Arber S, Han B, Mendelsohn M, Smith M, Jessell TM et al. (1999) Requirement for the homeobox gene Hb9 in the consolidation of motor neuron identity. Neuron 23: 659-674. doi:10.1016/S0896-6273(01)80026-X. PubMed: 10482234.
8. Nakano T, Windrem M, Zappavigna V, Goldman SA (2005) Identification of a conserved 125 base-pair Hb9 enhancer that specifies gene expression to spinal motor neurons. Dev Biol 283: 474-485. doi:10.1016/j.ydbio.2005.04.017. PubMed: 15913596. 05)00252-6 . PII. doi:10.1016/j.ydbio.2005.04.017
9. Vande Velde C, McDonald KK, Boukhedimi Y, McAlonis-Downes M, Lobsiger CS et al. (2011) Misfolded SOD1 associated with motor neuron mitochondria alters mitochondrial shape and distribution prior to clinical onset. PLOS ONE 6: e22031. doi:10.1371/journal.pone.0022031. PubMed: 21779368.
10. Iyer S, Ferreri DM, DeCocco NC, Minnear FL, Vincent PA (2004) VE-cadherin-p120 interaction is required for maintenance of endothelial barrier function. Am J Physiol Lung Cell Mol Physiol, 286: L1143-L1153. doi:10.1152/ajplung.00305.2003. PubMed: 14672921. 00305.2003 . PII.
11. Oas RG, Xiao K, Summers S, Wittich KB, Chiasson CM et al. (2010) p120-Catenin is required for mouse vascular development. Circ Res 106: 941-951. CIRCRESAHA doi:10.1161/CIRCRESAHA.109.207753. PubMed: 20110533. 109.207753. PII.
12. Albelda SM, Muller WA, Buck CA, Newman PJ (1991) Molecular and cellular properties of PECAM-1 (endoCAM/CD31): a novel vascular cell-cell adhesion molecule. J Cell Biol 114: 1059-1068. doi:10.1083/jcb.114.5.1059. PubMed: 1874786.
13. Alvarez JI, Dodelet-Devillers A, Kebir H, Ifergan I, Fabre PJ et al. (2011) The Hedgehog pathway promotes blood-brain barrier integrity and CNS immune quiescence. Science 334: 1727-1731. doi:10.1126/science.1206936. PubMed: 22144466. science.1206936 . PII . doi:10.1126/science.1206936
14. Odden JP, Holbrook S, Doe CQ (2002) Drosophila HB9 is expressed in a subset of motoneurons and interneurons, where it regulates gene expression and axon pathfinding. J Neurosci 22: 9143-9149. PubMed: 12417636. 22/21/9143. PII.
15. Thaler J, Harrison K, Sharma K, Lettieri K, Kehrl J et al. (1999) Active suppression of interneuron programs within developing motor neurons revealed by analysis of homeodomain factor HB9. Neuron 23: 675-687. doi:10.1016/S0896-6273(01)80027-1. PubMed: 10482235.
16. Li H, Arber S, Jessell TM, Edlund H (1999) Selective agenesis of the dorsal pancreas in mice lacking homeobox gene Hlxb9. Nat Genet 23: 67–70. doi:10.1038/12669. PubMed: 10471501.
17. Harrison KA, Thaler J, Pfaff SL, Gu H, Kehrl JH (1999) Pancreas dorsal lobe agenesis and abnormal islets of Langerhans in Hlxb9-deficient mice. Nat Genet 23: 71-75. doi:10.1038/12674. PubMed: 10471502.
18. Harrison KA, Druey KM, Deguchi Y, Tuscano JM, Kehrl JH (1994) A novel human homeobox gene distantly related to proboscipedia is expressed in lymphoid and pancreatic tissues. J Biol Chem 269: 19968-19975. PubMed: 7914194.
19. Deguchi Y, Kehrl JH (1991) Selective expression of two homeobox genes in CD34-positive cells from human bone marrow. Blood 78: 323-328. PubMed: 1712647.
20. Arkhipova V, Wendik B, Devos N, Ek O, Peers B et al. (2012) Characterization and regulation of the hb9/mnx1 beta-cell progenitor specific enhancer in zebrafish. Dev Biol 365: 290-302. doi:10.1016/j.ydbio.2012.03.001. PubMed: 22426004. 12)00133-9. PII.
21. Karsan A, Pollet I, Yu LR, Chan KC, Conrads TP et al. (2005) Quantitative proteomic analysis of sokotrasterol sulfate-stimulated primary human endothelial cells. Mol Cell Proteomics 4: 191-204. PubMed: 15611527. M400152-MCP200 . PII . doi:10.1074/mcp.M400152-MCP200
22. Vasudevan A, Bhide PG (2008) Angiogenesis in the embryonic CNS: a new twist on an old tale. Cell Adh Migr 2: 167-169: 6485 [pii] PubMed: 19262109.
23. Park KW, Crouse D, Lee M, Karnik SK, Sorensen LK et al. (2004) The axonal attractant Netrin-1 is an angiogenic factor. Proc Natl Acad Sci U S A 101: 16210-16215. doi:10.1073/pnas.0405984101. PubMed: 15520390. 0405984101. PII.
24. Park KW, Morrison CM, Sorensen LK, Jones CA, Rao Y et al. (2003) Robo4 is a vascular-specific receptor that inhibits endothelial migration. Dev Biol 261: 251-267. doi:10.1016/S0012-1606(03)00258-6. PubMed: 12941633. S0012160603002586 . PII.
25. Mukouyama YS, Shin D, Britsch S, Taniguchi M, Anderson DJ (2002) Sensory nerves determine the pattern of arterial differentiation and blood vessel branching in the skin. Cell 109: 693-705. doi:10.1016/S0092-8674(02)00757-2. PubMed: 12086669. S0092867402007572 . PII.
26. Liang X, Song MR, Xu Z, Lanuza GM, Liu Y et al. (2011) Isl1 is required for multiple aspects of motor neuron development. Mol Cell Neurosci 47: 215-222. doi:10.1016/j.mcn.2011.04.007. PubMed: 21569850. 7431(11)00092-3. PII.
27. Moretti A, Caron L, Nakano A, Lam JT, Bernshausen A et al. (2006) Multipotent embryonic isl1+ progenitor cells lead to cardiac, smooth muscle, and endothelial cell diversification. Cell 127: 1151-1165. doi:10.1016/j.cell.2006.10.029. PubMed: 17123592. 8674(06)01398-5 . PII . doi:10.1016/j.cell.2006.10.029
28. Keenan ID, Rhee HJ, Chaudhry B, Henderson DJ (2012) Origin of non-cardiac endothelial cells from an Isl1+ lineage. FEBS Lett 586: 1790-1794. doi:10.1016/j.febslet.2012.05.014. PubMed: 22613570. 5793(12)00389-4 . PII . doi:10.1016/j.febslet.2012.05.014
29. Vande Velde C, Miller TM, Cashman NR, Cleveland DW (2008) Selective association of misfolded ALS-linked mutant SOD1 with the cytoplasmic face of mitochondria. Proc Natl Acad Sci U S A 105: 4022-4027. doi:10.1073/pnas.0712209105. PubMed: 18296640.